

**Metal-rich Scales in the Reykjanes
Geothermal System, SW Iceland: Sulfide Minerals in
a Seawater-dominated Hydrothermal Environment**

Vigdís Hardardóttir



uOttawa

Thesis submitted to the Faculty of Graduate
and Postdoctoral Studies

In partial fulfillment of the requirements

For the PhD degree in Earth Sciences

**Department of Earth Sciences
Faculty of Science
University of Ottawa**

© Vigdís Hardardóttir, Ottawa, Canada, 2011

I dedicate this thesis to four strong women
for being the wind beneath my wings;
my sister Helga Hardardóttir,
and my daughters Steinunn, Sigrún Emma, and Elísabet Guðrún

Fyrir próf

Á litlum lærdómshesti
Ég legg í prófsins hyl.
Þótt allt mig annað bresti,
Ég eitt á samt: ég vil.

Þótt létt sé lærdómsnesti
Í léttum viskumal,
Þá er þar bitinn besti,
Sá bitinn er: ég skal.

Hannes Hafstein, Ljóðabók, 1951
(Icelandic statesman and poet,
1861-1922)

Before exam

Though small my horse of wisdom
My aim is up the hill.
As poor and lacking sure I am
One thing I have, - the will.

My haversack of learning
Is light, - and skill are few.
But still I have the best of all
I intend, - I can and shall.

Translator
Jón Þorsteinsson 2. Desember 2010.

Abstract

Downhole sampling of unboiled liquid at 1350 and 1500 m depth in the seawater-dominated Reykjanes high-temperature geothermal system shows that metal concentrations measured at surface (and by analogy, metal concentration measured in many black smoker vents) are minimum values due to mineral precipitation in the wells. Deep, unboiled fluids in the Reykjanes geothermal system react with mid-ocean ridge basalt at temperatures as high as 346°C and contain 9-140 ppm Fe, 14-17 ppm Cu, 5-27 ppm Zn, 120-290 ppb Pb, 1-6 ppb Au, and 28-107 ppb Ag. The concentrations of Fe, Cu, Zn and Pb are similar to those in the highest-temperature seafloor hydrothermal systems (~400°C), but the Au and Ag concentrations are one to two orders of magnitude higher. Fluids discharged at surface from the same wells have orders of magnitude lower metal concentrations due to precipitation caused by boiling and vapor loss during depressurization. Some seafloor vent fluids may also be depleted in metals compared to the deep liquids at Reykjanes because of deposition due to boiling, mixing, and/or conductive cooling prior to sampling at the seafloor. The low metal contents in some mid-ocean-ridge hydrothermal systems imply potentially significant losses of metal below the seafloor, if the deep liquids have metal concentrations similar to those at Reykjanes.

Boiling and gas loss causes the formation of mineral scales upstream and downstream of orifice plates (throttle points across which there are sharp pressure decreases) in the surface pipelines of Reykjanes. Detailed studies on scales collected along the surface pipelines of well RN-9, from the wellhead to the separation station, yielded the following results. Upstream of the orifice plate and at high pressure (40 bar, 252°C), the scales

consisted mainly of sphalerite and chalcopyrite with traces of galena and bornite. At the orifice plate, the pressure dropped to 11 bar (188°C) resulting in abundant precipitation mainly of amorphous silica accompanied by sphalerite and traces of chalcopyrite. The Fe content of the sphalerite (RN-9) increased from 3 wt.% (at 40 bar) to 5-8.5 wt.% (at 11 bar). At the orifice plate the sharp pressure decrease results in flashing (rapid boiling) of the geothermal liquid over a distance of a few centimetres which causes rapid deposition of very fine-grained sulfides. In the medium-pressure wells (average pressure at the wellhead of 37-30 bar), metals are deposited on fluid-flow control valves inserted into the orifice plate; in high-pressure wells (average pressure at the wellhead of 45-35 bar) most of the metals are deposited downstream of the orifice plate. A high degree of supersaturation of metals is indicated by the very fine grain size of the sulfides and dendritic textures. In the medium-pressure wells, the nearly quantitative deposition of metals on the fluid flow control valve results in the formation of a metastable Cu-Fe-S solid solution, rich in silver and gold, together with fine-grained intergrowths of galena and sphalerite. Concentrations of Au and Ag in these scales are up to 590 ppm and 2.3 wt.%, respectively. Postdepositional cooling causes the exsolution of bornite and digenite from the high-temperature solid solution (~250°C), and silver is expelled from the Cu-Fe-S solid solution and remobilized into late fractures in the scales. Gold appears to remain in solid solution or occurs as submicroscopic inclusions in the bornite and digenite.

The major metal precipitating at all pressures is Zn. Bulk concentrations in the scales vary between 40 and 60 wt.% Zn upstream and downstream of the orifice plate in the high-pressure wells. In well RN-9, the Zn contents are between 15 and 25 wt.% upstream and in the first 4 m downstream of the orifice plate, and diminishes from there. Iron contents

increase up in the well from 8 to ~20 wt.% due to precipitation of maghemite but also local contamination from the steel pipe. The Fe concentration decreases downstream of the orifice plate from 6 wt.% to 2 wt.% at the separation station. In the surface pipeline of well RN-9, Fe is forming an amorphous phase with silica. Copper contents are low downhole (~3 wt.%), but increase up to 25 wt.% on the fluid flow control valve and decrease from there. Lead is present at ppm concentrations downhole; at the wellhead Pb contents are ~3 wt.%, increasing to 15 wt.% at the fluid flow control valve and decreasing sharply from there. Gold and Ag concentrations in all scales are high, generally increasing from 80 ppm Au and 35 ppm Ag at 669 m depth to ~100 ppm Au and 3500 ppm Ag near the orifice plate.

In one year, well RN-9 precipitated in surface pipeline close to 2.5 tonnes of material downstream of the orifice plate, which contains ~0.6 ton of sphalerite, 0.2 ton of chalcopyrite and 1.6 tonnes of amorphous silica. This well became clogged downhole in 1993 and again in 2003. On the basis of mineralogy and phase densities; ~11 tonnes of sphalerite were precipitated downhole yearly from 1983 to 1993. Assuming an average fluid flow of 1.7×10^9 kg per year for RN-9 and an average of 10 mg/kg Zn from the downhole liquid (range 5-26 ppm), the total amount of metal is estimated to be 17 tonnes of Zn, close to the estimate from the volume of scale and its sphalerite content. Between 4 and 5 tonnes of scales are deposited by the high-pressure wells per year at surface, including 1.5 tonnes of Zn, 8 kg of Ag and ~1 kg of Au. Sulfide-rich scales that might be recovered from the five high-pressure wells examined in this study could contain metals valued at close to \$73,000 per year at today's metal prices January 2011.

To mitigate sulfide precipitation downhole, both in the casing as well as the reservoir wallrock, the wellhead pressure should be kept as high as possible. In the surface pipeline,

the pressure must be at least ~22 bar downstream of the pressure control valve, and the surface pipelines should be as straight as possible, avoiding bends and other disruptions of flow that cause more turbulence and scale deposition.

Sommaire

L'échantillonnage des liquides n'ayant pas subi d'ébullition, prélevées à des profondeurs de 1350 à 1500 mètres dans le système hydrothermal de Reykjanes où domine l'eau de mer, nous indique que les teneurs de métaux observées à la surface (et par analogie, dans les nombreux fumeurs noirs des fonds marins) sont des teneurs minimales à cause d'une précipitation dans les puits de forage. Les fluides du système géothermique de Reykjanes réagissent avec les basaltes de la dorsale océanique à des températures allant jusqu'à 346°C et contiennent de 9 à 140 ppm Fe, 14 à 17 ppm Cu, 5 à 27 ppm Zn, 120 à 290 ppb Pb, 1 à 6 ppb Au et 28 à 107 ppb Ag. Les teneurs de Fe, Cu, Zn et Pb sont comparables à celles des solutions hydrothermales des systèmes sous-marins aux températures les plus élevées (~400°C), sauf que les teneurs en Au et Ag sont une ou deux ordres de grandeur plus élevées. Les fluides qui sont déchargés à la surface dans ces mêmes puits possèdent des teneurs en métaux qui sont inférieures par plusieurs ordres de grandeurs à cause de la précipitation qui survient lors de l'ébullition et de la perte de vapeur engendrée lors de la dépressurisation. Il est aussi possible que les fluides de certaines des cheminées sous-marines soient eux aussi appauvries en métaux, soit par la déposition lors de l'ébullition, du mélange ou du refroidissement par conduction qui survient avant la prise de l'échantillon sur le fond marin. Les faibles teneurs en métaux observées dans les fluides de certains systèmes hydrothermaux sous-marins suggèrent qu'ils ont subi une perte importante de métaux sous le fond marin, si leur composition en profondeur est comparable à celle observée dans le système de Reykjanes.

L'ébullition et le dégazage favorisent la formation des dépôts et incrustations de minéraux dans les pipelines à la surface du champ de Reykjanes. Ces dépôts ou incrustations se retrouvent préférentiellement où surviennent les plus importantes chutes de pression dans les pipelines, soit en amont ou en aval des plaques d'orifice. L'étude détaillée de ces incrustations, prélevées le long du pipeline du puits RN-9, de la tête du puits jusqu'à la station de séparation, nous donne les résultats suivants. En amont de la plaque d'orifice, où la pression est élevée (40 bars, 252°C), les dépôts sont composés surtout de sphalérite et de chalcopryrite avec des traces de galène et de bornite. À la plaque d'orifice la pression diminue à 11 bars (188°C), ce qui provoque surtout la déposition de silice amorphe et de sphalérite avec des traces de chalcopryrite. La teneur en Fe de la sphalérite augmente de 3% pds (à 40 bars) jusqu'à 5 - 8,5% pds (à 11 bars). À la plaque même, la dépressurisation rapide provoque l'ébullition instantanée de la solution géothermique sur une distance de quelques centimètres, ce qui cause la déposition rapide de sulfures de granulométrie très fine. Dans les puits à moyenne pression (37 à 30 bars à la tête du puits), les métaux se déposent sur les vannes de contrôle d'écoulement qui sont insérées dans la plaque d'orifice alors que dans les puits à haute pression (45 à 35 bars à la tête du puits), la précipitation des métaux survient surtout en aval de la plaque d'orifice. La taille très fine des grains de sulfures ainsi que les textures en dendrites indiquent un haut niveau de sursaturation. Dans les puits à pression moyenne, la déposition quasi-quantitative des métaux sur les vannes de contrôle produit une solution solide métastable de Cu-Fe-S et enrichie en Au et Ag ainsi que de fines intercroissances de galène et de sphalérite. La teneur en Au et Ag de ces incrustations peut atteindre jusqu'à 590 ppm et 2,3% pds, respectivement. Après la déposition, le refroidissement de la solution solide à haute température (~250°C) entraîne l'exsolution de bornite et digénite ainsi que

l'expulsion de l'argent de la solution solide de Cu-Fe-S qui se remobilise au sein des fractures tardives dans les incrustations. L'or semble demeurer en solution solide ou se présente sous forme d'inclusions submicroscopiques dans la bornite ou la digénite.

Le principal métal à se précipiter à toutes les pressions est le zinc. Les teneurs de Zn, obtenus sur des échantillons en vrac en amont ou en aval de la plaque d'orifice dans les puits de haute pression, varient de 40 à 60% pds. Dans le puits RN-9, la teneur en Zn varie entre 15 à 25% pds en amont et parmi les premiers 4 mètres en aval de la plaque d'orifice, et diminue de ce point vers l'aval. La teneur en Fe s'accroît de 8 à ~20% pds vers le haut du puits. Cette augmentation en Fe est attribuée à la précipitation de maghémite mais doit aussi être en partie causée par la contamination provenant du tuyau en acier. La teneur en Fe diminue en aval de 6% à la plaque d'orifice jusqu'à 2% pds à la station de séparation. Dans le pipeline de surface du puits RN-9, on remarque la précipitation d'une phase amorphe de Fe et de silice. Les teneurs en Cu sont faibles dans le fond du puits (~3% pds) mais augmentent jusqu'à 25% pds à la vanne de contrôle et diminuent par la suite. Le plomb présente des teneurs en ppm dans le fond du puits ; à la tête du puits la teneur est à ~3% pds et augmente jusqu'à 15% pds sur les vannes de contrôle pour ensuite chuter rapidement. Les teneurs en Au et Ag dans les incrustations sont élevées, allant généralement de 80 ppm Au et 35 ppm Ag à 669 m de profondeur, et augmentant à ~100 ppm Au et 3 500 ppm Ag à la plaque d'orifice.

Durant une période d'une année, près de 2,5 tonnes de dépôts minéraux furent précipités en aval de la plaque d'orifice du pipeline de surface, contenant en moyenne ~0,6 tonne de sphalérite, 0,2 tonnes de chalcopryrite et 1,6 tonnes de silice amorphe. Ce puits est devenu bouché en profondeur en 1993, et à nouveau en 2003. En s'appuyant sur la composition minéralogique des dépôts et leur densité, on peut estimer que ~11 tonnes de

sphalérite furent précipitées annuellement en profondeur dans le puits de 1983 à 1993. En supposant pour le puits RN-9 un écoulement annuel moyen de 1.7×10^9 kg par année et une teneur moyenne de Zn de 10 mg/kg (étendue de 5 à 26 ppm), la masse totale de Zn estimée est 17 tonnes, soit près de la valeur prédite par le volume et la composition (en Zn) de dépôts. Environ 4 à 5 tonnes de dépôts et incrustations sont déposées annuellement à la surface, ce qui correspond à 1,5 tonnes de zinc, 8 kg d'argent et ~1 kg d'or. Au prix actuels du marché, les précipitations enrichies en sulfures des 5 puits à haute pression documentés dans cette étude représentent un revenu annuel d'environ 73 000\$.

Afin de prévenir la précipitation en profondeur, aussi bien dans le tubage du puits que dans la roche encaissante, il est important de maintenir la pression aussi élevée que possible. Dans les pipelines de surface, la pression doit être maintenue au moins à ~22 bars en aval de la soupape de contrôle de pression et les canalisations doivent, dans la mesure du possible, être droites afin d'éviter les bouleversements ou turbulences dans l'écoulement du fluide qui encouragent la précipitation des dépôts.

Table of Contents

Abstract	iii
Sommaire	vii
Table of Contents	xi
List of Tables	xiv
List of Figures	xvi
Acknowledgments	xx
CHAPTER 1: Iceland Geology, Geothermal Activity, and the Reykjanes High-temperature System	1
1.1 Introduction and Objectives.....	2
1.2 Volcanic setting of Iceland	3
1.2.1 Plate tectonics	5
1.2.2 Crustal thickness	5
1.2.3 The volcanic zones	6
1.2.4 The volcanic systems	7
1.2.5 The geologic history	8
1.3 Geothermal Systems in Iceland	10
1.3.1 Classification and characteristics	11
1.4 Reykjanes Geothermal System	20
1.4.1 Geological setting geothermal activity	22
1.4.2 Stratigraphy and alteration mineralogy	26
CHAPTER 2: Sulfide Mineralogy and Composition of Scales from the Reykjanes Geothermal System, Southwest Iceland	30
2.1. Introduction	31
2.2. Characteristics of Well RN-9	32
2.2.1 General information	32
2.2.2 Conditions in well RN-9	35
2.2.3 Conditions in the surface pipeline of RN-9	37
2.3. Scale Samples from RN-9: Occurrence, Characteristics and Textures	38
2.3.1 Group 1	45
2.3.2 Group 2	45
2.3.2 Group 3	50
2.4 Mineralogy, Mineral Chemistry, and Paragenesis of Scales in RN-9	50
2.4.1 Amorphous phases	51
2.4.2 Sphalerite	51

2.4.3	Chalcopyrite	56
2.4.4	Galena	57
2.4.5	Bornite	57
2.4.6	Pyrrhotite	58
2.4.7	Pyrite	58
2.4.8	Gold	59
2.4.9	Other minerals	59
2.4.10	Oxides	60
2.5	Scales in Newer Wells, RN-10 to RN-24	61
2.5.1	High-pressure wells	63
2.5.2	Medium-pressure wells	63
2.5.3	Low-pressure wells	67
2.6	Scaling Tests in 2002 and 2003 in RN-9, RN-11 and, RN-10	68
2.7	Downhole Scales in Well RN-22	69
2.8	Bulk Compositions of the Scales	75
2.8.1	Major elements	75
2.8.2	Normative calculations for well RN-9	102
2.8.3	Trace elements	103
2.9	Mass Accumulation in Well RN-9 Downhole and in the Surface Pipeline ...	112
2.10	Metals in the Altered Host Rock	113
2.11	Discussion	121
2.11.1	Scale deposition versus pressure change	121
2.11.2	Texture, mineralogy, composition and paragenesis versus pressure .	122
2.11.3	Mass balances of metals	125
2.12	Summary and Conclusions	126
CHAPTER 3: Cu-rich Scales in the Reykjanes Geothermal System, Iceland		130
	Abstract	131
	Introduction	132
3.1	The Reykjanes Geothermal System	133
3.1.1	Location and conditions of scale formation	135
3.2	Mineralogy and Chemical Composition of the Cu-rich Scales	139
3.2.1	Mineral analyses	143
3.3	Discussion	145
3.3.1	Sulfide textures and paragenesis	145
3.3.2	Mineral phase relations	147
3.3.3	Causes of sulfide mineral deposition	150
3.3.4	Comparison with Cu-rich black smoker chimneys	150

3.3.5 Comparison with sulfide scales from the Salton Sea	153
3.3.6 Cu-rich stockworks in volcanic-hosted massive sulfide ore deposits	154
3.4 Summary and Conclusions	155
Acknowledgements	156
Chapter 4: Metals in Deep Liquid of the Reykjanes Geothermal System, Southwest Iceland: Implications for the Composition of Seafloor Black Smoker Fluids	157
Abstract	158
Introduction	159
4.1 Geologic Background and Hydrothermal System	160
4.2 Results and Discussion	161
4.2.1 Comparison with seafloor black smoker fluids	163
4.2.2 Metal flux from Reykjanes and seafloor systems	166
Acknowledgements	167
Chapter 5: Composition of the Deep Liquid of the Reykjanes Geothermal System, Southwest Iceland: Geochemical Modeling of Fluid-Mineral Interaction	168
5.1. Introduction	169
5.2. Geothermal Fluids at Reykjanes	171
5.2.1 Calculation of reservoir liquid from the discharged fluid	171
5.2.2 Chemical characteristics of the Reykjanes geothermal fluid	175
5.3. Introduction to the Computational approach by CHILLER	182
5.3.1 Reconstruction of the downhole samples	182
5.3.2 Mineral equilibria	184
5.3.3 Results of boiling the reconstructed liquid	186
5.4. Discussion	189
5.5. Summary	192
Chapter 6: Summary and Comparison with Other Geothermal Systems	194
6.1 Summary	195
6.2 Comparison of Reykjanes Scales to Other Geothermal Systems	200
References	205
Appendixes	241
Appendix 2.1	242
2.1.1 Well logging in RN-9 in September 1993 and October 2004	242
2.1.2 The orifice plate and the fluid flow control valve (the cone)	247
Appendix 2.2	250
2.2.1 Microprobe analyses	250
2.2.2 Bulk chemical analyses	251

2.2.3 X-Ray diffractions (XRD analysis at ISOR)	253
2.2.4 Chemical analyses of water samples (at ISOR)	256
Appendix 2.3	258
Appendix 2.4	265
2.4.1 Scaling experiments 2002 and 2003	265
2.4.2 Test equipment	265
2.4.3 RN-9 results	269
2.4.4 RN-11 results	271
2.4.5 RN-10 results	272
Appendix 2.5	275
2.5.1 Normative calculations	275
2.5.2 Volume calculations	276
2.5.3 Amount of scales precipitated in well RN-9 from 1983 to 1993	276
2.5.4 Amount of scales in well RN-9 in 2003	279
Appendix 4	280
Appendix 4.1: Sampling and analytical methods, plus complications of discharge compositions of seafloor black smokers	282
Appendix 5	285
Appendix 5.1 Calculation of reservoir liquid composition from surface samples	286
Appendix 5.2	288

List of Tables

Table 1.1. Comparison of the compositions of downhole liquids in the high-temperature areas of Krafla, Námafjall, Nesjavellir, Hellisheidi, Svartsengi and Reykjanes	11
Table 2.1. Mineralogy of the scale samples from well RN-09	46
Table 2.2. Composition of minerals in scales from surface pipelines from well RN-9 ...	53
Table 2.3 Representative microprobe and SEM analyses of amorphous Fe-Silicate from well RN-9 (2002)	60
Table 2.4 Summary of physical parameters for the wells in this study, and scale characteristics	62
Table 2.5 Principal mineralogy and relative abundance of the minerals downhole in well RN-22 from cleaning in August 2009	70
Table 2.6 Compositions of minerals in scales from downhole well RN-22	73
Table 2.7 Bulk compositions of scales from RN-9 Reykjanes geothermal system	76
Table 2.8. Bulk composition of scales from high- (RN-11, 22, 23, 14, 10), medium- (RN-12, 21, 24) and low-pressure (RN-13, 15, 18) wells, Reykjanes geothermal system	85

Table 2.9 Bulk composition of scales from 2009 downhole RN-22 Reykjanes geothermal system	95
Table 2.10 Normative abundances of minerals by weight from well RN-9	99
Table 2.11 Correlation matrix for selected trace elements in scales from RN-9	100
Table 2.12. Concentrations of platinum group elements in selected gold-rich samples	109
Table 2.13. Major and trace element concentrations in altered rock from drill cuttings from downhole well RN-9 (500 to 1346 m depth)	114
Table 2.14. Volume and mass of scale deposited over one year period in surface pipeline of wells RN-9, RN-11, RN-22 and RN-23	126
Table 3.1. Calculated reservoir compositions of liquids from wells RN-9, 12, 21, and 24, and measured deep liquid (RN-12DL) in a downhole sample collected from well RN-12	133
Table 3.2. Summary of the physical parameters for the wells sampled in this study	137
Table 3.3. Mineralogy of scale samples from the Reykjanes wells compared to black smoker chimneys from the TAG hydrothermal field	140
Table 3.4. Major and trace element concentrations in scales from the Reykjanes wells and chimneys from the TAG hydrothermal field	142
Table 3.5. Representative electron microprobe analyses (wt.%) of metallic minerals in Cu-rich scales from RN-12, 21, and 24	144
Table 4.1. Composition of downhole liquids and surface fluid from Reykjanes, black smoker fluid of 21°N EPR, and seawater	162
Table 5.1. Major and trace element concentrations of the reservoir liquid from wells RN-9, 12, 19, 21, and 24 plus downhole liquid samples from wells RN-12, 19, 19, and 21: seawater near Reykjanes, and standard seawater composition	173
Table 6.1. High-temperature geothermal systems with various range of salinity compared to Reykjanes of seawater salinity	201
Table A2.1. Measured diameter of well RN-9 in 1983 when new, and 10 and 20 years later	242
Table A2.2. Pressure and corresponding temperature for water at saturated vapor pressure	243
Table A2.3 Brief description of sample treatment and analytical methods	254
Table A2.4. Fractionation of samples from high-enthalpy well; field treatment and elements determined	256
Table A2.5. Composition of sphalerites upstream (group 1, 40 bar) and downstream (group 2, 11 bar) of the orifice plate in well RN-09	258
Table A2.6. Bulk chemical compositions of scales from coupons from experiments wells, RN-9, RN-11, RN-10	261
Table A2.7. Pressure range and average pressure measured in scaling tests in 2002 and 2003 in well RN-9, RN-10, and RN-11	268
Table A2.8. XRD results on coupons from wells RN-9, RN-11, RN-10	268
Table A2.9. Normative calculations for well RN-9	275

Table A2.10. Volume of scales ($V (m^3) = \pi * r^2 * h$) formed in the first 8 m in the surface pipeline of RN-9	276
Table A2.11. The amount of each mineral formed in the first 8 m downstream of the orifice plate in RN-9	278
Table A2.12. Volume of scales in a new well RN-9 (1983), 10 years later (1993), and 20 years later (2003)	279
Table A4.1 Major and trace element concentration from selected seafloor black smoker vents	281
Table A5.1. Example of calculated species for discharge liquid RN-9 to reservoir liquid by adding in the vapor	288

List of Figures

Figure 1.1. Map showing Greenland, Scotland, and Iceland and their relation to the Mid-Atlantic Ridge, plus the location of the present Iceland hotspot	4
Figure 1.2. Geology map of Iceland	4
Figure 1.3. Geology map of Reykjanes Peninsula	8
Figure 1.4. Locations of drillholes at Reykjanes, as of June, 2007.....	24
Figure 1.5. Simplified stratigraphy and alteration mineralogy from well RN-9 and RN-12	27
Figure 2.1. Photograph of the pipeline from RN-9, wellhead to the discharge pond (the Gray Lagoon)	32
Figure 2.2. Drawing of the pipeline from the wellhead of RN-9 (362 m long to the separation station)	33
Figure 2.3. Production characteristics of well RN-9, Reykjanes, Iceland	34
Figure 2.4. Boiling-point curve and equivalent pressure curve for seawater	36
Figure 2.5. Photograph of scales in surface pipelines of well RN-9 and the Grey Lagoon	39
Figure 2.6. Representative samples of Group 2 and Group 3 scales from the surface pipeline of well RN-9, downstream of the orifice plate	41
Figure 2.7. Reflected light photomicrographs and electron backscatter (BS) images of scales from well RN-9	47
Figure 2.8. Mole % FeS in sphalerite in scales from downhole RN-22 and in the surface pipeline of RN-9	52
Figure 2.9. Correlation between Fe and Zn concentrations in sphalerite, showing Fe substitution for Zn in the sphalerite structure	55
Figure 2.10. Iron versus Cd in sphalerite in scales from downhole RN-22 and in the surface pipeline of RN-9	55
Figure 2.11. Selenium versus Cd in sphalerite in scales from downhole RN-22 and in the surface pipeline of RN-9	56
Figure 2.12. Al-Mg-Fe ternary diagram showing the compositions of smectites in scales from RN-9 pipeline	61
Figure 2.13. Photographs of the surface pipeline from upstream of the orifice plate	64

Figure 2.14. Photographs of the fluid-flow control valve (FFCV) in the surface pipeline	65
Figure 2.15. Photographs of scales in the pipelines downstream of the orifice plate	66
Figure 2.16. Scales cleaned from well RN14b in 2009	67
Figure 2.17. Backscattered electron image of drill cuttings from RN-22	71
Figure 2.18. Backscattered electron image of scale from 150 m depth in well RN-22 ...	71
Figure 2.19. Backscattered electron images of scales from downhole well RN-22	72
Figure 2.20. Concentrations of Zn, Cu, Fe and S in scales from downhole in RN-22 ...	98
Figure 2.21. Concentrations (ppm) of the major metals in scales versus pressure from all wells at Reykjanes	98
Figure 2.22. Bulk concentrations of major and trace elements in scales downstream of wellhead to the separation station in pipeline of well RN-9	101
Figure 2.23. Solubility of amorphous silica versus temperature, showing SiO ₂ concentrations at inflow temperatures 295° and 290°C and at pressures of 44, 18 and 11 bar	102
Figure 2.24. Multielement plots showing the correlations of Au, Ag, and Se with the major metals Cu, Zn, and Pb in scale from well RN-9	104
Figure 2.25. Plot of Zn versus Se in downhole samples RN-22 and surface pipeline RN-9	105
Figure 2.26. Plot of Se versus Pb concentrations in downhole scale samples from RN-22 and RN-9	105
Figure 2.27. Concentrations of Ag, Au, Pb, Co, and V in scales from downhole in well RN-22	107
Figure 2.28. Plot of Ag versus Pb concentrations in downhole scale samples from RN-22 and surface pipeline RN-9	107
Figure 2.29. Plot of Au/Ag ratio versus pressure in scale samples from RN-9, downhole RN-22, and the high-, medium- and the low-pressure wells	108
Figure 2.30. Plot of Ag versus Se concentrations in downhole scale samples from RN-22 and surface pipeline RN-9	109
Figure 2.31 Plots of iridium versus Au, Ir versus Pd, and Pt versus Pd in scales from ..	110
Figure 2.32. Rare earth element (REE) concentrations in scales from surface pipeline of RN-9 and from experiments in the pipeline of wells RN-11	112
Figure 2.33. Downhole distribution of the major elements in altered host rocks of well RN-9	118
Figure 2.34. Downhole distribution of trace elements in altered host rocks of well RN-9	119
Figure 2.35. Log (XH ₂ /XH ₂ S) versus temperature diagram showing sphalerite compositions in samples from wells RN-22 and RN-9.....	124
Figure 3.1. Location of the Reykjanes geothermal system	134
Figure 3.2. Schematic model of the geothermal wells in the Reykjanes geothermal system	136
Figure 3.3. Photographs of scales from wells RN-12, 21 and 24	138
Figure 3.4. False-color image of the surface of bornite-rich scale in RN-12	143

Figure 3.5. Phase relations in the central portion of the Cu-Fe-S system at 300°C	147
Figure 4.1. Location of the Reykjanes geothermal area on the Reykjanes peninsula, Iceland	159
Figure 4.2. Depth versus pressure profiles for wells RN-12, 19 and 21 during the deep liquid sampling of May, 2007	160
Figure 4.3. Trace-element concentrations in three downhole liquid samples from Reykjanes, and one sample collected from surface, the latter corrected for vapor loss	164
Figure 5.1. A spider diagram with all data normalized to seawater (logarithmic y-axis) for the few available species from the Reykjanes discharge fluid samples	169
Figure 5.2. Calculated steam fraction versus pressure for RN-9 liquid with the initial inflow temperature 295°C	171
Figure 5.3. Concentration of elements in the Reykjanes reservoir from 1983 to 2009, for discharges from wells RN-9, 12, 19, 21 and 24	176
Figure 5.4. Concentrations of Na versus Cl in the geothermal liquids from Reykjanes compared with the surrounding seawater and the groundwater	179
Figure 5.5. Concentrations of Ca versus Cl in the geothermal liquids from Reykjanes compared to local seawater	179
Figure 5.6. Concentrations of K versus Cl in the geothermal liquids from Reykjanes compared with the surrounding seawater	179
Figure 5.7. Log Q/K for minerals vs. temperature for liquid from well RN-19	185
Figure 5.8. pH change during boiling of reconstructed liquid RN-9	187
Figure 5.9. Boiling of the RN-19 reservoir liquid, reconstructed and with metal concentrations from the downhole sample from RN-19 (results from a CHILLER).....	187
Figure 5.10. Stability diagram of sulfide minerals in terms of log fO_2 versus log $(a^{2Cu^+}/a^{Fe^{2+}})$	192
Figure A2.1. Well RN-9, 28 September 1993 profile of scales, from surface to 600 m depth.....	244
Figure A2.2. Well logging of RN-9	245
Figure A2.3. Schematic model of geothermal wells in the Reykjanes geothermal system	248
Figure A2.4. Drawing of installed equipment in a typical geothermal well	257
Figure A2.5. Treatment of samples from two-phase geothermal wells	257
Figure A2.6. Photo and schematic of the equipment used in the scaling test experiments in 2002 and 2003, including the movable horizontal steam/water separator used for well output measurements	266
Figure A2.7. A) Results of pressure measurements in RN-9 at station 0.0 and in branch one at stations 1.1 to 1.6 as a function of time. (B) Pressure at branches two, three and four as a function of time	267

Figure A2.8. Electron backscatter image of scales precipitated in a scaling test in July 2002, in well RN-9	269
Figure A2.9. A) Results of pressure measurements in RN-11 at station 0.0 and branch one at stations 1.1 to 1.6. as a function of time. (B) Pressure at branches two, three and four as a function of time	271
Fig. A2.10. A) Results of pressure measurements in RN-10 at station 0.0 and branch one at stations 1.1 to 1.6 as a function of time. B) Pressure at branch two as a function of time	273
Figure A2.11. Electron backscatter image of scales formed during a test of scaling rate, October 2003, well RN-10	274
Figure A2.12. Schematic drawing of scaling in well RN-9	277
Figure A2.13. Drawing of a cut-off cone used to calculate the amount of precipitation in the RN-9 well	279

Acknowledgements

I am very lucky for having had the opportunity to go back to school. Having the opportunity to start a new life, meet new people who become your friends for life is priceless. I am also very fortunate for the opportunity to have my youngest daughter Steinunn with me in Canada. Having her with me, becoming my friend, is a something mother dreams of. Thank you, dear Steinunn for everything. To all you people who provided, supported, and encouraged in numerous ways throughout the work of my Ph.D., I am very grateful.

I would especially like to thank my company, Iceland GeoSurvey (ISOR), and its director Ólafur G. Flóvenz for all the support through this time; ISOR supported me for 5 months in the beginning, including supporting me with computers, access to all their staff whenever I needed the help and an office whenever I was in Iceland.

I would also like to thank Hitaveita Sudurnesja now HS Orka hf; Júlíus J. Jónsson and Albert Albertsson for their grant support for 3.5 years and paying for most of the bulk chemical analysis. This is very much appreciated.

My special thanks go to my supervisors, Jeff Hedenquist and Mark Hannington, for their endless patience, encouragement and help on my journey of maturity. It is not easy to guide a student of the same age or older than you are, especially a student with temper, but both of you did a fantastic job. Thank you both. This PhD project was funded by research grants from a the Natural Sciences and Engineering Research Council (NSERC) of Canada grant to JH (part time 2005, 2006, 2007, full time 2008 to 2009, to go to Salt Lake City, fall 2005, to DOE meeting in Arizona Oct 2006, to Iceland April/May and August 2007, to Denver Oct 2007, to Eugene Oregon April 2008, to Iceland IAVCEI August 2008) and

NSERC grant (MH) to make the thin sections, XRD analysis, bulk chemical analysis, and the microprobe analysis. The PGE analyses were paid by Dr. Ames. I would like to acknowledge the scholarships and travel grants from University of Ottawa (Salt Lake City, Tucson Arizona), a SEG grant 2007 (Hugh E. McKinstry Student Research Awards), and Alice E. Wilson Scholarship 2009.

I would like to name a few people who helped me to make this PhD dream become true and were always ready to help whenever I needed them: Hrefna Kristmannsdóttir, Sverrir Thórhallsson, Thráinn Fridriksson, and Gestur Gíslason. I would not have made this without you. Thank you. Gestur, my love, also helped with many of the photos, diagrams and set up the PhD document. Special thanks are to Dr. Kevin Brown, New Zealand for giving me his time when collecting the deep liquid and to Dr. Mark H. Reed, Eugene Oregon who guided me for a month on the CHILLIER computer program. Haukur Jóhannesson, Halldór Ármannsson, Jón Örn, Karl Grönvold, Niels Óskarsson, and Geir Thórólfsson, were always willing to help. My very good friends André and Lesia, Tony and Terry, Karin Hoal; I would like to thank you for your encouragement, friendship and helping me see the bright side all the time.

Special thanks to Brynja Jónsdóttir, Steinunn Hauksdóttir, Guðrún Sigríður Jónsdóttir, Sigríður Anna Thórarinsdóttir, Ragna Karlsdóttir, Ingibjörg Ásta Gunnarsdóttir, Ingibjörg Kaldal, Ástríður Hardardóttir, Júlíana Signý Gunnarsdóttir, Kristján Hrafn Sigurdsson, Kjartan Reynir Hauksson, Sigvaldi Thordarson, Sigurdur Sveinn Jónsson (who did many of the XRD analysis), Gunnlaugur M. Einarsson, Magnús Ólafsson, Hjalti Franzson, Kristján Saemundsson, Páll Ingólfsson, Guðmundur Steingrímsson, Benedikt Steingrímsson, Bjarni Kristinsson, Peter Eric Danielsen, Páll Jónsson, Guðni Axelsson, Ásgrímur Guðmundsson, Sigrún Gunnarsdóttir, Guðlaugur Hermannsson, Anette Mortensen, and Dadi Thorbjörnsson,

all at ÍSOR, Hilmar Sigvaldason OS and Rósa Jónsdóttir for her excellent service attitude at the library at Orkugardur, Gudmundur Ómar Fridleifsson and Ómar Sigurdsson HS Orka hf, Sigurdur Steinthórsson and Bryndís Brandsdóttir at the University of Iceland, Grétar Ívarsson at Orkuveitan, and Jón Matthiasson at former Idntaeknistofnun did most of the SEM work.

The thin sections were made by George Mrazek and thank you for all the talks George. Ingrid Kjarsgaard did most of the microprobe work, read over early manuscripts and thank you for your friendship and encouragement. Sandra Sheperd and Helene J. De Gouffe, thank you for being there and your endless help and support, encouragements and for being great friends all the time. Stephanie Doume, Bernie and Richard, Patricia, Keiko, Bahram and other staff of the geology department at University of Ottawa, thank you for your support. Jim Palandri, Eugene Oregon helped me with the computer programs. My student friends thank you all; Mike, Anastasia, Jamil, Lillian, Juraj and Katarina, Francoise, Nick, Michelle, Stephanie, Ryan, John, Raina. Thank you my very good friends, Monique, Joseph and Marie Clair. My friends in Iceland, Arna, Valgerdur, Áslaug Alfreds, Kristín and Valli, Gudrún and Laufey and my support group at Lindarbraut 23, Lóa and Elísabet, thanks. Thank you for your support class 6U MR 1976. My thanks go also to Lilja and Jón, Björn and Nanna for being very supportive and helping me with my daughters while I did my studies.

Steinunn, ambassador Markús Örn Antonsson, ambassador Sigridur Anna Thórdardóttir, Jón, Ólöf, all at the Icelandic Embassy in Ottawa, thank you for your friendship and support. My group of friends of the Icelandic community in Ottawa including Jack, Pauline, Völundur, Daeja, Unnur, Obba, Bjarki and Kim special thanks to all of you and specially for

opening your arms for my daughter Steinunn. Aranka my very dear friend who opened her house for me and my family and always welcomed me when I came back and hugged when I needed one. Hugs and kisses.

Finally I would like to thank my parents, Hördur and Gudrún and close family; Helga, Lárus, Gudmundur, Rut, my daughters Elísabet and Sigrún and Bjarni for being so supportive and giving me the basic values to be able to function and achieve my goals here in Canada.

CHAPTER 1

Iceland Geology, Geothermal Activity, and the Reykjanes

High-temperature Geothermal System

1.1 Introduction and Objectives

The main purpose of this study was to understand the reasons for deposition of mineral scale in wells and pipes of the Reykjanes high-temperature geothermal system, southwest Iceland. An important goal was to determine ways to mitigate the scaling, which is costly to deal with during operation for electricity generation. Scales that formed in the surface pipelines of well RN-9, and were collected during cleaning in the summer of 2000, were studied first. A number of initial questions were addressed. Where do the scales precipitate and what are the characteristics of the scales? How do the location and depositional conditions affect the mineralogy and composition of the scales? The study then extended to 12 other wells, to determine the difference in scale composition across the system as well as the metal concentration in the downhole liquids of three wells, prior to boiling. Finally, the study compared the high-temperature downhole liquid with black smoker fluids that discharge elsewhere along the Mid-Atlantic Ridge. An important question to address was why the fluids and scales at Reykjanes differ from black smokers, given the similar basaltic host rocks and dominantly seawater composition.

These questions are the main focus of the thesis, discussed in Chapters 2 to 5. The scales are described in Chapters 2 and 3, including their chemical, mineralogical, and physical characterization. The metal compositions of downhole liquids are presented in Chapter 4, and these are compared in Chapter 5 to chemical analyses of the geothermal fluids as sampled at the surface in terms of mineral-fluid equilibria and the effects of boiling.

The first part of the thesis (Chapter 2) focuses on scales from well RN-9 in its surface pipeline, as well as scales from surface pipelines from other wells and scale from downhole in well RN-22. The second part of the thesis (Chapter 3) focuses on scales at the point of

sharp pressure decrease from wells RN-12, RN-21, and RN-24, which have very different compositions compared to those formed in well RN-9 and are unique in their high precious metal contents and mineralogy. Chapters 3 and 4 (deep liquid composition) have been published. Chapter 6 provides a summary, and comparison with scales in other geothermal systems.

This introductory chapter reviews the low- and high-temperature geothermal systems in Iceland and their characteristics, with an emphasis on the geology and alteration of the Reykjanes geothermal system. Examples with different liquid compositions (e.g., Krafla, north Iceland) are presented for comparison with Reykjanes.

Early work in the Reykjanes geothermal area was focused on surface geothermal manifestations, including steam vents, mud pools and sulfur deposits (Thorkelsson, 1928). The Reykjanes geothermal area has since been in utilization for close to 40 years, for salt production, fish drying, and minor electricity production. From May, 2006, electricity generation capacity has grown to 100 MWe (Megawatt electric), and current plans are to expand the electrical power generation with an additional 30 to 50 MWe low-pressure turbine unit (Sigurdsson, 2010).

1.2 Volcanic setting of Iceland

Iceland, 103,000 km² in area, is the largest subaerial portion of a mid-oceanic ridge system worldwide. The country is located on the Mid-Atlantic Ridge between 63°20' N, 18°44' W and 66°11'N 18°50'W, on the boundary between the North America and Eurasia plates (Figs. 1. 1 and 1. 2). Iceland is part of a much larger volcanic province that extends from Greenland to Scotland, related to a deep mantle plume or a hotspot (Wilson, 1963; Schilling, 1973; Pálmasson and Saemundsson, 1974; Schilling et al., 1982; Óskarsson, et al., 1985; Einarsson, 1991, 2001, 2008; Bjarnason, 2008).

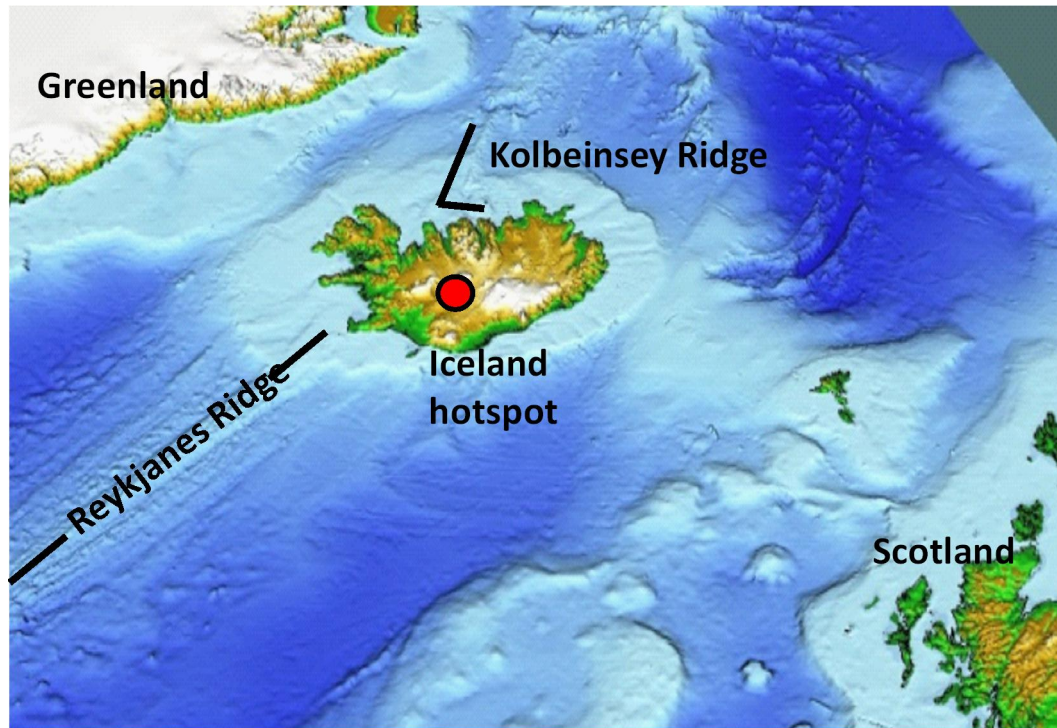


Figure 1. 1. Map showing Greenland, Scotland, and Iceland and their relation to the Mid-Atlantic Ridge, plus the location of the present Iceland hotspot (Bjarnason, 2008).

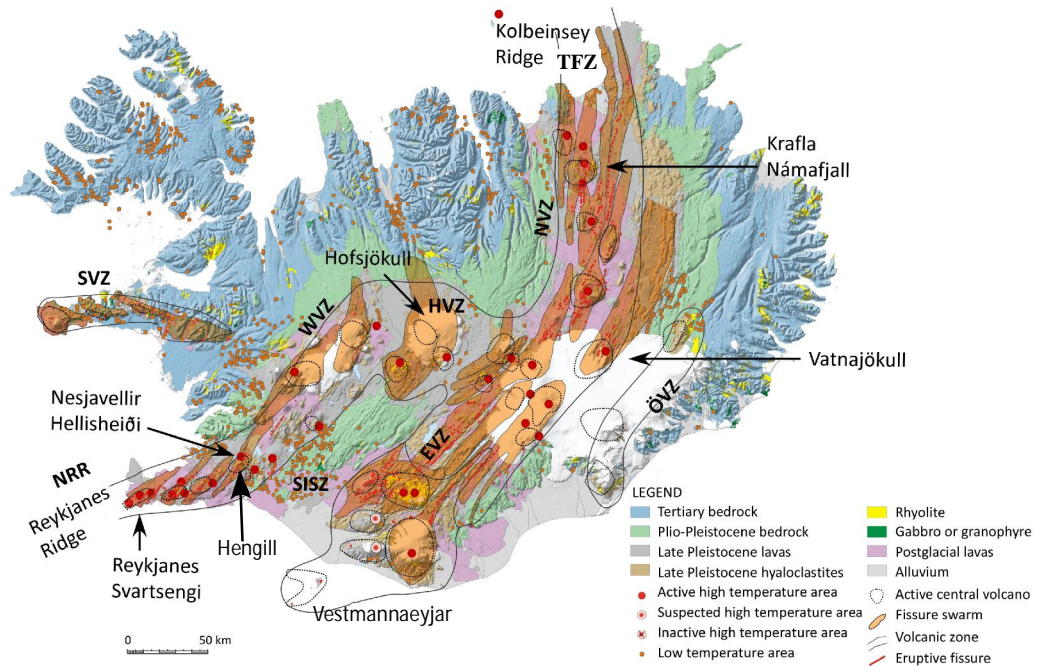


Figure 1. 2. Geology map of Iceland (Saemundsson and Jóhannesson, 2004) with names of the volcanic zones from Jakobsson et al. (2008). NRR = Northern Reykjanes Ridge; WVZ = Western Volcanic Zone; SISZ = South Iceland Seismic Zone; HVZ = Hofsjökull Volcanic Zone; NVZ = Northern Volcanic Zone; TFZ = Tjörnes Fracture Zone; ÖVZ = Öræfajökull Volcanic Zone; EVZ = Eastern Volcanic Zone; SVZ = Snæfellsnes Volcanic Zone.

1.2.1 Plate tectonics

The construction of Iceland began with the opening of the North Atlantic Ocean ~60 million years (m.y.) ago (Jolley and Bell, 2002). Due to the complex interaction of the Mid-Atlantic Ridge with the Iceland mantle plume, an area of mantle upwelling, Iceland has an average elevation of ~600 m above sea level, whereas the rest of the ridge is entirely submarine. The plate boundary has been moving westward relative to the mantle plume, with the center of the low-velocity anomaly located between Hofsjökull and Vatnajökull (Fig. 1.2). The crust tends to break up above the mantle plume, explaining why the main volcanic belts in Iceland are shifted eastward relative to the crest of the Mid-Atlantic Ridge (Óskarsson et al. 1985; Bjarnason, 2008). Traces of the hotspot are preserved at the aseismic Greenland-Iceland ridge on the North American plate and the aseismic Faeroe-Iceland ridge on the Eurasian plate (Bjarnason, 2008). Magnetic anomalies south of Iceland originally suggested in the 1960s indicate present-day spreading is ~1 cm/year in each direction, (Vine and Matthews, 1963; Vine 1966; Einarsson, 2008).

1.2.2 Crustal thickness

An understanding of the upper crustal structure was gained in the 1960s and 1970s, based on seismic refraction, wide-angle reflection experiments and surface wave dispersion analysis, including pioneering work of Båth (1960) and Tryggvason (1962), followed by Pálmason (1970, 1971). The modern image of the Iceland crust and the uppermost mantle is based on work by many authors (e.g., Tryggvason, 1962, Tryggvason et al., 1983; Pálmason and Saemundsson, 1974; Saemundsson, 1979; Angenheister et al., 1980; Eysteinnsson and Hermance, 1985; Menke et al., 1996; Brandsdóttir and Menke 2008). More recent studies indicate a cool (subsolidus) crust, ~11 to 14 km thick along the northernmost Reykjanes Ridge (Weir et al., 2001) to ~20 km thick beneath the Hengill central volcano (shown in

Fig. 1.2) (Bjarnason et al., 1993; Bjarnason, 2008), and close to ~40 km thick at the center of Iceland (Darbyshire et al. 1998, 2000).

1.2.3 The volcanic zones

The Mid-Atlantic Ridge surfaces on the Reykjanes Peninsula where it becomes a complex series of rift and transform zones as it crosses Iceland; it continues north of the island as the Kolbeinsey Ridge (Fig. 1.2; Jakobsson, 1972; Pálmason and Saemundsson, 1974; Saemundsson, 1979; Jakobsson et al., 2008). Three major rifts are active across Iceland; the Western Volcanic Zone extends from the Reykjanes Ridge and joins the Eastern Volcanic Zone and the Northern Volcanic Zone at Hofsjökull in the center of the island. The Eastern Volcanic Zone, today the most volcanically active zone in Iceland, extends from the south and meets the Northern Zone at Vatnajökull, which joins the Kolbeinsey Ridge in the Tjörnes Fracture Zone in the north (Jakobsson, 1972; Fig. 1.2). The transform zones, the South Iceland Seismic Zone (SISZ) and the Tjörnes Fracture Zone (TFZ) north of Iceland, connect the volcanic zones to the northern part of Reykjanes Ridge and the Kolbeinsey Ridge, respectively. The southern part of the East Volcanic Zone and the Öräfajökull Volcanic Zone are known as flank zones, with limited rifting activity (Jakobsson, 1972; Saemundsson, 1979). The Snaefellsnes Volcanic Zone (SVZ) is also a flank zone, but the older bedrocks of Snaefellsnes were formed in a now-extinct rift zone.

The activity of the Western Volcanic Zone (WVZ) and the Northern Volcanic Zone (NVZ) started ~6 to 7 m.y. ago, whereas activity in the Eastern Volcanic zone started ~2 to 3 m.y. ago (Saemundsson, 1979).

The volcanic pile in Iceland consists predominantly of basaltic rocks (80 to 85 volume %) with intermediate rocks and rhyolite constituting ~10% and sedimentary rocks

of volcanic origin ~5 to 10% (Saemundsson, 1979). The rhyolites are mainly associated with the central volcanoes (see below). Comprehensive studies of the postglacial volcanic products by Jakobsson (1972), Jakobsson and Shido (1978), and Jakobsson et al. (2008) show that the volcanic systems are strongly clustered (Fig. 1.2).

1.2.4 The volcanic systems

A volcanic system in Iceland is a spatial grouping of eruptions sites, with or without shallow magma chambers and with a swarm of volcanic and tectonic fissures. Each system has a typical lifetime of 0.5 (Saemundsson, 1979) to 2 m.y. (Jóhannesson, 1975; Franzson, 1978). They comprise one or even two central volcanoes with associated intermediate and silicic rocks that have distinct petrographic and geochemical characteristics (Walker, 1974; Saemundsson and Noll, 1974; Saemundsson, 1979; Jakobsson, 1979, 1980; Jakobsson et al., 1978). Almost every volcanic system hosts either an active or extinct high-temperature geothermal system, where temperatures exceeded $>200^{\circ}\text{C}$ in the uppermost 1000 m (Bödvarsson, 1961; Fridleifsson, 1979; Arnórsson, 1995a).

According to Jakobsson et al. (2008) there are 33 postglacial volcanic systems in Iceland (Fig. 1.2). These systems have been classified chemically into three main groups (Jakobsson 1972): alkali olivine basalt (alkali olivine basalt, hawaiite, mugearite, benmoreite, trachyte, alkaline rhyolite), transitional alkali basalt (ankaramite, transitional basalt, basaltic andesite, andesite, trachyte, comenditic rhyolite) and tholeiite (oceanite/picrite, olivine tholeiite, tholeiite, basaltic icelandite, icelandite, dacite, rhyolite). The alkalic systems are located on the Snaefellsnes Peninsula (SVZ, Fig. 1.2) and in Vestmanneyjar to the south. The Eastern Volcanic Zone is transitional alkalic in composition (EVZ, Fig. 1.2). The Northern Reykjanes Ridge (NRR, Fig. 1.2), the Western Volcanic Zone (WVZ) and the Northern Volcanic Zone (NVZ; Fig. 1.2) are all tholeiitic in composition.

The volcanic systems of the Reykjanes Peninsula are, from west to east, Reykjanes, Svartsengi, Krýsuvík, and Brennisteinsfjöll, and Hengill (Fig. 1.3). They lack central volcanos or intermediate to silicic rocks. The exception is the Hengill volcanic system, the easternmost, which is the only system that contains silicic rocks on the peninsula (Saemundsson, 1967; Hardardóttir, 1983).

1.2.5 The volcanic history

The volcanic rocks of Iceland range in age from present to ~16 Ma. Extensive work by Walker (1959, 1960, 1963), Saemundsson (1974, 1978, 1979, 1986) and Jóhannesson (Jóhannesson and Saemundsson, 2009) has led to a classification of the volcanic pile into four stratigraphic groups or series: Tertiary (older than 3.3 Ma), Plio-Pleistocene (0.8 to

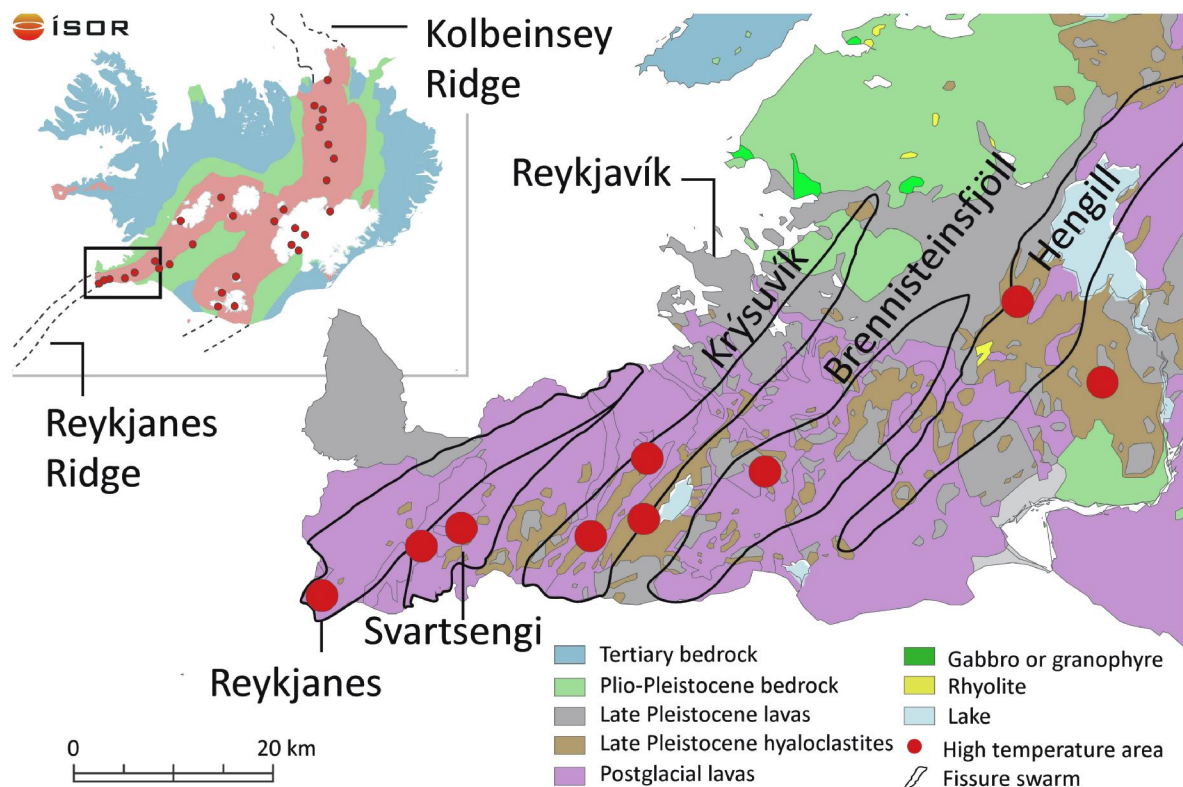


Figure 1.3. Geology map of Reykjanes Peninsula. Iceland in the inset with the location of the Reykjanes Peninsula, outlined. The high-temperature areas, from west to east, are Reykjanes, Svartsengi, Krýsuvík, Brennisteinsfjöll, and Hengill (including the associated geothermal systems of Hellisheidi and Nesjavellir) (from Saemundsson et al., 2010).

3.3 Ma), Upper Pleistocene (0.01 to 0.8 Ma), and post glacial (the past 10,000 to 13,000 y). The oldest rocks are found in the west, north and east, and become younger towards the center of the island; the youngest rocks occur in the active volcanic zone (Fig. 1.2).

The Tertiary sequences cover ~50,000 km² or close to half of the total area of Iceland and consist primarily of subaerial tholeiitic lavas with minor intermediate rocks and rhyolites. The characteristics of the stratigraphy are generally very regular, with 5 to 15 m thick flows separated by thin layers of red or red-brown clayey or tuffaceous material (Walker, 1959, 1963). This volcanic pile is rather flat and forms 800 to 900 m high lava plains which are broken up by at least 15 central volcanoes. However, based on the occurrence of differentiated rocks, an additional 40 central volcanoes are suspected to occur in the pile (Saemundsson, 1979). The fjörd landscape in the Tertiary region was formed by glacial erosion during the Plio-Pleistocene.

The Plio-Pleistocene rocks cover ~25,000 km² and are mainly located between the Tertiary rocks in the northwest, north, and east and the rocks formed in the active rifting zone in the center of the country (Fig. 1.2). The rocks from the Plio-Pleistocene time are very different in morphology compared to the Tertiary rocks. Unlike the high flat mountains with the red-brown interlayers, the Plio-Pleistocene rocks are characterized by brownish elongated ridges or conical hills of hyaloclastite and pillowed flows together with fluvio-glacial and moraine deposits. These structures were formed in periods of glaciations broken up by glacier-free warmer periods (Saemundsson, 1979). Subglacial eruptions of basalt formed pillow lava, hyaloclastite, irregular intrusions and cap lava flows. The term “tuya” (table mountain) refers to sequences that contain all these units, formed partly beneath a glacier, with the upper part extending above the ice cap, whereas “tindar” lack the cap lava flow (Jakobsson and Gudmundsson, 2008).

The Upper Pleistocene formations cover ~30,000 km² near the active volcanic zone. Hyaloclastite deposits are more extensive and glacial erosion features less common than in the Plio-Pleistocene record (Saemundsson, 1979). The volcanic rocks from the Upper Pleistocene are characterized by two types of formations based on morphology and structure. Subaerial lava flows erupted during interglacial periods, consisting of grey basalt or dolerite; pillow lavas and hyaloclastite, referred to as the palagonite formation, formed beneath glaciers (Saemundsson, 1979); tuyas are the most characteristic features from this time. Many of the currently active volcanic systems formed during this period. The Upper Pleistocene rocks together with the Post-glacial rocks comprise the Neovolcanic zone of Iceland (Saemundsson, 1979).

The post-glacial series span a time from 10,000 to 13,000 years b.p. on the Reykjanes Peninsula; in the highlands southwest of Vatnajökull, which is the largest glacier in Europe, these volcanic rocks have formed since about 9,000 years ago (Saemundsson, 1979; Jóhannesson and Saemundsson, 2009). The characteristic units of this time period include fresh lava flows, pyroclastic rocks, unconsolidated marine clays, fluvio-glacial and fluvial outwash, and soil formed after the deglaciation of the island (Saemundsson, 1979; Jóhannesson and Saemundsson, 2009). The compositions of the post-glacial volcanic rocks are essentially the same as during the last glacial and interglacial periods, with ~90 volume % basaltic rocks and 10% intermediate and rhyolitic rocks. The most characteristic features formed at this time are the shield volcanoes of olivine tholeiite composition.

1.3 Geothermal Systems in Iceland

In Icelandic geothermal systems the water is largely of meteoric or seawater origin, or a mixture of both. Magmatic volatiles have also been identified in some geothermal systems

(Arnórsson, 1995a). The lifetime of individual geothermal systems is variable depending on the heat source, and has been estimated in the Tertiary strata to be in the range of 200,000 to 300,000 years (H. Jóhannesson, pers. commun. 2010).

1.3.1 Classification and characteristics

In Iceland, geothermal systems are classified according to geological setting and drillhole data (mainly pressure/temperature measurements and drillhole cuttings) (Bödvarsson, 1961; Fridleifsson, 1979). A high-temperature geothermal system in Iceland is defined as one in which the temperature is above $\sim 200^{\circ}\text{C}$ in the uppermost 1000 m, whereas a low-temperature geothermal system is below $\sim 150^{\circ}\text{C}$ in the upper 1000 m. The

Table 1.1. Comparison of the composition of downhole liquid⁽¹⁾ in the high-temperature areas of Krafla, Námafjall, Nesjavellir, Hellisheidi, Svartsengi and Reykjanes.

	Krafla ⁽²⁾	Námafjall ⁽²⁾	Nesjavellir ⁽³⁾	Hellisheidi ⁽³⁾	Svartsengi ⁽⁴⁾	Reykjanes ⁽⁴⁾
Well No	58024	58313	95014	95135	16908	18909
Well	K-24	B13	NG-06	HE-35	SV-08	RN-09
Sample No	19881009	20070310	19880212	5095	20070104	20030169
Na/K T ($^{\circ}\text{C}$)	210	306	297	248	239	290*
T ($^{\circ}\text{C}$) max/ depth (m)	305 $^{\circ}$ /1384	334 $^{\circ}$ /2129	290 $^{\circ}$ /1000	308 $^{\circ}$ /2418	243 $^{\circ}$ /1559	295 $^{\circ}$ /1402
pH _{Na/K}	8.02	7.87	7.20	7.70	5.10	5.00**
Cl (ppm)	25	41.62	56	307	12524	17696
Na (ppm)	192	67.51	74	252	6327	8977
K (ppm)	17	17.8	18	38	934	1292
Ca (ppm)	3.3	0.15	1.2	2.3	1038	1429
SiO ₂ (ppm)	363	586.07	520	454	438	594
Mg (ppm)	0.001	0.002	0.016	0.06	0.539	0.806
Al (ppm)	-	2.11	-	1.31	0.0897	0.0601
Fe (ppm)	0.09	0.005	-	0.179	0.0069	0.3877
B (ppm)	-	1.38	-	0.759	7.1	7.5179
CO ₂ (ppm)	39	119	32	89	379	1067
H ₂ S (ppm)	33	251	458	94	5.7	27.1
NH ₃ (ppm)	-	-	-	-	-	-
H ₂ (ppm)	-	9.56	20	0.04	0.05	-
CH ₄ (ppm)	-	0.19	0.36	0.05	0.04	-
N ₂ (ppm)	0.02	8.47	5.08	4.5	6.63	-
TDS (ppm)	952	855	838	-	23204	-

⁽¹⁾ Based on surface samples which have been corrected for vapor loss to reservoir temperature (Henley et al., 1984); ⁽²⁾ With permission from Landsvirkjun; ⁽³⁾ with permission from Reykjavík Energy; ⁽⁴⁾ with permission from HS ORKA HF and ISOR; - not measured; * reservoir $^{\circ}\text{C}$; ** at 290°C ; TDS, total dissolved solids; ppm, mg/kg

geothermal waters, both high- and low-temperature, are generally weakly alkaline to neutral pH at surface. Under high-temperature reservoir conditions most of the high-temperature systems have a near neutral pH, whereas the seawater systems (Reykjanes and Svartsengi) are slightly acidic at high temperature (Table 1.1).

The low-temperature systems are widely distributed in Quaternary and Tertiary formations, mostly west and north of the active volcanic zones, with only a few areas east of the main rift zones (NVZ and EVZ, Figure 1.2; Arnórsson, 1995b; Jóhannesson and Saemundsson, 2009). The low-temperature areas are geographically not well defined and may have only one thermal spring at the surface, although clusters of springs are common. Permeability is fracture dominated, with springs associated with active fractures and faults. However, low-temperature geothermal systems have been discovered in Tertiary formations in many places where there are no surface manifestations (Axelsson et al., 2005). Surface conditions in the low-temperature areas are very grassy and cultivable due to the low-temperature alkaline water reaching the surface, quite different from the barren high-temperature areas.

The heat source for the low-temperature systems is a high thermal gradient in the host rock. In many cases they are related to faults and dykes which represent permeability anomalies along which the geothermal water ascends (Saemundsson and Fridleifsson, 1980; Björnsson et al., 1990). The low-temperature waters are dilute, with total dissolved solids of 200 to 400 mg/kg (Kristmannsdóttir, 1989).

Due to the low total dissolved solids, low-temperature liquids are commonly utilized directly for heating. The most common scale formed within low-temperature wells is calcite. Other scales have also been identified such as magnesium silicates, zinc silicates,

pyrrhotite and hematite, but these are generally only a minor problem (Kristmannsdóttir, 1989; Kristmannsdóttir et al., 1999).

The high-temperature systems in Iceland are located within or at the margin of the active volcanic zone, in rocks that are geologically young, and most of them are associated with active central volcanoes (Pálmason and Saemundsson, 1974). To date 30 high-temperature areas have been identified, mainly within the Western Volcanic Zone and the Northern Volcanic Zone (Jóhannesson and Saemundsson, 2009). The energy stored in high-temperature areas above 3 km depth is estimated to be $\sim 10^{23}$ J ($1 \text{ J} = [\text{kgm}^2]/\text{s}^2 = 1 \text{ Ws}$; Watt second; Pálmason, 1981; Arnórsson et al., 2008). High permeability is common in high-temperature systems due to the young age of the rocks, which have not yet been altered extensively. The high rate of thermal flow is due to the presence of hot intrusive bodies at relatively shallow depth in the crust that provide the heat for the high-temperature systems (Pálmason, 1981). Due to locations commonly in areas of high relief, the groundwater table is relatively depressed and consequently vapor vents can be the strongest surface manifestations. The vapor contains H_2S which oxidizes to elemental sulfur and which precipitates around the vents or forms sulfuric acid which results in a low pH (as low as 2) in the vapor condensate (Arnórsson, 1995a; Arnórsson, et al., 2008). The hot, acidic condensate reacts with the surrounding rocks, resulting in an intense alteration due to the glassy nature of the basalt and instability of igneous minerals (Arnórsson, 1995a). Elements such as Na, K, Ca and Mg are leached from the rock, and residual elements (including Si, Al and Ti) increase in relative concentration in the alteration products. These include kaolinite, anatase (titanium dioxide), amorphous silica (defined as showing no peaks when run in XRD), sulfate minerals, sulfur and pyrite (Sigvaldason, 1959; Arnórsson, 1995a).

Mudpools formed by acidic vapor-heated condensates are common in the high-temperature areas.

At present six high-temperature systems have been developed for their electrical energy; Krafla and Námafjall, in the Northern Volcanic Zone and Nesjavellir, Hellisheidi, Svartsengi and Reykjanes in the Western Volcanic Zone (Fig. 1.2). Due to the high total dissolved solids in the high-temperature geothermal water (note TDS in Table 1.1) it cannot be used directly for district heating.

Krafla and Námafjall

Both the Krafla and Námafjall geothermal systems in the Northern Volcanic Zone have well-defined upflows within the same fissure swarm; the swarm is ~100 km long and 5-10 km wide, and formed ~100,000 to 300,000 years ago (Saemundsson, 1974, 1978, 1983, 1991). The Krafla caldera is 8 by 10 km in size and formed ~110,000 y ago. The stratigraphy consists of basaltic lava flows, hyaloclastite and rhyolite. Surface studies, resistivity measurements, and drilling at Krafla indicate the geothermal system to be 40 km² in area (Mortensen et al., 2009a, b). In December, 1975, a major rifting episode started at Leirhnjúkur in the Krafla fissure swarm. Nine basaltic eruptions in 21 magmatic events took place in this rifting episode, which ended in September, 1984 (Björnsson et al., 1977, 1979). Seismic attenuation studies revealed a magma chamber at 3-7 km depth, partly underlying the currently drilled field (Einarsson, 1978).

Forty four wells have been drilled in the Krafla geothermal field since 1974; the deepest well is 2894 m deep and the highest temperature measured was 386°C at 2822 m depth. Three subfields have been drilled within the Krafla area, showing a complicated system of upflow, including (i) a relatively cool upper zone at Leirbotnar (190 to 220°C to ~1000 m depth) and hot lower zone (300 to 350°C from ~1200 m depth); (ii) an upper boiling zone at

Hvíthólar (~250°C at 700 m depth) with a cooler intermediate level (180°C at 1200 m gradually increasing to 240 to 250°C at 1800 m depth), and (iii) a system that is boiling at all depths at Suðurhlídar (Arnórsson, 1978a; Arnórsson et al., 1978; Kristmannsdóttir and Svantesson, 1978; Ármannsson, 1989). The upper zone in the Leirbotnar field and the lower zone of Hvíthólar are liquid dominated, whereas the rest of the system is vapor dominated (Ármannsson et al., 1989). The current power production at the Krafla geothermal power plant is 60 MW; it started at 7 MW in 1978 and rose to 30 MW from 1983 to 1998.

One of the wells in the Krafla geothermal system was drilled as part of the Iceland Deep Drilling Project (IDDP), where the objective was to drill to 4.5 km depth to sample supercritical fluid at temperature and pressure in excess 374°C and ~221 bar. This drilling started in June 2008 but ended in July 2009 at ~2100 m depth after drilling into rhyolitic magma. The highest recorded temperature in that well was measured at 346°C (<http://beta.isor.is/efni/djupborun-iddp>).

Results from stable isotope studies by Darling and Ármannsson (1989) indicate that the liquids from the Krafla system are dominantly locally derived meteoric water. However the chemical compositions of the Krafla liquids are quite variable depending on location and the depth of the well (Table 1.1, only one set of data shown). Changes in liquid composition have occurred due to utilization as well as injection of magmatic gases during the volcanic episode (Ármannsson et al., 1982, 1989; Gudmundsson and Arnórsson, 2002; Mortensen et al., 2009b; Gudmundsson et al., 2010; Christenson et al., 2010). Discharge liquids have low dissolved solids (~1000 to 1500 ppm total) with SiO₂ the most abundant dissolved solid in the range of 500 to 700 ppm. Cl is 20-30 ppm and Na 150 ppm (Arnórsson et al., 1978). The gas content in vapor varies from 2000 ppm to 40,000 ppm. CO₂ is the most abundant gas component, up to 90%; however, drilling in the last few years indicates that

gases of possible magmatic origin (i.e., SO_2 , He, H_2) are much more abundant than previously thought (Christenson et al., 2010). Where the magmatic gasses have modified the chemical characteristics of the reservoir fluids, very low pH values have been observed due to the high HCl concentration in the fluid. Other parts of the system have pH values that are neutral to slightly alkaline (Gíslason and Arnórsson, 1976; Arnórsson et al. 1978).

In the Krafla geothermal system, downhole scaling has been and still is a problem in a few wells. In the early days of utilization calcite was a problematic scale in some of the cooler wells and amorphous silica in the surface pipelines (Ármannsson, 1989). Calcite precipitated due to boiling in the liquid-dominated fields, mainly in the upper zone of Leirbotnar, where the temperature is 190° to 200°C . Precipitation of silica (amorphous silica, cristobalite), iron silicate (amorphous), iron sulfides (pyrite, FeS_2 ; pyrrhotite, FeS), iron oxide (magnetite; Fe_3O_4), and calcium sulfate (anhydrite) also occurred in some wells that tap liquids from both the upper and lower zones (Kristmannsdóttir and Svantesson, 1978; Arnórsson, 1978a; Arnórsson et al., 1978, Ármannsson, 1989). The sulfates and iron oxides precipitated in wells where magmatic gases were detected (Ármannsson et al., 1982). In recent years, corrosion of the steel liner has been observed in some wells (due to the magmatic gas component) as well as precipitation of minerals such as magnetite (Mortensen et al., 2008, 2009a, b).

The Námafjall geothermal system occurs on a hyaloclastite ridge, 2.5 km long and 0.5 km wide, located ~10 km south of Leirhnjúkur which is in the center of the Krafla caldera. The Námafjall geothermal system is estimated to be 3-4 km^2 in size at surface (Saemundsson, 1991). Exploration drilling started in 1963, with 15 wells located in the Bjarnarflag field in the western part of the Námafjall area; the deepest well is close to

2700 m and has the highest measured temperature of 334°C (ÍSOR database). The areal extent of the resistivity anomaly is about 20 km² at ~1000 m depth (Gudmundsson et al., 2010). Electricity production started in 1969 (3 MW), and a district heating plant was constructed in 1971 (Thórhallsson et al., 1975). Most of the wells were lost during the 1975-1984 rifting episode and a small eruption even took place through one of the wells in 1977.

The chemical composition of the Námafjall reservoir liquid is similar in all the wells (Table 1.1; Ármannsson, 1993; Gudmundsson and Arnórsson, 2002; Gudmundsson et al., 2010; Christenson et al., 2010). Discharge liquids corrected to reservoir concentrations are generally low in total dissolved solids (~1000 ppm). Silica is the most abundant dissolved solid, ranging from 400 to 650 ppm; Cl is 20-30 ppm and Na is 150 ppm (Arnórsson et al., 1978). The gas content in vapor ranges from 1000 to 7000 ppm, with CO₂ up to 50 volume %, with the sum of H₂S and H₂ typically being similar to the CO₂ concentration. The stable isotope composition of the total discharge indicates that the origin of the reservoir fluid is precipitation from higher elevation, probably in the vicinity of the Vatnajökull glacier in the south (Sveinbjörnsdóttir et al., 1986; Darling and Ármannsson, 1989; Ármannsson, 2005).

Scaling in the Námafjall wells or surface pipelines has never been a problem; amorphous silica originally precipitated in the district heating system but the direct piping of geothermal water was replaced with a heat-exchanger system in which cold groundwater is heated by steam and piped into the district heating system (Thórhallsson et al., 1975).

Hengill

The Nesjavellir and Hellisheidi high-temperature geothermal systems are hosted by the Hengill volcanic system, located within the active rift of the Western Volcanic Zone, 20 to

30 km east of the capital Reykjavík. The Hengill area is located just north of a triple junction where an oblique spreading ridge, tensional spreading axes and major seismic zone meet, at the location where the Reykjanes Peninsula begins (Figs. 1.3 and 1.2). Hengill is the only central volcano with a geothermal system where rhyolite is known (Saemundsson, 1967; Hardardóttir, 1983). Geothermal waters in the reservoirs at Nesjavellir and Hellisheidi are generally between 250° to 320°C and low salinity.

Exploration at the Hengill volcanic system started about 40 years ago (Saemundsson, 1967; Gunnarsson et al, 1992). Presently, 28 wells have been drilled at Nesjavellir to a depth ranging from 1000 to 2500 m; the highest measured temperature is over 380°C at 1900 and 2200 m depth (Steingrímsson et al., 1990). The well field covers an area of 3.5 km². The power plant went into operation in the autumn of 1990 (60 MWe), increasing production in steps up to the current 120 MWe, as well as 1640 l/s of water at 83°C, equivalent to 380 MWth (MW thermal), which is transported to Reykjavik for space heating.

The main outflow channel of the geothermal fluids from beneath Hengill volcano into the Nesjavellir system is related to 2000 and 5000 year-old NE-SW trending volcanic fissures (Franzson, 1998). The southern part of the reservoir nearest to the Hengill volcano is a two-phase boiling system, but the temperature decreases rapidly away from the volcanic fissures and the system becomes liquid dominated (Stefánsson, 1985). The reservoir fluid is low in total dissolved solids and gas and has neutral to alkaline pH (Table 1.1). Isotopic studies suggest that the Nesjavellir waters originate from a distant source, most likely the Langjökull glacier in the north (Mutonga et al., 2010).

The Hellisheidi geothermal area is located south of Hengill volcano, with a current installed production capacity of 213 MWe (February, 2009); power production started in 2006. Forty seven exploration and production wells have been drilled in the area, the

deepest to 3322 m, and the highest measured temperature in the system is 329°C. The majority of separated liquid is injected back into the geothermal system. Isotopic studies and the chemistry of the thermal fluids indicate that the Hellisheidi water is of local origin and is younger than that in the Nesjavellir system (Mutonga et al., 2010).

The main scaling problem from the geothermal fluids at Nesjavellir and Hellisheidi is the deposition of silica in surface piping as the fluid cools, either by boiling or conductive cooling. The scaling is mitigated by “aging” the supersaturated water in retention tanks for 1.5 hours, allowing the monomer silica to form suspended polymers so supersaturation with respect to amorphous silica is reduced (Ármannsson and Ólafsson, 2006). By mixing condensed steam with the treated water after “aging” supersaturation is avoided and the treated water can be reinjected without scaling problems (Gunnarsson et al., 2010).

Svartsengi

The Svartsengi geothermal system is located on the Reykjanes Peninsula about 15 km inland, to the east of the Reykjanes system (Fig. 1.3). Drilling in this area started in 1972 with two shallow exploration wells (239 and 402 m deep). Two pilot plants were built in 1972 and 1976, the first to examine problems of scaling. At present 20 wells (12 in production and one for reinjection) have been drilled to 1992 m depth. The geothermal plant is a combined heat and power plant which comprises two 1 MWe generators and four 12.5 MWth heat exchange- deaerator systems (based on thermal exchange, with a temperature decrease of hot water from 125°C to 40°C; Albertsson et al., 2010, Thórólfsson, 2010).

The wells are collared in lava erupted in 1226 AD (Jóhannesson and Einarsson, 1988); hydrothermal surface manifestations are evident over an area of ~4 km². The Svartsengi and Reykjanes fields exist in similar tectonic, volcanic and hydrological environments (see

below). Although these two systems are located close to each other, the stratigraphic succession differs significantly in that interglacial lava series are found at Svartsengi but are absent at Reykjanes (Franzson, 1995; Franzson et al., 2002)

The geothermal liquid has salinity approximately two thirds of seawater, with 22,000 ppm total dissolved solids at a reservoir temperature of $\sim 240^{\circ}\text{C}$ (Table 1.1). In the early years of operation, calcite scaling formed in the boiling zone at 600 to 500 m depth, and this scale was drilled out about every second year. The reservoir was depressurized by ~ 30 bar, due to drawdown caused by utilization (74 bar-g in 1976 and 44 bar-g in 2009: Jónsson et al., 2010). As a result, the geothermal system changed from being completely liquid-dominated to having a vapor cap (Thórólfsson, 2010). Many of the production wells draw dry vapor from the vapor cap to generate electricity, greatly reducing the problem of calcite scaling (Thórólfsson, 2010).

1.4 Reykjanes Geothermal System

The Reykjanes Peninsula is the landward continuation of the Reykjanes Ridge, the northern part of the Mid-Atlantic Ridge. Where the diverging plate margin interacts with the Iceland plume, there is a complex pattern of rifting and transcurrent faulting; the Reykjanes Ridge is 30° to 40° oblique to the spreading direction, resembling faster spreading ridges both in terms of topography and seismicity (Einarsson, 2001). The Reykjanes Peninsula is a part of the active Western Volcanic Zone of Iceland (Saemundsson, 1979; Jakobsson et al., 1978), and seismic activity is mainly confined to a 1 to 2 km-wide zone that trends $\sim \text{N}70^{\circ}\text{E}$, which is thought to mark the plate boundary on the peninsula (Figure 1.3; Guðmundsson, 1986; Sigurdsson, 1986; Clifton and Kattenhorn, 2007).

The westernmost 20 km of the peninsula is a flat coastal lowland, rising from ~ 20 m above sea level on the west coast to 250 m at mountain Thorbjörn, near Svartsengi. Further

east is Heiðin Há, the largest a shield volcano on the peninsula, 15 km in diameter and 525 m high (Jóhannesson and Saemundsson, 2009).

The Reykjanes Peninsula is constructed solely of volcanic rocks. The hyaloclastite deposits that form the highlands date from the past glaciations, whereas post-glacial lavas that erupted during the last 14,000 years cover most of the lowlands. The hyaloclastite deposits formed beneath glaciers and are preserved as elongated ridges and table mountains (tuyas). At least 160 post-glacial eruptive fissures or aligned craters and close to 30 lava shields have been identified by Jónsson (1978, 1983). The volcanic rocks are of basaltic composition, ranging from picrite shield lavas through olivine tholeiite shield lavas and fissure products; no intermediate or rhyolitic rocks outcrop west of the Hengill central volcano (Jakobsson et al., 1978).

Five volcanic systems are active on the Reykjanes Peninsula: from west to east, Reykjanes, Svartsengi, Krísuvík, Brennisteinsfjöll and Hengill at the eastern boundary of the peninsula (Figure 1.3). Svartsengi and Reykjanes are commonly shown as one volcanic system on geology maps (Jakobsson et al., 1978; Jóhannesson and Saemundsson, 2009). The Reykjanes Peninsula apparently lacks central volcanoes with shallow magma chambers (Saemundsson, 1979); the heat source is interpreted to be dikes intruded at depth (Franzson, 2004). The geothermal systems associated with the Krísuvík and Brennisteinsfjöll volcanic systems have yet to be harnessed, but the other three systems, Reykjanes, Svartsengi and Hengill, are being utilized.

The salinity of the geothermal liquids on the Reykjanes peninsula varies depending on proximity to the ocean (Björnsson et al., 1971, 1972a, b). The Reykjanes geothermal system is surrounded by the ocean on three sides, only 1.5 km from the shoreline and extends SW to the sea (Björnsson et al., 1971; Johnsson and Jakobsson, 1985), has reservoir liquid of

seawater salinity, but as noted above, Svartsengi salinity is two thirds of seawater, and the Hengill system has very low salinity fluids (Table 1.1; Björnsson et al., 1971, 1972a, b; Hauksson, 1981; Kristmannsdóttir, 1984; Bjarnason, 2002).

The δD and $\delta^{18}O$ values average -22.5‰ and -1.08‰ (ISOR data base) respectively, in the reservoir liquid from well RN-8, whereas seawater near Reykjanes has value of 1.7‰ and 0.21‰ , respectively (Ólafsson and Riley, 1978). Isotope measurements in calcite and quartz (Sveinbjörnsdóttir et al., 1986) have been suggested to indicate involvement of glacial meltwater. Further petrographic research done on the cuttings by Franzson (1995, 2004) and isotopic composition of epidote (Pope et al., 2009), and isotopic composition of anhydrite and epidote (Marks et al., 2010a, b) support indications that the Reykjanes geothermal system was dominated by meteoric water recharge at some time during the Pleistocene.

1.4.1 Geological setting geothermal activity

The Reykjanes Peninsula includes very diverse volcanic formations of both glacial and interglacial age as well as post-glacial lava flows (Jónsson 1978; Saemundsson et al. 2010). Surface geothermal manifestations include steam vents, mud pools and sulfur deposits (e.g., Thorkelsson, 1928; Jónsson, 1968; Ólafsson, 1975). Because the Mid-Atlantic Ridge comes ashore at the tip of the peninsula, the nature of the volcanism and geothermal activity reflect the spreading processes at ocean ridges (i.e., Björnsson et al., 1972a, b; Arnórsson et al., 1978; Kristmannsdóttir, 1984; Clifton and Schlische, 2003).

The peninsula is intensely fractured along a NE-SW trending fault zone. The fractures are small normal faults and tension cracks (e.g., Einarsson, 1991, 2008; Hreinsdóttir et al., 2001; Clifton and Schlische, 2003; Árnadóttir et al., 2004; Clifton and Kattenhorn, 2007)

and less conspicuous strike-slip faults that cut across the plate boundary at a high angle (dominantly N-S: Clifton and Schlische, 2003; Einarsson, 2008), indicating a strong relationship between the geothermal activity and the tectonic and magmatic anomalies. The geothermal systems occur at the intersection of the seismic zone with the fissure swarms (Arnórsson, 1978b; Jakobsson et al., 1978; Franzson et al., 2002; Franzson 2004).

The area near Reykjanes is mostly covered by post-glacial basalt lava flows with low hyaloclastite ridges of Pleistocene age protruding through the lava field in a few places. The most recent volcanic episode was in the late 12th and early 13th century (Sigurgeirsson, 1995, 2004). The recent volcanic activity was characterized by early shield volcanoes and later episodic fissure eruptions (Jónsson, 1978, 1983; Jakobsson et al., 1978; Sigurgeirsson, 2004).

Drilling to investigate the utilization potential of the Reykjanes geothermal area started in 1956, and in 1969 the first production well, RN-8, was completed. Well RN-9 was drilled in early 1983. Since 1998 drilling has been continuous, and to date 29 wells have been drilled, generally to the depth of 2000 to 2500 m (Fig. 1.4). The deepest well, RN-17, was the first IDDP well of opportunity (<http://www.iddp.is/>); it is 3082 m deep and had the primary economic objectives to locate and to investigate supercritical fluid as a potential energy resource, as well as to explore the geologic processes in an active spreading margin. Well RN-17 collapsed before the goal was reached, and IDDP shifted its focus to Krafla.

In the early days of the Reykjanes power plant, one well (RN-8) was in production to supply steam for fish drying and to produce salt, with only a minor electricity production (Líndal, 1975). Electricity production increased up to 100 MWe in June 2006, and current plans are to expand the electrical power generation by 50 MWe, as well as to possibly add a 30 to 50 MWe low-pressure turbine unit (Sigurdsson, 2010). The production increased by a

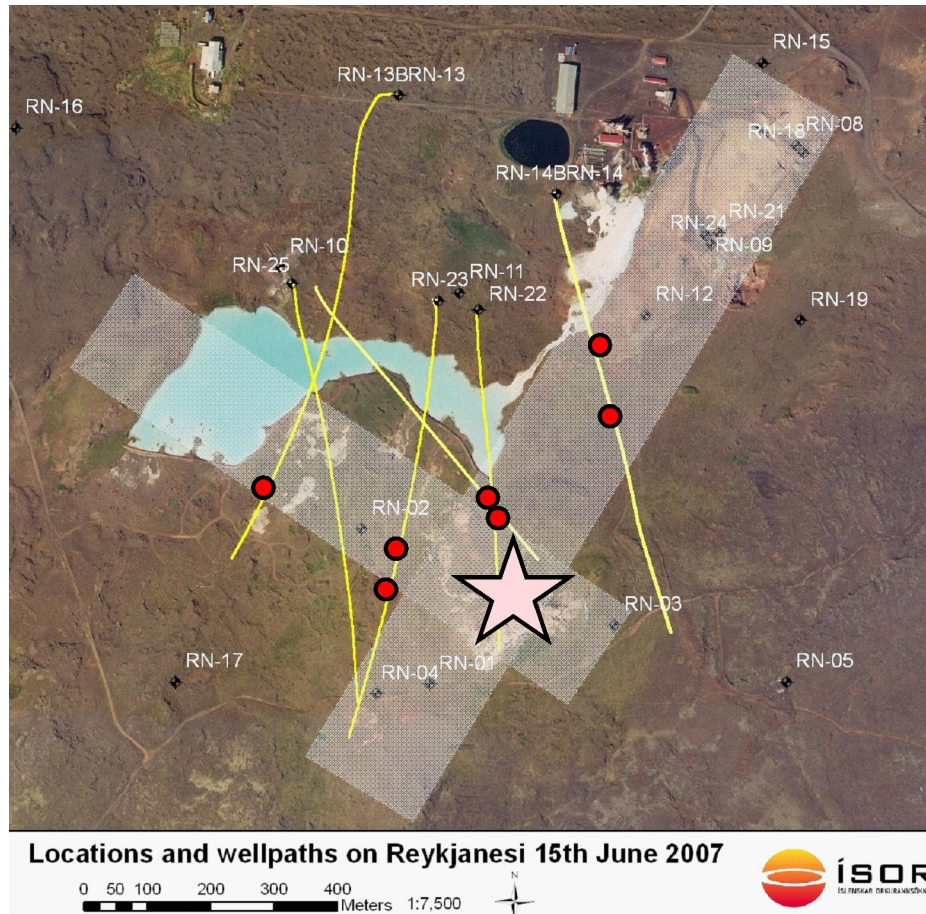


Figure 1.4. Locations of drillholes at Reykjanes, as of June, 2007. Yellow lines show the traces of deviated wells. Two main upflow zones are indicated by the shaded quadrangles, and the star represents the principal focus of upflow at Gunnuhver hot spring (simplified from Franzson, 2004 and Karlsdóttir, 2005). Red dots are locations of the major inflow zones of the deviated wells projected to the surface. Well RN-6 is ~600 m SW of well RN-4.

factor of 16, from ~50 to 800 kg/s between 1970 and 2007 (Hjartarson and Júlíusson, 2007), resulting in ~30 bar pressure decrease at 1500 m depth in the reservoir associated with drawdown in the first three years (Jónsson et al., 2010). This drawdown resulted in formation of a vapor cap over the liquid-dominated part of the reservoir which has resulted in the discharge of dry vapor (without a liquid phase) from shallow wells (Fridriksson et al., 2010). The enthalpy of the deep production wells has increased from 1210-1400 kJ/kg (liquid enthalpy at 275-310°C), prior to May 2006, to 1450-1950 kJ/kg in 2008, indicating excess enthalpy discharges (i.e., greater than the heat content for a liquid-only feed to the

discharging wells: Fridriksson et al., 2010; see Henley et al., 1984). The pressure drawdown also led to an increase in the depth of boiling in the system, with the level of first boiling moving downward. Thus the liquid-dominated system and more active boiling system has led to an increase in surface activity.

Surface manifestations cover about $\sim 1.5 \text{ km}^2$ and are typical of high-temperature areas; warm to hot ground, mud pools, steam vents, hot springs (Björnsson et al., 1970; Pálmason et al., 1985). The intensity of the surface activity is known to vary over time; it increases abruptly as a result of seismic activity and then decreases with time until the next seismic event.

The size of the geothermal system has been debated. Björnsson et al. (1972a, b) suggested that the extent of the 280°C isotherm at 1.5 km depth is about 1 km^2 ; however, resistivity measurements by Karlsdóttir (1997, 2005) suggest an areal extent up to 10 km^2 at 800 to 1000 m depth. Studies of hydrothermal alteration in the wells (RN-1 to RN-16) indicate that the alteration area is greater than 1 km^2 (Franzson, 2004). The upflow zone is controlled by N-S and NE-SW structures; with the main upflow located at the intersection of these structures below the principle surface activity at Gunnuhver, a hot spring south of well RN-22 (Fig. 1.4; Franzson, 2004). This location of the main upflow was later corroborated by resistivity measurements by Karlsdóttir (2005) and carbon dioxide soil emission measurements by Fridriksson et al. (2006). The estimated heat flow based on the CO_2 soil emission is $130 \pm 16 \text{ MW}$ (Fridriksson et al., 2006), which is consistent with earlier temperature surveys and resistivity surveys by Björnsson et al. (1971, 1972a, b). The young rocks above the geothermal system are highly permeable, as indicated by the low groundwater table which is near the surrounding seawater level and shows the effect of

tides (Björnsson et al., 1972a, b). This high surface permeability is also confirmed by the resistivity surveys (Karlsdóttir, 1997, 2005).

The reservoir liquid in the Reykjanes high-temperature geothermal system has salinity (~3.2 wt%) similar to seawater (3.5 wt%), with a fluid inflow temperature in wells between 275°C to 315°. The fluid inflow temperature was 290 to 295°C in well RN-09 and 275°C in well RN-08; both wells have a vapor-saturated liquid inflow (i.e., inflow liquid is just at the boiling point; Bjarnason, 2002).

1.4.2 Stratigraphy and alteration

The stratigraphy of the Reykjanes system was first determined by Björnsson et al. (1971) and Tómasson and Kristamannsdóttir (1972), who studied in detail the first eight wells; further drilling added to this knowledge (e.g., Franzson, 2000, 2004; Franzson et al., 1983, 2002). Based on cuttings sampled at 2 m intervals during drilling, the stratigraphy consists of hyaloclastite and breccias of reworked tuffaceous sediments to 1000 m depth interbedded with basaltic lava flows, and pillow basalts at greater depths. Some volcanic sedimentary horizons contain fragments of marine fossils (Franzson et al., 2002; Franzson, 2004). Dykes are common below ~1000 m depth and increase in abundance with depth (Franzson et al., 2002). A simplified stratigraphic section of well RN-9 (Fig. 1.5) shows the main fluid zones (feeder zones or circulation loss of drilling fluid); the distribution of the main alteration minerals is also shown. As this well was only ~1400 m deep, the stratigraphy to 2500 m is also shown for well RN-12, about 150 m to the southwest (Richter et al, 2003; Jónsson et al., 2003).

Based on the first 16 wells, Franzson et al. (2002) and Franzson (2004) built a conceptual model of the volcanic stratigraphy. Below ~1200 m depth the rocks consist largely of pillow basalt formed by submarine volcanic eruptions. As the depth of volcanic

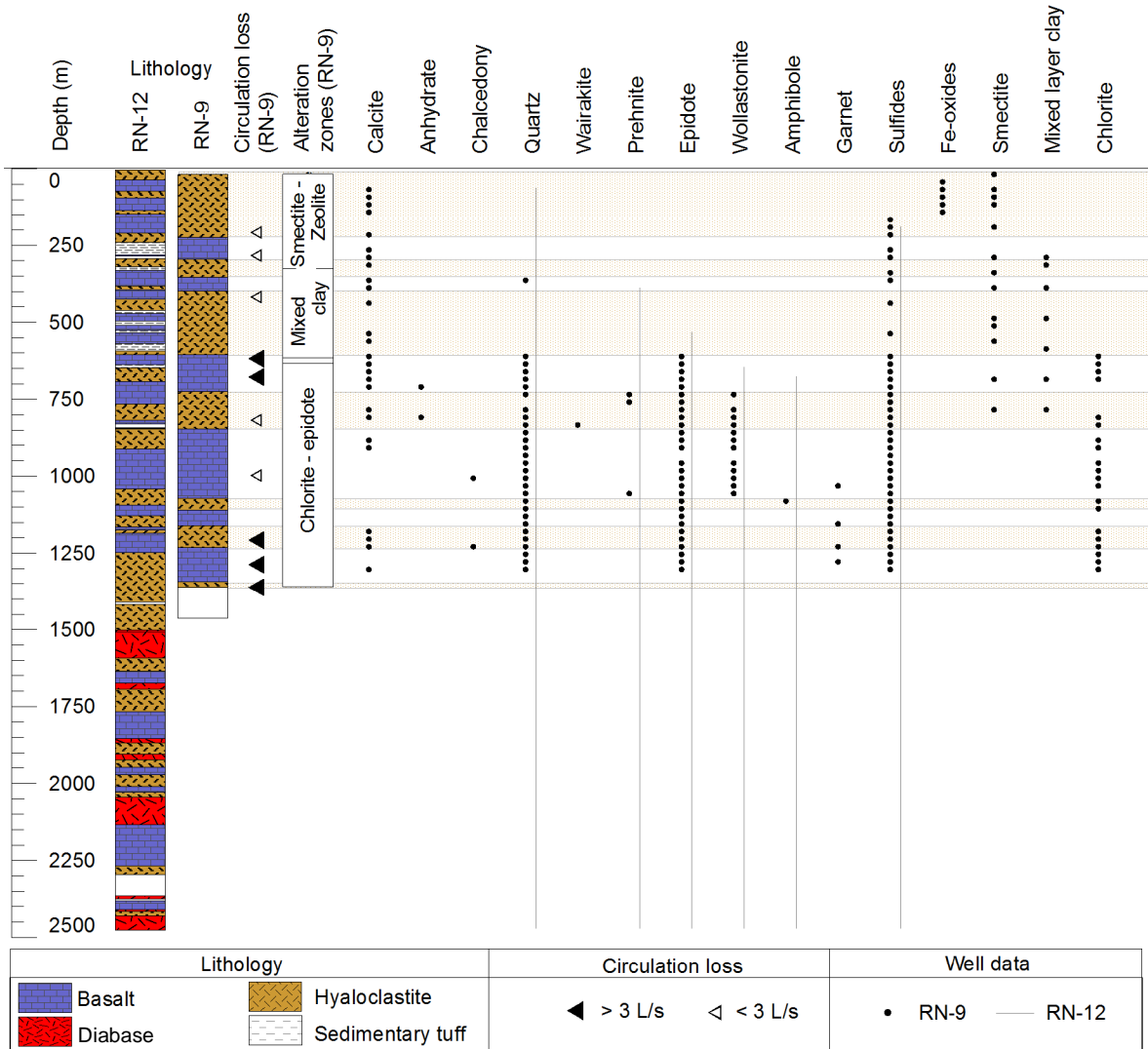


Figure 1.5. Simplified stratigraphy and alteration mineralogy from well RN-9 (Franzson et al., 1983; Mungania, 1993) and RN-12 (Richter et al., 2003; Jónsson et al., 2003).

effusion became shallower (i.e., lower pressure), gas exsolution in the magma increased and caused explosive reaction with the seawater, causing brecciation and formation of volcanoclastic material. Subsequent deposition of shallow marine volcanoclastic sedimentary horizons occurred, as indicated by the marine fossil fragments. The sequence is capped by pillow basalts and sub-aerial basalt flows of post-glacial age (<120 m depth).

Petrographic studies have been conducted on most of the drill cuttings from Reykjanes and detailed studies are available for selected wells (including RN-8, RN-9, RN-10 and RN-

17), on hydrothermal alteration, whole-rock geochemical and isotope compositions, and fluid inclusions (Tómasson and Kristmannsdóttir, 1972; Kristmannsdóttir, 1984; Sveinbjörnsdóttir et al., 1986; Lonker et al., 1993; Franzson, 2000, 2004; Franzson et al., 2002; Marks et al., 2010a, b).

The appearance and/or disappearance of alteration minerals between drill holes and with depth have been used to divide the high-temperature systems in Iceland into alterations zones. This work was pioneered by Tómasson and Kristmannsdóttir (1972) and Kristmannsdóttir (1975, 1984), followed by many geologists at ISOR (Franzson et al., 1983, 2002; Franzson, 2004; Fridleifsson, 2005). The minerals which are commonly used as indicators of temperature from lower ($\sim 100^{\circ}\text{C}$) to higher ($\sim 300^{\circ}\text{C}$) temperature are zeolites and smectite to chlorite, epidote and amphibole. The depth to each alteration zone varies between wells, depending on the lateral distance from the upflow zone, which appears to be mainly in the area of well RN-9 and ~ 600 m southwest of RN-9 (Fig. 1.4; Franzson, 2004; Karlsdóttir, 2005). The alteration zones in RN-9 and RN-12 are shown in Figure 1.5, together with the downhole distribution of other alteration minerals.

The zeolites (most commonly mordenite, heulandite, laumontite, analcime, wairakite) and smectite commonly form at temperatures less than 200°C and generally are not present at depths where the temperature reaches 250°C (Kristmannsdóttir, 1975); however, analcime is present below the main zeolite zone and wairakite occurs at higher temperature (Tómasson and Kristmannsdóttir, 1972; Kristmannsdóttir, 1984). The clay minerals are the most common sheet-silicates, and occur up to 280°C ; smectite (mainly montmorillonite) is stable up to $\sim 200^{\circ}\text{C}$, and chlorite appears in the temperature range 230 to 280°C . Between these two zones mixed-layer minerals, including chlorite and montmorillonite with a trace of illite, are common (Tómasson and Kristmannsdóttir, 1972). Prehnite occurs between the

chlorite and the epidote zone. Epidote is common at a temperature above 260°C, wollastonite at temperatures of ~270°C and amphibole (first hornblende followed by actinolite) above 280°C (Kristmannsdóttir, 1984; Franzson et al., 2002, Franzson, 2004). Quartz is a common mineral at all depth intervals. Quartz at Reykjanes occurs at temperatures above 180°C, but calcite commonly disappears at temperature above 300°C (Franzson et al., 2002; Franzson, 2004). Calcite is also common near aquifers in which the liquid is boiling (Franzson et al., 2002). Garnet occurs at temperatures of ~300°C, but Lonker et al. (1993) noted that it is most common at 320 to 330°C. Anhydrite is dispersed through the section, but where it occurs in large quantities it appears related to zones of cold water inflow. Pyrite is the most abundant sulfide and is also disseminated throughout the section, together with minor chalcopyrite and sphalerite. Detailed work on the IDDP well RN-17 identified sparse sphalerite from ~400 m to 1200 m, as well as chalcopyrite and galena (Marks et al., 2010a).

By studying the order in which minerals deposit into open spaces, Franzson et al. (2002) suggested that the geothermal system has been progressively heating, and shows no signs of cooling. By contrast, Lonker et al. (1993) concluded from oxygen isotope and fluid inclusion study that the system is cooling due to heat-source decay, cooler water incursion, or both. Franzson (2000) studied homogenization (T_h) and melting temperatures (T_m) of fluid inclusions in quartz, calcite, and plagioclase from cuttings from wells RN-9 and RN-10. The T_m data indicated a wide salinity range, from fresh water salinity to seawater salinity (0 to ~3.2 wt.%), interpreted as being due to a change from a dominantly fresh-water environment during glacial time to a more saline environment in post-glacial times.

CHAPTER 2

Sulfide Mineralogy and Composition of Scales from the Reykjanes Geothermal System, Southwest Iceland

Vigdís Hardardóttir^{1,2}, Jeffrey W. Hedenquist², Mark D. Hannington²
and Ingrid Kjarsgaard³

¹Iceland GeoSurvey, Grensásvegi 9, 108 Reykjavík, Iceland

²Department of Earth Sciences, University of Ottawa, Ottawa, Ontario, Canada, K1N 6N5

³Carleton University, Ottawa, Ontario, Canada, K1S 5B6

Manuscript in preparation

Presented at:

Water - Rock Interaction in June-July 2004 (WRI-11) in Saratoga Springs, USA

World Geothermal Congress (WGC2005), June 2005, Antalya, Turkey

The Geological Society of America Annual Meeting, October 2005, Salt Lake City, USA

2.1. Introduction

Scale deposition in production wells and pipelines is a common problem encountered during the exploitation of geothermal systems, particularly so in surface facilities at Reykjanes (Fig. 1.3). The objective of this study was to characterize the deposits and their origin and to suggest ways to mitigate the scaling, which is detrimental to the flow of hot fluid. Development plans at Reykjanes are to increase generation capacity to 150 MW which may result in the formation of a steam cap; if so production of steam should decrease the problem of scaling.

Reykjanes is a geothermal system in southwest Iceland that produces 100 MW electrical energy. Production of high-temperature (290°C) liquid of near-seawater composition results in a pressure decrease and boiling in the wells during ascent. The boiling causes cooling and gas loss, which leads to the precipitation of base metal-rich sulfide scales (mainly sphalerite and minor chalcopyrite) and amorphous Fe-bearing silica, both in the well and in surface pipes (unpublished data by H. Kristmannsdóttir, 1985; Hardardóttir et al., 2001, 2005, 2009; Hardardóttir, 2002, 2004a, b). This paper reports the results of a detailed study of the mineralogy and chemical composition of the scales, mainly from well RN-9 (Fig. 2.1). A summary description of the surface scales from the more recently drilled wells at Reykjanes is also presented.

Well RN-9 was chosen for a detailed study due to the availability of scale samples collected from the surface pipeline during cleaning in the summer 2000. In addition, detailed information on the production history of this well is available (i.e., pressure at the wellhead, periods and amount of discharge, scaling history, and composition of discharged fluid). Well RN 9 was drilled in 1983 but saw limited use at the time. Well RN-10 was not drilled until 1999. From 1999 to 2007, 15 wells (up to RN-24) were drilled in an area of



Figure 2.1. Photograph of the pipeline from RN-9 wellhead to the discharge pond (the Grey Lagoon). Red dots show the locations of samples, mostly collected in the year 2000. Missing are sample locations at the bridge which is out of view to the right and upstream from there to the last location at bend 4 (photo G. Ó. Fridleifsson). The separation station receives the two-phase flow from the geothermal wells and is where the vapor is separated from the liquid. The vapor is piped to the power plant and the liquid to a reinjection well or to a surface disposal pond. The vent house is where the liquid level-control valves of the separation station are housed, just before the silencer. In the silencer the flashed vapor escapes by a chimney and the liquid flows by gravity to the pond.

<1.5 km² (Fig. 1.4). The maximum measured temperatures (275°-320°C) and calculated deep liquid compositions of the newer wells are similar to those of well RN-9 (Chapter 5). The production history of well RN-9 and the mineralogy of surface scales form the main part of this chapter, followed by descriptions of the scales precipitated in the newer wells. The results of scaling tests, conducted in 2002 and 2003, are also summarized, followed by discussion of the bulk chemistry of the scales. Normative calculations and mass of scale accumulation in the surface pipelines are discussed, as well as compositions of altered whole rock from RN-9. Well RN-22 is discussed in detail at the end of this chapter, as it provides the only opportunity to characterize sub-surface scales formed at high pressure, up to ~52 bars.

2.2. Characteristics of Well RN-9

2.2.1 General information

Well RN-9 was drilled in 1983 and filled with concrete in 2005. The initial wellhead pressure was typically ~40 bar, but was as high as 47 bar and as low as 15 bar for a few

days or months during its production (Figs. 2.1, 2.2, and 2.3). From 1992 to 1994 the pressure was 30 to 25 bar, and from 2000 to the end of its production in 2003 the wellhead pressure was ~27 to 24 bar (Steingrímsson and Björnsson, 1994; all pressures are referred to as gauge-g, which is 0 at atmospheric pressure, unless otherwise noted). Early in 1992, the shut-in pressure was 38 bar (see Table A2.2 for pressure and corresponding temperature data). Temperature measurements indicated 4 to 5°C decrease with time, from a maximum of 295°C at 1405 m depth in 1983 (Steingrímsson and Björnsson, 1992). Pressure measurements indicated no drawdown of pressure due to utilization from 1983 to 1994.

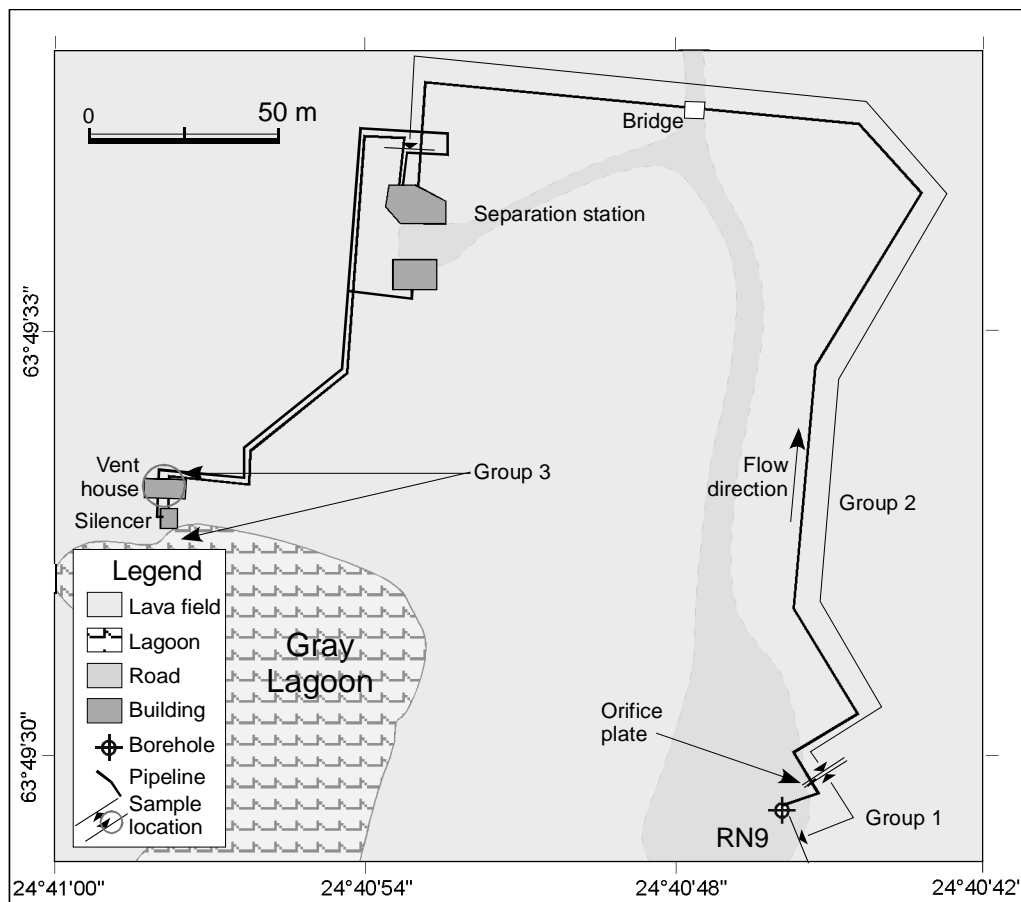


Figure 2.2. Drawing of the pipeline from the wellhead of RN-9 (362 m long to the separation station), showing the locations of the three sample groups based on pressure. Group 1, samples at the wellhead and ~14 m upstream of the orifice plate; group 2, samples on the orifice plate, where the pressure decreases sharply, and the next ~350 m downstream of the orifice plate to the separation station. Group 3, samples from the vent house and the Grey Lagoon, at atmospheric pressure and 100°C.

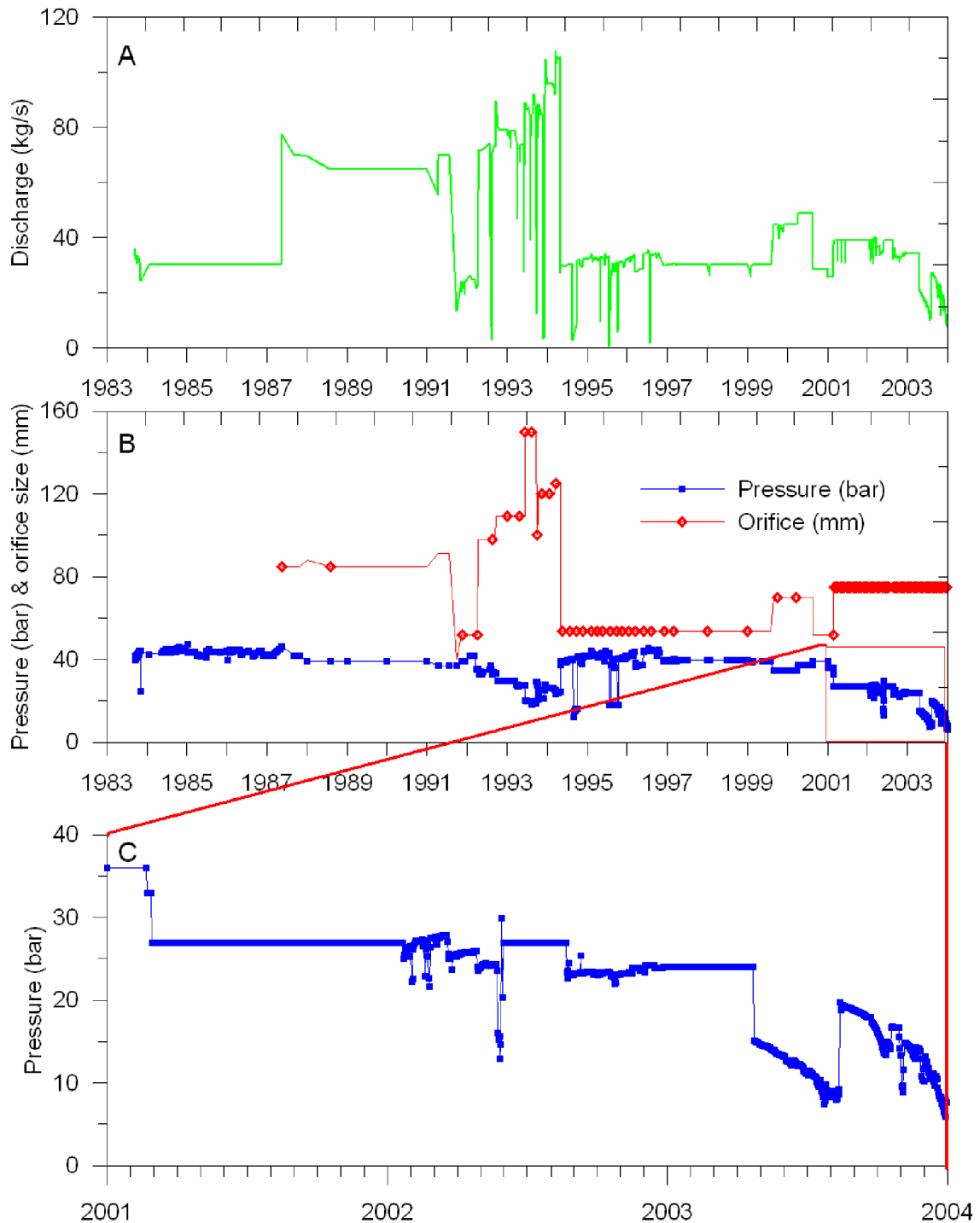


Figure 2.3. Production characteristics of well RN-9, Reykjanes, Iceland (Verkfræðistofan Vatnaskil sf, 2010). A) Discharged fluid (kg/s) = production, from 1983 to 2004. B) Wellhead pressure (bar-gauge; g) and the diameter of the orifice plate (mm). C) Wellhead pressure from 2001 to 2004.

Scaling initially occurred in a 2" pipeline at the wellhead used to insert well logging instruments (Steingrímsson and Björnsson, 1992). However the well became blocked by scale in late 1993 to a depth of at least 567 m. Due to a broken liner, the well could be cleaned only to a depth of 552 m (Steingrímsson and Björnsson, 1993; Figure A2.1). In late August, 1999, the 53.5 mm diameter of the opening in the orifice plate was increased to 70 mm (Verkfraedi-stofan Vatnaskil, 1993, 2000), resulting in a wellhead pressure drop to 34.5 bar. The pressure increased to ~37 bar when the surface pipeline was cleaned in July, 2000. By early 2001, the wellhead pressure declined to ~27 bar. In April, 2003, to late July, scaling in the well was suspected due to a lower wellhead pressure (Fig. 2.3). Pressure increased by 10 bar in July, 2003, suggesting temporary dislodging of scales, but the pressure declined again and finally the well stopped flowing in early January, 2004, due to scale deposition. For further details see Appendix 2.1.

2.2.2 Conditions in well RN-9

When RN-8 and RN-9 were the only producing wells at Reykjanes, downhole logging was limited to temperature and pressure surveys with mechanical clock-driven tools (Amerada and Kuster gauges). These measurements were not taken regularly and almost always conducted with the well shut-in (closed), whereas today wells are also measured while producing (dynamic flowing profiles). Temperature and pressure measurements indicate the depth that the ascending liquid starts to boil in the well or in the host rock before it enters the well (Appendix 2.1). Figure 2.4 shows the calculated boiling temperature for depth curve and the pressure profile for a hot liquid of seawater composition (3.5 wt.% NaCl; Haas, 1971), together with temperature and pressure logging data from well RN-9 during shut-in conditions. The temperature and pressure measurements date from September, 1983, and can be compared to the estimated reservoir temperature and

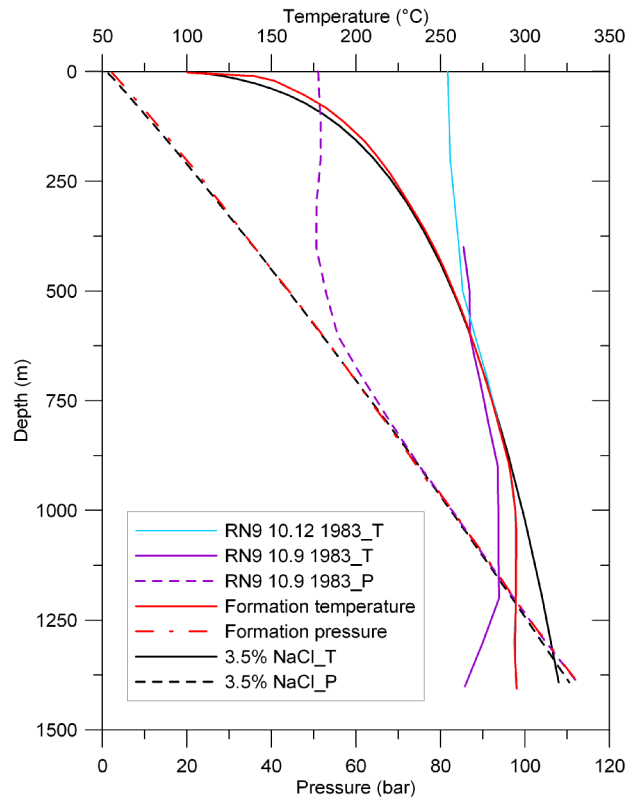


Figure 2.4. Boiling-point curve and equivalent pressure curve (lower x-axis) for seawater (black line, 3.5 wt.% NaCl; Haas, 1971) and measured pressure and temperature from September and December, 1983, in well RN-9 (dashed color lines). Formation temperature and pressure are equal to reservoir temperature and pressure before drilling started in the area (Hjartarson, 2004). The boiling-point curves for seawater are calculated assuming a 0 bar-g wellhead pressure. Indication of boiling can be seen by change in slope of the temperature and the pressure curves. The change in the slope is due to the transition from liquid to a boiling two-phase mixture. See text and Appendix 2 for further explanations.

pressure profiles in this location before drilling started in the area (Hjartarson, 2004). The well heated up from the time of drilling in late May, 1983, with the first survey occurring on September 10 while the well was closed. The wellhead pressure was 50 bar, and temperature at the feed-zone at 1200 m depth was 285°C. Boiling in the well appears to have started above ~850 m depth, as shown by the deviation of the pressure measurements from a hydrostatic pressure profile. Logging in December, 1993 (after cleaning the well) showed that the well had heated up during 10 years of flow and was 295°C from 1000 to 1400 m depth and 255°C at the wellhead when closed (Steingrímsson and Björnsson, 1993).

The initial boiling level in the well at that time was approximately 900 m (open well). In the following years, measurements showed that the boiling depth increased gradually from about 600 m depth (closed well) in 1983 to about 1000 m depth up to 2003 (S. Thórhallsson, pers. commun. 2009), due to increased utilization (Appendix 2.1). The temperature and pressure measurements from well RN-9 are discussed further in Chapter 5.

2.2.3 Conditions in the surface pipeline of RN-9

The production (discharge in kg/s; Fig. 2.3) from well RN-9 was controlled by the size of the orifice plate (Appendix 2.1.2). Pressure at the well head, generally between ~44 and 40 bar through the 1980s, was constant for the first ~14 m of the downstream pipe to the orifice plate, where it decreased sharply to ~11 bar due to expansion through the opening (throttle) in the orifice plate. This situation prevailed until ~1988, when the pressure after expansion was increased by 1 bar due to a change in turbine operation. Downstream of the orifice plate towards the separation station, ~348 m away, the pressure decreased by 1-2 bar. From the separation station two pipes lead to the vent house (Fig. 2.2), one for vapor and one for separated liquid. The liquid pipe was ~153 m long and the pressure was similar to that in the two-phase line coming from the well (10-12 bar).

Production from well RN-9 was constant at ~32 kg/s for the first five years, but was doubled in the years 1988 to 1993 by increasing the orifice diameter (Fig. 2.3). The total production from November, 1983 to September, 1993, when the well was cleaned, was 1.7×10^{10} kg fluid. The production varied considerably in the following years for various reasons, including scaling problems, but the total production from September, 1993 to July, 2000, when the surface pipes were cleaned, was 0.8×10^{10} kg. From the first blockage of the well in September, 1993, to the second blockage in 2003, when flow stopped, the well

produced 1.1×10^{10} kg. The total production from the well was $\sim 2.8 \times 10^{10}$ kg (ISOR database).

2.3. Scale Samples from RN-9: Occurrence, Characteristics and Textures

The amount of scale deposition in the 362 m long pipeline from the wellhead to the separation station was variable, depending on the pressure and temperature as well as obstacles in the pipe, such as bends (Fig. 2.5). At bends in the pipe, turbulent flow increased, as inferred from the very uneven appearances of the scales (see below). At the wellhead, scales a few mm thick lined the interior of the whole pipe (Fig. 2.5A). Upstream of the orifice plate (14 m from the wellhead), as far as could be observed visually into the pipe (~ 1.5 to 2 m), the scales were less than 0.5 cm thick and only occurred in the bottom of the pipe (Figs. 2.5B, C). Scale thickness increased sharply downstream from the orifice plate. When the pipeline was opened in July, 2000, scales that had formed in 1 to 1.5 years nearly clogged the 40 cm diameter pipeline ~ 4 to 8 m downstream of the orifice plate, leaving an opening only about 10 cm in diameter for the fluid to flow (Figs. 2.5D, E and 2.6A-D). The deposition decreased in thickness further downstream. Scales were only ~ 1 cm thick 150 m downstream of the orifice plate (Figs. 2.5H and 2.6A), but at bends and in the bottom of the pipeline in this interval, scales were thicker (Figs. 2.5F-K and 2.6J, L). When the pipe was cleaned in 2000, samples were collected both up- and downstream of the orifice plate; the sample locations are shown in Fig. 2.1.

The scale samples can be grouped depending on their location (Hardardóttir et al. 2001, 2005; Hardardóttir, 2002, 2004a), as well as by the prevailing pressure in the surface pipeline. There are three groups of scales formed at different temperatures, pressures and flow regimes within the pipeline:

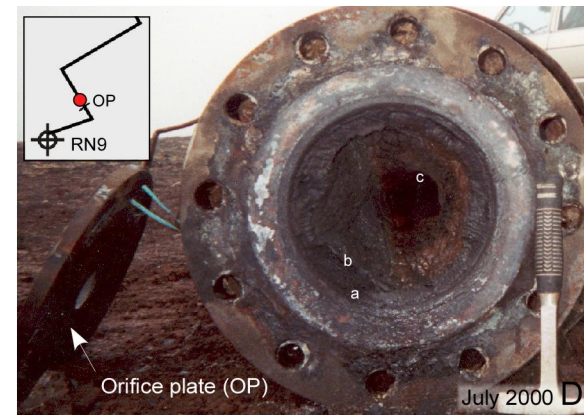
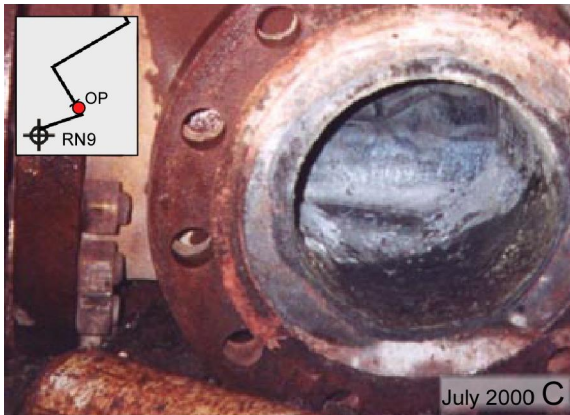
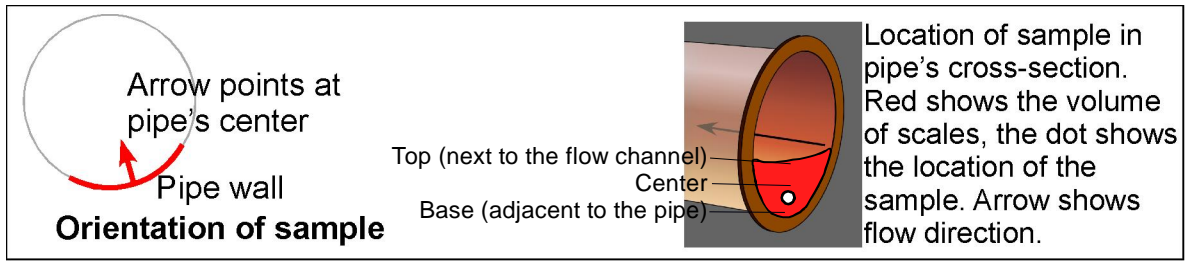
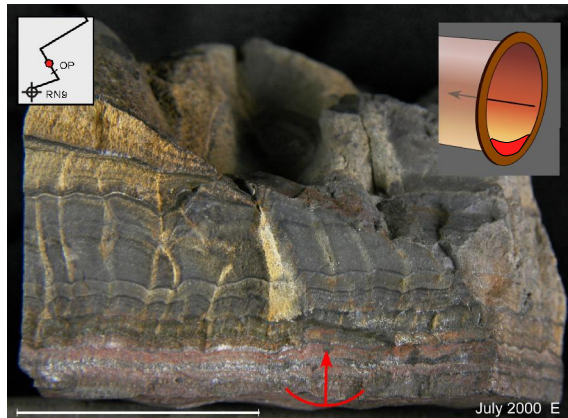
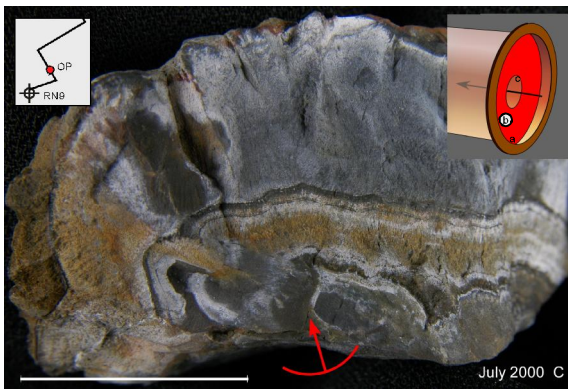
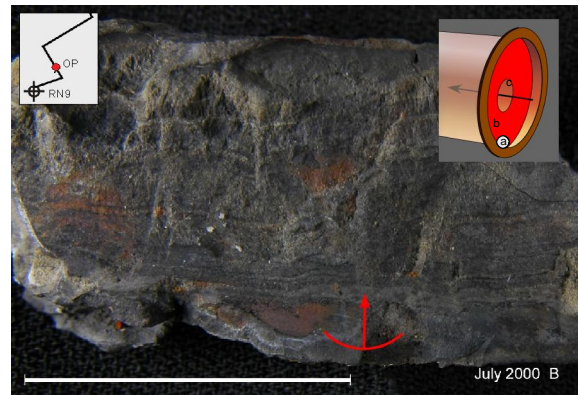
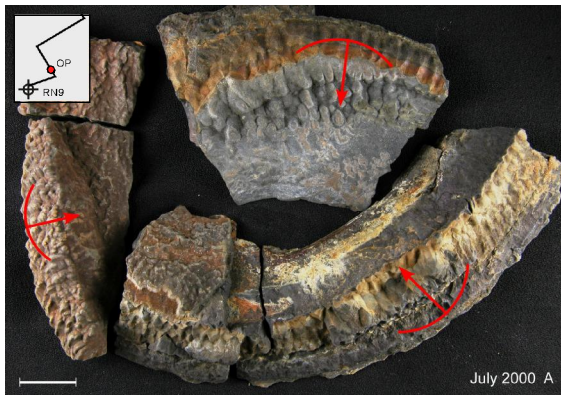


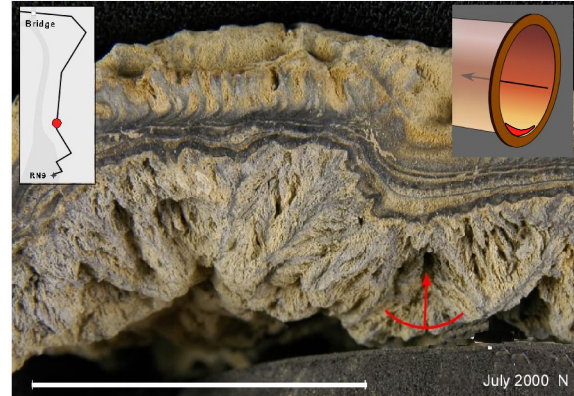
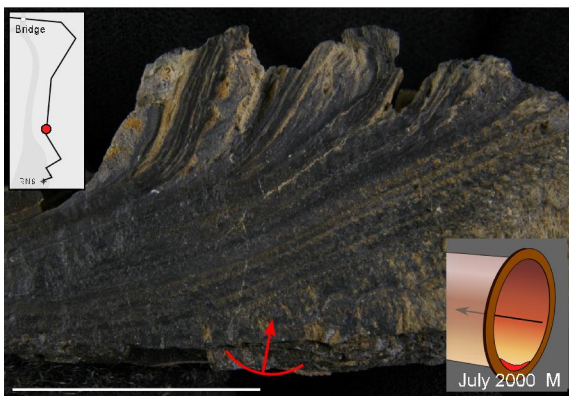
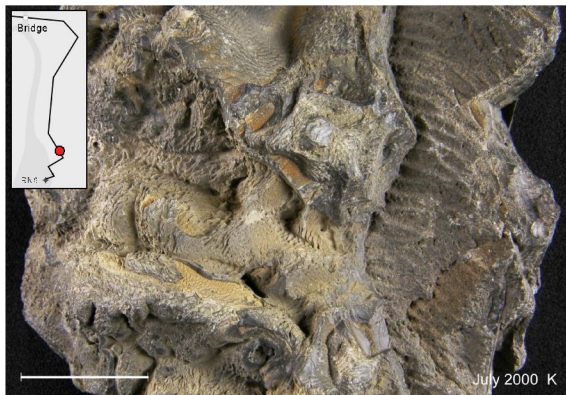
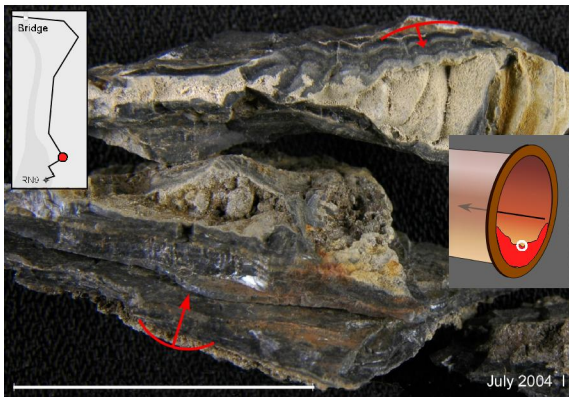
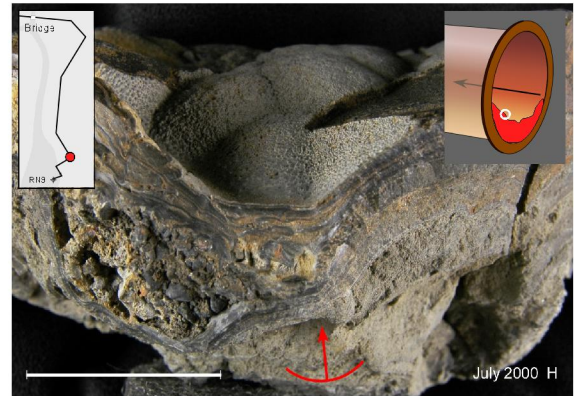
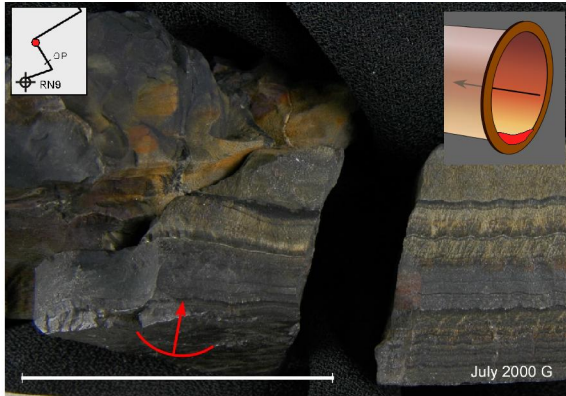


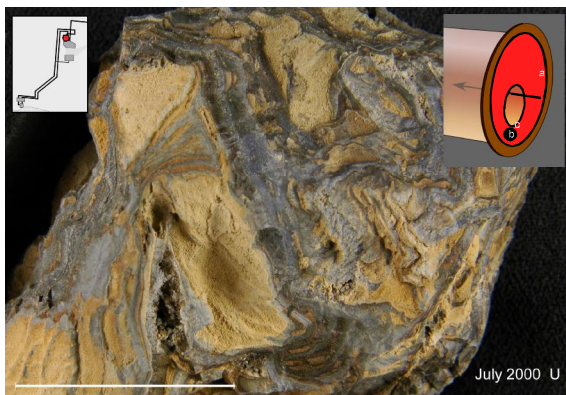
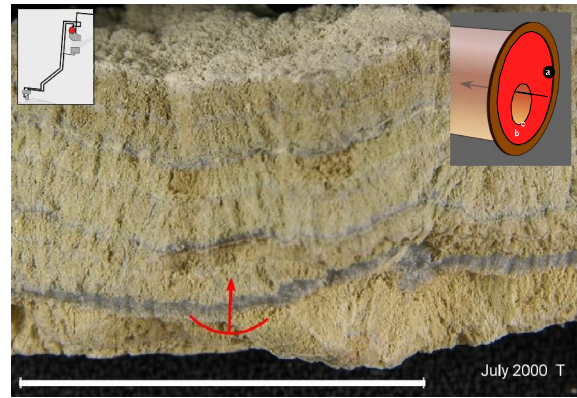
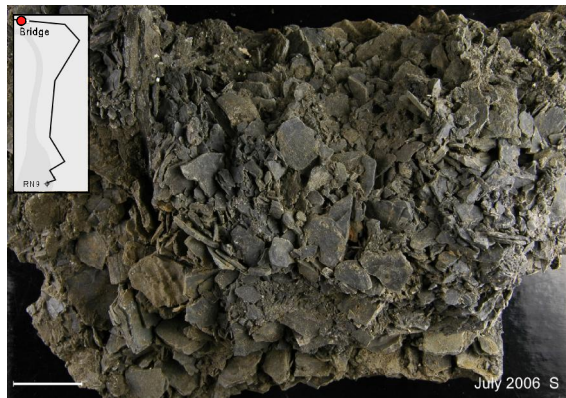
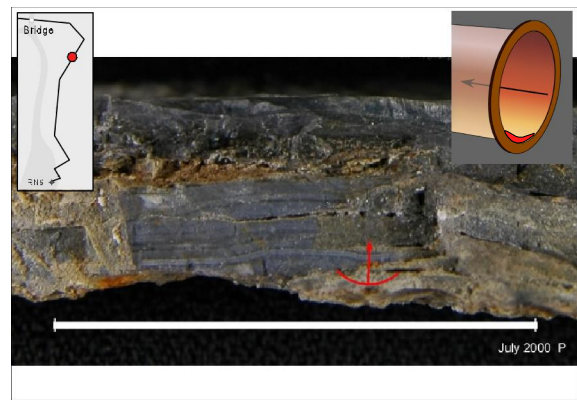
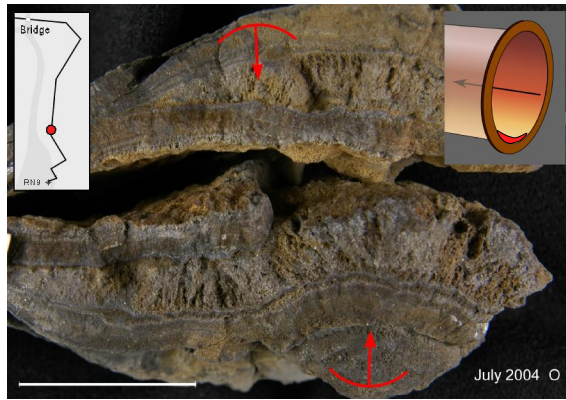
Figure 2.5. Photograph of scales in surface pipelines of well RN-9 and the Grey Lagoon. Diameter of the pipe in A is ~50 cm, M is ~30 cm, others ~40 cm. A) wellhead (wh) above the cellar. B) downstream (dst) of the wh. C) upstream (upst) of the orifice plate (op) ~12 m from wellhead, scale thickness <4 mm. D) downstream of op ~13 m from wh, opening of the fluid flow is ~10 cm; a-c sample locations. E) ~4 m from D, no opening for the fluid. F) bend three ~35 m from wh, downstream of location D, scale thickness ~10 cm. G) at bend four ~70 m from wh, downstream of location F, scale thickness ~2-3 cm. H) downstream of location G ~240 m from wh. I) ~270 m from wh. J) and K) at each side of the bridge ~300 m from the wh, scale thickness ~10 cm and ~4 cm. L) the liquid pipeline from the separation station (ss) ~350 m from wh, opening of the pipe was ~20 cm; a, b, c are sample locations. M) Same liquid pipeline as in L but closer to the vent house. N) Amorphous material from the Grey Lagoon.



Scale bar is 2 cm







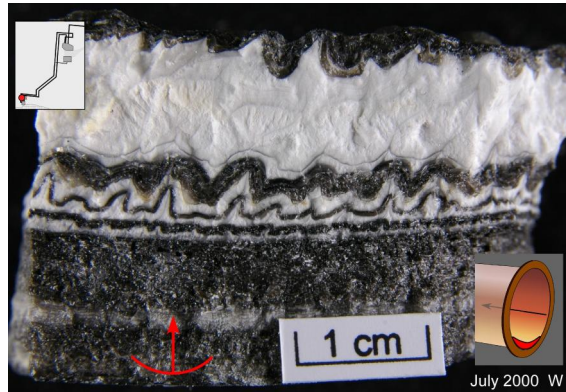


Figure 2.6. Representative samples of Group 2 (pressure 11 bar) and Group 3 (pressure 1 bar) scales from the surface pipeline of well RN-9, downstream of the orifice plate (op). The scale bar is 2 cm. Samples are presented from the orifice plate to the valve house. Group 2. A) Sample #31 from the orifice plate. B) #19, thin bands or layers parallel to the flow. C) #18, layers are thicker and bulbous due to growth of dendrites due to sudden change in temperature. White staining appeared after cleaning the sample with water and is probably salt. D) #16, elongated dendrites forming fans or ridges (or lobes). The orange colour is due to iron staining. Samples in B to D are from the same location (Fig. 2.5D), with B closest to the pipe wall, and D closest to the flow. E, F) #29, ~8 m downstream of the orifice plate, two views of the same sample. Layers are thin at the bottom and thicker in the upper part and coalesce. F to the left is closer to the flow showing cooling effects (cracks). Darker dots are remnants (?) of salt crystals. F to the right is the bottom part of scale with overlapping edges. G) #26 and 27, downstream of E ~12 m downstream of the op at the second bend showing horizontal layers or bands at various thickness to the right. The sample to the left shows thicker and more bulbous layers caused by the sudden increase of turbulence flow at the bend. H) #5. I) #1-2004 at the third bend downstream of sample #26 and 27, ~35 m from the op. Scales are more porous below a dense glassy (black) layer of amorphous Fe-Si (Table 2.3). Cavities contain clasts of layers from upstream scales and bigger crystals of sphalerite. J, K) #4, downstream and ~7 m from I and H. Sample mostly consists of amorphous silica and sphalerite laths. The surface is very uneven due to turbulent flow in the pipe. L) #stora, scale 40 cm long and 15 cm thick, ~8 m downstream of K. The scale is mostly layered amorphous material with a very porous structure and undulating surface. Clasts of scales from upstream are trapped in the layered material. M, N, and O) at bend four, ~70 m downstream of wellhead (wh), the scales consist of alternating layers of amorphous material with dendrites closer to the center of the pipe. The layers closer to the center of the pipe are broken (M). P is downstream of O, ~270 m from the wh and consists of a thin layer at the bottom of the pipe of amorphous material with clasts of scale from upstream. Q, R, S) 330 m downstream of the wh, the scales are ~10 cm thick and consist of casts of scales from upstream cemented by amorphous material (R is the top surface; S is the bottom surface). The scale alternates between dark gray and lighter coloured amorphous material. T, U, V) are from the same locations in front of the separation station but collected at different location in the pipe a, b and c shown in Fig. 2.5L. Complex overlapping layers are observed at the bottom of the pipe (U). The opening through the scale is 20 cm. Group 3. W) alternating layers of black amorphous Si (likely due to difference in particle size of the amorphous silica rather than opaque inclusions; Simmons and Browne, 2000) and white (pure amorphous silica). Scale bar is 2 cm long.

Group 1 scales formed from the wellhead to the orifice plate, representing the first 14 m of the surface pipe where the pressure was generally ~40 bar (252°C) (range 47 to 15 bar; ~262°C to 201°C, Fig. 2.3).

Group 2 scales formed on the downstream side of the orifice plate, where the pressure decreased sharply to ~11 bar (~188°C), and in the next ~348 m downstream of the orifice plate to the separation station (Figs. 2.6A-T).

Group 3 scales formed in the vent house (153 m downstream of the separation station) and at the Grey Lagoon (discharge pond), where the waste liquid was discharged to the surface at atmospheric pressure (Figs. 2.1, 2.5N, and 2.6T-W).

The scales in surface pipelines were collected at different times from 1993 until the well was closed in early 2004.

2.3.1 Group 1

Scales from Group 1 vary from a very fine black powder to gold- or green-colored stratified deposits, and locally brecciated sulfides, in layers <4 mm thick (Table 2.1). In thin section the minerals of the scale can be seen to have been deposited in alternating bands, <0.5 mm to 2 mm thick, of very fine-grained intergrowths and aggregates of anhedral sphalerite, chalcopyrite, ± bornite, ± galena. The sulfides are interlayered with Fe-rich amorphous silica bands. Coarser grained layers of the same minerals formed just in front of the orifice plate (upstream side: Figs. 2.7A-D). One sample collected during well logging came from inside the well somewhere above 450 m depth (sample 9RN08_2001).

2.3.2 Group 2

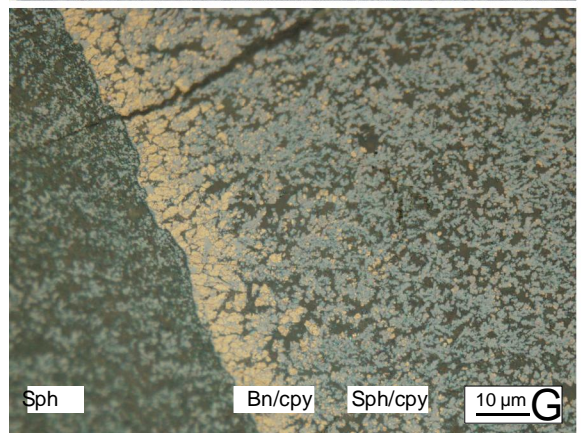
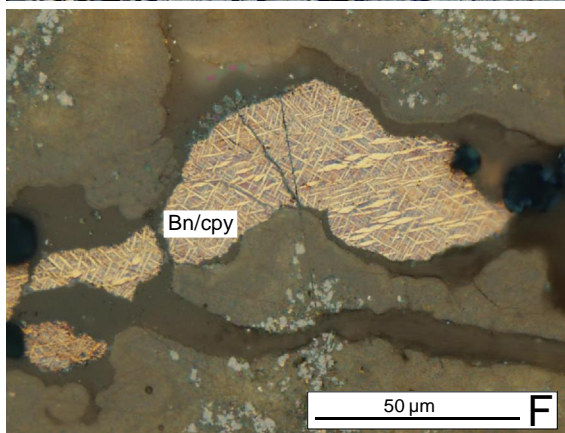
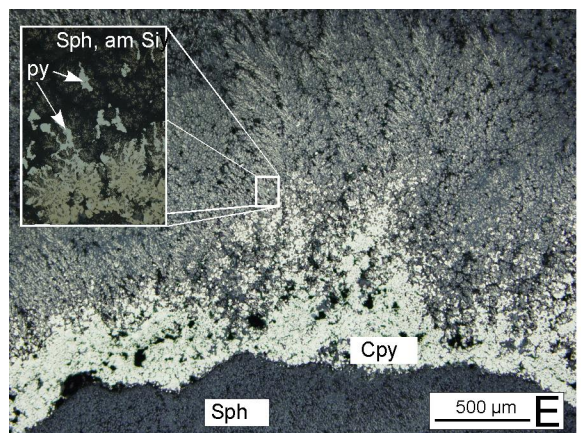
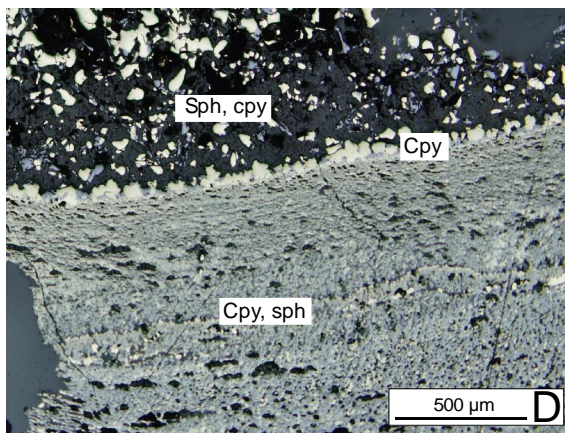
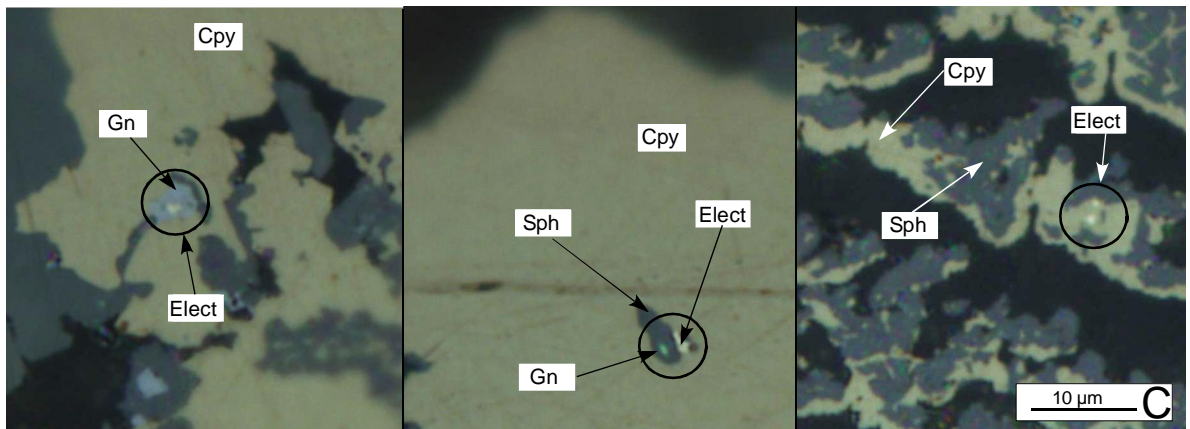
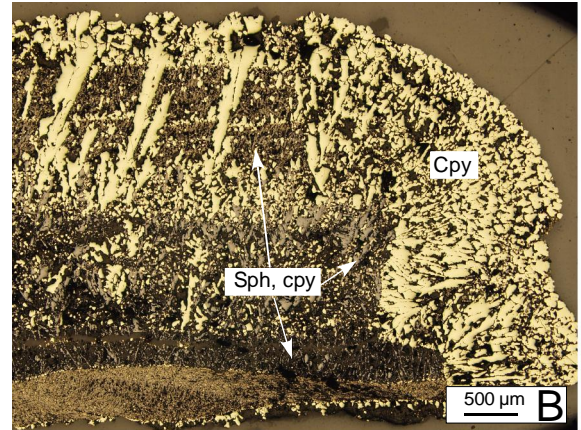
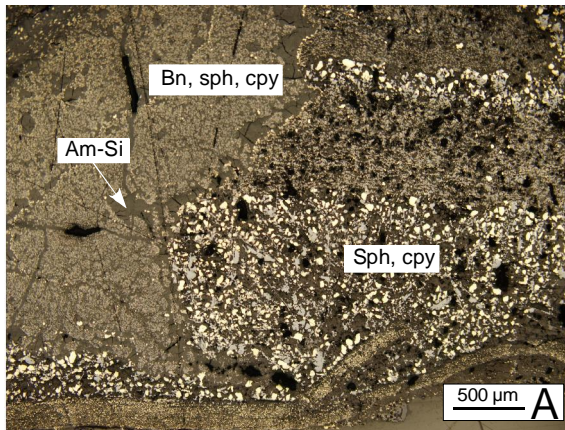
Group 2 scales are characterized by abundant amorphous silica with sulfides, mainly sphalerite and sparse chalcopyrite. The amount of amorphous silica increases downstream

of the orifice plate where it is least developed (Figs. 2.7E-L; Table 2.1). The very fine-grained orifice-plate sample consists of mainly sphalerite intergrown with bornite (?), locally chalcopyrite and trace galena (identified by XRD). Downstream from the orifice plate the scales form layers of very hard, glassy, bulbous precipitates of amorphous silica commonly containing dendrites of sphalerite (Fig. 2.5D, 2.6A, and 2.7). The layered scales consist of very fine, medium to light gray bulk precipitates that were overgrown by alternating dark gray to black, dense, vitreous layers. Sulfides include dendritic sphalerite with, traces of galena and minor chalcopyrite bands (Figs. 2.6B-D) locally grading into pyrite in the growth direction (Figs. 2.7E). The thickness of the layers increases inward toward the center of the pipe, where the thickest layers were typically <5 mm thick. The layers at the very bottom of the pipe conform to the curvature of the pipe (Fig. 2.6L, M, O). Broken layering is common next to the base adjacent to the pipe, where the clasts are commonly imbricated in the flow direction (Fig. 2.6F). Ten meters downstream of the orifice plate at bend 2 (Fig. 2.1), the layers contain abundant sphalerite, bornite and chalcopyrite, and became thicker and bulbous (Figs. 2.6G and 2.7G).

Table 2.1. Mineralogy of the scale samples from well RN-09

	Group 1	Group 2	Group 3
Temperature range (°C)	262-201	188	100
Pressure (bar)	47-15	11	1
sphalerite/ wurtzite (Zn,Fe)S	xx	xx	tr
chalcopyrite (CuFeS ₂)	xxx	x	
bornite (Cu ₅ FeS ₄)	tr	tr	
galena (PbS)	x		
covellite (CuS)	tr	tr	
pyrrhotite (Fe _{1-x} S _x)	tr	tr	
Ag+Au	tr	tr	
pyrite (FeS ₂)		tr	
amorphous phase (X-SiO ₂)	x	xxx	xxx
oxides		tr (?)	
clay	tr	tr	

Group 1 is from the wellhead and upstream of orifice plate. Group 2 is from the orifice plate and 350 m downstream. Group 3 is from the Vent house and Gray Lagoon. xxx, abundant; xx, major; x, minor; tr, trace



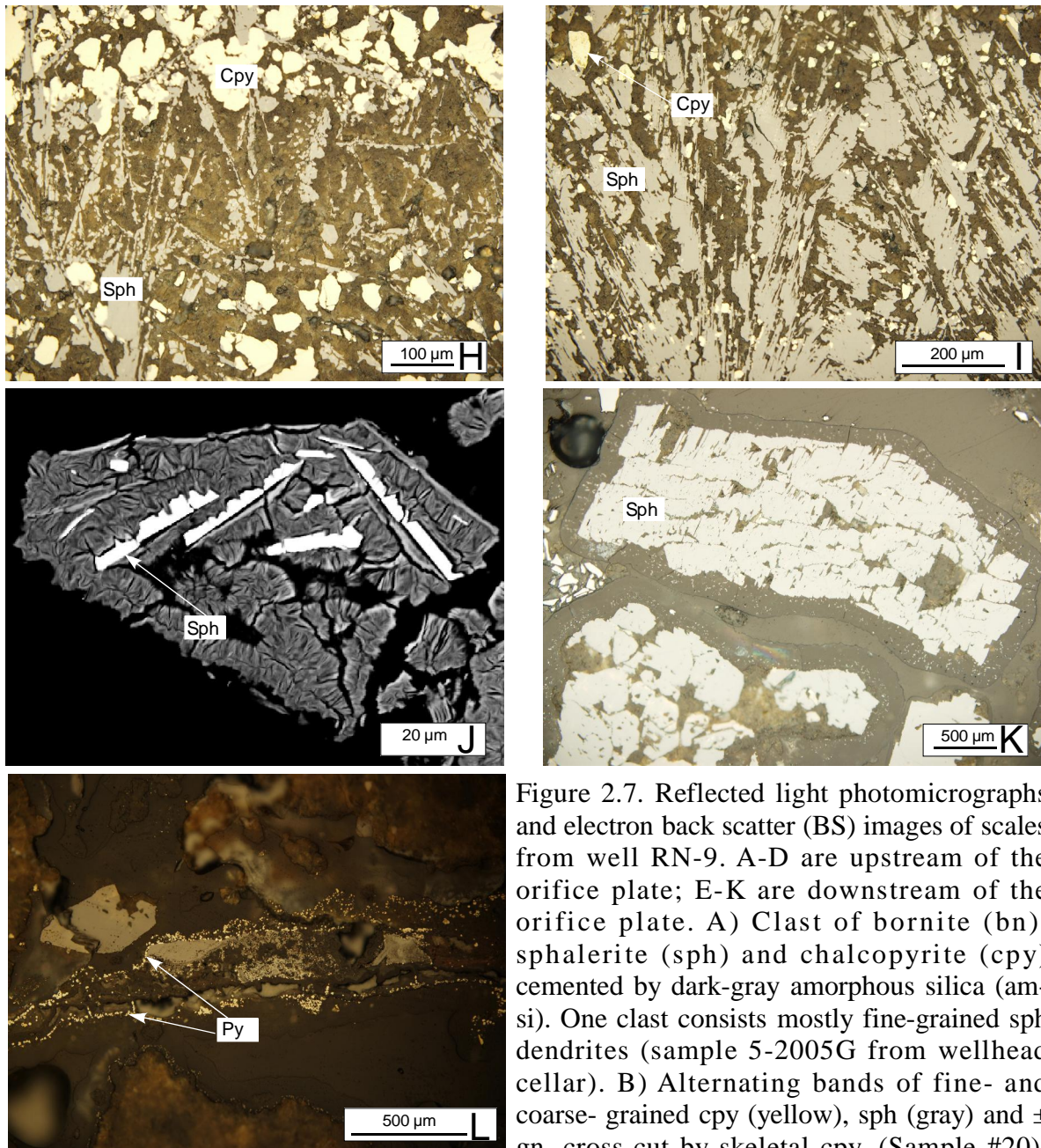


Figure 2.7. Reflected light photomicrographs and electron back scatter (BS) images of scales from well RN-9. A-D are upstream of the orifice plate; E-K are downstream of the orifice plate. A) Clast of bornite (bn), sphalerite (sph) and chalcopyrite (cpy) cemented by dark-gray amorphous silica (am-si). One clast consists mostly fine-grained sph dendrites (sample 5-2005G from wellhead cellar). B) Alternating bands of fine- and coarse-grained cpy (yellow), sph (gray) and \pm gn, cross-cut by skeletal cpy. (Sample #20).

C) Electrum (black circle). D) Two layers consisting of sph and cpy of various crystal size divided by band of mainly cpy. The lower layer consists of cpy moulded on sph. E) Dendritic layer of sph in amorphous groundmass, followed by cpy layer with few irregularly shaped py crystals (lighter yellow colour). Sample #29. F) Bn with exsolution lamellae of cpy (sample #19). G) Band of bn in between sph layers. Blue color is secondary cv (?) (sample #26). H and I) show skeletal partly dendritic sph in partly crystallized clay (?) groundmass. J) BS image of sph needles in a poorly crystallized clay matrix (sample #3-2006). K) Large crystals of sph, rimmed by amorphous material containing much smaller sph crystals (sample #3-2006). L) Pyrite crystals surrounding or nucleating on a fragment consisting of mostly very fine-grained sphalerite. Sample 40M_2000.

Between bend 3 and bend 4 (~30 to 63 m downstream of orifice plate) the thickness of the scales was 5 to 15 cm (Figs. 2.6H, L). At bend 3, only the most recently deposited scales, closest to the flow, were collected. These samples consisted of porous amorphous silica with discontinuous bands of chalcopyrite (<1 mm thick) and layers of dendritic sphalerite. Further downstream the scale thickness gradually decreased to ~1 cm close to bend 6 but then increased to 10 cm in a depression close to the bridge at the lowest point of the pipe (Fig. 2.1 and 2.2), ~300 m downstream of the orifice plate. Here the scales consisted mainly of fragile, brown to dark grey breccias cemented by amorphous silica (Figs. 2.2, 2.5 and 2.6Q-S). The increase in thickness was apparently due to settling of material at the lowest point of the pipe (Figs. 2.6Q-S). Layered scales up to 15 cm thick are medium gray and glassy, with a high porosity (Fig. 2.6L). Pieces of scales dislodged from further upstream were commonly stacked in open spaces. These scales were yellow to yellowish-brown to various shades of black in thin section. Further downstream (~150 m from the orifice plate), the scales diminished to less than 1 cm-thick and consisted of light-brown layers of dendritic amorphous silica (Figs. 2.6M-P).

The scales downstream from the separation station were collected from the waste liquid pipeline, where the temperature was ~180°C. The pressure in this pipe was controlled by a valve in the valve house and was the same as in the turbine, ~11 bar (Figs. 2.6T-V). Samples taken at one location in the pipe were thinly layered, alternating between light colors dominated by amorphous silica and dark gray to black layers of amorphous silica with traces of sphalerite, pyrite, chalcopyrite and galena.

2.3.2 Group 3

The scales from the vent house (Fig. 2.6W) were deposited in the liquid pipe (diameter ~16 cm; Figs. 2.5L-M and 2.6U-V), which led to the silencer and then to the discharge pool (Grey Lagoon: Fig. 2.2). The pressure was typically close to atmospheric but varied depending on whether the valve in this pipe was completely open (atmospheric pressure) or partly closed (higher but unknown pressure). The scale was ~3 cm thick and consisted mainly alternating layers, from <1 mm up to 1 cm, of dark gray to black and white amorphous silica with a trace of sphalerite (Figs. 2.5N and 2.6W). The samples from the Gray Lagoon, an open pool, were soft amorphous silica.

2.4. Mineralogy, Mineral Chemistry, and Paragenesis of Scales in RN-9

Cross-sectional slices of scale samples were cut for thin sections (Figs. 2.6A-W). Reflected- and transmitted-light microscopy, XRD, and scanning electron microscopy (SEM), were used for mineral identification and textural interpretation. Microprobe analyses were carried out on sphalerite/wurtzite, chalcopyrite, galena, pyrrhotite, pyrite, electrum, oxides, clays and the matrix of the Fe-rich amorphous silica.

The metallic minerals consist mainly of sphalerite and chalcopyrite, in a matrix of Fe-rich amorphous silica and smectite, with traces of galena, bornite, pyrrhotite, pyrite, electrum, and oxides. Generally the minerals are finely crystalline, ~5-50 μm in size, although larger crystals in the range of 20 to 200 μm (maximum 2000 μm) were found upstream of the orifice plate. Larger crystals also occurred locally at bends in the pipe downstream of the orifice plate (i.e., where the surfaces were sheltered from laminar flow), and in cavities of brecciated samples further downstream. The scales precipitated directly on the orifice plate and on the wall of the pipe immediately downstream of the orifice plate

show an intimate intergrowth of sphalerite, bornite, and chalcopyrite, indicating coprecipitation of sulfides (Fig. 2.7G).

2.4.1 Amorphous phases

Amorphous silica of low density constitutes most of the principal scale downstream of the orifice plate (up to 93 wt.% SiO₂ depending on sample location). In XRD analyses the typical opal hump (termed amorphous silica in text) was first identified in samples at the bend 2 in the pipe, or about 10-12 m downstream of the orifice plate and is seen in all samples downstream of bend 2. The term Fe-silica refers to Fe rich masses (FeO_t = 10 wt.%) rich in silica but lacking the typical opal hump (in XRD).

2.4.2 Sphalerite

Sphalerite [(ZnFe)S] is the major sulfide mineral in the scales (Table 2.1) and was commonly the first sulphide mineral to precipitate, as indicated by overgrowths of chalcopyrite and other minerals, both upstream and downstream of the orifice plate.

In Group 1 scales (pressure ~40 bar) sphalerite occurs as fine grains (<4 µm across) intergrown with chalcopyrite ±galena and locally with bornite (Fig. 2.7G). The fine-grained sphalerite crystals commonly occur in elongate aggregates and/or dendritic branches (Fig. 2.7E). Irregularly shaped, skeletal laths, 20 to 200 µm in length, are also common (Fig. 2.7H). Some skeletal crystals upstream of the orifice plate are distinctly V-shaped and up to 100 x 1000 µm in size (Fig. 2.7I); locally whole euhedral crystals also occur.

Downstream of the orifice plate in Group 2 samples (pressure ~11 bar), sphalerite occurs as small needles and as anhedral grains in the Fe-bearing amorphous silica. The scales immediately downstream of the orifice plate are much denser and contain more very

fine-grained sphalerite and extremely fine-grained chalcopyrite and bornite than the scales further downstream (Figs. 2.7E, G).

At bend 3, the sphalerite crystals form laths with saw-tooth-like margins (Figs. 2.7H, J), commonly $4 \times 20 \mu\text{m}$ across and aggregates with hexagonal outline, up to $2000 \mu\text{m}$ across, composed of groups of smaller crystals (Fig. 2.7K). These crystal habits might indicate early stages of wurtzite growth. These larger aggregates mostly occur in lees and voids between scale fragments. At the separation station, sphalerite crystals occur as small anhedral grains.

Microprobe analyses (methodology summarized in Appendix 2.2.1) of sphalerite from Group 1 (~40 bar) and Group 2 scales (~11 bar) indicate a uniform composition upstream of the orifice plate, with Fe contents of ~3 wt%, whereas downstream of the orifice plate sphalerite has higher Fe contents of ~5 to 8.5 wt.% (Fig. 2.8, Tables 2.2 and A2.4). The sphalerites furthest downstream at the bridge location of RN-9 are the most Fe-rich (Fig.

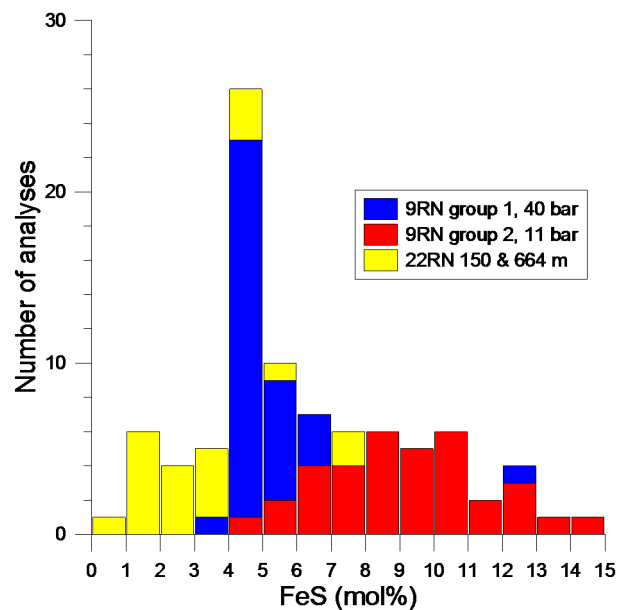


Figure 2.8. Mole % FeS in sphalerite in scales from downhole RN-22 and in the surface pipeline of RN-9 from group 1 (~40 bar) and 2 (~11 bar) showing the increase in Fe content in group 2.

Table 2.2 Compositions of minerals in scales from surface pipelines from well RN-9

Sample No.	Group	Well RN-9	Zn	Fe	Cu	Pb	S	Au	Ag	As	Sb	Co	Se	Ni	Cd	Te	Mn	Bi	Total	
			wt%																	
Wellhead																				
9RN5-2005	1	sphalerite	64.56	3.27	-	<0.01	32.14	<0.01	<0.02	0.02	0.01	0.03	0.07	0.03	0.03	0.03	0.05	--	100.22	
9RN5_2005G	1	sphalerite	63.21	3.51	-	0.09	33.61	<0.01	<0.01	<0.01	0.01	0.01	0.09	<0.01	0.14	<0.01	0.05	--	100.72	
9RN1_2005G	1	sphalerite	58.12	7.54	-	0.21	33.71	<0.01	0.01	<0.01	<0.01	0.01	0.03	0.01	0.22	0.03	0.13	--	100.02	
9RN1_2005G	1	sphalerite	62.29	4.03	-	0.61	32.44	<0.01	0.03	<0.01	<0.01	<0.01	0.06	<0.01	0.16	<0.01	0.07	--	99.69	
		~ 13 m downstream of wh, upstream of orifice plate (OP), 47-15 bar																		
9RN20_2000	1	sphalerite	64.68	3.30	-	0.02	32.71	<0.01	<0.01	0.02	<0.01	0.02	0.05	0.01	0.06	0.03	0.04	--	100.91	
9RN21_2000	1	sphalerite	63.88	3.22	-	0.09	33.43	<0.01	0.01	0.05	0.02	0.01	0.09	0.02	0.07	0.02	0.07	--	100.98	
9RN21C-2000	1	sphalerite	65.01	2.70	-	0.18	33.18	<0.01	<0.01	0.05	<0.01	0.02	0.08	<0.01	0.10	0.01	0.07	--	101.38	
9RN21C_2000	1	sphalerite	63.62	2.58	-	<0.01	33.56	<0.01	<0.01	<0.01	0.03	<0.01	0.07	0.01	0.06	<0.01	0.07	--	100.00	
		~30-70 m downstream of OP, ~11 bar																		
9RN1_2004_2	2	sphalerite	63.27	3.17	-	0.02	33.03	<0.01	<0.01	0.03	0.01	0.01	0.11	<0.01	0.19	<0.01	0.07	--	99.88	
9RN1_2004_2	2	sphalerite	61.04	5.36	-	0.22	33.17	<0.01	0.06	0.03	<0.01	<0.01	0.08	<0.01	0.51	0.01	0.15	--	100.63	
9RN4B_2000	2	sphalerite	62.84	3.77	-	0.17	32.21	<0.01	<0.01	<0.01	<0.01	0.01	0.09	<0.01	0.41	<0.01	0.12	--	99.61	
9RN4B_2000	2	sphalerite	60.93	4.79	-	<0.01	32.92	<0.01	<0.01	<0.01	<0.01	0.01	0.09	<0.01	0.40	0.01	0.10	--	99.25	
		~250 m downstream of OP, the bridge, ~11 bar																		
9RN-3-2006	2	sphalerite	61.94	5.38	-	0.09	32.49	<0.01	0.02	0.03	0.02	0.03	0.05	0.01	0.39	0.03	0.08	--	100.55	
9RN3_2006	2	sphalerite	61.37	5.21	-	0.12	32.27	<0.01	<0.01	<0.01	<0.01	0.02	0.05	<0.01	0.45	0.01	0.09	--	99.60	
9RN-3-2006	2	sphalerite	58.48	7.22	-	<0.01	33.15	<0.01	<0.01	0.01	<0.01	0.04	0.08	<0.01	0.23	<0.01	0.12	--	99.33	
		Well RN-9																		
9RN5_2005G	1	chalcopyrite	0.86	30.50	33.62	0.40	35.26	<0.01	<0.01	<0.01	<0.01	0.01	<0.01	0.01	<0.01	0.02	0.01	--	100.69	
9RN09_2001	1	chalcopyrite	<0.01	31.55	34.60	0.03	34.31	<0.01	0.02	0.02	<0.01	0.02	<0.01	0.01	<0.01	<0.01	0.01	--	100.57	
9RN09_2001	1	chalcopyrite	0.07	31.36	35.08	<0.01	34.28	<0.01	<0.01	<0.01	<0.01	<0.01	0.03	<0.01	<0.01	0.02	0.01	--	100.85	
9RN20_2000	1	chalcopyrite	0.17	31.34	33.31	0.07	34.83	<0.01	<0.01	<0.01	<0.01	<0.01	0.06	<0.01	0.01	0.02	0.01	--	99.82	
9RN20_2000	1	chalcopyrite	0.10	31.31	34.00	0.03	34.28	<0.01	0.02	0.04	<0.01	<0.01	0.03	<0.01	<0.01	<0.01	0.02	--	99.83	
9RN1_2004_2	2	chalcopyrite	0.19	29.75	34.43	0.20	33.96	0.20	0.05	<0.01	<0.01	<0.01	0.03	<0.01	<0.01	0.02	0.05	--	98.88	
		Well RN-9																		
9RN23	1	galena	1.05	1.73	2.76	87.14	13.36	0.50	1.01	0.04	<0.01	0.01	0.53	<0.01	0.04	0.07	<0.01	<0.01	108.23	
9RN23	1	galena	1.72	0.95	1.42	87.94	13.34	<0.01	0.02	<0.01	<0.01	<0.01	0.53	0.03	<0.01	<0.01	<0.01	<0.01	105.96	
9RN23	1	galena	2.36	1.86	2.63	83.65	13.94	0.10	0.23	<0.01	<0.01	0.02	0.28	0.03	<0.01	<0.01	0.03	<0.01	105.10	
9RN23	1	galena	4.32	0.82	1.11	83.44	12.76	0.05	0.31	0.01	<0.01	0.03	0.71	<0.01	<0.01	<0.01	0.03	<0.01	103.59	
9RN23	1	galena	0.76	2.97	3.98	77.18	12.95	0.05	1.00	<0.01	0.02	0.03	0.41	<0.01	0.02	0.10	<0.01	<0.01	99.46	
9RN5_2005G	1	galena	2.71	2.56	0.63	79.94	13.39	<0.01	0.08	<0.01	<0.01	<0.01	0.24	<0.01	<0.01	<0.01	0.03	<0.01	99.58	

Table 2.2. (continued)

Sample No.	Group	wt%														Total wt%			
		Zn	Fe	Cu	Pb	S	Au	Ag	As	Sb	Co	Se	Ni	Cd	Te		Mn	Bi	
9RN2005G	1	pyrrhotite	0.22	61.51	0.14	0.30	38.23	0.04	0.08	0.03	<0.01	0.01	<0.01	0.03	0.01	0.04	0.02	--	100.64
9RN5_2005G	1	pyrrhotite	0.34	64.26	0.09	0.04	38.32	<0.01	<0.01	<0.01	<0.01	<0.01	<0.01	0.01	0.02	0.01	0.01	--	103.10
9RN5_2005G	1	pyrrhotite	0.45	61.91	0.11	0.34	37.28	<0.01	0.08	0.03	<0.01	0.01	<0.01	<0.01	<0.01	0.04	<0.01	--	100.25
9RN5_2005G	1	pyrrhotite	0.23	59.37	2.53	0.56	34.88	0.10	0.05	<0.01	<0.01	<0.01	<0.01	0.01	0.08	<0.01	0.05	--	97.86
9RN5_2005G	1	pyrrhotite	0.25	60.72	1.50	0.26	36.58	<0.01	0.03	0.05	<0.01	<0.01	<0.01	0.01	0.07	0.05	0.04	--	99.56
9RN1_2005G	?	pyrrhotite	0.04	61.11	0.16	0.25	38.54	0.03	<0.01	0.02	<0.01	<0.01	<0.01	0.03	<0.01	<0.01	0.02	--	100.20
9RN1_2005G	?	pyrrhotite	0.17	61.50	0.11	<0.01	38.87	0.05	<0.01	<0.01	<0.01	<0.01	<0.01	0.03	0.01	<0.01	<0.01	--	100.74
		Well RN-9																	
9RN14	2	pyrite	0.11	46.21	1.47	<0.01	54.68	<0.01	0.04	0.03	<0.01	<0.01	<0.01	<0.01	<0.01	<0.01	0.05	0.23	102.83
9RN14	2	pyrite	0.14	45.64	0.78	0.02	53.36	<0.01	0.16	0.01	<0.01	<0.01	<0.01	0.02	0.05	0.03	0.02	0.15	100.38
9RN14	2	pyrite	0.03	46.33	0.55	0.21	53.57	<0.01	0.08	0.01	<0.01	<0.01	<0.01	<0.01	<0.01	<0.01	0.06	0.21	101.05
9RNstora	2	pyrite	0.13	44.26	1.64	0.03	51.79	<0.01	0.01	0.15	<0.01	<0.01	<0.01	0.02	<0.01	<0.01	0.09	0.27	98.42
		Well RN-9																	
9RN1_2004	1	maghemite	<0.01	67.35	<0.01	0.12	0.03	<0.01	<0.01	<0.01	<0.01	<0.01	<0.01	0.02	<0.01	<0.01	<0.01	--	67.52
9RN1_2004	1	maghemite	0.04	65.48	<0.01	<0.01	0.03	0.03	0.04	<0.01	<0.01	<0.01	<0.01	<0.01	<0.01	<0.01	0.06	--	65.70
9RN21	1	smithsonite	61.92	3.12	0.03	<0.01	<0.01	<0.01	<0.01	<0.01	<0.01	<0.01	<0.01	0.02	<0.01	<0.01	0.05	--	65.14

-- Not measured

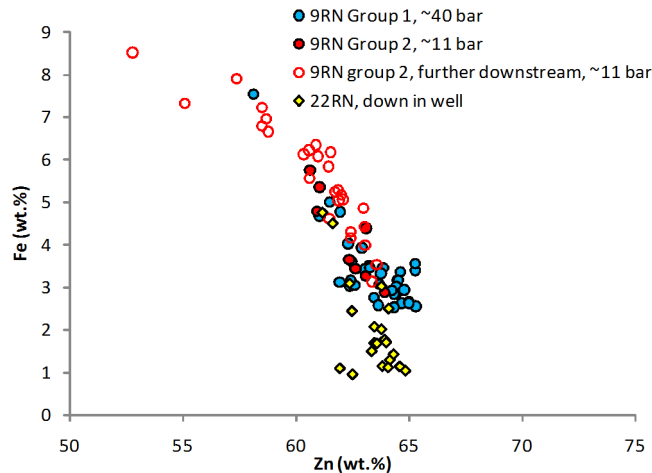


Figure 2.9. Correlation between Fe and Zn concentrations in sphalerite, showing Fe substitution for Zn in the sphalerite structure. The data are from scales collected at 150 and 670 m depth in well RN-22 and the surface pipeline of RN-9 from group 1 (~40 bar) and 2 (~11 bar).

2.9). Cadmium contents average 0.23 wt.% (range 0.03 to 0.51 wt.%; Fig. 2.10) and Se contents are 0.02-0.13 wt% (Fig. 2.11). A trace of Mn (~0.07 wt.%) was also found in the sphalerites, as well as Cu and Pb, probably due to sub-microscopic inclusions of chalcopyrite and galena. About one third (22 of 69 analyses) of the sphalerite grains also contain Ag, up to 0.16 wt.%, most likely present as sub-microscopic inclusions of native silver or Ag-rich galena.

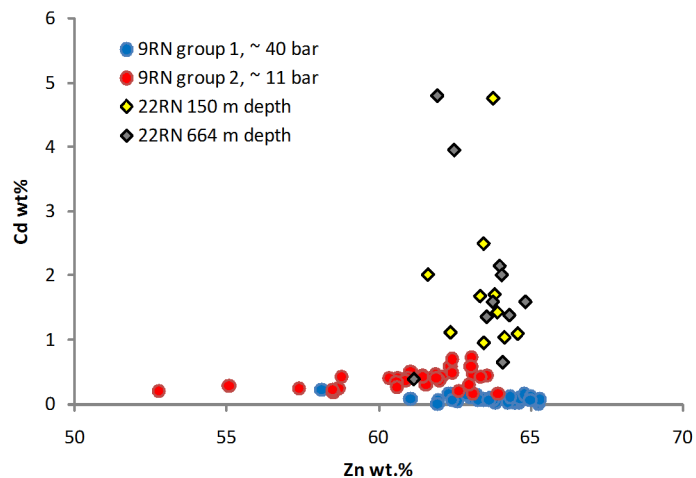


Figure 2.10. Zinc versus Cd (wt.%) in sphalerite in scales from downhole RN-22 and in the surface pipeline of RN-9 from group 1 (~40 bar) and 2 (~11 bar) showing the decrease in Cd with increasing Fe content.

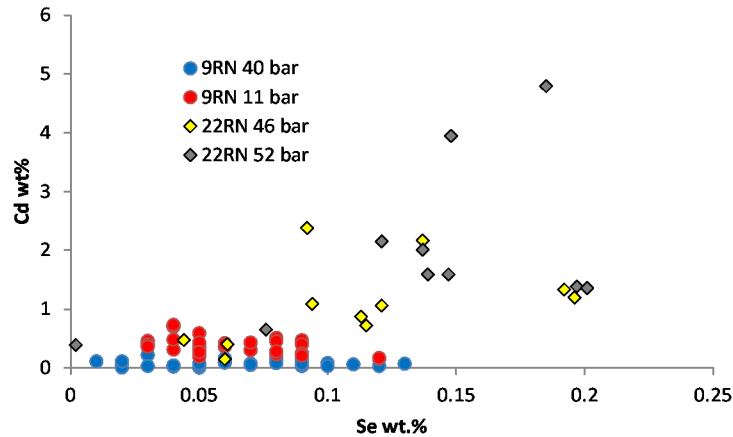


Figure 2.11. Selenium versus Cd (wt.%) in sphalerite in scales from downhole RN-22 and in the surface pipeline of RN-9 from group 1 (~40 bar) and 2 (~11 bar) showing an apparent increase in Se content with increasing Cd content.

2.4.3 Chalcopyrite

Chalcopyrite (CuFeS_2) occurs in all RN-9 samples; it is abundant at the wellhead and upstream of the orifice plate (Group 1), decreasing downstream towards bend 3 (Group 2 ~30 m downstream of orifice plate), with only traces found in the valve house (Group 3: Table 2.1). Upstream of the orifice plate chalcopyrite coprecipitated with sphalerite, as indicated by the intimate intergrowth of these minerals (Fig. 2.7E). Locally, chalcopyrite precipitated with bornite, galena, and pyrite.

In Group 1 scales, chalcopyrite occurs as anhedral grains, ~2 μm across, and skeletal laths or blades, 1200 x 100 μm , growing across several layers perpendicular to the layering (Fig. 2.7B). The smallest crystals are commonly overgrown by bornite and sphalerite. Upstream of the orifice plate, chalcopyrite typically forms monomineralic bands, 20 to 200 μm thick (Fig. 2.7B, C). In Group 2, downstream of the orifice plate, the chalcopyrite crystals are smaller, mainly ~2-4 μm in size, and form elongated dendrites intergrown with sphalerite \pm bornite \pm pyrite (Fig. 2.7E). Thirty m downstream of the orifice plate, chalcopyrite occurs only as trace disseminations, up to 30 μm across, and as more angular crystals in lees of fluid flow at bends in the pipe.

The chalcopyrite crystals in Group 1 are close to stoichiometric CuFeS_2 in composition (Table 2.2). Trace element concentrations are typically < 0.05 wt%, except for Zn and Pb, which are up to 1 wt.% and most likely represent inclusions of sphalerite and galena. Other elements detected are Mn (up to 0.05 wt.%) and Se (up to 0.06 wt.%), possibly in inclusions of sphalerite and galena. Traces of Te, Co and Ni were also identified, close to the detection limits of the microprobe (~ 0.01 wt.%). Gold and Ag are present as inclusions in the chalcopyrite and were detected at concentrations up to 0.2 wt.% and 0.05 wt.%, respectively.

2.4.4 Galena

Galena (PbS) is present only as a trace mineral in the first 14 m of the pipeline, upstream of the orifice plate (Group 1), and was mainly identified by XRD analyses in Groups 2 and 3 (~ 11 bar). Where observed, galena precipitated after sphalerite and chalcopyrite (at the rims) as small crystals from 2 to 25 μm (typically ~ 5 μm), and seldom as individual grains except in scales upstream of the orifice plate. At the wellhead galena occurs as anhedral, irregularly shaped grains, interstitial to and at the rims of sphalerite and/or chalcopyrite crystals (Fig. 2.7D), or isolated in Fe-rich silica.

Microprobe analyses of galena were complicated by the small grain size and contamination by sphalerite, chalcopyrite and possibly bornite (Table 2.2). Se (up to 0.7 wt.%) and up to 1 wt% Ag may be present as sub-microscopic silver grains or selenides.

2.4.5 Bornite

Due to the very small grain size, much of the bornite (Cu_5FeS_4) in RN-9 scales was identified only by X-ray diffraction (XRD). Chemical analyses of the bulk scale and normative calculations (see 2.7) suggest that bornite should be more abundant than is observed under the microscope. Bornite occurs only as a trace constituent intimately

intergrown with chalcopyrite and sphalerite with a characteristic pink-bluish to brick red color (Fig. 2.7G). Bornite occurs in samples from the wellhead (Group 1) as lamellae within chalcopyrite grains, on and around the orifice plate (Fig. 2.7F), and at bend 2 (Group 2, ~10 m downstream of the orifice plate, sample #26, Fig. 2.7G). Immediately downstream of the orifice plate, bornite occurs as individual grains $<3 \mu\text{m}$ across in amorphous silica; however, at bend 2 it forms discontinuous bands, up to $150 \mu\text{m}$ thick (Fig. 2.7G) in concave features, together with chalcopyrite and sphalerite dendrites. Visible bornite also occurs in cavities 150 m downstream of the orifice plate.

The intimate intergrowth of bornite with chalcopyrite in RN-9 makes a clear paragenetic relationship difficult to determine, but locally chalcopyrite is seen to rim the bornite, suggesting that bornite precipitated before chalcopyrite. At the wellhead, bornite surrounds sphalerite grains, replaces larger chalcopyrite crystals, and occurs in fractures.

2.4.6 Pyrrhotite

Pyrrhotite ($\text{Fe}_{1-x}\text{S}_x$) occurs only as a trace mineral at the well head and 1 m downstream of the well head. It occurs in amorphous iron silica at the bottom of the pipe, in layers close to the fluid flow, and locally in fractures in these scales. Pyrrhotite forms needles up to $40 \times 6 \mu\text{m}$ in size or hexagonal or rectangular shapes, $36 \times 25 \mu\text{m}$.

The analyzed pyrrhotite has a range of compositions ($\text{Fe}_{0.91-0.98}\text{S}$; Table 2.2), with Fe/(Fe+S) mole ratios between 0.46 and 0.49, however, most of the analyses are contaminated by chalcopyrite, sphalerite and galena.

2.4.7 Pyrite

Pyrite (FeS_2) occurs primarily ~5 m downstream of the orifice plate, where it locally overgrows dendritic chalcopyrite (Fig. 2.7E). Typically it is euhedral and fine grained

(~5µm). Further downstream it occurs in small aggregates, commonly in concave features, as discontinuous bands in an amorphous silica coating, as inclusions in sphalerite (Fig. 2.7L), and after chalcopyrite (Fig. 2.7E). A few grains of marcasite are also present.

Microprobe analyses of pyrite indicate 0.5 to ~1.5 wt% Cu and up to 0.14 wt% Zn, likely due to contamination. Silver and As are up to 0.16 wt% and Pb up to 0.2 wt%. Mn contents are less than 0.1 wt.% and Ni and Se are still lower (Table 2.2).

2.4.8 Gold

Minute grains of electrum or native gold are common in the Group 1 samples (Fig. 2.7D). These grains are typically <2 µm in diameter but locally as large as 4 µm. They occur as inclusions in chalcopyrite and sphalerite but occur mainly in chalcopyrite bands and commonly are associated with galena. Gold likely co-precipitated together with these three minerals. Only two grains were seen downstream of the orifice plate in the first-formed chalcopyrite band (closest to the wall of the pipe). Only two grains could be analysed by microprobe, with Au/Ag ratios of 0.34 and 0.60, indicating electrum.

2.4.9 Other minerals

Anglesite (PbSO₄) and cotunnite (PbCl₂) were identified by XRD, both upstream and downstream of the orifice plate, as well as natokite (CuCl) and other salts, halite (NaCl) and sylvite (KCl), most likely formed due to evaporation of the hot liquid when the pipe was being opened. Anglesite and cotunnite are secondary products from Pb and Cu sulfides and occur in samples that could have been in the pipe from early production years (as early as 1983).

A poorly crystallized clay mineral was found upstream and downstream (~150 m and ~240 m) of the orifice plate and identified as smectite by XRD. Electron microprobe

Table 2.3. Representative semiquantitative microprobe and SEM analysis⁽¹⁾ of amorphous Fe-rich silica (silicate?) from well RN-9. The samples are from wellhead (#08_01 and #09_01) and upstream in front of the orifice plate #21 and #23

Sample	SiO ₂	Al ₂ O ₃	MgO	FeO
No. 9RN23	wt%	wt%	wt%	wt%
23_145*	9.3	53.6	1.3	10.9
23_147*	4.5	45.1	0.7	10.4
23_158*	11.4	46.7	3.0	9.1
23_140*	46.5	4.6	9.2	24.7
23_141*	46.7	4.5	9.2	24.7
23_142*	46.7	4.3	10.0	24.1
23_144*	40.7	4.5	9.0	24.7
23_151*	44.8	4.7	9.6	23.2
23_152*	45.9	4.9	9.9	22.8
23_153*	44.1	4.9	9.8	23.9
23_154*	45.5	5.8	9.6	22.3
23_157*	43.4	4.9	9.4	21.4
23_161*	45.0	4.8	9.5	23.5
23_162*	43.8	5.2	9.5	22.5
23_163*	40.7	5.6	9.2	22.5
08_01**	41.9	4.5	11.6	20.3
09_01**	58.1	3.0	16.0	17.0
21_00**	34.8	4.5	8.7	19.7

*Microprobe; **SEM Scanning electron microscope; ⁽¹⁾Other elements analyzed are Cl, Na, K, Ca, Mn, Cu, Zn and S, all <1 wt.%

analyses of this material upstream of the orifice plate indicate a highly variable composition (Fig. 2.12, Table 2.3). The most likely origin of this material is from the transformation of amorphous iron-rich silica to poorly crystallized smectite and opaline silica. Montmorillonite (smectite) is also the dominant sheet silicate in the Reykjanes drill-cuttings, formed at temperatures up to ~200°C (Tómasson and Kristmannsdóttir, 1972).

2.4.10 Oxide minerals

A light-gray material with blue to pinkish tint, at bend 3 (~30 m downstream of the orifice plate; Group 2) has been tentatively identified as maghemite. It has an Fe concentration of ~66 wt.% (Table 2.2) which is closer to hematite (69.9 wt.%) than to magnetite (72.4 wt.%). However, it lacks the reddish color of hematite and the material is magnetic.

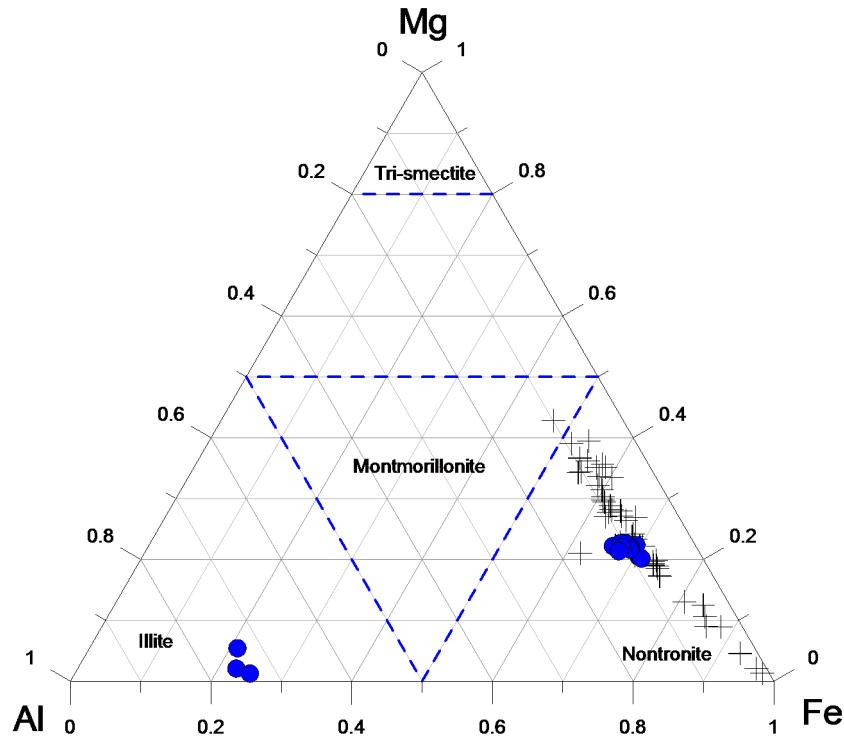


Figure 2.12. Al-Mg-Fe ternary diagram showing the compositions of smectites in scales from RN-9 pipeline. Data are from energy dispersive analyses by SEM (+) and microprobe analyses (blue circles, Table 2.3).

2.5. Scales in Newer Wells, RN-10 to RN-24

Most scales sampled from these wells were collected during a maintenance period in the summer of 2007, and some scales were collected after production tests (RN-10, RN-15, RN-13) prior to utilization (e.g., RN-11; Fig. A2.4). The physical parameters for each of the wells sampled in this study are summarized in Table 2.4. The new wells have pressure control valves inserted into the orifice plate (Appendix 2.1 and Chapter 3). In these new wells the pressure was maintained at ~22 bar after the orifice, because of the design of the newer turbines, compared to ~11 bar in well RN-9. Most of the newer wells started production in May, 2006, except for well RN-12, which produced from 2004. These wells are identified in the present study as high-, medium-, and low-pressure wells, depending on the initial wellhead pressure (Table 2.4).

Table 2.4. Summary of physical parameters for the wells used in this study, and scale characteristics

Well	Year drilled - Total depth (m)	T °C max depth (m)	Reservoir T °C 2006/2007*	Average P at WH (Sept 2006 to May or August)	Downstream of OP P (bar)	ΔT °C	Pipe upstream of orifice	FFCV	Presence of scaling			Further down-stream	
									Upstream	Orifice plate	Down-stream		
High pressure													
RN-9	1983-1445 m	295°C 1402 m	290°C	44-40-25 ⁽¹⁾	11	257-252-230	xx	no valve	no info	no info	xx	xxxx	xxx
RN-11	2002-2248 m	296°C 2172 m	295°C	42	22	255 °C - 220°C	x	x	no info	no info	x	xxxx	no info
RN-22	2006-1680 m	305°C 1105 m	300/290°C	35	22	244°C - 220°C	c	no info	no info	no info	no info	xxxx	no info
RN-23	2006-1924 m	314°C 1847 m	300°C	45	22	259°C - 220°C	x	x	no info	no info	xx	xxxx	xx
RN-14B	2004-2426 m	290°C 1040 m	300°C	40 ⁽²⁾	22	252-220	c	x	no info	no info	x	x	no info
RN-10	1999-2046 m	319°C 1900 m	310°C	25	22	226°C - 220	c	c	c	c	x	c	no info
Medium pressure													
RN-12w	2002-2506 m	314°C 2495 m	295°C	37	22	247°C - 220°C	c	xxx	no info	no info	x	x	no info
RN-21w	2005-1664 m	285°C 1593 m	285°C	32	22	239°C - 220°C	c	xxx	no info	no info	no info	x	no info
RN-24	2006-2114 m	286°C 1269 m	280°C	30	22	236°C - 220°C	c	xxx	no info	no info	x	x	no info
Low pressure													
RN-19w	2005-2235 m	302°C 2226 m	275°C	27	22	230°C - 220°C	c	x	c	c	c	x	no info
RN-15	2004-2507 m	284°C 2154 m	284°C	25	22	226°C - 220°C	c	x	no info	no info	x	c	no info
RN-18	2004-1815 m	292°C 1386 m	285°C	22	22	220°C - 220°C	x	c	no info	no info	no info	x	no info
RN-13	2004/2457 m	286°C 2475 m	295°C	collapsed	22	no info	no info	no info	no info	no info	no info	no info	no info
		295°C 1300m		2006									

OP, orifice plate; ΔT= T °C at wellhead - T downstream of the orifice plate; xxxx, precipitation up to 10 cm thick; xxx, precipitation decreases but reaches at least 30 m downstream of the orifice plate; xx, = 2 cm; x, trace < 0.5 cm; c, colour change, commonly blue; w, deep fluid sampled; ⁽¹⁾ well RN-9 is not in use at this time, see text for further explanation; ⁽²⁾ only active from middle of April 2007; FFCV, fluid-flow control valve inseted into the orifice plate * Fridriksson and Giround, 2008.

2.5.1 High-pressure wells

The wellhead pressure of RN-10, RN-11, RN-14b, RN-22 and RN-23 ranged between 32 and 50 bar from September, 2006, to September, 2007 (ÍSOR data base, Table 2.4). RN-11, RN-22 and RN-23 were drilled from the same well pad (Fig. 1.4). Well RN-10 and RN-11 were drilled vertically, and RN-14b, RN-22, and RN-23 were drilled inclined to the south (Fig. 1.4). The maximum measured temperature in these wells is 319°C in well RN-10, with reservoir temperatures between 290 and 300°C (Fridriksson and Giround, 2008).

Abundant precipitation of sulfides occurred downstream of the orifice plate of these wells, whereas there was only trace scaling (<1 mm thick) upstream of the orifice plate, and locally on the fluid-flow control valve (Figs. 2.13 – 2.15). The samples from RN-10 were taken during a production test in the autumn of 2003, at a wellhead pressure between 45 and 52 bar. The scales from well RN-11 were collected at the wellhead and the critical pressure pipe (see Fig. A2.4, Appendix 2.4) during the production test in 2002. The wellhead pressure was unstable during this time, so the pressure at which the sample was collected is uncertain. Samples upstream and downstream of the orifice plate were collected in 2007. Scales from well RN-14b, RN-22, and RN-23 were collected up- and downstream of the fluid-flow control valve (previously the location of the orifice plate). Well RN-14b, with wellhead pressure ranging between 20 and 50 bar, was sampled in August 2007, up- and downstream of the orifice plate. During maintenance in the summer of 2009, the pipeline downstream of RN-14b orifice plate was cleaned of hundreds of kg of scales (Fig. 2.16).

2.5.2 Medium pressure wells

From September, 2006, to September, 2007, the wellhead pressure for wells RN-12, RN-21 and RN-24 ranged from 28 to 37 bar (Table 2.4). The wells were drilled vertically,



Figure 2.13. Photographs of the surface pipeline, looking upstream from the orifice plate, from high-pressure wells (HP) RN-10, RN-11, RN-14, RN-22, RN-23, medium-pressure wells (MP), RN-21, RN-24 and low-pressure wells (LP), RN-15, RN-18, RN-19. All photos are upstream of the orifice plate. RN-9 is shown for comparison with thin sulfide scales (<0.3 cm). Other photos show that there is little scale deposition in a year in the upstream pipelines (diameter of the pipelines 300–400 mm). Photographs were taken in May and August, 2007, during maintenance.



Figure 2.14. Photographs of the fluid-flow control valve (FFCV) in the surface pipeline (cone points in the direction of the fluid flow) from high-pressure wells (HP) RN-10, RN-11, RN-14, RN-23, medium-pressure wells (MP) RN-12, RN-21, RN-24 (cone points in the direction of fluid flow) and low-pressure wells (LP) RN-15, RN-18, RN-19, showing variable scale formation on the cone inserted into the orifice plate.

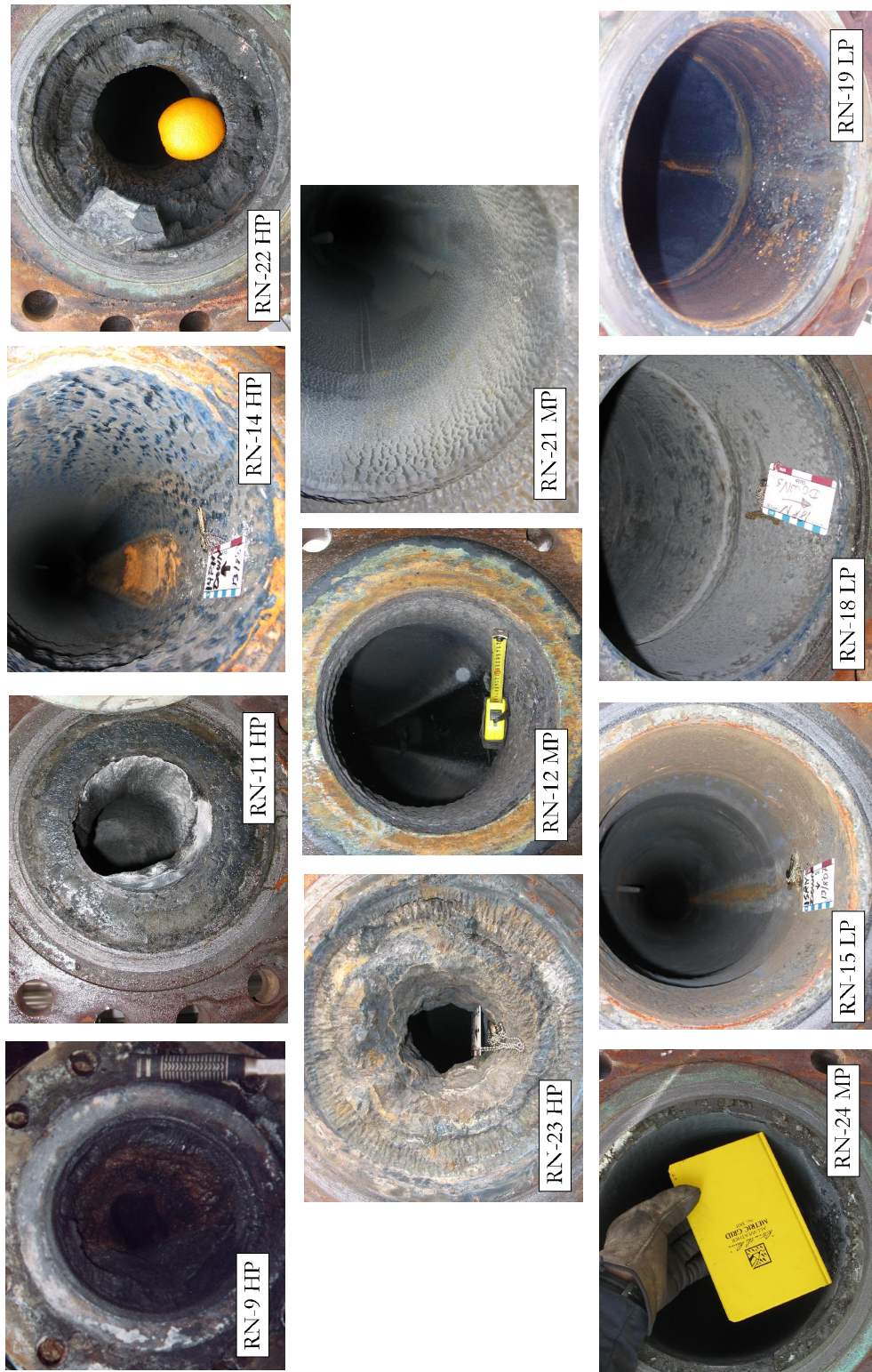


Figure 2.15. Photographs of scales in the downstream pipelines (looking downstream of the orifice plate) from high-pressure wells (HP) RN-11, RN-14, RN-22, RN-23, medium-pressure wells (MP) RN-12, RN-21, RN-24 and low-pressure wells (LP) RN-15, RN-18, RN-19, showing variable scale formation. Well RN-9 shown for comparison.



Figure 2.16. Scales cleaned from well RN14b in 2009, downstream of the fluid-flow control valve showing the volume deposited in one year within ~5 of pipeline.

and the maximum measured temperature was 314°C in well RN-12. The reservoir temperature ranged between 285 to 295°C (Fridriksson and Giround, 2008).

Scales formed mainly on the fluid-flow control valve (Figs. 2.14E-G) and on the orifice plate (downstream). Scales were not present in the pipes upstream of the fluid-flow control valve, and only a trace of scaling occurred downstream of the orifice plate, seen as a bluish color in the pipeline (Fig. 2.15). The scales that formed on the fluid-flow control valve (here-after referred to as the “cone”) consist mainly of an intimate intergrowth of sphalerite, bornite and digenite, dusted with isometric grains of galena (Chapter 3); silver grains and silver in fractures are also common. The scales get thicker from the base of the cone to the tip, in the direction of fluid flow. The thickest scale was 1.8 cm.

2.5.3 Low-pressure wells

This group includes wells RN-13, RN-15, RN-18 and RN-19, which had wellhead pressures between 25 and 28 bar. All wells were drilled vertically (Table 2.4), except for well RN-13, which collapsed and was drilled again inclined. The reservoir temperature

measured in these wells ranged between 275° (RN-19) and 295°C (RN-13; Fridriksson and Giround, 2008); the highest measured temperature (311°C) was in well RN-13.

In September, 2006, to September, 2007, the low-pressure wells experienced little scale deposition in the surface pipelines, although a trace of scale formed on the fluid-flow control valve in some of the wells (Figs. 2.13 – 2.15). Scales were collected from well RN-13 as well as from RN-15 during production tests in late 2004 and early 2005; the other scale samples were collected during maintenance periods. The small amount of scaling in the low-pressure wells consist of sphalerite, chalcopyrite, galena, bornite and a trace of pyrite, as indicated by XRD.

2.6. Scaling Tests in 2002 and 2003 in RN-9, RN-11 and RN-10

Scaling tests were conducted by inserting metal coupons into pipes using the fluid discharged from the wells. The first tests were conducted in July 2002 in well RN-9, then in October 2002 in well RN-11 and in October 2003 in RN-10. The purpose was to determine the relationship between pressure and the characteristics of the scales, as well as scaling rate. The following section summarizes the results for each well. Details on equipment and procedures are provided in Appendix 2.4.

The scales formed on coupons were precipitated under a range of pressures, from ~22 bar to 6 bar in RN-9, and ~50 bar to 5 bar in RN-11 and RN-10. At ~20 bar and ~7 bar in well RN-9, the scaling rate was ~1.2 mm and 6 mm per year, respectively, whereas in well RN-11 the scaling rate was 6 mm per year at ~41 bar and 12 mm per year at 15 bar. The scaling rate for well RN-10 was 2.4 to 11 mm per year at 50 and 7 bar, respectively. The high scaling rates of 6 mm (RN-11) and 2.4 mm (RN-10) per year were interpreted to be due to local pressure decreases, by 13 bar, during the experiments.

The amount of scale deposits increased as the pressure decreased. The variation in mineralogy with pressure in these small experiments was the same as that observed between the different wells. XRD analyses showed that sphalerite and/or wurtzite precipitated at all pressures on the substrate of coupons exposed to liquid from all wells. Trace galena was detected at ~20 bar down to 5 bar but generally was not observed at higher pressures. Chalcopyrite was only detected at the highest pressure in well RN-10 (~50 bar wellhead pressure) and well RN-9 (20 to 14 bars), and at all pressures in well RN-11. Bornite was only detected as a trace mineral in scales on the coupons from well RN-9. Amorphous silica precipitated on the coupons at and below 11 bar in all wells.

Sphalerite with very high Fe contents was found in the highest pressure experiments (56 wt.% ZnS, 42 wt.% FeS and 2 wt.% CuS). The FeS content ranged from 27 to 60 mole% (Hardardóttir et al., 2005). The high Fe contents of the sphalerite from the scaling tests (17-60 mole% FeS) are dramatically different from the low Fe contents in the other pipeline scales and downhole in RN-22 (see below). This suggests that the conditions of the scaling experiments were not the same as the conditions in which the bulk of the scales were formed.

2.7. Downhole Scales in Well RN-22

Well RN-22 was cleaned of down-hole scales to a depth of 685 m in the summer of 2009. A small amount of scale was recovered from 141 m depth (measured pressure 46 bar) to ~685 m depth (52 bar). The samples were studied in polished thin section, analysed for bulk composition, and a few minerals analysed by microprobe (Table 2.5).

The drill cuttings of scale from RN-22 consist mainly of skeletal and euhedral sphalerite and wurtzite (Fig. 2.17). XRD analysis indicates the presence of wurtzite from 210 m down

to 685 m depth, and the abundance of wurtzite as well as chalcopyrite increases downhole (S.S. Jónsson, pers. commun. 2009; ISOR data base). In thin section, chalcopyrite and sphalerite crystals were observed to increase in size with depth. Chalcopyrite is the second most abundant mineral followed by a trace of bornite (Table 2.5). Some pyrrhotite grains are present in samples from 664 m and a few at 141 m depth, together with colloform goethite and hematite (Fig. 2.18). Other minerals identified were pyrite (as inclusions in chalcopyrite), gold (commonly electrum inclusions in chalcopyrite), and hematite/maghemite, which are more abundant in the upper part of the well. A weak pattern of magnetite was also identified by XRD in the upper samples and as a trace in the deepest samples. Some of the drill cuttings contain a strongly magnetic fraction that most likely was derived from the steel casing. This is a distinct from the weakly magnetic maghemite identified in a number of samples (see below).

Sphalerite, wurtzite, bornite, pyrrhotite, pyrite, electrum, hematite and/or maghemite from 150 and 669 m depth were analyzed by electron microprobe (Table 2.6). The wurtzite and sphalerite have a low Fe content, ranging from 1 to 4.7 wt.% (average 2 wt.%: Figs 2.8 and 2.9), with no difference between the two depth intervals. These Fe contents are also

Table 2.5. Principal mineralogy and relative abundance of the minerals downhole in well RN-22 from cleaning August 2009

Depth (m)	sph/w	cpy	bn	am-Si	po	py	Ag+Au	other
141	xxx	x	x	x	tr		tr	Hm/maghem, goe
150	xxx	x	x	tr			tr	Hm/maghem, goe
160	xxx	x	tr	tr				
270	xxx	x	tr	tr				
350	xxx	x	tr	tr				
449	xxx	x		tr				
570	xxx	x		tr				
618	xxx	x		tr	tr			
664	xxx	xx			tr	tr	tr	

xxx, abundant; xx, major; x, minor; tr, trace; sph, sphalerite; w, wurtzite; cpy, chalcopyrite; bn, bornite; am-si, amorphous SiO₂; po, pyrrhotite; py, pyrite; hm, hematite; maghem, maghemite; goe, goethite

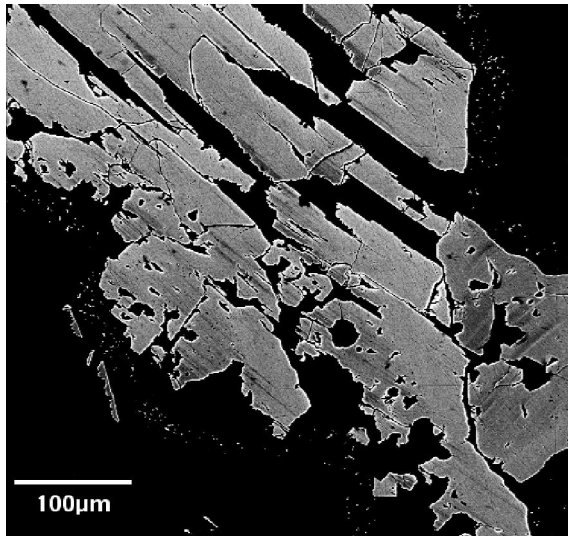


Figure 2.17. Backscattered electron image of drill cuttings of scale from RN-22 (depth 150 m) consisting mainly of skeletal or splintery spherulitic and wurtzite.

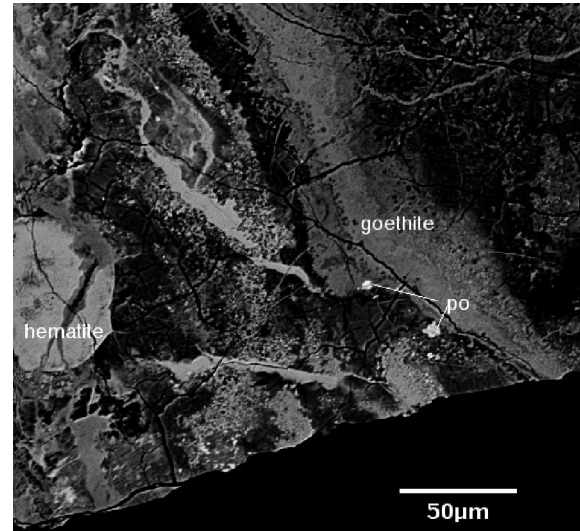


Figure 2.18. Backscattered electron image of scale from 150 m depth in well RN-22 showing pyrrhotite grains in amorphous mass together with goethite and hematite (?).

generally lower than those measured in surface pipeline in well RN-9. The spherulitic contains traces of Se (0.04 to 0.2 wt.%) and high Cd (~ 0.5 wt.%, up to 4.7 wt.%: Fig. 2.10) which are considerably higher than in spherulitic from surface pipeline of well RN-9. The presence of CdS and CdSe solid solutions within the spherulitic structure is suggested (e.g., Fig. 2.11) where CdS and CdSe substitute for FeS (Bethke and Barton, 1971).

Bornite has a non-stoichiometric composition (55 and 57 wt.% Cu versus 63 wt.% for stoichiometric bornite, and up to 14.6 wt.% Fe compared to 11.1 wt.%). The bornite is Ag-rich (0.5 to 1.5 wt.%: Table 2.6), and in some samples small silver grains appear to have exsolved from it (Fig. 2.19).

One small grain of pyrrhotite has a low S content. The pyrite contains 0.04 and 0.2 wt.% As. Due to the small sizes of electrum grains, only the Au/Ag ratio could be determined, which is 3-4 at 669 m depth (4 grains) and 1 at 150 m depth (1 grain). This is considerably higher than the ratio measured in well RN-9 (0.3-0.6).

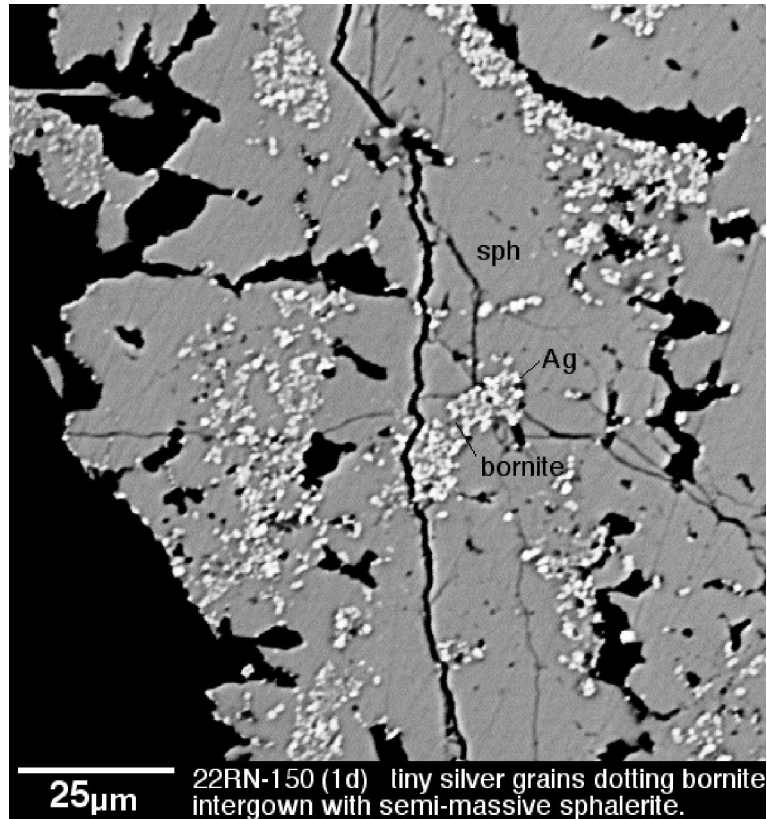


Figure 2.19. Backscattered electron images of scales from downhole well RN-22 showing intergrown sphalerite and bornite, highlighting the distribution of silver (labelled).

Analyses of a few grains of the maghemite from 150 m depth range from ~65 to 70 wt.% Fe with a trace of Zn, Mn and Si (generally <0.5 wt.%: Table 2.6). The composition is close to hematite, but the magnetic character of the grains confirms maghemite ($\gamma\text{-Fe}_2\text{O}_3$) (Haneda and Morrish, 1977). The XRD diffraction pattern of maghemite is similar to that of magnetite, which was originally identified in these scale samples by XRD.

Chemical (XRF) analyses on the downhole scales in RN-9 showed that they mainly consisted of Fe-sulfides together with Zn and Cu and trace of SiO_2 and Mg (unpublished data by H. Kristmannsdóttir, 1985; Hardardóttir, 2002; ISOR data base).

Table 2.6. Compositions of minerals in scales from downhole well RN-22

Sample no	Depth (m)	Mineral	Zn wt%	Fe** wt%	Cu wt%	Pb wt%	S wt%	Au wt%	Ag wt%	As wt%	Sb wt%	Co wt%	Se wt%	Ni wt%	Cd wt%	Te wt%	Mn wt%	Bi wt%	Total wt%
22RN	150	sphalerite	63.91	1.78	-	<0.01	31.85	<0.01	0.06	<0.01	<0.01	0.05	0.12	<0.01	0.72	<0.01	<0.01	0.15	98.6
22RN	150	sphalerite	64.14	1.30	-	<0.01	31.75	<0.01	<0.01	<0.01	0.03	0.03	0.19	0.01	1.33	<0.01	<0.01	0.07	98.9
22RN	150	sphalerite	64.58	1.15	-	<0.01	32.12	<0.01	0.03	<0.01	<0.01	0.02	0.20	<0.01	1.20	0.02	0.02	0.11	99.4
22RN	150	sphalerite	63.82	1.16	-	<0.01	31.76	0.03	<0.01	0.01	<0.01	0.03	0.09	<0.01	2.38	<0.01	0.03	0.17	99.5
22RN	150	sphalerite	61.62	4.50	-	0.15	32.01	<0.01	<0.01	0.02	0.02	<0.01	0.06	<0.01	0.15	0.05	0.07	0.04	98.7
22RN	150	sphalerite	63.45	1.70	-	<0.01	31.65	0.01	<0.01	<0.01	<0.01	0.03	0.12	<0.01	1.06	0.03	<0.01	<0.01	98.0
22RN	150	sphalerite	63.34	1.50	-	0.08	31.75	<0.01	<0.01	0.01	<0.01	0.06	0.14	<0.01	2.17	0.02	0.02	0.08	99.2
22RN	150	sphalerite	63.77	3.03	-	<0.01	31.95	<0.01	0.03	<0.01	<0.01	0.03	0.06	0.02	0.40	<0.01	<0.01	0.05	99.3
22RN	150	sphalerite	62.36	3.09	-	<0.01	32.20	0.01	0.03	<0.01	<0.01	0.03	0.04	0.03	0.47	<0.01	0.03	0.11	98.4
22RN	150	sphalerite	63.46	2.08	-	0.10	31.87	0.02	<0.01	0.02	<0.01	<0.01	0.09	0.01	1.09	<0.01	0.03	0.18	98.9
22RN	150	sphalerite	62.47	2.45	-	<0.01	32.00	<0.01	<0.01	<0.01	<0.01	0.04	0.11	<0.01	0.87	0.10	0.02	0.19	98.2
22RN	664	sphalerite	64.30	1.44	-	<0.01	29.20	<0.01	0.02	<0.01	0.02	0.02	0.20	<0.01	1.38	<0.01	<0.01	<0.01	96.6
22RN	664	sphalerite	64.83	1.05	-	<0.01	29.59	<0.01	<0.01	0.01	<0.01	0.03	0.14	0.03	1.59	<0.01	0.02	0.09	97.4
22RN	664	sphalerite	61.94	1.10	-	<0.01	31.95	<0.01	<0.01	0.01	<0.01	0.05	0.19	0.02	4.79	<0.01	0.02	0.14	100.2
22RN	664	sphalerite	63.99	1.71	-	<0.01	32.29	<0.01	0.06	<0.01	<0.01	0.01	0.12	0.02	2.15	0.03	0.01	<0.01	100.4
22RN	664	sphalerite	63.77	2.02	-	0.18	31.97	<0.01	<0.01	0.03	<0.01	0.04	0.15	0.03	1.59	0.04	<0.01	0.07	99.9
22RN	664	sphalerite	64.09	2.50	-	<0.01	31.98	<0.01	<0.01	<0.01	<0.01	0.02	0.08	<0.01	0.65	<0.01	0.03	0.04	99.4
22RN	664	sphalerite	63.56	1.69	-	<0.01	32.27	<0.01	0.08	0.01	<0.01	0.05	0.20	<0.01	1.36	<0.01	0.03	0.10	99.3
22RN	664	sphalerite	61.16	4.76	-	<0.01	31.17	<0.01	0.07	<0.01	<0.01	<0.01	0.01	0.01	0.39	0.03	0.04	0.13	97.8
22RN	664	sphalerite	64.06	1.13	-	<0.01	31.73	0.03	<0.01	<0.01	<0.01	0.05	0.14	0.02	2.01	<0.01	0.01	<0.01	99.2
22RN	664	sphalerite	62.49	0.96	-	0.12	32.17	0.03	<0.01	<0.01	<0.01	0.03	0.15	0.02	3.95	<0.01	0.01	0.05	100.0
22RN-2	150	bornite	0.58	14.86	57.05	0.18	27.62	<0.01	0.50	0.02	<0.01	<0.01	0.06	<0.01	<0.01	<0.01	0.01	0.04	100.9
22RN-1b	150	bornite	2.54	12.92	55.14	0.13	25.43	<0.01	0.89	<0.01	<0.01	<0.01	0.27	0.04	0.07	<0.01	<0.01	0.08	97.5
22RN-1b	150	bornite	1.74	14.37	56.38	0.06	27.37	<0.01	0.65	0.02	<0.01	<0.01	0.11	0.00	0.11	<0.01	<0.01	0.05	100.9
22RN-1c	150	bornite	1.78	12.91	56.07	0.43	26.65	<0.01	1.59	<0.01	<0.01	<0.01	0.16	0.01	0.08	0.03	<0.01	0.10	99.8
22RN-1	150	pyrrhotite	0.20	62.78	0.02	<0.01	24.00	<0.01	<0.01	<0.01	<0.01	<0.01	<0.01	0.03	0.00	0.02	0.10	<0.01	87.2
22RN-1	664	pyrite	0.52	46.36	0.30	<dl	52.10	<dl	<dl	0.20	<dl	0.07	<dl	0.03	<dl	0.00	0.03	<0.01	99.6
22RN-1	664	pyrite	0.62	45.30	0.67	<dl	51.67	<dl	<dl	0.04	<dl	0.31	0.01	0.04	<dl	0.00	<dl	<0.01	98.7

Table 2.6 (continued)

Depth (m)	Normalized			Depth (m)	Well	RN-22	Zn	Fe	O	Si	Ca	Mg	Cr	Al	Ti	V	Mn	Total	
	Au	Ag	Au/Ag																
22RN-2	150	electrum	50.5	49.5	1.0														
22RN-0	664	electrum	76.2	23.8	3.2														
22RN-1	664	electrum	81.6	18.4	4.4														
22RN-1	664	electrum	80.5	19.4	4.1														
22RN-2	664	electrum	75.5	24.5	3.1														
22RN	150	maghemite	0.01	69.94	29.99	<0.01	<0.01	<0.01	<0.01	<0.01	<0.01	<0.01	0.04	0.01	0.02	0.01	<0.01	<0.01	100.0
22RN	150	maghemite	<0.01	69.34	30.61	<0.01	<0.01	<0.01	<0.01	<0.01	<0.01	<0.01	0.03	<0.01	0.01	<0.01	<0.01	<0.01	100.0
22RN	150	maghemite	0.09	68.23	30.59	0.49	0.16	<0.01	<0.01	0.49	0.16	<0.01	0.06	<0.01	0.01	<0.01	<0.01	<0.01	100.0
22RN	150	maghemite	0.12	66.71	31.98	0.53	0.15	<0.01	<0.01	0.53	0.15	<0.01	0.12	<0.01	0.02	<0.01	<0.01	<0.01	100.0
22RN	150	maghemite	0.14	67.36	31.32	0.60	0.12	<0.01	<0.01	0.60	0.12	<0.01	0.10	<0.01	0.01	0.02	<0.01	<0.01	100.0
22RN	150	maghemite	0.12	67.59	31.11	0.59	0.13	<0.01	<0.01	0.59	0.13	<0.01	0.03	0.01	<0.01	<0.01	<0.01	<0.01	100.0
22RN	150	maghemite	0.12	66.34	32.02	0.82	0.14	<0.01	<0.01	0.82	0.14	<0.01	0.10	0.02	0.01	0.01	0.01	0.40	100.0
22RN	150	maghemite	0.08	65.05	33.26	0.47	0.43	<0.01	<0.01	0.47	0.43	<0.01	0.10	0.01	0.03	0.02	0.02	0.56	100.0
22RN	150	maghemite	0.11	65.98	32.55	0.62	0.29	<0.01	<0.01	0.62	0.29	<0.01	0.09	<0.01	0.08	0.01	<0.01	0.35	100.0
22RN	150	maghemite	0.08	67.17	31.62	0.51	0.31	<0.01	<0.01	0.51	0.31	<0.01	0.08	0.01	0.01	<0.01	<0.01	0.22	100.0
22RN	150	maghemite	0.09	67.05	31.54	0.49	0.29	<0.01	<0.01	0.49	0.29	<0.01	0.08	<0.01	0.08	<0.01	<0.01	0.47	100.0
22RN	150	maghemite	0.06	67.39	31.18	0.55	0.28	<0.01	<0.01	0.55	0.28	<0.01	0.15	<0.01	0.02	<0.01	<0.01	0.37	100.0
22RN	150	maghemite	0.05	66.80	31.82	0.63	0.21	<0.01	<0.01	0.63	0.21	<0.01	0.06	<0.01	<0.01	<0.01	<0.01	0.42	100.0
22RN	150	maghemite	0.09	65.71	32.79	0.68	0.33	<0.01	<0.01	0.68	0.33	<0.01	0.09	0.01	<0.01	<0.01	<0.01	0.30	100.0
22RN	150	maghemite	0.44	66.42	31.82	0.88	0.13	<0.01	<0.01	0.88	0.13	<0.01	0.00	<0.01	0.01	0.01	0.01	0.30	100.0
22RN	150	maghemite	0.19	66.84	31.87	0.60	0.14	<0.01	<0.01	0.60	0.14	<0.01	0.02	0.01	<0.01	0.02	0.02	0.32	100.0
22RN	150	maghemite	0.37	65.61	33.05	0.50	0.16	<0.01	<0.01	0.50	0.16	<0.01	0.01	<0.01	0.01	0.03	0.26	100.0	
22RN	150	maghemite	0.26	66.63	31.89	0.52	0.13	<0.01	<0.01	0.52	0.13	<0.01	0.00	<0.01	<0.01	0.01	0.56	100.0	
22RN	150	maghemite	0.03	65.92	31.77	1.81	0.11	<0.01	<0.01	1.81	0.11	<0.01	0.04	0.01	<0.01	<0.01	<0.01	0.31	100.0
22RN	150	maghemite	0.03	68.34	30.12	1.20	0.03	<0.01	<0.01	1.20	0.03	<0.01	0.11	0.03	<0.01	<0.01	<0.01	0.13	100.0
22RN	150	maghemite	0.01	69.95	29.25	0.41	<0.01	<0.01	<0.01	0.41	<0.01	<0.01	0.11	0.03	<0.01	0.01	0.22	100.0	
22RN	150	maghemite	0.93	66.60	31.68	0.23	0.11	<0.01	<0.01	0.23	0.11	<0.01	0.01	0.01	<0.01	0.01	0.41	100.0	
22RN	150	maghemite	0.20	67.48	31.21	0.40	0.13	<0.01	<0.01	0.40	0.13	<0.01	0.10	0.01	0.01	<0.01	0.46	100.0	
22RN	150	maghemite	0.04	71.07	28.40	0.02	<0.01	<0.01	<0.01	0.02	<0.01	0.03	0.13	0.01	0.07	0.17	0.06	100.0	
22RN	150	maghemite	<0.01	69.73	30.23	<0.01	<0.01	<0.01	<0.01	<0.01	<0.01	<0.01	<0.01	0.03	0.01	<0.01	<0.01	<0.01	100.0

, Cu in analyses of individual sphalerite grains was assumed to have been present as inclusions of chalcopyrite smaller than the resolution of the microprobe beam (~3 µm). Results of these analyses were corrected for excess Fe by subtracting an amount of Fe equal to Cu on an atomic basis. -- not analysed; <0.01 below the detection limits of the microprobe 0.01 wt.%; ** Cations on the basis of 32 oxygen

2.8. Bulk Compositions of the Scales

The bulk composition of the scales at Reykjanes is dominated by SiO₂, Zn, S, Fe, and Cu, reflecting the major mineralogy: at high pressure (>22 bar), sphalerite is the most abundant phase, whereas at lower pressure (~15 bar and lower), amorphous silica is the most abundant phase, followed by sphalerite, amorphous Fe-silicate and chalcopyrite ± bornite.

Of the 40 scale samples collected from the RN-9 pipeline (Table 2.4), the majority were analyzed for major and trace elements (Table 2.7), including the scale experiments in RN-9. Representative analyses of samples from well RN-9 are listed in Table 2.7 from the wellhead to the orifice plate, downstream to the end of the pipe at the separation station, and from there to the vent house and the Gray Lagoon. The bulk compositions of scales from the high-, medium- and low-pressure wells (45 and 25 bar) are presented in Table 2.8. The downhole scales collected from well RN-22 formed at the highest pressure (52 to 46 bar), and their bulk composition is listed in Table 2.9. Normative abundances of the minerals, calculated by weight, are presented in Table 2.10 and correlation coefficients for elements analyzed from well RN-9 are listed in Table 2.11.

2.8.1 Major elements

Zinc is the major metal precipitating at all pressures; between 20 and ~52 bar, the concentrations of Zn in the scales are between 40 and 60 wt.% (Table 2.8). Copper concentration is low (~3 wt.%) at high pressure (~45 bar) but is slightly higher than Zn at the fluid flow control valve (~20 -26 wt.%; Figs. 2.20 and 2.21A, B) and similar on the downstream side of the orifice plate in well RN-9 (Fig. 2.22). Iron concentrations are highest (~20 wt.%) at ~40 bar in well RN-9. One sample from ~160 m depth in well RN-22

Table 2.7. Bulk compositions of scales from RN-9 Reykjanes geothermal system (see Appendix 4.1 for analytical methods)

Wellhead	pressure bar	Zn	Fe	Cu	Pb	S	SO4	C Total	SiO2	Al2O3	CaO	Na2O	K2O	MnO	MgO	LOI	Total	
		ICP-OES 0.001	INAA 0.01	ICP-OES 0.001	ICP-OES 0.003	IR 0.01	IR	IR	IR	FUS-ICP 0.01	FUS-ICP 0.01	FUS-ICP 0.01	FUS-ICP 0.01	FUS-ICP 0.01	FUS-ICP 0.001	FUS-ICP 0.01	%	%
08_01*	47-15	7.1	18.7	1.0	3.2		na	na	33.4	3.5	1.2	1.1	0.1	0.5	9.1	na	78.8	
5_05G	47-16	19.1	12.7	5.7	2.0	15.8	na	0.08	23.0	2.4	0.7	0.4	0.2	0.4	5.5	15.0	102.8	
6_01*	47-17	13.8	14.5	5.8	1.0	10.0	<0.05	na	26.9	2.7	0.8	0.7	0.2	0.4	6.6	13.7	97.2	
1_05G	47-18	7.9	13.8	6.9	4.6	11.5	na	0.08	31.7	2.5	0.5	0.6	0.4	0.6	3.4	16.5	100.7	
9_01*	47-19	20.7	20.0	19.7	0.6	24.9	1.00	na	4.8	0.6	0.1	0.1	0.0	0.1	1.1	14.3	108.0	
~13 m downstream of wellhead																		
20_00	47-15	17.7	17.5	18.0	0.1	27.6	na	0.05	6.1	0.7	0.2	0.1	0.1	0.1	1.5	15.0	104.8	
21_00	47-15	18.4	18.8	19.0	0.3	29.0	na	0.04	5.4	0.8	1.2	0.2	<0.01	0.1	1.3	15.6	110.0	
23_00	47-15	17.9	17.3	20.7	0.6	29.8	na	0.06	4.5	0.6	0.2	0.3	0.2	0.1	1.1	14.9	108.1	
~14 m downstream of wellhead																		
31A_00	11	23.6	6.0	16.0	5.9	19.1	na	0.06	14.4	0.5	0.6	0.4	0.1	0.7	0.6	14.9	102.9	
31B_00	11	23.9	5.3	19.3	8.0	20.9	na	0.08	13.0	0.3	2.2	0.2	0.1	0.5	0.4	11.5	105.5	
<1 m downstream of orifice plate																		
2_05G	11	14.7	4.4	14.6	12.9	16.0	na	0.06	26.9	2.9	0.6	0.8	0.7	0.1	0.1	10.2	105.1	
3_05G	11	16.4	4.5	16.1	14.3	17.2	na	0.04	21.3	2.4	0.7	0.7	0.5	0.1	0.1	10.6	105.0	
16_00inter	11	30.7	6.5	21.2	7.3	26.6	na	0.09	2.3	0.2	0.1	0.2	<0.01	0.2	0.2	15.1	110.4	
17_00c	11	14.1	4.9	9.4	4.1	12.3	na	0.07	33.7	1.7	1.1	0.7	0.4	0.5	0.3	20.3	103.4	
18A_00exter	11	12.4	5.6	7.2	3.7	11.8	na	0.07	39.5	2.2	1.4	0.6	0.5	0.6	0.2	18.7	104.4	
~4 m downstream of orifice plate																		
29_00*	11	12.3	4.4	6.2	1.8	11.0	1.23	na	47.0	2.9	0.9	0.8	0.6	0.7	0.3	14.3	104.2	
29_00	11	9.2	4.1	4.4	2.6	8.4	na	0.04	54.6	3.3	1.4	0.9	0.6	0.8	0.3	12.0	102.4	
28_00	11	10.4	4.5	5.2	3.0	9.9	na	0.08	49.8	2.8	1.4	0.8	0.5	0.6	0.2	15.2	104.2	
27B_00	11	9.5	4.5	4.7	2.7	9.0	na	0.05	53.4	3.3	1.2	1.0	0.6	0.7	0.3	12.2	103.0	
~10 downstream of orifice plate; 2 nd bend																		
26_00	11	17.7	5.0	13.6	5.8	15.9	na	0.05	29.2	1.8	0.5	0.4	0.2	0.5	0.3	13.9	104.7	
~30 downstream of orifice plate; 3 rd bend																		
1_00	11	10.2	5.4	5.4	3.7	9.3	na	0.05	50.1	3.2	0.9	0.8	0.8	0.9	0.2	12.2	103.1	
~30-70 m downstream of orifice plate																		
5_00	11	9.8	3.0	5.3	3.4	8.8	na	0.02	53.1	3.5	0.8	1.0	0.9	0.4	0.2	12.6	102.8	
30_2A_00	11	4.8	2.4	2.2	1.4	4.2	na	0.03	72.3	2.6	0.7	0.8	0.5	0.6	0.3	8.6	101.3	
30_00*	11	7.5	3.3	3.1	2.3	5.9	1.00	na	66.5	2.2	0.6	0.8	0.5	0.8	0.4	10.0	104.9	
1_04	11	5.7	3.5	2.6	2.4	5.4	na	0.04	64.7	3.7	0.8	1.0	0.9	0.5	0.6	7.5	99.4	
1_04_3	11	13.8	3.9	14.6	13.3	14.8	na	0.06	28.3	2.2	0.5	0.6	0.5	0.1	0.2	9.7	102.6	

Table 2.7. (continued)

	Zn	Fe	Cu	Pb	S	SO4	C Total	SiO2	Al2O3	CaO	Na2O	K2O	MnO	MgO	LOI	Total
	ICP-OES	INAA	ICP-OES	ICP-OES	IR	IR	IR	FUS-ICP	%	%						
bar	0.001	0.01	0.001	0.003	0.01			0.01	0.01	0.01	0.01	0.01	0.001	0.01	%	%
~30-70 m downstream of orifice plate																
4_05G	11	5.2	2.3	3.2	5.1	na	0.10	65.5	4.3	0.8	1.1	1.2	0.2	0.2	8.0	100.7
4_00*	11	2.3	2.4	3.3	1.6	0.36	na	82.6	1.7	0.5	0.9	0.5	0.8	0.3	6.4	104.2
40N_00*ex	11	0.6	1.0	0.2	0.5	<0.05	na	93.1	0.5	0.6	0.3	0.1	0.1	0.5	3.4	101.0
40M_00*c	11	1.1	2.7	0.2	1.1	<0.05	na	71.2	1.2	1.0	5.6	0.5	0.9	0.5	14.2	100.4
40E_00*in	11	0.9	3.1	0.2	0.8	<0.05	na	81.8	2.2	0.2	1.0	0.5	1.0	0.4	6.7	99.0
~70-100 downstream of OP																
6A_00*	11	1.9	2.9	0.4	1.4	1.41	na	81.6	1.8	0.6	1.1	1.3	0.8	0.8	5.2	101.7
6B_00*	11	3.7	3.7	1.1	3.3	2.31	na	70.9	4.7	1.1	1.6	1.7	0.8	0.3	6.9	103.6
2_04_2A	11	2.4	2.0	1.2	2.5	na	0.02	77.8	5.9	1.4	1.7	1.4	0.4	0.4	8.4	106.7
2_04_3	11	2.4	2.5	0.8	2.0	na	0.02	75.3	4.2	1.0	1.2	1.0	0.4	0.6	7.9	100.0
2_04_1A	11	2.5	2.7	0.9	2.1	na	0.03	75.6	3.6	1.1	1.4	1.0	0.6	0.4	8.2	100.7
7_00	11	2.5	6.1	1.4	2.6	na	0.07	68.1	3.0	0.9	1.4	0.8	1.7	0.4	10.5	100.2
41_00*	11	0.8	3.1	0.2	0.7	<0.05	na	82.6	2.3	0.5	0.8	0.5	1.0	0.4	6.4	99.5
The bridge																
1_06	11	0.6	3.2	0.1	0.2	na	0.04	69.8	3.0	1.3	3.7	1.5	1.6	0.7	13.3	99.3
~250 m downstream of OP																
2_06	11	0.5	2.5	0.1	0.2	na	0.04	78.2	1.3	1.1	3.3	1.0	1.2	0.5	9.5	99.5
3_06	11	2.2	2.9	0.4	1.5	na	0.04	73.7	5.6	1.2	1.3	1.2	0.4	1.1	8.1	100.0
Separation station (ss)																
14_00	11	0.4	3.2	0.0	0.4	na	0.04	82.1	2.7	0.7	1.4	0.9	0.4	0.6	6.0	98.8
~345 m downstream of OP																
15_00	11	0.7	3.2	0.2	0.5	na	0.04	85.8	0.8	0.5	1.2	0.4	0.9	0.7	5.4	100.5
13_00*	11	0.6	4.1	0.1	0.5	0.21	na	81.4	1.4	0.5	0.9	0.4	1.3	0.6	7.3	99.3
11_00	11	0.3	3.1	0.0	0.2	na	0.03	78.8	1.4	0.6	1.2	0.5	0.9	0.4	7.0	94.4
~153 m downstream of separation station; valve house																
42_00*	1	0.0	0.2	0.1	0.0	0.30	na	92.2	0.1	0.3	0.5	0.2	0.1	<0.01	6.4	100.3
42_00	1	0.0	0.2	0.1	0.0	na	0.02	93.0	0.1	0.3	0.3	0.1	0.1	<0.01	6.5	100.6
Grey Lagoon = discharge pond																
1G1*	1	<0.01	0.1	0.0	0.0	na	na	84.1	0.1	0.6	2.9	0.4	0.02	0.0	12.0	100.2
2G106	1	0.0	0.5	0.0	<0.003	na	0.02	56.6	0.4	1.1	3.2	0.8	0.02	0.2	34.8	97.6
3G106	1	0.0	<0.01	0.0	<0.003	na	0.02	50.8	0.1	1.1	4.6	0.8	0.03	0.1	37.3	94.9
Scale pressure experiments																
RN-9	18	17.2	3.8	14.7	11.9	15.5	na	24.7	3.3	0.8	1.0	0.7	0.1	0.1	8.1	101.8
RN-9	17	18.7	5.7	15.3	15.3	17.7	na	13.5	1.5	0.6	0.6	0.3	0.5	0.2	8.7	98.5

Table 2.7. (continued)

Surface pipeli	pressure	Ag	Au	Se	As	Sb	Cd	Hg	Tl	Ga	Ge	Mo	Co	Ni	Bi	In
bar	ppm	ppm	ppm	ppm	ppm	ppm	ppm	ppm	ppm	ppm	ppm	ppm	ppm	ppm	ppm	ppm
	INAA	INAA	INAA	INAA	INAA	INAA	INAA	INAA	FUS-MS	FUS-MS	FUS-MS	FUS-MS	INAA	INAA	FUS-MS	FUS-MS
	5	2	3	0.5	0.1	0.5	1	0.1	1	1	1	2	1	20	0.4	0.2
Wellhead																
08_01*	47-15	na	na	na	na	na	na	na	na							
5_05G	47-16	439	213	<0.5	<0.1	220	<1	<0.1	14	14	<1	6	7	<20	2.2	<0.2
6_01*	47-17	415	90	<1	<0.2	125	na	<0.1	18	18	1	3	26	15	<0.4	<0.2
1_05G	47-18	907	73	214	4	40	12	<0.2	10	<1	<1	3	<1	<20	0.6	0.4
9_01*	47-19	164	147	282	<1	236	na	<0.1	3	<1	<1	<2	5	<1	<0.4	<0.2
13 m downstream of wellhead																
20_00	47-15	405	143	256	<0.5	200	<1	0.1	4	4	<1	3	6	<20	0.6	<0.2
21_00	47-15	382	158	236	<0.5	230	<1	0.1	3	3	<1	23	<1	<20	<0.4	<0.2
23_00	47-15	667	121	232	<0.5	200	<1	0.1	3	3	<1	23	4	<20	<0.4	<0.2
14 m downstream of wellhead																
31A_00	11	5110	137	270	35	12	200	<1	2	2	<1	<2	<1	<20	0.8	<0.2
31B_00	11	6060	176	346	180	30	160	<1	<1	<1	<1	<2	5	<20	<0.4	<0.2
<1 m downstream of orifice plate																
2_05G	11	6790	48	299	154	31	<30	<1	0.2	2	<1	2	<1	<20	<0.4	<0.2
3_05G	11	7890	53	344	184	<0.1	40	<1	0.3	1	<1	<2	7	<20	<0.4	<0.2
16_00inter	11	9980	164	383	<0.5	<0.1	260	<1	<0.1	<1	<1	<2	<1	<20	0.7	<0.2
17_00c	11	3230	115	223	67	12	120	<1	0.3	4	<1	5	<1	<20	2.9	<0.2
18A_00exter	11	2440	98	212	19	9	80	<1	0.1	5	<1	7	<1	<20	2.7	<0.2
4 m downstream of orifice plate																
29_00*	11	2000	92	199	41	10	100	na	0.2	6	<1	<2	51	10	<0.4	<2
29_00	11	1640	74	152	110	<0.1	60	<1	0.2	6	<1	3	<1	<20	1.5	<0.2
28_00	11	1920	85	191	62	<0.1	140	<1	<0.1	5	<1	<2	<1	<20	0.7	<0.2
27B_00	11	1740	80	153	113	12	60	<1	0.2	6	<1	4	<1	<20	1.7	<0.2
10 downstream of orifice plate, 2 nd bend																
26_00	11	4400	127	231	132	17	110	13	0.3	3	<1	3	<1	<20	2.4	<0.2
30 downstream of orifice plate, 3 rd bend																
1_00	11	2740	79	204	117	17	70	<1	0.3	7	<1	5	<1	<20	1.9	<0.2
30-70 m downstream of orifice plate																
5_00	11	1900	72	149	209	19	50	<1	0.3	6	<1	3	<1	<20	1.2	<0.2
30_2A_00	11	866	39	104	334	<0.1	<30	<1	0.1	8	<1	5	<1	<20	0.8	<0.2
30_00*	11	110	48	113	36	7	63	na	0.3	8	<1	<2	32	15	<0.4	<2
1_04	11	1450	14	113	127	19	150	<1	0.3	9	<1	6	8	<20	0.4	<0.2
1_04_3	11	6610	50	291	78	19	<30	<1	0.3	3	<1	<2	<1	<20	<0.4	<0.2

Table 2.7. (continued)

	pressure bar	Ag		Au		Se		As		Sb		Cd		Hg		Tl		Ga		Ge		Mo		Co		Ni		Bi		In	
		ppm INAA																													
30-70 m downstream of orifice plate																															
4_05G	11	1770	20	107	159	<0.1	<30	<1	0.3	6	<1	11	3	<20	<0.4	<0.2															
4_00*	11	200	13	28	38	2	14	na	<0.1	10	<1	<2	63	37	<0.4	<2															
40N_00*ex	11	112	4	<3	5	1	15	na	0.1	6	<1	<2	206	132	<0.4	<2															
40M_00*c	11	95.3	7	13	14	1	14	na	<0.1	9	<1	<2	84	37	<0.4	<2															
40E_00*in	11	62.6	5	12	37	1	6	na	<0.1	12	<1	<2	55	34	<0.4	<2															
70-100 downstream of OP																															
6A_00*	11	165	11	28	57	2	31	na	<0.1	10	<1	<2	3	<1	<0.4	<2															
6B_00*	11	390	20	67	25	4	15	na	0.2	9	<1	<2	2	<1	<0.4	<2															
2_04_2A	11	704	8	50	143	18	<30	<1	0.2	7	<1	3	4	<20	<0.4	<2															
2_04_3	11	482	11	44	156	21	<30	<1	0.2	8	<1	4	4	<20	<0.4	<2															
2-04_1A	11	363	9	39	64	5	<30	<1	0.1	8	<1	5	<1	<20	<0.4	<2															
7_00	11	208	17	62	15	<0.1	50	<1	<0.1	11	<1	8	<1	<20	<0.4	<2															
41_00*	11	79	6	<3	25	2	4	na	0.1	11	<1	<2	226	47	<0.4	<2															
The bridge																															
1_06	11	63	10	29	<0.5	1	<30	<1	<0.1	8	<1	4	4	<20	<0.4	<2															
250 m downstream of OP																															
2_06	11	50	5	23	5	1	<30	<1	<0.1	8	<1	5	6	<20	<0.4	<2															
3_06	11	203	6	33	37	5	80	<1	0.5	8	<1	5	<1	<20	<0.4	<2															
Separation station (ss)																															
14_00	11	38	4	9	8	1	<30	<1	0.1	10	<1	6	2	<20	<0.4	<2															
345 m downstream of OP																															
15_00	11	111	6	<3	<0.5	1	<30	<1	<0.1	12	<1	8	4	<20	<0.4	<2															
13_00*	11	47.1	0.4	<3	14	1	12	na	<0.1	16	<1	<2	560	70	<0.4	<2															
11_00	11	26	2	<3	5	<0.1	<30	<1	<0.1	11	<1	7	<1	<20	<0.4	<2															
153 m downstream of separation station; valve house																															
42_00*	1	10	0.2	5	1	3	<0.3	<1	<0.1	63	<1	<2	1	<1	<0.4	<2															
42_00	1	21	0.3	<3	<0.5	4	<30	<1	<0.1	65	<1	7	<1	<20	<0.4	<2															
Grey lagoon = discharge pond																															
1GL*	1	0.15	<0.01	<3	2	1	<0.7	na	<0.1	na	<1	<1	2	<1	<2	<2															
2GL06	1	<5	0.3	20	10	<0.1	<30	<1	<0.1	<1	<1	<2	<1	<20	<0.4	<2															
3GL06	1	<5	0.4	<3	11	<0.1	<30	<1	<0.1	<1	<1	<2	<1	<20	<0.4	<2															
Scale pressure experiments																															
RN-9	18	1052	67	320	2500	1	32	na	0.1	2	<0.1	7	<1	19	<0.4	<2															
RN-9	17	1819	102	440	6370	1	44	na	<0.1	1	<0.1	33	<1	49	<0.4	<2															

Table 27. (continued)

	Sn	W	V	Cr	Nb	Zr	Hf	Ta	Sc	Ti	Ir	Ba	Sr	Rb	Cs	
	ppm	ppm	ppm	ppm	ppm	ppm	ppm	ppm	ppm	ppm	ppb	ppm	ppm	ppm	ppm	
pressure	FUS-MS	INAA	FUS-ICP	INAA	FUS-MS	FUS-ICP	INAA	FUS-MS	INAA	FUS-ICP	INAA	FUS-ICP	FUS-ICP	FUS-MS	FUS-MS	
bar	1	1	5	5	1	4	1	0.1	0.1	10	5	3	2	2	0.5	
Wellhead																
08_01*	na	na	79	na	1	na	na	na	<0.1	144	na	26	35	na	na	
5_05G	21	<1	17	<5	<1	8	<1	<0.1	<0.1	60	<5	18	25	7	<0.5	
6_01*	14	220	14	<5	<1	14	<1	7.1	<0.1	78	<5	21	24	5	<0.5	
1_05G	<1	<1	<5	32	<1	<4	<1	<0.1	<0.1	60	<5	37	22	24	2.5	
9_01*	2	<1	<5	<5	<1	8	<1	0.8	<0.1	78	<5	6	4	<2	<0.5	
13 m downstream of wellhead																
20_00	<1	<1	<5	<5	<1	8	2	<0.1	0.7	24	<5	4	7	<2	<0.5	
21_00	<1	<1	6	<5	<1	7	<1	<0.1	<0.1	24	<5	9	7	<2	<0.5	
23_00	<1	<1	12	<5	<1	8	<1	<0.1	<0.1	24	<5	7	5	<2	<0.5	
14 m downstream of wellhead																
31A_00	2	<1	<5	<5	<1	4	<1	<0.1	<0.1	24	<5	10	7	3	<0.5	
31B_00	<1	<1	<5	<5	<1	<4	<1	<0.1	<0.1	24	0.02	7	5	<2	<0.5	
<1 m downstream of orifice plate																
2_05G	2	<1	<5	75	<1	14	5	<0.1	<0.1	24	<5	143	38	22	1.0	
3_05G	1	<1	<5	59	<1	12	7	<0.1	<0.1	24	<5	111	33	19	0.8	
16_00inter	14	<1	<5	<5	<1	11	<1	<0.1	<0.1	24	<5	3	4	<2	<0.5	
17_00c	2	<1	<5	36	<1	<4	<1	<0.1	<0.1	36	53	77	28	15	0.6	
18A_00exter	<1	<1	<5	<5	<1	9	<1	0.8	<0.1	30	<5	96	36	16	0.7	
4 m downstream of orifice plate																
29_00*	<1	403	<5	<5	3	7	<1	13.9	<0.1	54	<5	134	38	24	1.0	
29_00	<1	<1	<5	44	<1	6	<1	<0.1	<0.1	<10	<5	157	47	27	1.2	
28_00	<1	<1	<5	47	<1	<4	<1	<0.1	<0.1	<10	<5	133	41	20	0.9	
27B_00	<1	<1	<5	50	<1	8	<1	<0.1	<0.1	24	<5	157	47	29	1.3	
10 downstream of orifice plate, 2 nd bend																
26_00	<1	<1	<5	<5	<1	8	<1	<0.1	<0.1	84	<5	60	20	11	<0.5	
30 downstream orifice plate, 3 rd bend																
1_00	2	<1	<5	78	<1	<4	<1	<0.1	<0.1	24	<5	152	44	32	1.4	
30-70 m downstream of orifice plate																
5_00	<1	<1	<5	<5	<1	4	<1	<0.1	<0.1	24	<5	165	44	36	1.6	
30_2A_00	<1	<1	<5	81	<1	<4	<1	<0.1	<0.1	<10	<5	116	33	28	1.4	
30_00*	1	193	5	<5	2	5	<1	6.6	<0.1	60	<5	83	27	26	1.1	
1_04	<1	<1	7	88	<1	<4	<1	<0.1	<0.1	30	<5	164	41	44	1.9	
1_04_3	<1	<1	<5	52	<1	21	<1	<0.1	<0.1	30	<5	110	26	25	0.9	

Table 27. (continued)

	pressure bar	Sn		W		V		Cr		Nb		Zr		Hf		Ta		Sc		Ti		Ir		Ba		Sr		Rb		Cs	
		FUS-MS ppm	INAA ppm	FUS-ICP ppm	INAA ppm	FUS-ICP ppm	INAA ppm	FUS-MS ppm	FUS-ICP ppm	INAA ppm																					
30-70 m downstream of orifice plate																															
4_05G	11	10	<1	<5	74	<1	<1	<0.1	<0.1	<1	<4	<1	<1	<1	<1	<0.1	<0.1	<0.1	<0.1	18	<5	<5	214	50	49	2.2					
4_00*	11	1	292	<5	<5	5	<1	10.6	<0.1	6	6	<1	<1	<1	10.6	<0.1	<0.1	<0.1	60	<5	<5	67	21	20	1.0						
40N_00*ex	11	1	884	13	<5	4	<1	8.3	<0.1	9	9	<1	<1	8.3	<0.1	<0.1	<0.1	120	<5	<5	20	7	6	<0.5							
40M_00*c	11	4	443	10	6	18	<1	13.8	<0.1	9	9	<1	<1	13.8	<0.1	<0.1	<0.1	96	<5	<5	63	35	18	1.2							
40E_00*in	11	29	259	<5	<5	28	<1	33.5	<0.1	9	9	<1	<1	33.5	<0.1	<0.1	<0.1	78	<5	<5	79	25	24	1.1							
70-100 downstream of OP																															
6A_00*	11	<1	<1	8	<5	3	<1	<0.1	<0.1	3	<1	<1	<1	<0.1	<0.1	<0.1	<0.1	<10	<5	<5	59	24	36	0.9							
6B_00*	11	<1	<1	<5	<5	3	<1	<0.1	<0.1	3	4	<1	<1	<0.1	<0.1	<0.1	<0.1	108	<5	<5	218	58	68	2.8							
2_04_2A	11	7	<1	6	36	<1	<1	<0.1	0.3	<1	<4	<1	<1	<0.1	<0.1	<0.1	<0.1	36	<5	<5	308	82	58	2.5							
2_04_3	11	4	<1	7	70	<1	<1	<0.1	<0.1	<1	<4	<1	<1	<0.1	<0.1	<0.1	<0.1	30	<5	<5	197	53	45	2.0							
2-04_1A	11	<1	<1	10	52	<1	<1	<0.1	<0.1	<1	7	<1	<1	<0.1	<0.1	<0.1	<0.1	<10	<5	<5	175	54	37	1.7							
7_00	11	<1	<1	6	100	<1	<1	<0.1	<0.1	<1	<4	<1	<1	<0.1	<0.1	<0.1	<0.1	12	<5	<5	115	37	30	1.4							
41_00*	11	2	1970	7	<5	13	<1	66.4	<1	5	5	<1	<1	66.4	<1	<1	<1	78	<5	<5	90	26	24	1.1							
The bridge																															
1_06	11	1	<1	19	57	<1	<1	0.7	<0.1	<1	<4	<1	<1	0.7	<0.1	<0.1	<0.1	54	<5	<5	153	57	57	1.6							
250 m downstream of OP																															
2_06	11	<1	<1	<5	73	<1	<1	<0.1	<0.1	<1	17	<1	<1	<0.1	<0.1	<0.1	<0.1	30	<5	<5	87	42	40	1.4							
3_06	11	7	<1	18	78	<1	<1	<0.1	0.4	<1	<4	<1	<1	<0.1	<0.1	<0.1	<0.1	42	<5	<5	267	69	59	2.6							
Separation station (ss)																															
14_00	11	<1	<1	13	113	<1	<1	<0.1	<0.1	<1	<4	<1	<1	<0.1	<0.1	<0.1	<0.1	18	<5	<5	126	34	33	1.3							
345 m downstream of OP																															
15_00	11	<1	<1	13	112	<1	<1	<0.1	<0.1	<1	<4	<1	<1	<0.1	<0.1	<0.1	<0.1	18	<5	<5	31	16	11	<0.5							
13_00*	11	3	5520	6	<5	34	<1	177	1.0	6	6	<1	<1	177	<0.1	<0.1	<0.1	120	<5	<5	38	17	14	0.7							
11_00	11	<1	<1	9	110	<1	<1	<0.1	<0.1	<1	6	<1	<1	<0.1	<0.1	<0.1	<0.1	18	<5	<5	47	22	18	0.8							
153 m downstream of separation station; valve house																															
42_00*	1	<1	8	<5	<5	1	<1	<0.1	<0.1	<1	<1	<1	<1	<0.1	<0.1	<0.1	<0.1	<10	<5	<5	20	4	6	<0.5							
42_00	1	<1	<1	<5	137	<1	<1	<0.1	0.2	<1	6	<1	<1	<0.1	<0.1	<0.1	<0.1	<10	<5	<5	8	5	6	<0.5							
Grey lagoon = discharge point																															
1GL*	1	na	<1	<2	<5	-5	<1	<0.1	na	11	11	<1	<1	<0.1	<0.1	<0.1	<0.1	24	<5	<5	22	20	<15	<0.5							
2GL06	1	<1	<1	20	<5	<1	<1	<0.1	2.1	6	6	<1	<1	<0.1	<0.1	<0.1	<0.1	258	<5	<5	36	36	14	<0.5							
3GL06	1	<1	<1	6	47	<1	<1	<0.1	1.1	<1	<4	<1	<1	<0.1	<0.1	<0.1	<0.1	30	<5	<5	41	43	15	<0.5							
Scale pressure experiments																															
RN-9	18	<1	<1	<5	<5	<1	<1	<0.2	<0.1	<1	<5	<1	<1	<0.2	<0.1	<0.1	<0.1	36	<5	<5	191	44	26	1							
RN-9	17	<1	<1	<5	<5	<1	<1	<0.2	<0.1	<1	<5	<1	<1	<0.2	<0.1	<0.1	<0.1	12	<5	<5	86	24	11	<5							

Table 2.7. (continued)

	pressure bar	Be ppm	Br ppm	P ppm	U ppm	Th ppm	Y ppm	La ppm	Ce ppm	Pr ppm	Nd ppm	Sm ppm	Eu ppm	Gd ppm	Tb ppm	Dy ppm	
																	FUS-ICP
Wellhead																	
08_01*	47-15	na	44				4										
5_05G	47-16	<1	<0.5	<44	<0.1	<0.1	<2	<0.5	0.7	0.07	0.3	<0.1	<0.05	<0.1	<0.1	<0.1	
6_01*	47-17	<1	<1	<44	<0.1	<0.1	<1	0.4	0.4	0.06	0.2	<0.1	<0.05	<0.1	<0.1	<0.1	
1_05G	47-18	<1	<0.5	<44	0.1	0.1	<2	<0.5	0.7	0.07	0.3	<0.1	<0.05	<0.1	<0.1	<0.1	
9_01*	47-19	<1	<1	<44	0.2	<0.1	<1	0.2	0.2	<0.05	<0.1	<0.1	<0.05	<0.1	<0.1	<0.1	
13 m downstream of wellhead																	
20_00	47-15	<1	<0.5	<44	<0.1	<0.1	<2	1.9	<0.1	<0.05	<0.1	<0.1	<0.05	<0.1	<0.1	<0.1	
21_00	47-15	<1	<0.5	<44	<0.1	<0.1	<2	2	<0.1	<0.05	<0.1	<0.1	<0.05	<0.1	<0.1	<0.1	
23_00	47-15	<1	<0.5	<44	<0.1	<0.1	<2	1	0.1	<0.05	<0.1	<0.1	<0.05	<0.1	<0.1	<0.1	
14 m downstream of wellhead																	
31A_00	11	<1	<0.5	<44	<0.1	<0.1	<2	3.4	<0.1	<0.05	<0.1	<0.1	<0.05	<0.1	<0.1	<0.1	
31B_00	11	<1	<0.5	<44	<0.1	<0.1	<2	<0.5	<0.1	<0.05	<0.1	<0.1	<0.05	<0.1	<0.1	<0.1	
<1 m downstream of orifice plate																	
2_05G	11	<1	<0.5	<44	<0.1	<0.1	<2	2.7	<0.1	<0.05	<0.1	<0.1	<0.05	<0.1	<0.1	<0.1	
3_05G	11	<1	<0.5	<44	<0.1	<0.1	<2	<0.5	<0.1	<0.05	<0.1	<0.1	<0.05	<0.1	<0.1	<0.1	
16_00inter	11	<1	<0.5	<44	<0.1	<0.1	<2	<0.5	<0.1	<0.05	<0.1	<0.1	<0.05	<0.1	<0.1	<0.1	
17_00c	11	<1	28.3	<44	<0.1	<0.1	<2	1.1	0.6	0.07	0.3	<0.1	<0.05	<0.1	<0.1	<0.1	
18A_00exter	11	<1	16.6	<44	<0.1	<0.1	<2	<0.5	0.5	0.05	0.2	<0.1	<0.05	<0.1	<0.1	<0.1	
4 m downstream of orifice plate																	
29_00*	11	<1	6.1	<44	<0.1	<0.1	<1	0.3	<0.1	<0.05	<0.1	<0.1	<0.05	<0.1	<0.1	<0.1	
29_00	11	<1	<0.5	<44	0.3	<0.1	<2	<0.5	0.1	<0.05	<0.1	<0.1	<0.05	<0.1	<0.1	<0.1	
28_00	11	<1	<0.5	<44	0.3	<0.1	<2	<0.5	<0.1	<0.05	<0.1	<0.1	<0.05	<0.1	<0.1	<0.1	
27B_00	11	<1	<0.5	<44	<0.1	<0.1	<2	1.2	0.1	<0.05	<0.1	<0.1	<0.05	<0.1	<0.1	<0.1	
10 m downstream of orifice plate, 2nd bend																	
26_00	11	<1	<0.5	<44	<0.1	0.1	<2	<0.5	0.8	0.09	0.4	<0.1	<0.05	<0.1	<0.1	<0.1	
30 m downstream of orifice plate, 3rd bend																	
1_00	11	<1	29.2	<44	<0.1	<0.1	<2	1.3	0.4	<0.05	0.2	<0.1	<0.05	<0.1	<0.1	<0.1	
30-70 m downstream of orifice plate																	
5_00	11	<1	14.3	<44	<0.1	<0.1	<2	0.7	0.2	<0.05	<0.1	<0.1	<0.05	<0.1	<0.1	<0.1	
30_2A_00	11	<1	<0.5	<44	0.6	<0.1	<2	<0.5	<0.1	<0.05	<0.1	<0.1	<0.05	<0.1	<0.1	<0.1	
30_00*	11	<1	17.1	<44	<0.1	<0.1	<1	<0.5	<0.1	<0.05	<0.1	<0.1	<0.05	<0.1	<0.1	<0.1	
1_04	11	<1	<0.5	<44	<0.1	<0.1	<2	<0.5	<0.1	<0.05	<0.1	<0.1	<0.05	<0.1	<0.1	<0.1	
1_04_3	11	<1	<0.5	<44	<0.1	<0.1	<2	<0.5	<0.1	<0.05	<0.1	<0.1	<0.05	<0.1	<0.1	<0.1	

Table 2.7. (continued)

	Ho	Er	Tm	Yb	Lu
	ppm	ppm	ppm	ppm	ppm
pressure	FUS-MS	FUS-MS	FUS-MS	FUS-MS	FUS-MS
bar	0.1	0.1	0.05	0.2	0.05
Wellhead					
08_01*	47-15				
5_05G	<0.1	<0.1	<0.05	<0.2	<0.05
6_01*	<0.1	<0.1	<0.05	<0.1	<0.05
1_05G	<0.1	<0.1	<0.05	<0.2	<0.05
9_01*	<0.1	<0.1	<0.05	<0.1	<0.05
~13 m downstream of wellhead					
20_00	<0.1	<0.1	<0.05	<0.2	<0.05
21_00	<0.1	<0.1	<0.05	<0.2	<0.05
23_00	<0.1	<0.1	<0.05	<0.2	<0.05
~14 m downstream of wellhead					
31A_00	11	<0.1	<0.05	<0.2	<0.05
31B_00	11	<0.1	<0.05	<0.2	<0.05
<1 m downstream of orifice plate					
2_05G	11	<0.1	<0.05	<0.2	<0.05
3_05G	11	<0.1	<0.05	<0.2	<0.05
16_00inter	11	<0.1	<0.05	<0.2	<0.05
17_00c	11	<0.1	<0.05	<0.2	<0.05
18A_00exter	11	<0.1	<0.05	<0.2	<0.05
~4 m downstream of orifice plate					
29_00*	11	<0.1	<0.05	<0.1	<0.05
29_00	11	<0.1	<0.05	<0.2	<0.05
28_00	11	<0.1	<0.05	1.3	<0.05
27B_00	11	<0.1	<0.05	<0.2	<0.05
~10 downstream of orifice plate; 2 nd bend					
26_00	11	<0.1	<0.1	<0.2	<0.05
~30 downstream of orifice plate; 3 rd bend					
1_00	11	<0.1	<0.1	<0.2	<0.05
~30-70 m downstream of orifice plate					
5_00	11	<0.1	<0.1	<0.2	<0.05
30_2A_00	11	<0.1	<0.1	<0.2	<0.05
30_00*	11	<0.1	<0.1	<0.2	<0.05
1_04	11	<0.1	<0.1	<0.2	<0.05
1_04_3	11	<0.1	<0.1	<0.2	<0.05

*Sample analyzed in 2002 - 2004; ICP-OES, Inductively coupled plasma optical emission spectrometry; FUS-MS, Fusion mass spectrometry; FUS-ICP, Fusion Inductively coupled plasma; IR, infrared; INAA, instrumental neutron activation analysis; LOI, loss of ignition; <, below detection limits (dl); na- not analyzed; number below method are below dl.

Table 2.7. (continued)

	Ho	Er	Tm	Yb	Lu
	ppm	ppm	ppm	ppm	ppm
pressure	FUS-MS	FUS-MS	FUS-MS	INAA	INAA
bar	0.1	0.1	0.05	0.2	0.05
30-70 m downstream of orifice plate					
4_05G	11	<0.1	<0.05	<0.2	<0.05
4_00*	11	<0.1	<0.05	<0.1	<0.05
40N_00*ex	11	<0.1	<0.05	<0.1	<0.05
40M_00*c	11	<0.1	<0.05	<0.1	<0.05
40E_00*in	11	<0.1	<0.05	<0.1	<0.05
70-100 downstream of OP					
6A_00*	11	<0.1	<0.05	<0.1	<0.05
6B_00*	11	<0.1	<0.05	<0.1	<0.05
2_04_2A	11	<0.1	<0.05	<0.2	<0.05
2_04_3	11	<0.1	<0.05	<0.2	<0.05
2-04_1A	11	<0.1	<0.05	<0.2	<0.05
7_00	11	<0.1	<0.05	<0.2	<0.05
41_00*	11	<0.1	<0.05	<0.1	<0.05
The bridge					
1_06	11	<0.1	<0.1	<0.2	<0.05
250 m downstream of OP					
2_06	11	<0.1	<0.1	<0.2	<0.05
3_06	11	<0.1	<0.1	<0.2	<0.05
Separation station (ss)					
14_00	11	<0.1	<0.1	<0.2	<0.05
345 m downstream of OP					
15_00	11	<0.1	<0.1	<0.2	<0.05
13_00*	11	<0.1	<0.1	<0.1	<0.05
11_00	11	<0.1	<0.1	<0.2	<0.05
153 m downstream of separation station; valve house					
42_00*	1	<0.1	<0.1	<0.1	<0.05
42_00	1	<0.1	<0.1	<0.2	<0.05
Grey Lagoon = discharge pond					
1GL*	1				
2GL06	1	<0.1	<0.1	<0.2	<0.05
3GL06	1	<0.1	<0.1	<0.2	<0.05
Scale pressure experiments					
RN-9	18	<0.1	<0.1	<0.1	<0.1
RN-9	17	<0.1	<0.1	<0.1	<0.1

Table 2.8. Bulk composition of scales from high (RN-11, 22, 23, 14, 10), medium (RN-12, 21, 24) and low pressure (RN-13, 15, 18) wells Reykjanes geothermal system (see Appendix 4.1 for analytical methods)

Surface pipelines	Locations	pressure	bar	Zn	Fe	Cu	Pb	S	SO ₄	C _{Total}	SiO ₂	Al ₂ O ₃	CaO	Na ₂ O	K ₂ O	MnO	MgO	LOI	Total
				ICP- OES	INNA OES	ICP- OES	IR	IR	IR	FUS- ICP	FUS- ICP	FUS- ICP	FUS- ICP	FUS- ICP	FUS- ICP	FUS- ICP	FUS- ICP	FUS- ICP	FUS- ICP
Well RN-11																			
HP1_11RN5T_02G	Wellhead 19/11		40	25.1	13.5	1.3	0.1	12.3	na	na	23.9	2.0	0.6	0.4	0.2	0.2	4.7	13.1	97.3
HP2_11RN1-07	Upstream of FFCV		43	40.8	8.4	7.8	0.2	25.9	na	0.06	9.2	0.6	0.3	0.2	0.1	0.2	1.3	14.9	110.0
HP3_11RNE1-2_07	FFCV		43	37.7	8.2	11.4	0.7	25.3	na	0.05	9.3	0.6	0.3	0.1	<0.01	0.2	1.1	14.8	109.7
HP4_11RN3_07	Downstream of OP		22	38.3	7.9	8.1	0.2	24.2	na	0.05	11.5	0.8	0.3	0.3	0.1	0.3	1.5	15.4	108.7
HP5_11RN4-07	Downstream of OP		22	20.8	8.4	15.6	4.7	18.1	na	0.06	12.3	0.5	0.8	0.5	0.2	0.8	0.3	15.6	98.6
<i>Scale pressure experiments</i>																			
RN-11	1.1		41	21.9	16.4	3.9	0.6	15.3	na	na	20.5	3.2	1.0	1.3	0.7	0.3	2.8	16.0	103.9
RN-11	1.2		41	26.7	15.8	7.5	1.7	20.6	na	na	14.1	1.5	0.9	0.6	0.2	0.4	1.6	14.7	106.3
Well RN-23																			
HP9_23RN1-07	Upstream of OP		43	58.7	3.1	2.0	0.0	34.4	na	0.02	1.8	0.2	0.0	<0.01	0.0	0.03	0.2	16.0	116.5
HP10_23RNEO-07	Upstream of OP		43	56.3	3.4	0.7	0.0	31.2	na	0.03	2.3	0.4	0.2	<0.01	0.1	0.02	0.4	16.5	111.6
HP11_23RNE2-07	FFCV		43	49.4	2.8	10.9	0.1	30.8	na	0.03	2.5	0.5	0.1	<0.01	0.1	0.03	0.2	15.1	112.6
HP12_23RN3D-07	OP (?)		22	58.9	2.5	2.0	0.0	33.2	na	0.04	0.4	0.1	0.0	<0.01	<0.01	0.02	0.1	16.0	113.2
HP13_23RN4-07	Downstream of OP		22	40.9	4.3	15.5	0.4	26.4	na	0.04	4.2	0.3	0.4	0.8	0.2	0.10	0.2	15.8	109.4
HP14_23RN5-07	Downstream of OP		22	44.6	3.1	13.8	0.1	30.6	na	0.04	1.9	0.2	0.1	0.1	0.0	0.04	0.2	15.6	110.2
HP15_23RNG6-07	Downstream of OP (~32m)		22	44.9	5.1	13.8	0.6	29.8	na	0.02	2.8	0.6	0.3	0.3	0.2	0.06	0.3	14.2	113.0
HP16_23RN1_06RE	Downstream of OP		22	33.3	6.4	12.4	0.5	25.0	na	na	<0.01	0.3	<0.01	<0.01	<0.01	<0.01	<0.01	0.0	77.9
HP17_23RN1_09	Downstream of OP		22	43.2	4.8	11.8	1.9	29.1	na	na	<0.01	0.2	<0.01	<0.01	<0.01	<0.01	<0.01	0.0	91.0
Well RN-14																			
HP18_14RN1-07	Upstream of OP		34	57.5	1.8	4.1	0.1	31.2	na	0.04	1.0	0.1	0.1	<0.01	0.1	0.03	0.2	19.9	116.2
HP19_14RN2-07	Downstream of OP		22	42.7	3.4	19.9	1.3	28.7	na	0.07	2.0	0.4	0.2	0.1	<0.01	0.1	0.5	13.7	112.8
Well RN-10																			
HP20_10RN8_03	Downstream of FFCV		22	37.5	7.4	15.1	0.5	25.8	na	0.09	2.8	0.4	0.1	<0.01	<0.01	0.1	0.1	23.0	112.9
<i>Scale pressure experiments</i>																			
RN-10	1.1		34	31.4	23.3	1.4	0.7	30.1	na	na	5.5	0.4	0.3	0.6	0.1	0.3	0.3	14.0	108.3
RN-10	3.1		18	21.4	21.9	1.2	2.2	22.3	na	na	21.9	0.4	0.3	0.8	0.1	0.6	0.2	12.3	105.5
RN-10	4.1		20	21.9	22.5	1.2	1.8	22.3	na	na	22.5	0.4	0.3	0.8	0.2	0.5	0.2	12.6	107.2

Table 28. (continued)

Surface pipelines	Locations	Ag	Au	Se	As	Sb	Cd	Hg	Tl	Ga	Ge	Mo	Co	Ni	Bi	In
	pressure	ppm	ppm	ppm	ppm	ppm	ppm	ppm	ppm	ppm	ppm	ppm	ppm	ppm	ppm	ppm
	bar	INAA	INAA	INAA	INAA	INAA/ FUS-MS	TD-ICP	INAA	FUS- MS	FUS- MS	FUS- MS	FUS- MS	INAA	INAA	FUS-MS	FUS- MS
		5	2	3	0.5	0.1/0.5	0.5	1	0.1	1	1	2	1	20	0.4	0.2
Well RN-11																
High pressure wells																
HP1_11RN5T_02G	Wellhead 19/11	44	115	320	53	1	272	na	0.1	12	15	18	13	7	< 0.4	<0.2
HP2_11RN1-07	Upstream of FFCV	43	464	345	<0.5	<0.1	600	<1	<0.1	4	<1	<2	15	<20	9.4	<0.2
HP3_11RNE1-2_07	FFCV	43	1160	822	490	<0.1	580	<1	<0.1	5	<1	4	25	<20	28.7	0.8
HP4_11RN3_07	Downstream of OP	22	956	948	<3	<0.1	600	<1	<0.1	5	<1	4	<1	<20	16.8	<0.2
HP5_11RN4-07	Downstream of OP	22	1670	247	290	16	220	<1	<0.1	2	<1	6	5	<20	1.1	<0.2
Scale pressure experiments																
RN-11	1.1	41	234	273	33	7	145	na	0.1	10	15	33	13	432	<5	<0.2
RN-11	1.2	41	1856	296	360	23	121	na	<0.1	7	8	77	20	68	<5	<0.2
Well RN-23																
HP9_23RN1-07	Upstream of OP	43	128	385	923	<0.1	13300	<1	<0.1	1	<1	<2	395	<20	38.2	<0.2
HP10_23RNEO-07	Upstream of OP	43	193	341	923	<0.5	12600	<1	<0.1	5	<1	5	364	<20	0.6	<0.2
HP11_23RNE2-07	FFCV	43	1350	109	659	23	7240	<1	<0.1	3	<1	4	190	<20	2.0	<0.2
HP12_23RN3D-07	OP (?)	22	522	288	781	176	17100	<1	<0.1	8	<1	10	331	<20	0.8	<0.2
HP13_23RN4-07	Downstream of OP	22	2250	54.6	367	396	4730	<1	<0.1	<1	<1	22	135	<20	<0.4	<0.2
HP14_23RN5-07	Downstream of OP	22	1670	116	578	27	8930	<1	<0.1	<1	<1	7	213	<20	1.1	<0.2
Well RN-14																
HP15_23RN6-07	Downstream of OP (~32m)	22	1290	82.4	497	25	5220	<1	<0.1	1	<1	2	129	<20	0.7	<0.2
HP16_23RN1_06RE	Downstream of OP	22	2830	87.2	454	589	3650	20	0.3	1	<0.7	70	136	<10	<2	<0.2
HP17_23RN1_09	Downstream of OP	22	3000	64.1	606	747	4900	13	0.1	1	<0.7	10	138	<10	<2	<0.2
Well RN-10																
HP18_14RN1-07	Upstream of OP	34	22000	12.2	181	3030	6470	<1	<0.1	14	<1	119	387	<20	<0.4	<0.2
HP19_14RN2-07	Downstream of OP	22	7200	4.51	149	1010	1720	5	<0.1	4	<1	33	146	<20	<0.4	<0.2
HP20_10RN8_03	Downstream of FFCV	22	5260	110	441	733	3650	<1	<0.1	<1	<1	12	168	<20	0.5	<0.2
Scale pressure experiments																
RN-10	1.1	34	1129	161	245	5	180	na	<0.1	5	<0.1	9	9	62	0.6	<0.2
RN-10	3.1	18	3258	151	172	34	76	na	<0.1	13	<0.1	11	6	19	10.7	<0.2
RN-10	4.1	20	3027	150	180	23	79	na	<0.1	13	<0.1	11	4	48	0.8	<0.2

Table 28. (continued)

Surface pipelines	Locations														
	Sn	W	V	Cr	Nb	Zr	Hf	Ta	Sc	Ti	Ir	Ba	Sr	Rb	Cs
	ppm FUS-MS	ppm INAA	ppm FUS-ICP	ppm INAA	ppm FUS-MS	ppm FUS-ICP	ppm INAA/ FUS-MS I/0.2	ppm FUS-MS	ppm INAA	ppm FUS-ICP	ppb INAA	ppm FUS-ICP	ppm FUS-MS	ppm FUS-MS	ppm FUS-MS
	bar	1	5	5	1	4	1/0.2	0.1	0.1	10	5	3	2	2	0.5
Well RN-11															
HP1_11RN5T_02G	Wellhead 19/11	40	<1	195	<5	1	<0.2	<0.1	0.6	66	<5	12	20	17	0.7
HP2_11RN1-07	Upstream of FFCV	43	<1	9	<5	<1	<0.2	<0.1	<0.1	12	<5	15	11	<2	<0.5
HP3_11RNE1-2_07	FFCV	43	25	8	<5	4	<0.2	0.2	<0.1	102	<5	26	12	2	<0.5
HP4_11RN3_07	Downstream of OP	22	<1	13	<5	<1	<0.2	<0.1	<0.1	42	<5	18	13	2	<0.5
HP5_11RN4-07	Downstream of OP	22	<1	6	<5	<1	<0.2	<0.1	<0.1	18	<5	23	13	2	<0.5
<i>Scale pressure experiments</i>															
RN-11	1.1	41	5	81	662	13	0.7	0.3	0.8	533	<5	87	34	36	1.5
RN-11	1.2	41	3	73	187	8	0.3	0.2	1.1	258	<5	30	26	12	0.6
Well RN-23															
HP9_23RN1-07	Upstream of OP	43	12	30	<5	<1	<0.2	<0.1	<0.1	60	<5	<3	<2	<2	<0.5
HP10_23RNEO-07	Upstream of OP	43	1	76	<5	<1	<0.2	<0.1	<0.1	162	<5	28	7	<2	<0.5
HP11_23RNE2-07	FFCV	43	<1	51	<5	2	0.3	0.2	<0.1	156	<5	67	47	<2	<0.5
HP12_23RN3D-07	OP (?)	22	<1	14	<5	<1	<0.2	<0.1	<0.1	30	<5	<3	<2	<2	<0.5
HP13_23RN4-07	Downstream of OP	22	<1	18	<5	<1	<0.2	<0.1	<0.1	138	<5	12	9	<2	<0.5
HP14_23RN5-07	Downstream of OP	22	<1	22	<5	<1	<0.2	<0.1	<0.1	90	<5	6	4	<2	<0.5
HP15_23RN6-07	Downstream of OP	22	<1	119	<5	<1	<0.2	<0.1	<0.1	174	<5	15	7	6	<0.5
HP16_23RN1_06RE	Downstream of OP	22	<0.5	13	35	<2.4	<1	<0.2	<0.1	na	<5	9	5	<0.4	<0.1
HP17_23RN1_09	Downstream of OP	22	<0.5	35	<5	<2.4	<1	<0.2	<0.1	na	<5	<3	<3	1	<0.1
Well RN-14															
HP18_14RN1-07	Upstream of OP	34	2	147	<5	<1	<0.2	<0.1	<0.1	84	<5	<3	2	<2	<0.5
HP19_14RN2-07	Downstream of OP	22	<1	187	<5	<1	<0.2	<0.1	<0.1	234	<5	5	3	<2	<0.5
Well RN-10															
HP20_10RN8_03	Downstream of FFCV	22	<1	<1	<5	<1	<0.2	0.1	<0.1	174	<5	8	5	<2	<0.5
<i>Scale pressure experiments</i>															
RN-10	1.1	34	<1	48	<5	<1	0.2	<0.1	0.8	54	<5	18	6	3	<0.5
RN-10	3.1	18	<1	96	27	<1	<0.2	<0.1	0.6	144	<5	21	6	7	<0.5
RN-10	4.1	20	<1	99	55	<1	<0.2	<0.1	<0.1	288	<5	21	15	7	<0.5

Table 2.8. (continued)

Surface pipelines	Locations	pressure	Be	Br	P	U	Th	Y	La	Ce	Pr	Nd	Sm	Eu	Gd	Tb	Dy
		bar	ppm FUS-ICP	ppm INAA	ppm FUS-ICP	ppm FUS-MS	ppm FUS-MS	ppm FUS-ICP	ppm FUS-MS	ppm MS	ppm MS	ppm MS	ppm INAA	ppm FUS-MS	ppm MS	ppm FUS-MS	ppm MS
Well RN-11																	
High pressure wells																	
HP1_11RN5T_02G	Wellhead 19/11	40	<1	<0.5	<44	<0.1	<0.1	<1	0.7	0.5	0.12	0.3	<0.1	<0.05	<0.1	<0.1	<0.1
HP2_11RN1-07	Upstream of FFCV	43	<1	<0.5	<44	<0.1	<0.1	<2	0.4	0.6	0.06	0.2	<0.1	<0.05	<0.1	<0.1	<0.1
HP3_11RNE1-2_07	FFCV	43	<1	<0.5	<44	0.2	0.4	<2	1.6	3.5	0.39	1.3	<0.1	0.06	0.2	<0.1	0.2
HP4_11RN3_07	Downstream of OP	22	<1	<0.5	<44	<0.1	<0.1	<2	0.4	0.7	0.08	0.3	<0.1	<0.05	<0.1	<0.1	<0.1
HP5_11RN4-07	Downstream of OP	22	<1	<0.5	<44	<0.1	<0.1	<2	0.2	0.2	<0.05	<0.1	<0.1	<0.05	<0.1	<0.1	<0.1
<i>Scale pressure experiments</i>																	
RN-11	1.1	41	<1	47.5	458	0.4	1.2	1	2.7	4.5	0.53	1.7	0.3	0.12	0.3	<0.1	0.2
RN-11	1.2	41	<1	42.5	<44	0.2	0.7	1	2.8	3.9	0.58	1.9	0.4	0.09	0.3	<0.1	0.2
Well RN-23																	
HP9_23RN1-07	Upstream of OP	43	<1	<0.5	<44	<0.1	<0.1	<2	0.1	0.3	<0.05	0.2	<0.1	<0.05	<0.1	<0.1	<0.1
HP10_23RNE0-07	Upstream of OP	43	<1	<0.5	<44	0.2	<0.1	<2	0.6	1.4	0.14	0.6	<0.1	<0.05	0.1	<0.1	0.2
HP11_23RNE2-07	FFCV	43	<1	<0.5	<44	0.2	0.3	<2	1.4	3.2	0.31	1.1	<0.1	0.07	0.2	<0.1	0.2
HP12_23RN3D-07	OP (?)	22	<1	<0.5	<44	<0.1	<0.1	<2	<0.1	0.2	<0.05	0.2	<0.1	<0.05	<0.1	<0.1	<0.1
HP13_23RN4-07	Downstream of OP	22	<1	46.4	<44	<0.1	<0.1	<2	<0.1	0.4	<0.05	0.2	<0.1	<0.05	<0.1	<0.1	<0.1
HP14_23RN5-07	Downstream of OP	22	<1	<0.5	<44	0.1	0.2	<2	0.3	1.1	0.09	0.4	<0.1	<0.05	<0.1	<0.1	<0.1
HP15_23RN6-07	Downstream of OP	22	<1	<0.5	<44	<0.1	0.1	<2	0.3	1	0.09	0.4	<0.1	<0.05	0.1	<0.1	0.1
HP16_23RN1_06RE	Downstream of OP	22	<3	<0.5	<44	<0.1	<0.1	0.4	<0.4	<0.8	<0.1	<0.4	0.2	<0.1	<0.1	<0.1	<0.3
HP17_23RN1_09	Downstream of OP	22	<3	<0.5	<44	<0.1	<0.1	0.2	<0.4	<0.8	<0.1	<0.4	<0.1	<0.1	<0.1	<0.1	<0.3
Well RN-14																	
HP18_14RN1-07	Upstream of OP	34	<1	<0.5	<44	0.2	<0.1	<2	0.3	0.9	0.09	0.4	<0.1	<0.05	<0.1	<0.1	<0.1
HP19_14RN2-07	Downstream of OP	22	<1	<0.5	<44	<0.1	<0.1	<2	0.2	0.5	0.07	0.4	<0.1	<0.05	0.1	<0.1	0.1
Well RN-10																	
HP20_10RN8_03	Downstream of FFCV	22	<1	<0.5	<44	0.1	0.2	<2	0.9	1.9	0.19	0.9	<0.1	<0.05	0.2	<0.1	0.1
<i>Scale pressure experiments</i>																	
RN-10	1.1	34	<3	17	<44	3.1	<0.1	<1	1	0.7	0.17	0.4	0.1	<0.05	<0.1	<0.1	<0.1
RN-10	3.1	18	<3	11.6	<44	1.2	<0.1	<1	1.1	0.7	0.19	0.5	0.1	<0.05	<0.1	<0.1	<0.1
RN-10	4.1	20	<3	21.7	<44	3.3	<0.1	<1	1.3	0.9	0.23	0.6	0.2	<0.05	<0.1	<0.1	<0.1

Table 2.8. (continued)

Surface pipelines	Locations	pressure bar	Ho ppm FUS-MS 0.1	Er ppm FUS-MS 0.1	Tm ppm FUS-MS 0.05	Yb ppm INAA 0.2	Lu ppm INAA 0.05
Well RN-11							
High pressure wells;							
HP1_11RN5T_02G	Wellhead 19/11	40	< 0.1	< 0.1	< 0.05	< 0.2	< 0.04
HP2_11RN1-07	Upstream of FFCV	43	< 0.1	< 0.05	< 0.05	< 0.2	< 0.04
HP3_11RNE1-2_07	FFCV	43	< 0.1	0.1	< 0.05	< 0.2	< 0.04
HP4_11RN3_07	Downstream of OP	22	< 0.1	< 0.1	< 0.05	< 0.2	< 0.04
HP5_11RN4-07	Downstream of OP	22	< 0.1	< 0.1	< 0.05	< 0.2	< 0.04
<i>Scale pressure</i>							
<i>experiments</i>							
RN-11	1.1	41	< 0.1	0.1	< 0.05	0.1	< 0.04
RN-11	1.2	41	< 0.1	0.1	< 0.05	0.1	< 0.04
Well RN-23							
HP9_23RN1-07	Upstream of OP	43	< 0.1	< 0.1	< 0.05	< 0.2	< 0.04
HP10_23RNEO-07	Upstream of OP	43	< 0.1	< 0.1	< 0.05	< 0.2	< 0.04
HP11_23RNE2-07	FFCV	43	< 0.1	< 0.1	< 0.05	< 0.2	< 0.04
HP12_23RN3D-07	OP (?)	22	< 0.1	< 0.1	< 0.05	< 0.2	< 0.04
HP13_23RN4-07	Downstream of OP	22	< 0.1	< 0.1	< 0.05	1.9	< 0.04
HP14_23RN5-07	Downstream of OP	22	< 0.1	< 0.1	< 0.05	< 0.2	< 0.04
HP15_23RN6-07	Downstream of OP	22	< 0.1	< 0.1	< 0.05	< 0.2	< 0.04
<i>(~32m)</i>							
HP16_23RN1_06RE	Downstream of OP	22	< 0.2	< 0.1	< 0.1	< 0.1	< 0.05
HP17_23RN1_09	Downstream of OP	22	< 0.2	< 0.1	< 0.1	< 0.1	< 0.05
Well RN-14							
HP18_14RN1-07	Upstream of OP	34	< 0.1	< 0.1	< 0.05	< 0.2	< 0.04
HP19_14RN2-07	Downstream of OP	22	< 0.1	< 0.1	< 0.05	< 0.2	< 0.04
Well RN-10							
HP20_10RN8_03	Downstream of FFCV	22	< 0.1	< 0.1	< 0.05	< 0.2	< 0.04
<i>Scale pressure</i>							
<i>experiments</i>							
RN-10	1.1	34	< 0.1	< 0.1	< 0.05	< 0.1	< 0.04
RN-10	3.1	18	< 0.1	< 0.1	< 0.05	< 0.1	< 0.04
RN-10	4.1	20	< 0.1	< 0.1	< 0.05	< 0.1	< 0.04

Table 2.8. (continued)

Surface pipelines	Locations	pressure	Zn % ICP- OES	Fe % INNA	Cu % ICP- OES	Pb % ICP- OES	S % IR	SO ₄ % IR	C _{Total} % IR	SiO ₂ % FUS- ICP	Al ₂ O ₃ % FUS- ICP	CaO % FUS- ICP	Na ₂ O % FUS- ICP	K ₂ O % FUS- ICP	MnO % FUS- ICP	MgO % FUS- ICP	LOI % FUS- ICP	Total %	
																			bar
Well RN-12																			
Medium pressure wells																			
MP1_12RNE1	FFCV		37	20.0	9.6	19.9	13.1	19.8	na	6.72	0.47	0.34	0.14	0.02	0.30	1.44	12.5	104.3	
MP2_12RNE2	FFCV		22	21.3	8.9	25.7	15.7	23.6	na	1.51	0.10	0.09	0.05	<0.01	0.14	0.19	12.2	109.5	
MP3_12RN2-07	Inside OP diameter		22	18.9	7.4	23.4	14.9	22.4	na	0.06	4.65	0.31	0.23	0.19	0.05	0.49	0.17	12.7	105.8
MP4_12RN1-07	Downstream of OP		22	13.9	9.3	20.4	10.5	16.5	na	0.09	12.53	0.81	0.53	0.11	1.16	1.15	15.3	102.9	
Well RN-21																			
MP5_21RNE1	FFCV		28	24.6	6.4	25.9	12.4	24.9	na	0.68	0.05	0.04	0.07	<0.01	0.06	0.07	11.7	106.8	
MP6_21RNE2	FFCV		22	26.0	5.9	24.1	13.3	24.4	na	0.90	0.06	0.04	0.11	0.05	0.07	0.07	12.1	107.1	
MP7_21RN2-07	OP		22	22.6	5.4	22.8	13.1	20.9	na	0.12	5.38	0.40	0.19	0.23	0.02	0.35	0.53	13.2	105.2
Well RN-24																			
MP9_24RNE1	Downstream of OP		22	20.7	7.4	26.3	16.7	23.3	na	0.84	0.06	0.04	0.07	<0.01	0.08	0.01	10.7	106.2	
MP8_24RNE2	FFCV		30	22.2	7.8	23.6	15.3	22.1	na	2.14	0.15	0.11	0.09	<0.01	0.26	0.18	na	93.9	
Well RN-13																			
LP1_13TRN4-04	Downstream of FFCV		28-26	2.8	1.1	1.4	1.4	2.2	na	0.06	84.0	1.5	0.4	0.5	0.1	0.030	5.7	101.5	
Well RN-15																			
LP4_15RN6-05	Downstr. of FFCV, upstream of OP		24.5	8.5	2.2	9.5	5.6	8.7	na	0.18	48.9	4.6	1.1	1.3	1.1	0.1	0.2	10.8	102.5
LP8_15RN1-07	Upstream of FFCV		24	6.9	15.5	12.0	7.0	14.6	na	0.07	22.8	2.2	0.6	0.4	0.3	0.6	6.8	13.3	103.1
LP9_15RN2-07	FFCV		26	16.3	5.8	31.2	14.4	23.2	na	0.17	2.1	0.1	0.1	0.1	<0.01	0.1	0.5	11.0	105.0
LP10_15RN3-07	Downstream of OP		22	13.6	7.8	23.5	10.6	17.6	na	0.14	10.9	0.7	0.3	0.2	0.1	0.7	2.7	13.1	101.8
Well RN-18																			
LP11_18RN2-07	Downstream of OP		22	17.9	7.0	26.8	11.5	22.2	na	0.15	5.3	0.4	0.2	0.3	0.020	0.4	0.8	11.5	104

Table 2.8. (continued)

	Locations	pressure	Ag ppm	Au ppm	As ppm	Sb ppm	Cd ppm	Hg ppm	Tl ppm	Ga ppm	Ge ppm	Mo ppm	Co ppm	Ni ppm	Se ppm	Bi ppm	In ppm	
		bar	INAA	INAA	INAA	US-MS INAA/F	TD-ICP	INAA	FUS-MS	FUS-MS	FUS-MS	FUS-MS	INAA	INAA	INAA	FUS-MS	FUS-MS	
Surface pipelines																		
Well RN-12																		
MP1_12RNE1	FFCV	37	6920	589	68	1	223	18	< 0.1	3	< 1	< 2	170	< 20	1199	0.5	< 0.2	
MP2_12RNE2	FFCV	22	9480	554	88	< 0.5	221	21	< 0.1	< 1	< 1	< 2	19	< 20	1199	< 0.4	< 0.2	
MP3_12RN2-07	Inside OP diameter	22	6620	370	35	5	150	32	< 0.1	< 1	< 1	< 2	< 1	< 20	707	0.4	< 0.2	
MP4_12RN1-07	Downstream of OP	22	6060	328	471	45	100	< 1	< 0.1	3	< 1	< 2	< 1	< 20	546	1.1	< 0.2	
Well RN-21																		
MP5_21RNE1	FFCV	28	17500	154	53	< 0.5	435	15	< 0.1	< 1	< 1	< 2	< 1	< 20	721	< 0.4	< 0.2	
MP6_21RNE2	FFCV	22	16300	127	175	8	391	14	0.1	< 1	< 1	< 2	< 1	< 20	764	< 0.4	< 0.2	
MP7_21RN2-07	OP	22	10800	201	174	48	230	< 1	< 0.1	1	< 1	< 2	< 1	< 20	354	< 0.4	< 0.2	
Well RN-24																		
MP9_24RNE1	Downstream of OP	22	15200	359	100	4	233	46	0.2	< 1	< 1	< 2	< 1	< 20	1350	< 0.4	< 0.2	
MP8_24RNE2	FFCV	30	13800	326	153	20	192	24	0.2	< 1	< 1	< 2	22	< 20	1328	0.9	< 0.2	
Well RN-13																		
LP1_13TRN4-04	Downstream of FFCV	28-26	1410	229	56	35	< 30	< 1	0.2	43	< 1	10	< 1	< 20	53	< 0.4	< 0.2	
Well RN-15																		
LP4_15RN6-05	Downstr. of FFCV, upstream of OP	24.5	6570	414	46	47	80	14	0.1	9	< 1	12	< 1	< 20	382	< 0.4	< 0.2	
LP8_15RN1-07	Upstream of FFCV	24	1260	136	< 0.5	< 0.1	140	< 1	< 0.1	14	< 1	4	3	< 20	446	0.4	< 0.2	
LP9_15RN2-07	FFCV	26	23200	163	< 0.5	< 0.1	160	< 1	< 0.1	2	< 1	< 2	< 1	< 20	587	0.4	< 0.2	
LP10_15RN3-07	Downstream of OP	22	14100	137	< 0.5	10	120	< 1	< 0.1	7	< 1	7	19	< 20	490	< 0.4	< 0.2	
Well RN-18																		
LP11_18RN2-07	Downstream of OP	22	21300	32	< 0.5	< 0.1	160	< 1	0.2	3	< 1	13	12	< 20	530	0.4	< 0.2	

Table 28. (continued)

Surface pipelines	Locations	pressure bar	Sn ppm FUS-MS	W ppm INAA	V ppm FUS-ICP	Cr ppm INAA	Nb ppm FUS-MS	Zr ppm FUS-ICP	Hf ppm US-MS	Ta ppm MS	Sc ppm INAA	Ti ppm ICP	Ir ppb INAA	Ba ppm FUS-ICP	Sr ppm ICP	Rb ppm FUS-MS	Cs ppm MS
Well RN-12																	
MP1_12RNE1	FFCV	37	< 1	3	< 5	45	< 1	< 4	< 0.2	< 0.1	< 1	12	< 5	7	6	< 2	< 0.5
MP2_12RNE2	FFCV	22	< 1	< 1	< 5	< 5	< 1	< 4	< 0.2	< 0.1	2	< 6	< 5	3	< 2	< 2	< 0.5
MP3_12RN2-07	Inside OP diameter	22	< 1	< 1	9	< 5	< 1	10	< 0.2	< 0.1	< 0.1	24	< 5	10	7	< 2	< 0.5
MP4_12RN1-07	Downstream of OP	22	< 1	< 1	20	< 5	< 1	< 4	< 0.2	< 0.1	< 0.1	24	< 5	26	12	4	< 0.5
Well RN-21																	
MP5_21RNE1	FFCV	28	< 1	< 1	< 5	34	< 1	< 4	< 0.2	< 0.1	< 1	12	< 5	3	< 2	< 2	< 0.5
MP6_21RNE2	FFCV	22	< 1	< 1	< 5	34	< 1	< 4	< 0.2	< 0.1	< 1	12	< 5	3	< 2	< 2	< 0.5
MP7_21RN2-07	OP	22	< 1	< 1	45	< 5	< 1	< 4	< 0.2	< 0.1	< 0.1	48	< 5	8	6	< 2	< 0.5
Well RN-24																	
MP9_24RNE1	Downstream of OP	22	< 1	< 1	< 5	43	< 1	< 4	< 0.2	< 0.1	< 1	12	< 5	5	< 2	< 2	< 0.5
MP8_24RNE2	FFCV	30	< 1	< 1	< 5	< 5	< 1	< 4	< 0.2	< 0.1	2	< 6	< 5	4	2	< 2	< 0.5
Well RN-13																	
LP1_13TRN4-04	Downstream of FFCV	28-26	< 1	< 1	67	123	< 1	< 4	< 0.2	< 0.1	< 0.1	18	< 5	31	10	18	0.9
Well RN-15																	
LP4_15RNG-05	Downstr. of FFCV,	24.5	1	< 1	72	< 5	< 1	17	0.4	0.5	< 0.1	246	< 5	185	57	41	2.1
LP8_15RN1-07	Upstream of FFCV	24	1	< 1	201	< 5	< 1	7	0.2	0.1	0.4	90	< 5	16	23	5	< 0.5
LP9_15RN2-07	FFCV	26	< 1	< 1	20	< 5	< 1	< 4	< 0.2	< 0.1	< 0.1	24	160	< 3	2	< 2	< 0.5
LP10_15RN3-07	Downstream of OP	22	< 1	< 1	111	< 5	< 1	< 4	< 0.2	< 0.1	< 0.1	24	< 5	8	8	< 2	< 0.5
Well RN-18																	
LP11_18RN2-07	Downstream of OP	22	< 1	< 1	41	< 5	< 1	< 4	< 0.2	< 0.1	< 0.1	24	< 5	5	5	< 2	< 0.5

Table 2.8. (continued)

Surface pipelines	Locations	pressure bar	Be		P	U	Th	Y	La	Ce	Pr	Nd	Sm	Eu	Gd	Tb	Dy
			ppm FUS-ICP	ppm INAA													
Well RN-12																	
Medium pressure wells																	
MP1_12RNE1	FFCV	37	< 1	< 0.5	<44	<0.1	< 0.1	<0.2	< 0.1	< 0.1	< 0.05	< 0.1	< 0.1	< 0.05	< 0.1	<0.5	< 0.1
MP2_12RNE2	FFCV	22	< 1	< 0.5	<44	<0.1	< 0.1	<0.2	< 0.1	< 0.1	< 0.05	< 0.1	0.1	< 0.05	< 0.1	<0.5	< 0.1
MP3_12RN2-07	Inside OP diameter	22	< 1	< 0.5	<44	<0.1	< 0.1	<0.2	< 0.1	< 0.1	< 0.05	< 0.1	< 0.1	< 0.05	< 0.1	<0.1	< 0.1
MP4_12RN1-07	Downstream of OP	22	< 1	< 0.5	<44	<0.1	< 0.1	<0.2	< 0.1	< 0.1	< 0.05	< 0.1	< 0.1	< 0.05	< 0.1	<0.1	< 0.1
Well RN-21																	
MP5_21RNE1	FFCV	28	< 1	< 0.5	<44	<0.1	< 0.1	<0.2	< 0.1	< 0.1	< 0.05	< 0.1	0.3	< 0.05	< 0.1	<0.5	< 0.1
MP6_21RNE2	FFCV	22	< 1	< 0.5	<44	<0.1	< 0.1	<0.2	< 0.1	< 0.1	< 0.05	< 0.1	0.3	< 0.05	< 0.1	<0.5	< 0.1
MP7_21RN2-07	OP	22	< 1	< 0.5	<44	<0.1	< 0.1	<0.2	0.2	0.3	< 0.05	0.2	< 0.1	< 0.05	< 0.1	<0.1	< 0.1
Well RN-24																	
MP9_24RNE1	Downstream of OP	22	< 1	< 0.5	<44	<0.1	< 0.1	<0.2	< 0.1	< 0.1	< 0.05	< 0.1	0.2	< 0.05	< 0.1	<0.5	< 0.1
MP8_24RNE2	FFCV	30	< 1	< 0.5	<44	<0.2	< 0.1	<0.2	< 0.1	< 0.1	< 0.05	< 0.1	0.2	< 0.05	< 0.1	<0.5	< 0.1
Well RN-13																	
LP1_13TRN4-04	Downstream of FFCV	28-26	2	2.8	<44	< 0.1	< 0.1	< 0.2	0.3	0.3	< 0.05	0.1	< 0.1	< 0.05	< 0.1	< 0.1	< 0.1
Well RN-15																	
LP4_15RN6-05	Downstr. of FFCV, upstream of OP	24.5	1	< 0.5	<44	0.3	0.4	< 0.2	1.5	2.7	0.3	1.2	< 0.1	0.08	0.2	< 0.1	0.2
LP8_15RN1-07	Upstream of FFCV	24	< 1	< 0.5	<44	0.1	0.2	< 0.2	1	1.5	0.19	0.6	< 0.1	< 0.05	0.1	< 0.1	< 0.1
LP9_15RN2-07	FFCV	26	< 1	< 0.5	<44	< 0.1	< 0.1	< 0.2	< 0.1	< 0.1	< 0.05	< 0.1	< 0.1	< 0.05	< 0.1	< 0.1	< 0.1
LP10_15RN3-07	Downstream of OP	22	< 1	< 0.5	<44	< 0.1	< 0.1	< 0.2	0.1	0.2	< 0.05	0.2	< 0.1	< 0.05	< 0.1	< 0.1	< 0.1
Well RN-18																	
LP11_18RN2-07	Downstream of OP	22	< 1	< 0.5	<44	< 0.1	< 0.1	< 0.2	< 0.1	< 0.1	< 0.05	< 0.1	< 0.1	< 0.05	< 0.1	< 0.1	< 0.1

Table 2.8. (continued)

Surface pipelines	Locations	pressure bar	Ho	Er	Tm	Yb	Lu
			ppm FUS-MS	ppm FUS-MS	ppm FUS-MS	ppm INAA	ppm INAA
Well RN-12	Medium pressure wells						
MP1_12RNE1	FFCV	37	< 0.1	< 0.1	< 0.05	< 0.1	< 0.04
MP2_12RNE2	FFCV	22	< 0.1	< 0.1	< 0.05	< 0.1	< 0.04
MP3_12RN2-07	Inside OP diameter	22	< 0.1	< 0.1	< 0.05	< 0.2	< 0.04
MP4_12RN1-07	Downstream of OP	22	< 0.1	< 0.1	< 0.05	< 0.2	< 0.04
Well RN-21							
MP5_21RNE1	FFCV	28	< 0.1	< 0.1	< 0.05	< 0.1	< 0.04
MP6_21RNE2	FFCV	22	< 0.1	< 0.1	< 0.05	< 0.1	< 0.04
MP7_21RN2-07	OP	22	< 0.1	< 0.1	< 0.05	< 0.2	< 0.04
Well RN-24							
MP9_24RNE1	Downstream of OP	22	< 0.1	< 0.1	< 0.05	< 0.1	< 0.04
MP8_24RNE2	FFCV	30	< 0.1	< 0.1	< 0.05	< 0.1	< 0.04
Well RN-13	Low pressure wells						
LP1_13TRN4-04	Downstream of FFCV	28-26	< 0.1	< 0.1	< 0.05	< 0.2	< 0.04
Well RN-15							
LP4_15RN6-05	Downstr. of FFCV, upstream of OF	24.5	< 0.1	< 0.1	< 0.05	< 0.2	< 0.04
LP8_15RN1-07	Upstream of FFCV	24	< 0.1	< 0.1	< 0.05	< 0.2	< 0.04
LP9_15RN2-07	FFCV	26	< 0.1	< 0.1	< 0.05	< 0.2	< 0.04
LP10_15RN3-07	Downstream of OP	22	< 0.1	< 0.1	< 0.05	< 0.2	< 0.04
Well RN-18							
LP11_18RN2-07	Downstream of OP	22	< 0.1	< 0.1	< 0.05	< 0.2	< 0.04

ICP-OES, Inductively coupled plasma optical emission spectrometry; FUS-MS, Fusion mass spectrometry; FUS_ICP, Fusion Inductively coupled plasma; IR, infrared; INAA, instrumental neutron activation analysis; LOI, loss on ignition; TD-ICP, Total Digestion; number below methods are dl. Inductively coupled plasma; na- not analyzed; <, below detection limits (dl) of the method; number below analytical methods are dl.

Table 2.9. Bulk composition of scales from 2009 downhole RN-22 Reykjanes geothermal system

Downhole RN-22	Depth (m)	pressure bar	Zn	Fe	Cu	Pb	S	C _{total}	SiO ₂	Al ₂ O ₃	CaO	Na ₂ O	K ₂ O	MnO	MgO	LOI	Total
			%	%	%	%	%	%	%	%	%	%	%	%	%	%	%
22RN669	669	~52 bar	44.8	7.0	3.5	0.003	28.6	na	<0.02	0.9	0.13	0.38	<0.12	0.05	1.2	na	86.6
22RN618	618	(267°C)	48.0	6.2	2.1	0.003	28.2	na	<0.02	1.0	0.17	0.38	<0.12	0.05	1.1	na	87.2
22RN570	570		45.9	5.7	1.2	0.003	27.4	na	<0.02	1.1	0.20	0.40	<0.12	0.05	1.2	na	83.3
22RN449	449		42.2	8.3	1.6	0.003	24.1	na	<0.02	1.6	0.34	0.62	<0.12	0.08	2.2	na	81.0
22RN350Fe*	350		38.2	8.9	1.8	0.006	22.8	na	<0.02	1.8	0.53	0.65	<0.12	0.10	2.3	na	77.1
22RN270Fe*	270		32.5	13.2	3.4	0.008	22.1	na	11.3	1.6	0.62	0.70	<0.12	0.11	1.9	na	87.4
22RN160Fe*	160		25.6	23.1	2.9	0.020	16.4	na	<0.02	1.2	0.56	0.51	<0.12	0.28	1.4	na	71.9
22RN150	150		41.0	8.0	3.7	0.014	25.5	na	<0.02	1.6	0.70	0.43	<0.12	0.10	1.8	na	82.8
22RN141	141	~46 (260°C)	44.4	7.0	3.8	0.014	25.0	na	<0.02	1.6	0.35	0.43	<0.12	0.08	1.8	na	84.5
Surface pipeline RN-22																	
HP7_22RN5-07	Upstream of OP	32	47.8	2.7	11.0	0.3	30.3	0.07	3.6	0.5	0.2	0.02	0.0	0.4	0.030	14.8	111.7
HP8_22RN16-07	Downstream of OP	22	42.3	3.8	17.8	1.0	28.3	0.04	1.9	0.1	0.1	0.09	0.1	0.1	0.1	16.4	112.0
Downhole RN-22	Depth (m)	pressure bar	Ag	Au	Se	As	Sb	Cd	Hg	Tl	Ga	Ge	Mo	Co	Ni	Te	Bi
			ppm	ppm	ppm	ppm	ppm	ppm	ppm	ppb	ppm	ppm	ppm	ppm	ppm	ppm	ppm
22RN669	669	~52 (267°C)	5	2	3	0.5	0.1	2	5	0.1	0.2	0.7	1	1	10	6	2
22RN618	618		35	89	1600	<0.5	<0.1	>5000	13	0.1	13	<0.7	<1	226	20	17.0	<2
22RN570	570		38	85	1490	<0.5	<0.1	>5000	8	<0.1	13	<0.7	<1	240	20	15.0	<2
22RN449	449		37	82	1360	<0.5	<0.1	>5000	6	<0.1	12	<0.7	<1	251	20	12.0	<2
22RN350Fe*	350		57	82	1180	<0.5	<0.1	>5000	6	<0.1	13	<0.7	<1	219	20	13.0	<2
22RN270Fe*	270		85	80	1010	<0.5	<0.1	>5000	11	0.2	11	<0.7	6	195	30	11.0	<2
22RN160Fe*	160		129	81	975	9	2.2	4770	18	0.2	10	<0.7	7	180	40	9.0	<2
22RN150	150	~46 (260°C)	378	75	664	28	7.4	4080	34	1.4	12	2.2	36	131	180	<6	<2
22RN141	141		584	125	1110	<0.5	<0.1	>5000	14	0.1	12	<0.7	2	180	20	7.0	<2
Surface pipeline RN-22																	
HP7_22RN5-07	Upstream of OP	32	887	106	982	<0.5	<0.1	8900	<1000	<0.1	3	<1	3	206	<20	-	<0.4
HP8_22RN16-07	Downstream of OP	22	3510	79.9	379	454	21	4380	<1000	<0.1	1	<1	10	88	<20	-	0.8

Table 2.9. (continued)

Downhole RN-22	Depth (m)	pressure bar	In	Sn	W	V	Cr	Nb	Zr	Hf	Ta	Sc	Ti	Ir	Ba	Sr	Rb	FUS-	
																		MS	MS
22RN669	669	~52 (267°C)	< 0.2	6.9	< 0.7	192	< 5	< 2.4	na	3	< 0.2	< 0.1	< 100	< 5	8	7	1.0		
22RN618	618		< 0.2	5.8	< 0.7	256	37	< 2.4	na	< 1	< 0.2	< 0.1	< 100	< 5	7	9	1.3		
22RN570	570		< 0.2	4.2	1	269	< 5	< 2.4	na	< 1	< 0.2	< 0.1	< 100	< 5	7	9	1.3		
22RN449	449		< 0.2	3.6	1.5	442	37	< 2.4	na	< 1	< 0.2	0.6	< 100	< 5	11	15	2.0		
22RN350Fe*	350		< 0.2	4.2	22.5	458	122	< 2.4	na	< 1	< 0.2	1.9	200	< 5	15	18	1.9		
22RN270Fe*	270		< 0.2	5.8	4.6	378	157	< 2.4	na	3	< 0.2	< 0.1	100	< 5	22	14	2.0		
22RN160Fe*	160		< 0.2	18	2.7	466	155	< 2.4	na	< 1	< 0.2	1.6	300	< 5	55	18	1.7		
22RN150	150	~46 (260°C)	< 0.2	3.5	< 0.7	814	< 5	< 2.4	na	< 1	< 0.2	1.3	600	< 5	26	14	1.9		
22RN141	141		< 0.2	4.2	< 0.7	847	< 5	< 2.4	na	< 1	< 0.2	1.6	200	< 5	8	13	2.0		
Surface pipeline RN-22																			
HP7_22RN5-07	Upstream of OP	32	< 0.2	< 1	< 1	79	< 5	< 1	< 4	0.5	0.1	< 0.1	144	< 5	12	9	< 2		
HP8_22RN16-07	Downstream of OP	22	< 0.2	< 1	< 1	10	92	< 1	7	< 0.2	< 0.1	< 0.1	66	< 5	5	4	< 2		

Downhole RN-22	Depth (m)	pressure bar	Cs	Li	Be	B	Br	P	U	Th	Y	La	Ce	Pr	Nd	Sm	Eu	FUS-	
																		MS	MS
22RN669	669	~52 (267°C)	< 0.1	3	< 3	10	8	130	< 0.1	< 0.1	0.2	< 0.4	< 0.8	< 0.1	< 0.4	< 0.1	< 0.1		
22RN618	618		< 0.1	< 3	< 3	< 10	< 0.5	90	< 0.1	< 0.1	0.2	< 0.4	< 0.8	< 0.1	< 0.4	< 0.1	< 0.1		
22RN570	570		< 0.1	< 3	< 3	< 10	9.5	80	< 0.1	< 0.1	0.2	< 0.4	< 0.8	< 0.1	< 0.4	< 0.1	< 0.1		
22RN449	449		< 0.1	< 3	< 3	10.0	< 0.5	< 50	< 0.1	< 0.1	0.2	< 0.4	< 0.8	< 0.1	< 0.4	< 0.1	< 0.1		
22RN350Fe*	350		< 0.1	< 3	< 3	30.0	< 0.5	100	< 0.1	< 0.1	0.6	< 0.4	< 0.8	< 0.1	< 0.4	< 0.1	< 0.1		
22RN270Fe*	270		0.1	< 3	< 3	20.0	8.8	270	< 0.1	< 0.1	< 0.1	< 0.4	< 0.8	< 0.1	< 0.4	< 0.1	< 0.1		
22RN160Fe*	160		< 0.1	18.0	< 3	< 10	12	240	< 0.1	< 0.1	0.8	< 0.4	< 0.8	< 0.1	< 0.4	0.1	< 0.1		
22RN150	150	~46 (260°C)	0.5	3.0	< 3	< 10	< 0.5	250	< 0.1	< 0.1	0.5	< 0.4	< 0.8	< 0.1	< 0.4	< 0.1	< 0.1		
22RN141	141		< 0.1	5.0	< 3	< 10	< 0.5	190	< 0.1	< 0.1	0.5	< 0.4	< 0.8	< 0.1	< 0.4	< 0.1	< 0.1		
Surface pipeline RN-22																			
HP7_22RN5-07	Upstream of OP	32	< 0.5	< 3	< 1	-	< 0.5	< 44	0.3	0.4	< 2	1.3	2.8	0.28	1	< 0.1	0.07		
HP8_22RN16-07	Downstream of OP	22	< 0.5	-	< 1	-	< 0.5	< 44	0.5	0.1	< 2	0.4	1.1	0.1	0.4	< 0.1	< 0.05		

Table 2.9. (continued)

Downhole RN-22	Depth (m)	pressure bar	Gd ppm FUS- MS	Tb ppm FUS- MS	Dy ppm FUS- MS	Ho ppm FUS-MS	Er ppm FUS-MS	Tm ppm FUS- MS	Yb ppm FUS- MS	Lu ppm FUS- MS
22RN669	669	~52 (267°C)	< 0.1	< 0.1	< 0.3	< 0.2	< 0.1	< 0.1	< 0.1	< 0.05
22RN618	618		< 0.1	< 0.1	< 0.3	< 0.2	< 0.1	< 0.1	< 0.1	< 0.05
22RN570	570		< 0.1	< 0.1	< 0.3	< 0.2	< 0.1	< 0.1	< 0.1	< 0.05
22RN449	449		< 0.1	< 0.1	< 0.3	< 0.2	< 0.1	< 0.1	< 0.1	< 0.05
22RN350Fe*	350		< 0.1	< 0.1	< 0.3	< 0.2	< 0.1	< 0.1	< 0.1	< 0.05
22RN270Fe*	270		< 0.1	< 0.1	< 0.3	< 0.2	< 0.1	< 0.1	< 0.1	< 0.05
22RN160Fe*	160		0.1	< 0.1	< 0.3	< 0.2	< 0.1	< 0.1	< 0.1	< 0.05
22RN150	150	~46 (260°C)	< 0.1	< 0.1	< 0.3	< 0.2	< 0.1	< 0.1	< 0.1	< 0.05
22RN141	141		< 0.1	< 0.1	< 0.3	< 0.2	< 0.1	< 0.1	< 0.1	< 0.05
Surface pipeline RN-22										
HP7_22RN5-07	Upstream of OP	32	0.1	< 0.1	0.2	< 0.1	< 0.1	< 0.05	2.1	< 0.05
HP8_22RN16-07	Downstream of OP	22	< 0.1	< 0.1	< 0.1	< 0.1	< 0.1	< 0.05	< 0.2	< 0.05

263°-268°C both P (bar) and T°C measured in May 2008, latter measurement at 700 m depth; wh, wellhead; OP; orifice plate; FFCV, fluid flow control valve; ICP-MS, Inductively coupled plasma mass spectrometry; ICP-OES, Inductively coupled plasma optical emission spectrometry; FUS-ICP, Fusion Inductively coupled plasma; COUL, coulometry; FUS-MS Na2O2, Fusion mass spectrometry with Na2O2; IR, infrared; INAA, instrumental neutron activation analysis; LOI, loss of ignition *samples contaminated with Fe (magnetic pieces) from the steel pipe; SiO2, Al2O3, CaO, Na2O, K2O, MgO and TiO2 measured as Si, Al, Ca, Na, K, Mg and Ti with detection limits (dl) 0.01 wt.% and MnO as Mn with detection limits (dl) 0.001; Zn measured with a detection limit of ppm 3; number below analytical methods are dl.

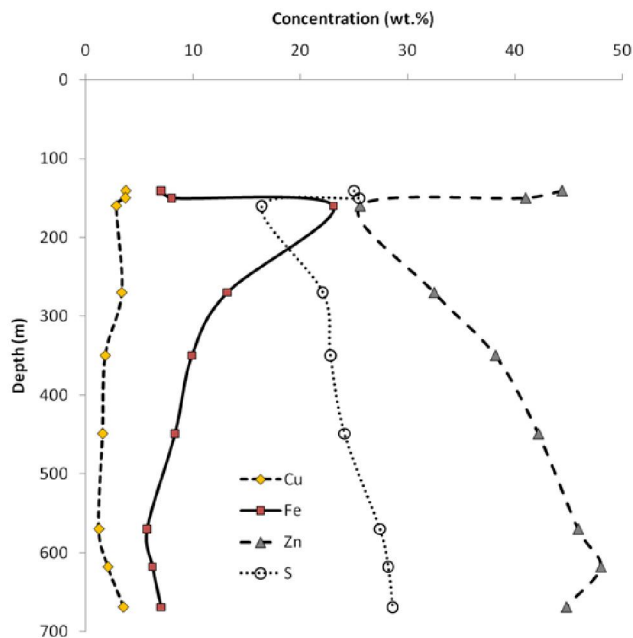


Figure 2.20. Concentrations of Zn, Cu, Fe and S in scales from downhole in RN-22, showing the antithetic behaviour of Zn and Fe and rather constant concentration of Cu. Sulfur tracks Zn. The increase in Fe concentration is most likely due to formation of maghemite. Zinc concentration decreases with lowering HS- concentration due to degassing of the boiling liquid as H₂S moves into the vapor phase.

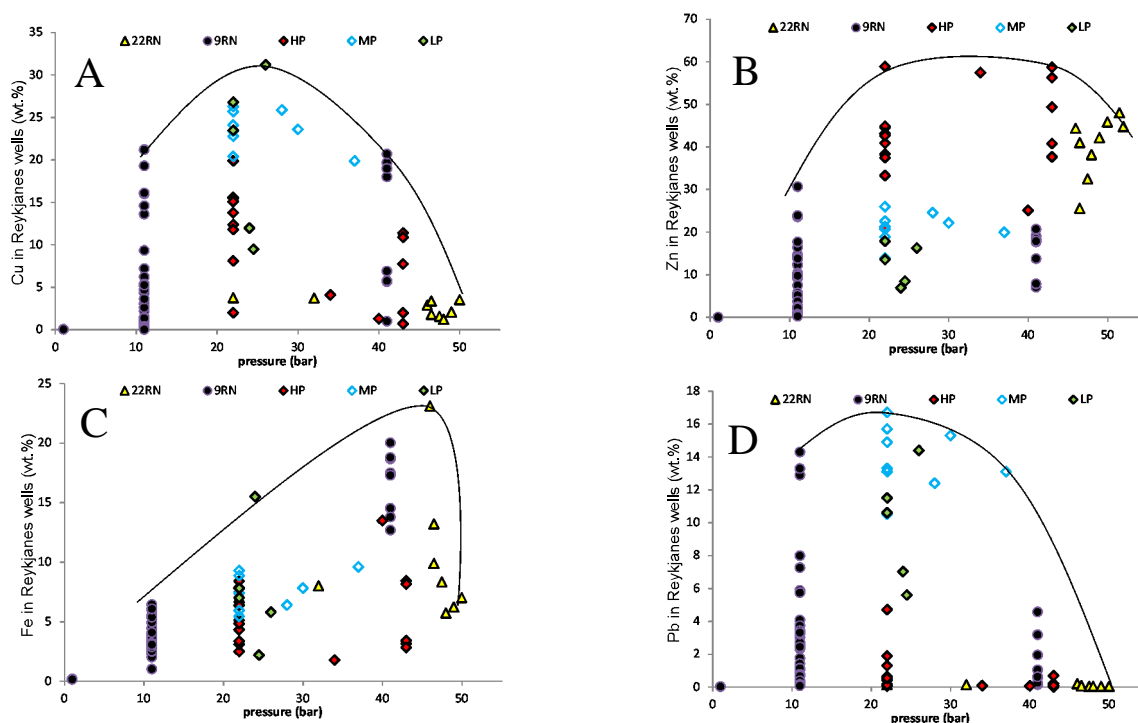


Figure 2.21. Concentrations (wt.%) of the major metals in scales versus pressure from all wells at Reykjanes. A) Cu, B) Zn, C) Fe, D) Pb. The black line illustrates the general trend of the concentrations for each element. These data shows that Zn and Fe are mainly deposited at higher pressure and Cu and Pb at lower pressure. HP, MP, LP are high, medium and low pressure wells.

Table 2.10 Normative abundances of minerals by weight from well RN-9

	Locations	sphale rite wt%	galena wt%	chalco pyrite wt%	bornite wt%	SiO ₂ wt%	Total oxides wt%	LOI wt%	Totals wt%
9RN20-2000	upstream of orifice plate	27.6	0.2	52.0	nc	6.1	2.7	15.0	104.4
9RN31A-2000	downstream on orifice plate	36.9	6.8	2.3	24.0	14.4	3.0	14.9	103.6
9RN2-2005G	< 1m downstream of orifice plate	23.0	14.9	2.1	21.9	26.9	5.2	10.2	104.8
9RN3-2005G	< 1m downstream of orifice plate	25.6	16.5	2.3	24.2	21.3	4.5	10.6	105.3
9RN29	~4 m downstream of orifice plate	19.1	2.0	9.0	4.9	47.0	6.1	14.3	103.0
9RN29-2000	~4 m downstream of orifice plate	14.3	3.0	8.4	2.3	54.6	7.1	12.0	102.5
9RN28-2000	~4 m downstream of orifice plate	16.2	3.5	10.0	1.3	49.8	6.2	15.2	102.8
9RN27B-2000	~4 m downstream of orifice plate	14.8	3.1	9.1	2.5	53.4	7.0	12.2	103.0
9RN4	~30 m downsteam of orifice plate	3.5	3.8	1.6	nc	82.6	4.6	6.4	102.7

nc, not calculated (not seen in thin sections)

(~45 bar) contained 23 wt.% Fe, but most of this is considered to be precipitation of maghemite and contamination from the steel pipe (Fig. 2.21C and Table 2. 9). Grains of maghemite occur in the scale up the well, and these likely account for the remainder of the Fe downhole. Lead is at the ppm level downhole in RN-22, consistent with the lack of galena seen in thin section. The Pb concentration increases at lower pressure and is highest in scales on the fluid-flow control valve and immediately downstream of the orifice plate in well RN-9 (Figs. 2.21D and 2.22).

The scales in the surface pipeline of well RN-9 also vary in composition with distance from the well head (Fig. 2.22A-D). The highest concentrations of Zn, Cu, Fe and Pb occur in scales near the orifice plate and decrease downstream from there. Locally, high concentrations of metals also occur in scales formed in “traps” (e.g., at bends ~30 m downstream of the orifice plate).

The SiO₂ concentration in scales is below detection (<0.01 wt.%) in downhole samples, with one exception. In the surface pipelines SiO₂ concentrations increased as pressure

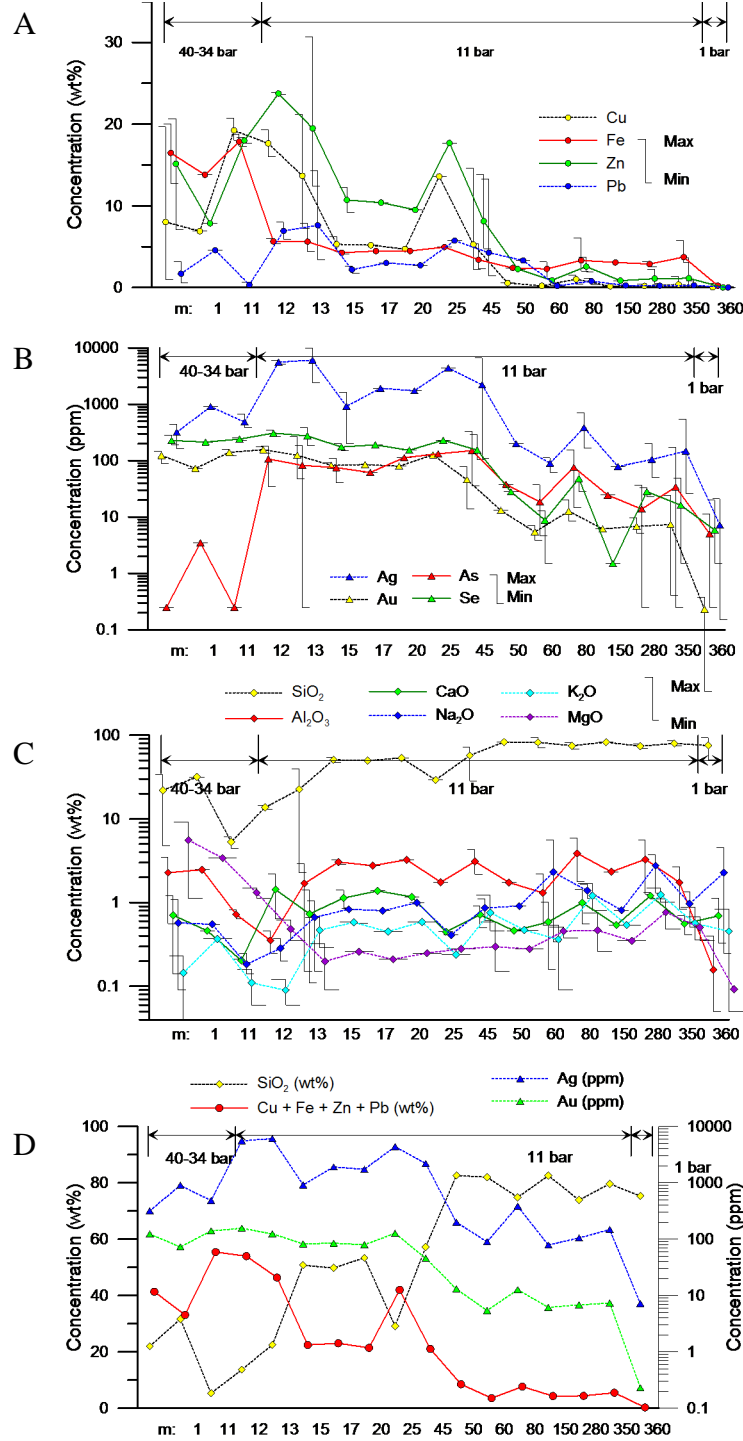


Figure 2.22. Bulk concentrations of major and trace elements in scales downstream of well-head to the separation station in pipeline of well RN-9. The intervals between the numbers indicate groups 1 (40-34 bar) to 3 (<1 bar). A) Cu, Fe, Zn and Pb. B) Ag, Au, Se, and As. C) Oxides. D) Average of Cu+Fe+Zn+Pb, SiO₂, Au and Ag. The main trends are the sulfides reach their highest concentration around the orifice plate where As starts to precipitate and Ag increases in concentration downstream of the orifice plate. Gold and Se are rather constant the first 25 m downstream of the wellhead. Silica starts to precipitate downstream of the orifice plate.

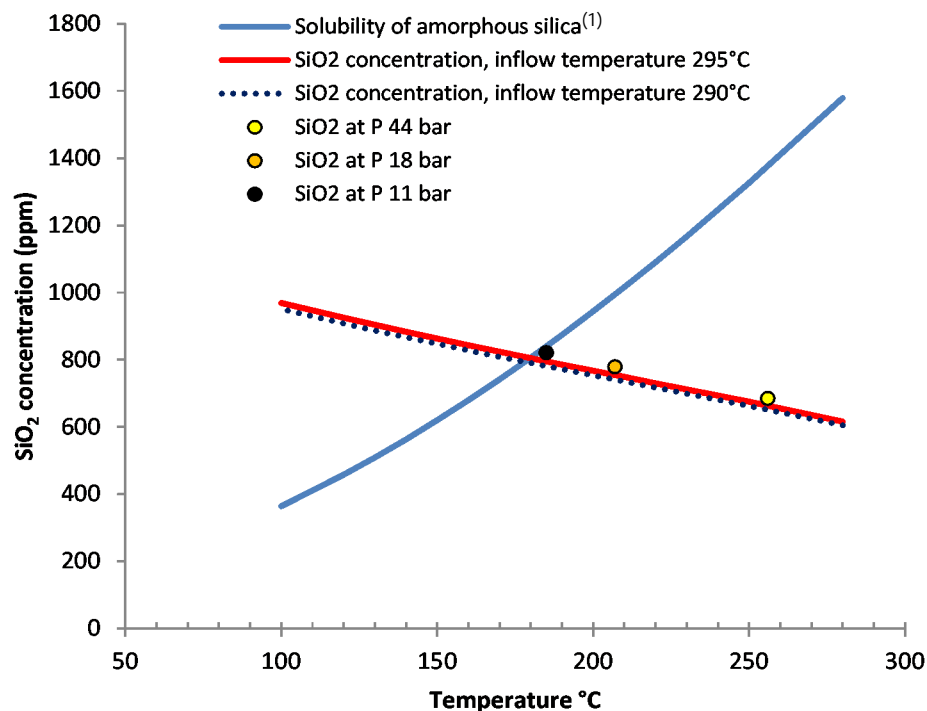


Figure 2.23. Solubility of amorphous silica versus temperature, showing SiO_2 concentrations at inflow temperatures 295° and 290°C and at pressures of 44, 18 and 11 bar. Where the solubility and the concentration lines meet below $\sim 180^\circ\text{C}$, precipitation of SiO_2 starts.

⁽¹⁾Fournier and Rowe, 1977

decreased below the solubility of amorphous silica in the fluids. This only occurs downstream of the orifice plate at a pressure of ~ 11 bar (188°C ; Table A2.2) in RN-9, as shown on Figure 2.23. Al_2O_3 and MgO concentrations are typically 1 to 5 wt.%; however, scales at the wellhead in RN-9 contain as much as 9 wt.% MgO in clay minerals (most likely Mg- and Fe-bearing smectite). Na_2O , K_2O , and CaO are typically <1 wt.% each (Figs. 2.22C, D). These are most likely incorporated in the poorly crystallized clay identified by XRD or as salts.

2.8.2 Normative calculations for well RN-9

From these data it is clear that the sphalerite, chalcopyrite and bornite account for all the Zn and Cu in the samples and some of the Fe, whereas galena accounts for all the Pb. Normative calculations based on weight percent of the major elements compare well with the

bulk mineralogy of the scales. For these calculations it was assumed that the sum of sulfides + balance of Fe + wt.% SiO₂ + oxides (Al, Mn, Mg, Ca, Na, K) + loss on ignition (LOI) totals 100 wt.%. All Zn was assumed to be in sphalerite, Pb in galena, and Cu in chalcopyrite and bornite. The Fe content of sphalerite was based on the average Fe concentration measured in sphalerites. The remaining Fe was apportioned first to chalcopyrite then to bornite. The proportion of chalcopyrite to bornite was estimated from thin section and then all remaining Fe was attributed to those minerals in the proportion given in Table A2.8. The results of these calculations are shown in Table 2.10 and in Appendix 2.5 Table A2.8.

According to the normative calculations, sphalerite, bornite and galena all reach their maximum immediately downstream of the orifice plate, ~37, ~25 and ~15 wt.%, respectively, where chalcopyrite is at its minimum ~2 wt.% (Table 2.10). Chalcopyrite is at its maximum upstream of the orifice plate where the pressure is highest. Galena and bornite decrease sharply, whereas sphalerite diminishes gradually, (to 1-5 wt.%) about 30 m downstream of the orifice plate. Chalcopyrite increases again to ~10 wt.% in the next 4 m downstream of the orifice plate and decreases from there; in the same interval, amorphous silica increases from ~5 wt.% upstream of the orifice plate to 55 wt.% ~4 m downstream. Amorphous silica accounts for ~80% of the scale downstream of the orifice plate.

2.8.3 Trace elements

The concentrations of most trace metals in the scales are remarkably low considering the high concentrations of major metals, except for Cd, Se, Au, and Ag. A number of components of the scales appear to account for most of the variance in the trace metal concentrations, indicated by the correlation matrix (Table 2.11). The polymetallic suite (Zn, Cu, Pb, Fe, S, Cd, Se, Au and Ag) shows the strongest correlations (Fig. 2.24), consistent

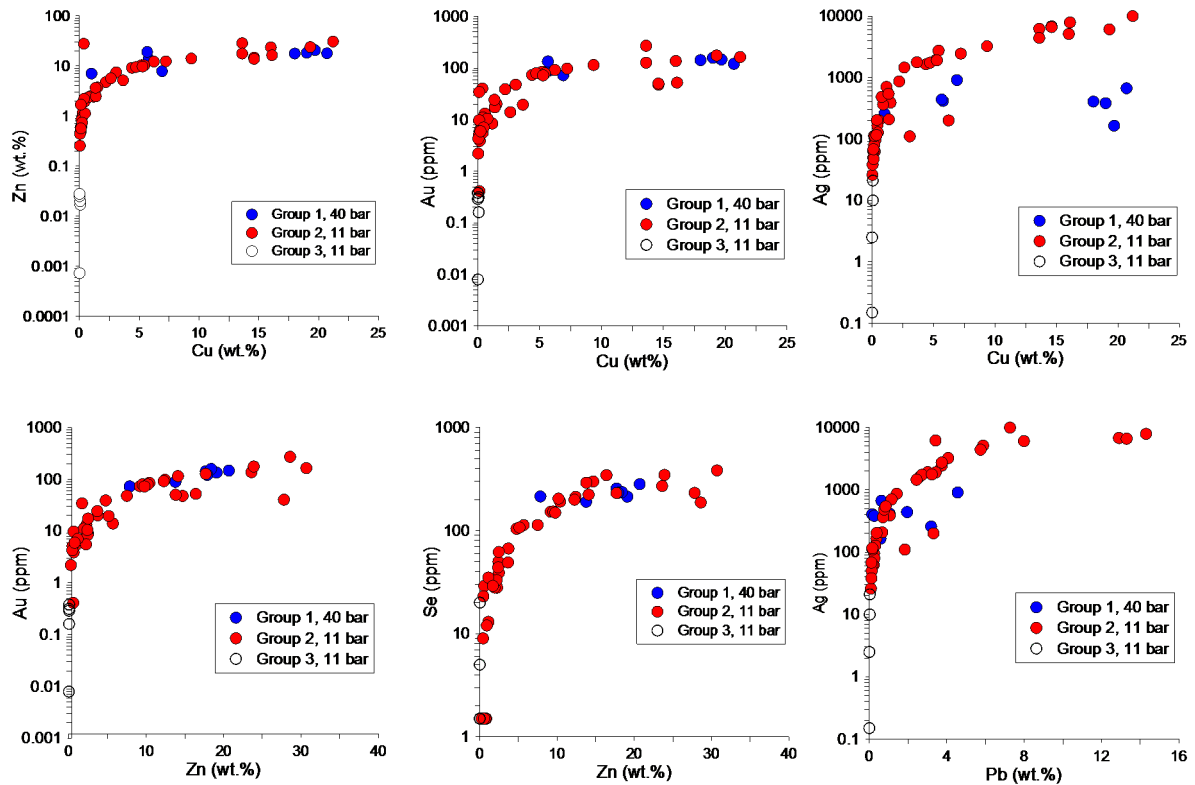


Figure 2.24. Multielement plots showing the correlations of Au, Ag, and Se with the major metals Cu, Zn, and Pb in scale from well RN-9. Group 1 scales are formed at ~40 bar, group 2 scales at 11 bar and group 3 at 1 bar.

with the coprecipitation of Zn, Cu, Pb sulfides and the high Fe, Cd, and Se content of the sphalerite (Figs. 2.8, 2.10, 2.11), which is the most abundant of the sulfides.

The highest concentrations of Se are apparently in solid solution in sphalerite (replaces S; Fig. 2.25), although some Se may be present in galena or clausthalite (PbSe) (Fig. 2.26). A distinct bimodal distribution is seen in Figure 2.25, which may reflect direct substitution of Se in sphalerite at lower concentration and a coupled substitution with Cd at higher concentrations. The distribution of Se suggests a strong positive temperature dependence, with the highest concentration downhole in RN-22 (660-1600 ppm), decreasing to 200-400 ppm in the surface pipeline in RN-9 (the first 40 m downstream of the orifice plate) to less than 50 ppm at bend 3. In the newer wells, Se concentrations in the scales are also generally between 200 to 1000 ppm.

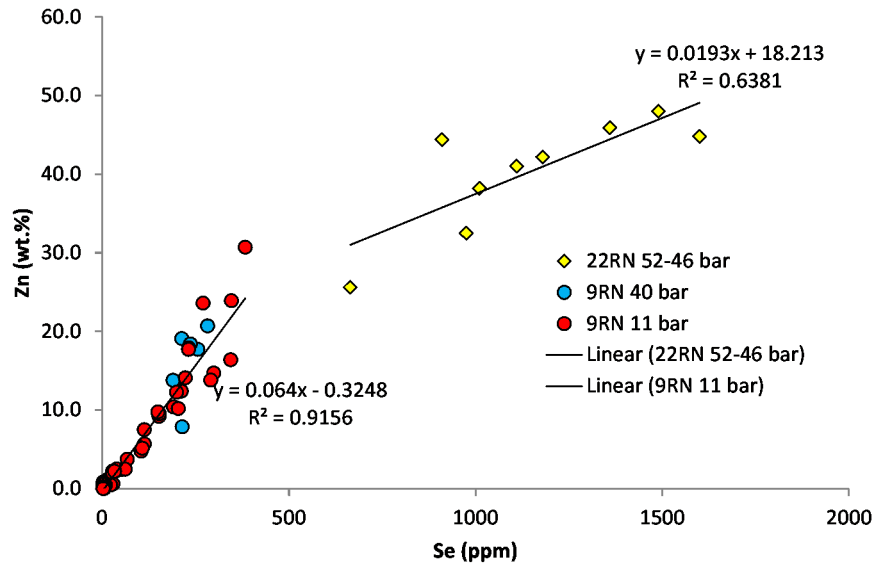


Figure 2.25. Correlations between Zn and Se in downhole samples RN-22 and surface pipeline RN-9. Bimodal distribution of Se in sphalerite is due to substitution of Se for S as the latter decreases in the liquid (see Fig. 2.20), whereas Se correlates with Pb (as galena) at surface as seen in Figure 2.26.

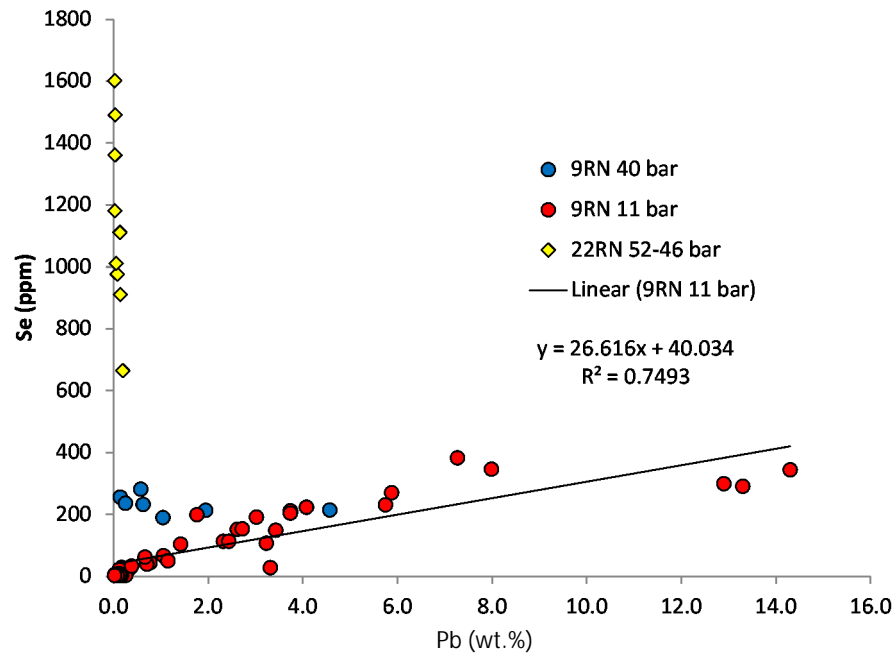


Figure 2.26. Plot of Se versus Pb concentrations in downhole scale samples from RN-22 and surface pipeline RN-9. Selenium is in solid solution in sphalerite in RN-22 whereas Se is in galena or possibly in clausthalite (PbSe) in RN-9, see Figure 2.25.

Like Se, the Cd concentrations downhole in RN-22 are >5000 ppm, mainly present in sphalerite. Cadmium in well RN-9 is lower (up to 260 ppm), and decreases downstream of the orifice plate to <0.3 ppm in the valve house. Mercury concentrations are generally below detection limit (1 ppm), but a few samples on the fluid flow-control valve in the medium-pressure wells have between ~20 to 50 ppm Hg, also likely in sphalerite.

Gold reaches its maximum concentration near the orifice plate/fluid flow control valve and is present at concentrations up to ~950 ppm just downstream of the orifice plate in the high-pressure well RN-11. In well RN-9 the highest Au value is from a sample located on the downstream side of the orifice plate (176 ppm). Gold concentrations decrease downstream of the orifice plate in all wells (Fig. 2.22B). Upstream of the orifice plate in well RN-9, fine inclusions of electrum were observed in most galena grains, as well as in chalcopyrite, sphalerite (Figs. 2.7A), and locally in pyrrhotite. At depth in RN-22, gold concentrations are uniformly high (~80 ppm) in the well scales down to ~670 m, suggesting that gold precipitation commenced in the well at the point of first boiling (Fig. 2.27)

The gold is most closely associated with the Cu-rich scales, and is only moderately correlated with Ag (Table 2.11). Silver is present in electrum, commonly associated with galena (Figs. 2.7C and 2.28), but it may also be present in bornite, as indicated by microprobe data from bornite samples in the newer wells (see Chapter 3 and Table 2.6). The high Au/Ag ratios of the bulk scales (Fig. 2.29) and the electrum may reflect the source or the physical separation of Au and Ag in different parts of the system. Gold and Ag are uniformly high in the scales of the medium-pressure wells close to the orifice plate, but the Au/Ag ratio decreases downstream of the orifice plate, suggesting that the Ag is transported to lower temperatures than the gold (Fig. 2.22B). This is consistent with the relative

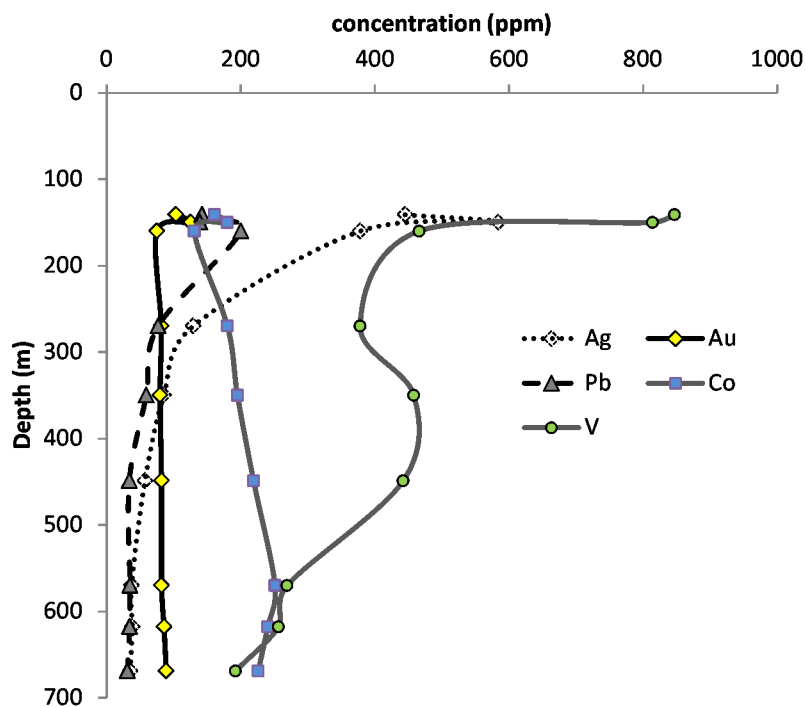


Figure 2.27. Concentrations of Ag, Au, Pb, Co, and V in scales from downhole in well RN-22 (669 m to 140 m depth). Lead and Ag regularly increase up the well due to boiling, whereas Au is constant. Vanadium likely precipitates in the maghemite; the reason for the sharp increase in V concentration is not known. Cobalt precipitates with the Cu-minerals.

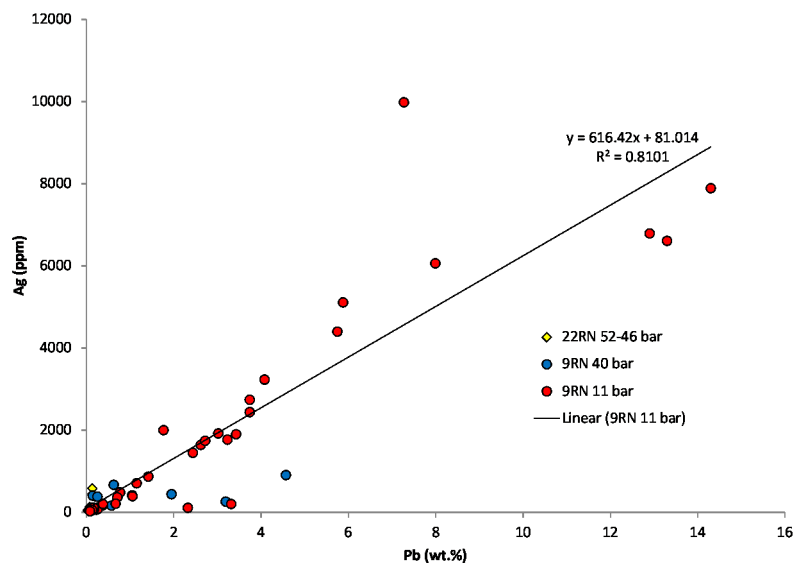


Figure 2.28. Plot of Ag versus Pb concentrations in downhole scale samples from RN-22 and surface pipeline RN-9. Silver is either as inclusions in galena or as Pb-Ag sulfide.

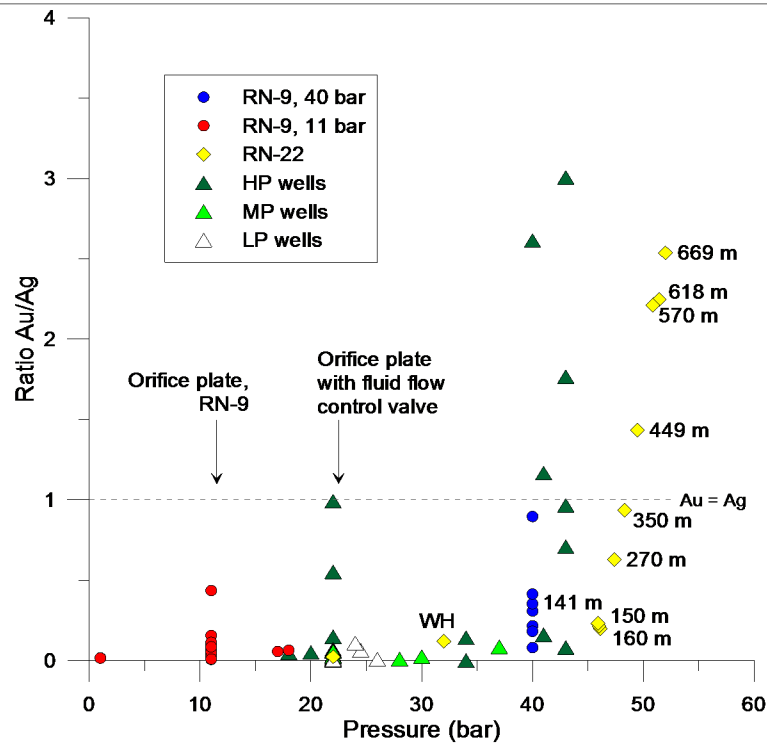


Figure 2.29. Plot of Au/Ag ratio versus pressure from scale samples from RN-9, downhole RN-22, and the high-, medium- and the low-pressure wells. At high pressure, Au precipitates in higher concentration than Ag (i.e., gold in solution becomes oversaturated at higher temperature/pressure than silver), but as pressure decreases the Au/Ag ratio declines sharply, as the gold was previously deposited from the liquid. As a result the Ag concentration in scale in surface pipes is more than ten times higher than Au. The numbers indicate location of samples in wells in meters from surface. The dotted line equals 1:1 Au and Ag. WH=wellhead.

solubilities of Au and Ag as aqueous sulfur and aqueous chloride complexes, respectively (e.g, Seward, 1973; Stefánsson and Seward, 2003, 2004).

Silver concentrations are also positively correlated with Pb, As, Sb and Se, which may indicate the presence of Ag-bearing sulfosalts with galena (Figs. 2.28 and 2.30) and native silver that were not identified (Fig. 2.30). Arsenic and Sb are generally below detection limits (<0.5 ppm and 0.1 ppm) upstream of the orifice plate but increase downstream (Tables 2.7 – 2.9). Arsenic concentrations reach 330 ppm in scales from well RN-9 and much higher in the scaling test samples in the same well (~6400 ppm). Antimony concentrations are up to ~800 ppm in the scaling test samples and up to ~300 ppm in other wells.

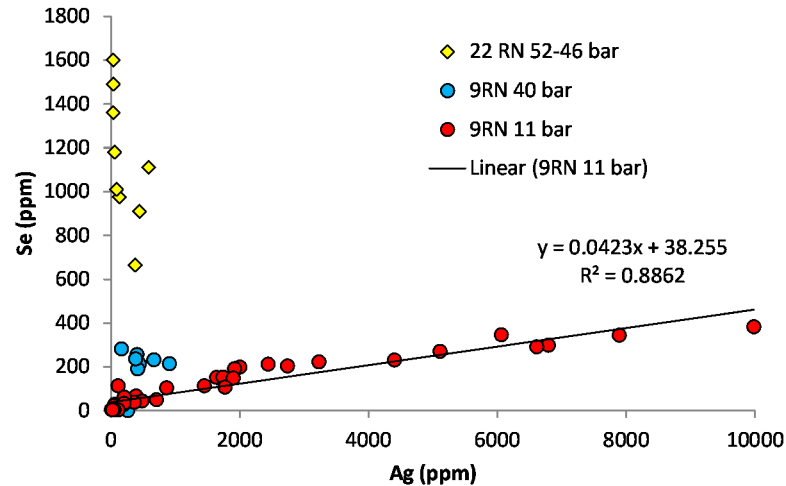


Figure 2. 30. Plot of Ag versus Se concentrations in downhole scale samples from RN-22 and surface pipeline RN-9. Selenium occurs in sphalerite downhole but in surface pipeline in galena or clausthalite (PbSe) or as Ag_2Se (caumannite).

Several samples were analyzed for PGE to determine if an enriched mantle or MORB source might be contributing to the high Au contents of the scales (Table 2.12). Pd was detected in the range of 4 – 12 ppb, Pt 0.2 – 0.5 ppb, Ir 0.02 – 0.14 ppb and Rh and Ru close to or below the detection limits. The Pt/Pd and Ir/Pd values are more than an order of magnitude below MORB and MORB sulfide values and the absolute concentrations of the PGE are low (Table 2.12 and Fig. 2.31). This suggests that the high gold content of the scale does not represent an enriched mantle or MORB sulfide source.

Table 2.12. Concentrations of Platinum Group Elements in selected gold-rich samples

Sample	Location	pressure	Au	Ir	Pd	Pt	Rh	Ru	Pt/Pd
			ppm	ppb	ppb	ppb	ppb	ppb	
				IMP-	IMP-	IMP-	IMP-	IMP-	
				200	200	200	200	200	
				0.01	0.12	0.17	0.02	0.08	
9RN31_00	Orifice plate (OP)	11	176	0.02	4.09	0.22	<0.02	<0.08	0.05
HP15_23RN6-07	Downstream of OP (~32m)	22	82.4	0.06	11.94	0.51	<0.02	<0.08	0.04
MP2_12RNE2	Fluid flow control valve	22	554	0.14	6.07	0.46	0.02	0.09	0.08
LP10_15RN3-07	Downstream of OP	22	137	0.04	5.85	0.32	<0.02	<0.08	0.05
Primitive Mantle ⁽¹⁾			0.001	3.2	3.9	7.1	0.9	5	1.82
MORB BULK ⁽²⁾			0.002	0.16	3.9	8.7	-	-	2.23
MORB sulfide ⁽²⁾			10.5	520	27,800	29,300	-	140	1.05

⁽¹⁾McDonough and Sun (1995); ⁽²⁾ Peach et al., (1990)

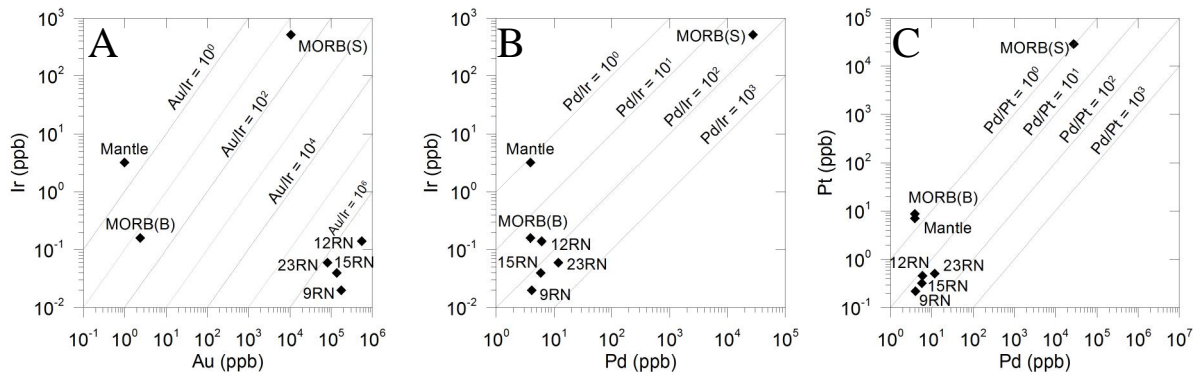


Figure 2.31 Iridium versus Au, Ir versus Pd, and Pt versus Pd plots (A, B, and C) illustrating extreme enrichment of Au relative to other PGE in the scales from Reykjanes geothermal system. See Tables 2.7 and 2.8 for sample locations. Values from mantle (McDonough and Sun, 1995), MORB(B) (bulk) and MORB(S) sulfides (Peach et al., 1990) are shown for comparison.

Cobalt concentrations are ~240 to 160 ppm downhole in RN-22 and up to 400 ppm in the high pressure well RN-23 (Fig. 2.27). Concentrations in the surface pipelines are generally lower. The samples from well RN-9 with high Co concentrations (26-560 ppm) have higher concentrations of Ni, W, Cr, Nb, Ta, Ti, and Mn, some of which could be from contamination from the steel pipeline or grinding of the samples in a steel mill. Molybdenum correlates with As and Sb but no Mo mineral was identified. Contamination from the steel pipes cannot be ruled out as a source of the Mo, as it was commonly detected in samples with magnetic flakes (Tables 2.9).

Unexpected enrichments in Bi (up to 40 ppm) and Sn (up to 20 ppm) occur in the scales from the high pressure wells (at the wellhead in RN-11 and upstream of the orifice plate in RN-23), suggesting precipitation at the highest temperatures.

Vanadium concentrations range from 190 ppm to 850 ppm in well RN-22 but decrease to ~80 ppm at the wellhead (Fig. 2.27). Up to 0.2 wt.% V was found in maghemite at 150 m depth in well RN-22. However, unusually high concentrations of V are correlated with Mg and Ti, suggesting that the V may be present in Mg-rich clay minerals. Titanium ranges

from 60 up to 600 ppm in RN-22, upstream of the orifice plate, and between 20 and ~250 ppm downstream of the orifice plate. It may also be present in magnetite or Mg-rich clay minerals.

Manganese and Ga appear to be most strongly correlated with SiO_2 and likely are trace constituents in the clays or amorphous silica precipitates. The samples in the valve house of RN-9 contain up to 65 ppm Ga, which correlates with SiO_2 and may substitute for Al in associated clay minerals. Thallium correlates with K_2O and is likely present in an illite-like clay. Barium, Sr, and Rb concentrations also appear to be related to a clay component in the scales. Barium minerals were not seen in thin section, but XRD analysis of a few samples downstream of the orifice plate indicated the presence of barian celestine, a secondary sulfate ($\text{Ba}_{0.25}\text{Sr}_{0.75}\text{SO}_4$). Sodium and Br are most likely present in salts. Bromine is present in most of the samples downstream of the orifice plate in well RN-9, ranging from ~10 to 100 ppm in the pipelines and up to 430 ppm in the samples from the discharge pond.

REE concentrations are very low in the analyzed scales, except in the scaling experiments formed at the highest pressure in well RN-11 (Fig. 2.32). The LREE-enriched profile is typical of fluids in geothermal systems, but the REE show little influence of seawater, except in one sample with a small negative Ce anomaly. It is noteworthy that the scales with highest REE concentrations do not show the negative Eu, and one sample may have a slight positive Eu anomaly, typical of seafloor hydrothermal systems.

Almost none of the trace elements mentioned above are found in the samples from the Gray Lagoon, indicating that the entire trace element load of the downhole liquids is deposited before reaching the discharge pond.

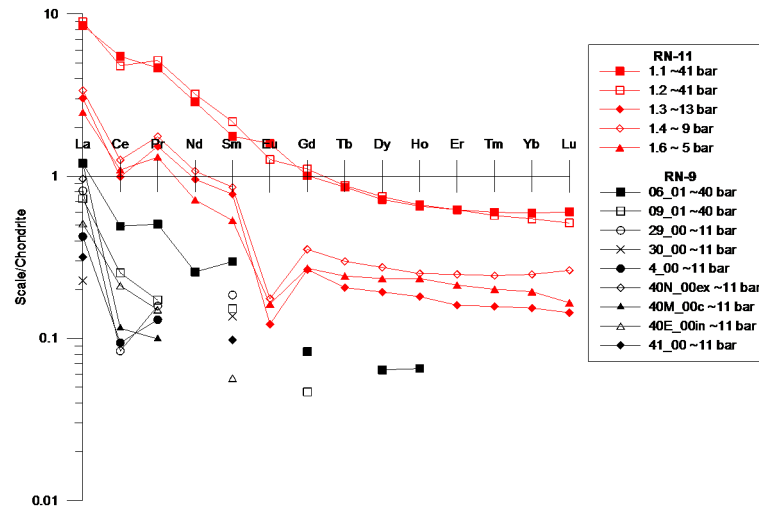


Figure 2.32. Rare earth element (REE) concentrations in scales from scale samples from surface pipeline RN-9 and from scale samples from experiments in the pipeline of wells RN-11. RN-11 (low pressure), is a typical LREE profile of seawater-dominated hydrothermal system; Ce anomaly and Eu anomaly where no Eu anomaly is seen at high pressure.

2.9. Mass Accumulation in Well RN-9 Downhole and in the Surface Pipeline

The scale deposit upstream of the orifice plate in the surface pipeline of well RN-9 had an average thickness of <0.5 cm of mainly sulfides, but just downstream of the orifice plate extensive amorphous material nearly filled the 40 cm diameter opening over a minimum 8 m length of the pipe line, with only a 10 cm opening for fluid flow (Fig. 2.5D). The 8 m length of the pipe contained about 0.94 m³ of scales deposited in ~1 year (see calculations in Appendix 2.5, Table A2.9). To determine the mineral composition of the scale, the average chemical composition of samples precipitated four and eight meters downstream of the orifice plate was used. All Zn and measured Fe (from microprobe) and all Pb were assumed to reside in sphalerite and galena, respectively. All Cu was assumed to reside in chalcopyrite, plus stoichiometric Fe, with the remaining Fe forming in Fe silicate (minnesotaite was used here as a proxy for the actual amorphous iron silicate); the balance of Si was assumed to have precipitated as amorphous silica (Table A2.10).

The results for the first 4 m downstream of the orifice plate indicate that ~50 vol.% (see calculations, Table A2.11) of the scales are sulfides, consisting of 28 vol.% sphalerite, 18 vol.% chalcopryrite, and 3 vol.% galena, with 20 vol.% amorphous iron silicate and 30 vol.% amorphous silica. Four meters further downstream, sulfides account for 22 vol.% of the deposition, including 15 % sphalerite, 6% chalcopryrite, and 1% galena, with the remainder consisting of amorphous iron silicate and/or Fe-rich silica (5%) and amorphous silica (72%). About 2.5 tonnes precipitated in this 8 m long pipeline, containing close to 0.6 tonnes of sphalerite, 0.2 tonnes of chalcopryrite and about 1.6 tonnes of amorphous silica (Table A2.11).

RN-9 was clogged in 1993 and again in 2003. In order to calculate the volume of scales that precipitated in the well at that time, the following assumptions were made. Boiling started at 1000 m depth, and scales precipitated evenly from the initial boiling point (Appendix 2.5). The volume of the empty well was ~58 m³ to 1000 m depth, whereas the open volume in 1993 was ~29 m³ based on internal measurements (Figs. A2.1 and A2.4). Thus, ~28 m³ of scale was deposited in 10 years (Table A2.11). Based on the bulk mineralogy and densities, ~11 tonnes of sphalerite (~7 tonnes Zn) was precipitated downhole per year from 1983 to 1993.

2.10 Metals in the altered host rock

The metal concentrations in the altered host rock (tholeiites) were determined from analysis of cuttings from well RN-9 collected at 50 m intervals, starting at a depth of 500 m down to 1346 m depth. Analytical methods are discussed in Appendix 2.3.

Major and trace element concentrations of altered rocks from well RN-9 are listed in Table 2.13 and plotted in Figures 2.33 and 2.34. For comparison, data for altered rock from

Table 2.13. Major and trace elements concentrations in altered rock from drill cuttings from downhole well RN-9 (500 to 1346 m depth). For comparison, fresh Reykjavík dolerite (international standard BIR-1, Flanagan, 1984) and olivine tholeiite sample RE-25 from Reykjanes are included (Jakobsson et al., 1978)

	SiO ₂	Al ₂ O ₃	CaO	Na ₂ O	K ₂ O	MnO	MgO	FeO _t	TiO ₂	P ₂ O ₅	LOI	S	Total	Zn	Cu	As
	%	%	%	%	%	%	%	%	%	%	%	%	%	ppm	ppm	ppm
Detection Limit	0.01	0.01	0.01	0.01	0.01	0.001	0.01	0.01	0.001	0.01	0.001	0.001	0.001	1	1	0.5
Analysis Method	FUS-ICP	FUS-ICP	FUS-ICP	FUS-ICP	FUS-ICP	FUS-ICP	FUS-ICP	FUS-ICP	FUS-ICP	FUS-ICP	FUS-ICP	TD-ICP	TD-ICP	TD-ICP	TD-ICP	INAA
BIR-1	47.96	15.50	13.30	1.82	0.03	0.18	9.70	10.19	0.96	0.02	-	-	-	70	125	0.44
RE25	49.30	15.07	12.68	1.98	0.11	0.20	7.66	11.77	1.24	0.09	0.27	-	-	-	-	-
Well RN-9, depth in meters																
500 H	44.35	13.63	10.04	2.00	0.70	0.14	8.16	8.94	1.26	0.15	9.52	0.25	99.14	61	109	< 0.5
550 H	45.59	13.42	12.03	1.63	0.42	0.16	6.92	11.29	1.80	0.21	5.39	0.20	98.86	75	127	< 0.5
604 B	47.73	13.82	11.99	1.86	0.22	0.23	7.61	10.08	1.19	0.11	2.80	0.15	97.63	129	148	< 0.5
620 B	49.87	14.06	12.63	1.95	0.13	0.20	7.80	10.19	0.98	0.06	1.32	0.16	99.20	109	239	2.0
646 B	48.20	14.77	12.09	2.06	0.14	0.21	6.59	11.41	1.69	0.13	1.24	0.10	98.53	87	192	< 0.5
656 B	48.06	14.51	12.54	2.02	0.08	0.21	7.37	10.52	1.13	0.10	1.13	0.32	97.67	79	177	< 0.5
692 B	49.25	14.32	11.69	1.98	0.07	0.19	8.14	7.65	1.72	0.11	2.98	0.31	98.09	88	145	< 0.5
748 H	43.34	13.17	10.31	1.40	0.19	0.20	8.37	11.17	1.85	0.22	7.18	0.11	97.39	90	166	1.9
802 H	46.88	14.19	11.17	2.20	0.22	0.19	8.06	7.78	1.86	0.10	5.61	0.36	98.26	85	156	< 0.5
848 B	48.57	13.86	12.02	2.08	0.05	0.18	7.14	10.07	1.34	0.10	1.93	0.31	97.33	68	129	2.8
898 B	48.21	14.71	12.00	2.49	0.09	0.18	6.74	9.61	1.33	0.14	2.14	1.04	97.63	57	122	< 0.5
946 B	48.92	14.16	12.90	1.91	0.04	0.22	7.71	10.75	1.27	0.06	1.33	0.50	99.27	113	314	3.0
1102 B	48.85	14.90	12.27	1.71	0.05	0.19	9.29	8.59	0.72	0.02	2.61	0.10	99.20	91	142	< 0.5
1200 H	55.62	12.05	10.23	1.54	0.12	0.19	4.93	9.48	1.19	0.09	3.14	0.41	98.58	271	369	2.8
1250 B	46.63	14.35	13.16	1.74	0.08	0.19	7.36	11.04	1.44	0.11	2.27	0.10	98.36	65	97	< 0.5
1298 B	48.44	15.92	13.35	1.84	0.06	0.14	8.31	8.24	0.85	0.10	2.40	0.09	99.65	67	79	< 0.5
1320 B	47.53	14.75	12.51	1.91	0.05	0.18	7.62	9.52	1.26	0.13	2.11	0.19	97.57	82	95	< 0.5
1346 H/B	47.63	14.55	10.02	2.19	0.14	0.16	7.89	9.66	1.42	0.14	4.53	0.24	98.33	98	135	3.4

' - ', data not available; H, hyaloclastites; B, basalt/pillow lava; elements present at concentrations below detection limit are; Pb < 5, Ag < 0.3, Se < 3, Bi < 0.4, In < 0.2, Cs < 0.5 all in ppm and Au < 2 and Ir < 5 ppb; FUS-ICP, Fusion mass Inductively coupled plasma; FUS-MS, Fusion mass spectrometry; TD-ICP, Total Digestion Inductively coupled plasma; INAA, instrumental neutron activation analysis; Hg-FIMS, Cold Vapor, Flow injection mercury system

Table 2.13 (continued)

Detection Limit	Analysis Method	Sb	Cd	Hg	Co	Ni	Mo	Sn	Ge	Ga	W	V	Cr	Zr	Nb	Hf	Ta
		ppm	ppm	ppb	ppm	ppm											
	INAA	0.58	-	-	52	170	-	-	-	16	-	310	370	18	0.6	0.60	-
BIR-1																	
RE25													137	-	-	-	-
Well RN-9, depth in meters																	
500 H		<0.2	<0.5	47	42	97	<2	2	<1	15	<1	287	392	75	12	2.3	0.7
550 H		1.1	<0.5	36	48	100	<2	3	2	17	<1	328	297	84	12	2.5	0.8
604 B		<0.2	0.8	35	44	88	<2	1	2	14	<1	311	278	77	7	2.1	0.4
620 B		0.4	0.6	42	54	75	4	2	2	15	<1	307	259	44	5	1.5	0.3
646 B		<0.2	<0.5	23	46	74	3	2	2	17	7	387	180	88	10	2.3	0.9
656 B		<0.2	<0.5	23	48	78	2	1	2	15	6	329	182	53	5	1.4	0.4
692 B		0.4	<0.5	20	22	113	<2	<1	<1	11	<1	343	329	84	12	2.1	0.8
748 H		<0.2	<0.5	8	50	150	<2	1	2	15	2	324	392	106	14	2.7	0.9
802 H		<0.2	<0.5	18	29	138	<2	2	<1	9	<1	276	365	122	14	3.3	1.0
848 B		<0.2	<0.5	29	46	74	3	1	2	15	7	365	283	68	7	1.9	4.8
898 B		0.3	<0.5	35	42	74	<2	1	2	15	5	297	197	86	10	2.1	0.9
946 B		<0.2	<0.5	46	50	83	3	1	2	15	6	345	255	57	5	1.6	0.5
1102 B		<0.2	<0.5	53	45	125	2	<1	2	12	5	262	454	32	2	0.9	0.2
1200 H		0.4	1.9	65	36	48	7	1	2	14	6	312	169	62	6	1.6	0.6
1250 B		0.4	<0.5	27	34	104	<2	2	2	14	<1	318	365	83	10	2.2	0.6
1298 B		<0.2	<0.5	25	37	113	<2	4	2	13	2	259	385	74	10	2.4	0.6
1320 B		<0.2	0.5	57	41	103	2	<1	2	14	<1	298	374	71	9	1.9	0.5
1346 H/B		<0.2	<0.5	104	40	93	<2	1	2	15	<1	268	304	81	8	2.5	0.5

Table 2.13 (continued)

Detection Limit	Analysis Method	Sc	Ba	Sr	Rb	Be	U	Th	Y	La	Ce	Pr	Nd	Sm	Eu	Gd	Tb
		ppm	ppm	ppm	ppm	ppm	ppm	ppm	ppm	ppm	ppm	ppm	ppm	ppm	ppm	ppm	ppm
	INAA	0.1	3	2	2	1	0.1	0.1	2	0.1	0.1	0.05	0.1	0.1	0.05	0.1	0.1
	FUS-ICP																
BIR-1		44	7.00	110	-	0.58	-	-	16	0.63	1.90	-	2.50	1.10	0.55	1.80	-
RE25		-	-	-	-	-	-	-	-	-	-	-	-	-	-	-	-
Well RN-9, depth in meters																	
500 H		41.3	185	173	12	20	0.3	0.7	19	7.5	18.1	2.42	11.4	3.0	1.05	3.5	0.6
550 H		43.1	133	182	7	21	0.3	1.2	24	10.0	23.9	3.28	15.2	4.0	1.38	4.5	0.8
604 B		48.9	121	134	<2	<1	0.1	0.4	19	5.6	14.1	1.71	8.4	2.5	0.90	3.0	0.6
620 B		47.9	83	110	<2	7	<0.1	0.5	18	3.3	8.9	1.34	6.7	2.1	0.83	2.8	0.5
646 B		48.5	71	149	<2	<1	0.2	0.5	23	9.1	20.9	2.79	13.2	3.6	1.28	4.3	0.8
656 B		49.8	52	113	<2	<1	<0.1	0.3	17	5.1	11.8	1.62	7.9	2.4	0.87	3.2	0.6
692 B		46.3	40	145	<2	<1	0.1	0.3	24	6.5	16.9	2.09	10.7	3.0	1.10	3.6	0.7
748 H		41.0	100	175	<2	<1	0.1	0.4	24	8.9	22.8	2.74	13.6	3.8	1.34	4.4	0.7
802 H		40.0	120	201	4	1	0.2	2.3	25	8.5	21.9	2.62	12.6	3.4	1.25	3.9	0.7
848 B		52.5	30	124	<2	<1	0.3	0.4	24	6.8	15.8	2.16	10.5	3.0	1.09	3.8	0.7
898 B		45.4	42	150	<2	<1	0.3	0.5	20	9.4	21.1	2.79	12.7	3.3	1.17	3.9	0.7
946 B		52.2	25	118	<2	<1	0.1	0.3	20	5.2	12.6	1.77	8.7	2.6	0.99	3.5	0.6
1102 B		46.7	20	97	<2	<1	<0.1	0.1	13	2.4	5.9	0.85	4.4	1.5	0.60	2.2	0.4
1200 H		37.5	98	161	<2	<1	0.2	0.4	19	7.5	16.8	2.21	10.1	2.8	1.01	3.4	0.6
1250 B		45.5	40	200	<2	<1	0.3	0.5	23	7.6	18.8	2.18	10.5	3.0	1.21	3.6	0.7
1298 B		44.5	26	111	5	<1	0.2	0.5	19	4.0	9.7	1.41	6.3	1.9	0.72	2.5	0.5
1320 B		46.6	31	138	<2	<1	0.3	0.4	21	6.8	17.3	2.05	9.9	2.7	0.99	3.3	0.6
1346 H/B		43.6	71	138	<2	5	0.1	0.4	22	6.1	15.3	2.23	10.7	3.1	1.19	3.7	0.7

Table 2.13 (continued)

	Dy	Ho	Er	Tm	Yb	Lu
	ppm	ppm	ppm	ppm	ppm	ppm
Detection Limit	0.1	0.1	0.1	0.05	0.1	0.04
Analysis Method	FUS-MS	FUS-MS	FUS-MS	FUS-MS	FUS-MS	FUS-MS
BIR-1	4	-	-	-	1.70	0.26
RE25	-	-	-	-	-	-
Well RN-9, depth in meters						
500	3.8	0.8	2.1	0.32	2.1	0.31
550	4.7	1.0	2.7	0.39	2.6	0.38
604	3.5	0.7	2.0	0.32	2.1	0.30
620	3.4	0.8	2.1	0.32	2.2	0.31
646	4.7	1.0	2.7	0.39	2.7	0.39
656	3.6	0.8	2.2	0.31	2.2	0.32
692	3.9	0.8	2.3	0.34	2.2	0.31
748	4.5	0.9	2.5	0.39	2.4	0.35
802	4.2	0.9	2.4	0.36	2.3	0.34
848	4.3	0.9	2.6	0.37	2.6	0.37
898	4.1	0.9	2.4	0.34	2.3	0.33
946	4	0.9	2.4	0.32	2.4	0.34
1102	2.8	0.6	1.7	0.23	1.8	0.26
1200	3.7	0.8	2.2	0.29	2.2	0.32
1250	3.9	0.8	2.3	0.34	2.3	0.33
1298	3.2	0.7	2.1	0.32	2.1	0.26
1320	3.7	0.8	2.2	0.33	2.2	0.32
1346	4.3	0.9	2.6	0.38	2.5	0.36

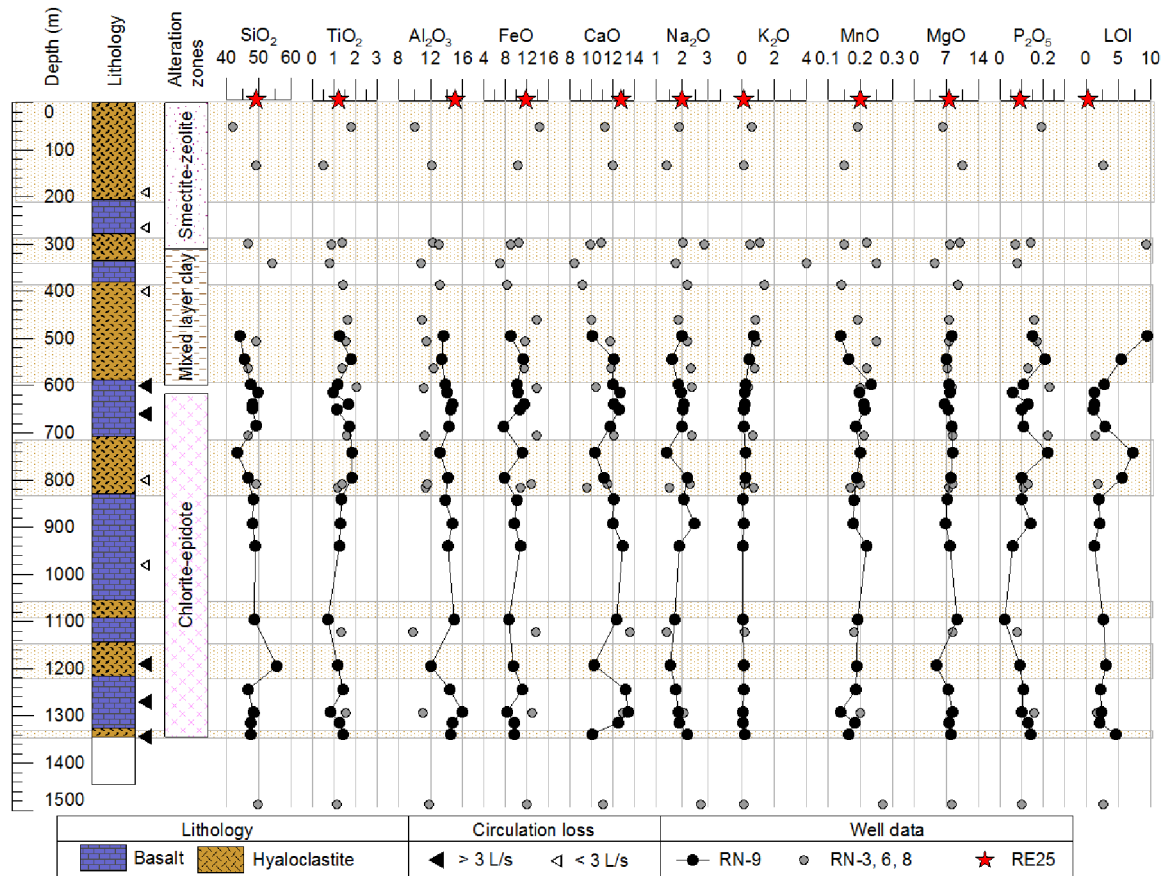


Figure 2.33. Downhole distribution of the major elements in altered host rocks of well RN-9 (Table 2.13). Well RN-09 was cased to ~500 m depth, with slotted liner down to the bottom of the well (Franzson et al., 1983; Mungania, 1993). The aquifer zones are located mainly between 600 and 700 m depth and below 1200 m depth. The compositions of altered wallrock from other wells (RN-3, RN-6, and RN-8) are shown in this interval (gray dots in the upper 500 m). The red star shows the composition of a fresh, coarse-grained olivine tholeiite lava, (sample RE-25) from surface (Jakobsson et al., 1978). Lithostratigraphy and the major alteration zones are shown to the left of the diagram. The concentrations of SiO₂, Al₂O₃, FeO, MnO, and CaO are generally lower in the hyaloclastite zones than in the fresh surface basalt, whereas the TiO₂, K₂O and P₂O₅ concentrations are similar or slightly higher.

wells RN-3, RN-6, and RN-8 are also shown (Kristmannsdóttir, 1984). These data are compared to unaltered basalt from the surface (sample RE25, shield volcano; Jakobsson et al., 1978), as well as data from an Icelandic dolerite (international standard BIR-1, Flanagan, 1984).

The loss on ignition (LOI) is high in the altered hyaloclastite, tuff and sedimentary rocks, ranging between 3 and ~10 wt.%, compared to ~0.3 wt.% LOI for fresh basalt. The higher

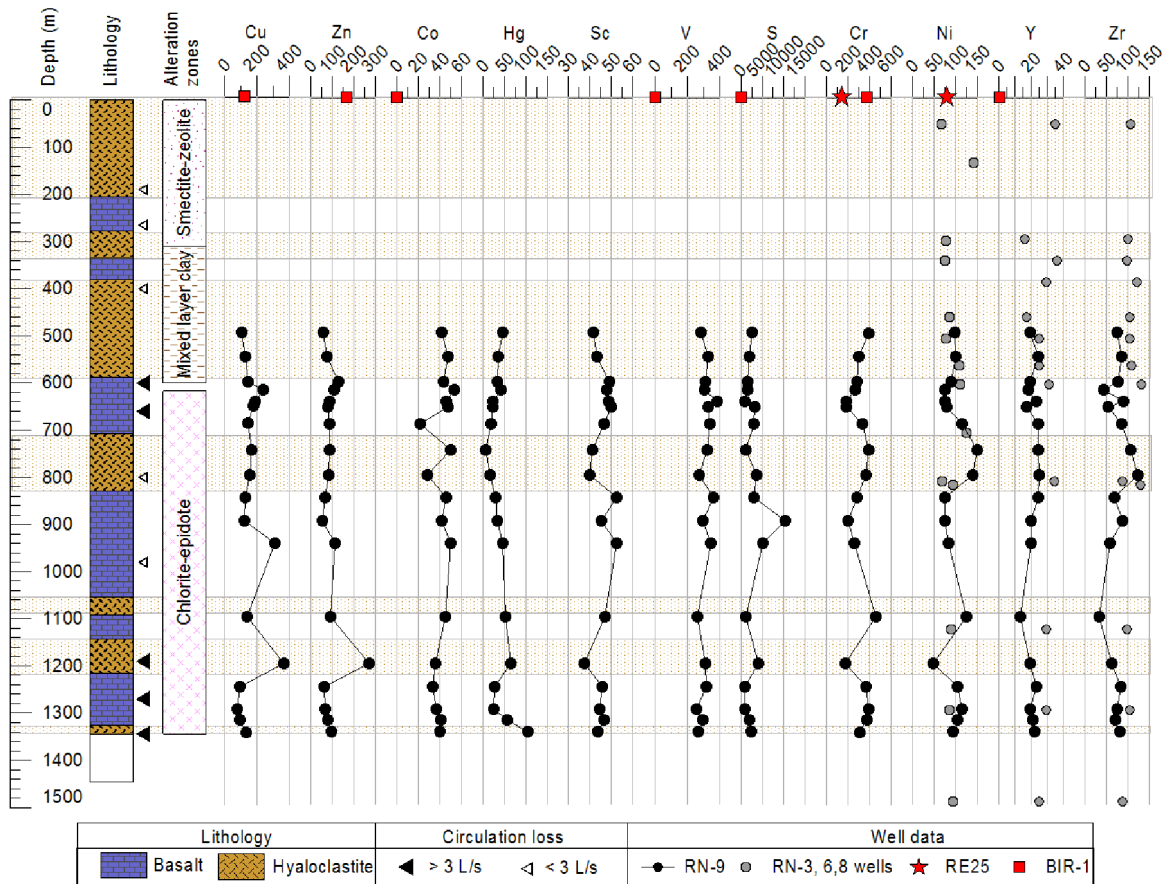


Figure 2.34. Downhole distribution of trace elements in altered host rocks of well RN-9 (Table 2.13). A few trace element compositions from wells RN-3, RN-6 and RN-8 are shown for comparison (Kristmannsdóttir, 1984; gray dots), as well as the trace element composition from Reykjavik dolerite, a fresh olivine tholeiite lava flow from a shield volcano, erupted during the youngest interglacial period (red square; international standard BIR-1, Flanagan, 1984). The Cu concentration range between 80 and 370 ppm where Zn concentrations range between 60 and 270 ppm.

values occur in the upper half of the well, where clay minerals dominate the alteration, consistent with recent results from well RN-17 (Marks et al., 2010a). In the basalt flow-dominated intervals, LOI is generally between 1 and 2 wt.%. The concentrations of SiO₂, Al₂O₃, FeO, MnO, and CaO are generally lower in the hyaloclastite zones than in the fresh surface basalt, whereas the TiO₂, K₂O and P₂O₅ concentrations are similar or slightly higher. In general the K₂O concentration increases from 0.05 to 0.70 wt.% below 1300 m depth to 500 m depth and up to 1.3 wt.% in the tuffaceous sediments at ~390 m depth in well RN-3 (Kristmannsdóttir, 1984). MgO concentration ranges from 5 to 9.3 wt.%, similar to fresh

basalt (~7.7 wt.%). Sodium is relatively constant (2 wt.%) and also similar to fresh basalt. In general, the major elements show remarkably little variation, indicating relatively small mass gains or losses due to hydrothermal alteration. The “immobile” elements, Zr, Nb, and Hf, are somewhat higher than in fresh dolerite, but similar to basalts from well RN-17 (Marks et al., 2010a), reflecting a slightly different parent composition. There is little difference in the lithology of the host rocks of these two wells, although the highest measured temperature in well RN-9 was 295°C compared to ~340°C in RN-17 at greater depth (ÍSOR data base).

The Cu concentration in altered rock ranges between 80 and 370 ppm (average 163 ppm), compared to 125 ppm in the Reykjavik dolerites (BIR-1). The highest values are located at 1200 m and ~950 m depth, and in the interval 620 to 650 m. Zinc concentrations range between 60 and 270 ppm (average 95 ppm), compared to 70 ppm in BIR-1, with an increase in the same intervals as Cu. Copper and Zn have higher concentrations close to points of fluid inflow (i.e., circulation loss at 600 to 700 m depth and below ~1200 m depth, Fig. 2.33 and 2.34), especially in hyaloclastite zones, which is consistent with the observed alteration in the drill cuttings (Franzson et al., 1983).

The average of Cu concentration in altered rocks of RN-9 is slightly higher (163 compared 113 ppm) than those in well RN-17 (Marks et al., 2010a), which is ~1100 m to the southwest (Figure 1.4). On the other hand the Zn concentration in the altered rocks of RN-9 is slightly lower (95 compared to 146 ppm). The trace elements Pb (<5 ppm), Cd (<0.5 ppm), Au (<2 ppb) and Ag (<0.3 ppm) are below detection in most samples. The Ba concentration is 185 ppm (at 500 m depth) and decreases to 20 ppm at the bottom of the hole (consistent with data from RN-17: Marks et al., 2010a); fresh dolerite contains 7 ppm. The distribution of Ba is similar to K₂O and may reflect some enrichment in clays at

shallow depth. The fact that the metals and most other elements are not depleted in the cuttings suggests that the immediate wall rocks were probably not the source of elements in the scales.

2.11 Discussion

2.11.1 Scale deposition versus pressure change

In 2006 to 2007 precipitation of scales upstream of the orifice plate in all wells caused a color change in the pipelines, but <1 mm of scales formed in most cases (Figure 2.13). The upstream scales in well RN-9 were somewhat thicker (<0.5 cm) but likely formed over a much longer time, since the well was in production, with few interruptions, from 1983 to the end of 2003. The wellhead pressure during production in these wells ranged from 52 bar down to ~25 bar but was as low as 15 bar in well RN-9 for short periods. This observation suggests that if the well had been maintained at a high pressure (~20 bar), sulfides would only have formed a thin skin coating on the pipelines.

Precipitation of scale downstream of the orifice plate was variable between wells, because pressure decreased to ~22 bar in the newer wells (RN-10 to RN-24) and ~11 bar in well RN-9. Heavy precipitation of sulfides downstream of the orifice plate occurred in wells with a high wellhead pressure (HP wells in Table 2.4 with pressure at wellhead ranging from ~52 to ~25 bar (267°C to 226°C)). The pressure decrease, or differential, between the upstream and downstream sides of the orifice plate in these HP wells was variable but large in all cases. This sharp decrease in pressure and consequent abrupt change in temperature due to boiling appears to be the main cause of the massive precipitation of scale downstream of the orifice plate. By contrast, a small amount of scale formed in the pipelines downstream of the orifice plate in wells with a lower wellhead

pressure, in the range of 27 and 25 bar (LP wells; Figure 2.15) and a decrease of 3 to 5 bars across the orifice plate. Medium pressure wells (MP), with average wellhead pressures of ~37 and ~30 bar, develop scales mainly on the fluid-flow control valve with only traces downstream of the orifice plate. In these wells, the pressure difference across the orifice plate ranged from ~14 bar for well RN-12 to between 10 and 6 bar for RN-21 and RN-24 (Table 2.4).

Well RN-18 (a LP well) does not have good permeability, and the pressure is much lower than in other wells (Jónsson, 2008). Liquid in RN-18 appears to boil all the way from the bottom of the well (~1800 m) to the surface as the fluid ascends, whereas the HP wells start boiling between 1300 and 1200 m depth. This has been shown directly by temperature and pressure measurements in wells RN-18 and RN-23 in 2007 (Jónsson, 2008). The low permeability indicate higher precipitation rates in the host rock.

Thus, the high pressure in the HP wells keeps scales from precipitating at depth, within the well or in the rock formation, until the sharp drop in pressure (and temperature) at the orifice plate. The LP wells have already boiled and arguably deposited scale at depth.

2.11.2 Texture, mineralogy, composition and paragenesis versus pressure

Upstream of the orifice plate in well RN-9 the most common texture in the scales is thin bands (<1 mm) or layers of mainly skeletal sphalerite and chalcopyrite, forming crystals <5 μm up to 2 mm in length (Figures 2.7B and C). Downstream of the orifice plate the sulfides are mainly dendritic, forming bulbous layers of various thickness (Figure 2.7E). An intimate intergrowth of sulfide minerals is also common. The skeletal minerals upstream of the orifice plate form due to a decrease in temperature from ~290°C (reservoir temperature for RN-9) to ~230°C (at the wellhead), as the fluid depressurized and boiled from deep in

the well (Chapter 5). This skeletal texture is also the main texture seen in scale samples recovered from within the casing of well RN-22. Much finer-grained intergrowths and dendritic growths of sphalerite and chalcopyrite, and locally of bornite, downstream of the orifice plate are typical of the products of rapid cooling, as observed in hydrothermal experiments, and are characteristic of a high degree of supersaturation (Stanton, 1972; Rimstidt, 1997). The alternating bands of sphalerite and chalcopyrite likely reflect changes in temperature due to frequent pressure (flow) changes at the wellhead (Chapter 5).

Downstream of the orifice plate in well RN-9 amorphous silica is the main precipitate, together with the sulfides. Distinctive colloform-banded amorphous silica, with white and black bands, precipitated in the valve house (Figure 2.6W) due to cooling from 180°C (9 bar) to 100°C (1 bar). Similar scales are very common in the geothermal pipes at Broadlands-Ohaaki, New Zealand, where the light and dark bands have been attributed to differences in particle size of amorphous silica rather than presence of very fine-grained opaque minerals (Simmons and Browne, 2000). In the newer wells (RN-11, 14, 22, 23), amorphous silica is not a major scale due to the higher separation pressure (22 bar vs 11 bar in RN-9), although sphalerite and Cu-sulfide minerals are present. The smaller pressure (temperature) decrease at the orifice is designed to maintain the temperature and to prevent saturation with amorphous silica (Fig.2.23).

Downhole in well RN-22 the first mineral to precipitate appears to have been sphalerite/wurtzite, but coprecipitation of chalcopyrite also occurred. Bornite started to precipitate ~at 350 m depth and became more abundant as the pressure decreased in the upper part of the well. Pyrite occurs as inclusions in chalcopyrite, and pyrrhotite may have formed. Oxides, maghemite and goethite (possible corrosion products) formed in the upper

part of the well. The phases that precipitated upstream of the orifice plate in the surface pipeline of RN-9 were also dominated by sphalerite, chalcopyrite with trace of bornite and galena. Wurtzite (identified by XRD) was also the first precipitate in the scaling test from well RN-10, which had the highest measured temperature at the time ($\sim 315^\circ\text{C}$), at least 20°C higher than the temperature in well RN-9.

The downhole sphalerite in well RN-22 which formed at a temperature in the range of 300° to 290°C has a low Fe concentration (1 to 4.7 wt.% Fe (average ~ 2 wt.%), 2-7 FeS mole%). Microprobe analyses show that group 1 sphalerite (40 bar) has Fe contents of ~ 3 wt% (4 to 5 FeS mole%, formed at ~ 230 up to 257°C , based on pressure measurements),

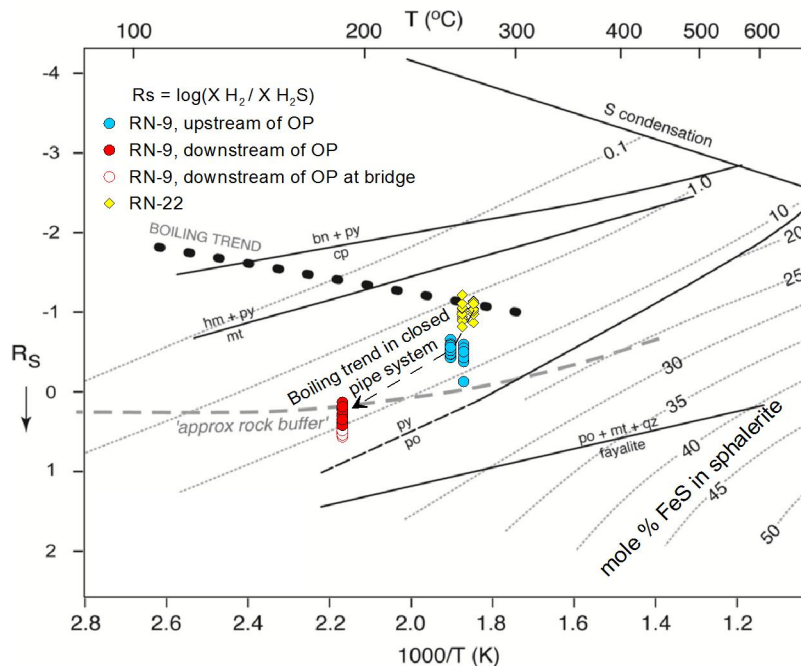


Figure 2.35. $\log(X\text{H}_2/X\text{H}_2\text{S})$ versus temperature diagram from Einaudi et al. (2003). Dash-dot line is the theoretical trend of gas loss due to liquid boiling from 300 to 150°C (Giggenbach 1980). The FeS composition of sphalerites (sph) from wells RN-22 and RN-9 are plotted versus the temperature as determined from the pressure at the sample locations. The unexpected increase in the FeS content of sphalerite (the Fe in sph is contoured in terms of H_2 and H_2S) downstream of the orifice plate does not follow the trend expected for boiling and equilibrium gas loss. Therefore, some other process, not known at the present, is controlling the change in Fe content of sph with decreasing temperature. X = mole fraction of the gas.

whereas group 2 sphalerite downstream from the orifice plate (11 bar) has Fe contents of ~5 to 8.5 wt.% (~6 to 14 FeS mole %, formed at ~188°C: Table 2.2, Figures 2.9 and 2.8). On a plot of the mole % FeS in sphalerite from group 1 and 2 on a diagram of sulfidation state versus temperature, the trend of the data has a different slope from that expected for H₂ and H₂S loss during boiling (calculated by Einaudi et al. 2003; Fig.2.35). This indicates that boiling and gas loss is unlikely to be the cause of the increase in the FeS content of sphalerite at lower temperature.

The high Fe contents of the sphalerite from the scaling tests (17-60 mole% FeS) are dramatically different from the low Fe contents in the other pipeline scales and downhole in RN-22. This suggests that the conditions of the scaling experiments were not the same as the conditions in which the bulk of the scales were formed.

2.11.3 Mass balances of metals

The high-pressure wells precipitate abundant scales downstream of the orifice plate. These wells (RN-11, RN-22 and RN-23) together with well RN-9 produced 5.2 tonnes of scales in about one year as shown in Table 2.14 (see calculations in Appendix 2.5 and in Tables A2.13 – A2.15). The total amount of scales in RN-9 was ~2.8 tonnes (including ~1 tonne of Zn+ Cu+ Fe+ Pb+ Ag+ Au). The total amount precipitated in the three new wells was 2.4 tonnes, including ~ 0.9 tonne Zn, close to 0.3 tonne Cu, ~0.2 tonne Fe, ~22 kg Pb, 5 kg Ag and close to 1 kg (700 g) Au. The volume of basalt that would have to be leached to obtain that amount of Cu and Zn is in the range of 10³ to 10⁴ m³ per year (Table 2.14). If the size of the Reykjanes geothermal system is considered to be 3.8 – 19.2 km³ (2 km² to 10 km² at 1000 m: Björnsson et al., 1972a, b; Karlsdóttir, 2005) and 2 km minimum depth, it would take about 25,000 to 130,000 years to leach out all the Ag and Au in the host rock

Table 2.14. Volume and mass of scale deposited over one year period in surface pipeline of wells RN-9, RN-11, RN-22 and RN-23. Mass of metals in surface pipeline and the volume of fresh basalt needed to leach to obtain that amount of metal. For calculation see Appendix 2.5

	RN-9		RN-11		RN-22		RN-23		Sum	
Density (0-4 m)	3,370	kg/m ³	3990	kg/m ³	3990	kg/m ³	3990	kg/m ³		
Density (4-8 m)	2,710	kg/m ³								
Pipeline diameter	40	cm	30	cm	30	cm	30	cm		
Scale thickness	15	cm	7	cm	7	cm	7	cm		
	Mass in pipeline (kg)	Basalt to leach (m ³)	Mass in pipeline (kg)	Basalt to leach (m ³)	Mass in pipeline (kg)	Basalt to leach (m ³)	Mass in pipeline (kg)	Basalt to leach (m ³)	Mass in pipeline (kg)	Basalt to leach (m ³)
Cu	147	406	46	127	144	397	94	259	431	1,189
Zn	435	2,387	196	1,080	342	1,875	358	2,000	1,331	7,342
Fe	135	0.7	130	0.6	31	0.2	36	0.2	331	2
Pb	112	14,960	9	1,190	8	1,080	5	650	134	17,880
Ag	10	115,600	1	12,100	2.8	32,400	1	13,600	15	173,700
Au	0.3	40,060	0.5	64,700	0.1	8,610	0.1	18,300	1	131,670
Sum of metals	839		383		528		494		2,243	
other (S + SiO ₂ + Mn+..)	2,026		425		279		313		3,043	
Total scale	2,865		807		807		807		5,286	

Concentration of the metals in the basaltic rocks; Fe 80800 ppm, Cu 125 ppm, Zn 70 ppm, Pb 3 ppm, Ag, 0.035 ppm, Au 0.003. See Tables A2.13 and A2.14

(Table 2.14). Strongly leached host rock, including around the deposits, is not seen.

The mass accumulation rate per year from one high-pressure well is close to 1 tonne; the five high-pressure wells in production (Table 2.14) produce scales in surface pipeline of between 4 and 5 tonnes per year. If the scales from the high-pressure wells were collected once in a year the value of the contained metal would be close to \$73,000 or about 8 million Icelandic krónur, at present metal prices.

2.12. Summary and Conclusions

Research at the Reykjanes geothermal field started when the first well was drilled in 1956; the first production well, RN-8, was discharged from 1969 to 1985. Well RN-9 was drilled in 1983 and was discharged intermittently over the next 20 years. In 1993 and 2003, RN-9 became blocked with scale and was first cleaned to a depth of 552 m (Steingrímsson

and Björnsson, 1993); it was filled with concrete in 2005. Since 1999 drilling has been continuous, and to date 29 wells have been drilled to depths of 2000 to 2500 m. Scales that precipitated at pressures between ~52 and 1 bar were studied here, including from downhole in RN-22 (to 685 m depth) and in surface pipelines of wells RN-10 to RN-24, as well as scales collected in 2000 from well RN-9. The wells can be classified as high- (30 to 52 bar), medium- (28 to 32 bar), and low-wellhead pressure (25 to 28 bar; Table 2.5), each with different scaling characteristics.

The amount of scale formation depends on the pressure difference across the orifice plates of the wells; precipitation in high-pressure wells, with a large pressure drop across the orifice plate, was up to 15 cm thick. Scale in the low-pressure wells downstream of the orifice plate was only seen as a colored thin patina coating the pipelines, where separation pressure was maintained at ~22 bar, arguably due to prior precipitation down the well caused by deep boiling. The medium-pressure wells had scales that only formed on the fluid flow control valve.

The scales in well RN-9 formed in 12 to 18 (?) months, due to the low separation pressure (11 bar) at the time, and nearly clogged the 40 cm diameter pipeline. In mid 2000 the surface pipeline from well RN-9 was cleaned out. Pressure at the well head, generally between ~44 bar (~257°C) to 40 bar (~252°C) through the 1980s, was constant for the first ~14 m of the pipe to the orifice plate, where it decreased sharply due to expansion through the opening in the orifice plate, to ~11 bar (188°C). The pressure decreased a further 1-2 bar to the separation station, ~348 m downstream from the orifice plate. The nature and chemical composition of the scales from wellhead to the orifice plate and downstream to the separation station depended on the pressure, obstacles in the pipelines, and bends in the pipeline.

Downstream of the orifice plate (at 22 bar) in the high-pressure wells, the scales consist mainly of sphalerite together with minor chalcopyrite. In the medium-pressure wells, intergrown bornite and digenite are the major Cu minerals together with the sphalerite and variable amounts of galena. However, where the pressure was allowed to decrease to 11 bar, amorphous silica was the major scale component. Further downstream from the orifice plate less sulfides precipitated; ~8 m downstream of the orifice plate SiO_2 comprised ~50 wt.% of the scale, and ~80% ~70 m further downstream. Where the pressure was allowed to decrease to 11 bar in RN-9, vapor loss and the resulting increase in the silica in solution as well as cooling of the liquid, resulted in massive amorphous silica precipitation.

Scales from downhole were only collected from well RN-22. The main mineral crystallizing in these scales is sphalerite; other minerals are minor or trace. Maghemite started to precipitate in the upper part of the well but decreased suddenly at 150 m depth explaining the sudden Fe decrease where the Zn and S concentration increased. The reason is not known.

The main texture in the downhole scales (well RN-22), as well as upstream of the orifice plate pipeline in well RN-9, is skeletal or splintery sphalerite. The crystals are larger than downstream of the orifice plate. Downstream of the orifice plate, layers of dendrites are the principal texture, which indicates rapid precipitation due to supersaturation of the liquid. Chalcopyrite and bornite are intimately intergrown with this sphalerite. The Fe concentration in sphalerite in the surface pipeline is higher than downhole in RN-22 (5-8 wt.% compared to ~2 wt.%), which is inconsistent with the trend expected if gas loss due to boiling (H_2 faster than H_2S) was the factor controlling the Fe content of the sphalerite at lower temperature.

Zinc is the major component of the scales downhole and near the orifice plate, accounting for up to 60 wt. % of the scales in the high-pressure wells. Copper is low in downhole scale (~3 wt%) but increases at the surface, reaching ~20 wt.% upstream of the orifice plate to a maximum concentration of 25 wt.% in scales on the fluid-flow control valve in the medium-pressure wells. Similarly, Pb contents of the scales are ~6 wt.% upstream of the orifice plate and reach a maximum on the fluid-flow control valve or within a few cm downstream of the orifice plate. Iron concentrations in sulphides, oxides and silicates vary considerably and are generally low. Most Fe in downhole samples is considered to be in maghemite and some is due to contamination from the steel casing. The gold and silver concentrations in scale tend to increase with decreasing pressure. Measured concentrations are ~30 ppm Au and ~80 ppm Ag in scale downhole, and reach a maximum 950 ppm Au and 2.3 wt.% Ag near the orifice plate.

Pressure and temperature changes as well as the extent of boiling are the major factors controlling the precipitation of sulfide minerals and amorphous silica from the geothermal discharge. The most effective measure taken to prevent scaling and clogging of pipelines is to keep the pressure as high as possible in the two-phase line (22 bar), downstream of the orifice plate and upstream of the steam separation unit, as well as avoiding variations in the fluid flow (i.e., due to fluctuations in the wellhead pressure and bends in the surface pipe).

The amount of scales precipitated in the high-pressure wells in the first year of production was about 2.2 tonnes containing up to 900 kg Zn, 430 kg Cu, close to 200 kg Fe, 22 kg Pb, 5 kg Ag and close to 1 kg Au. Calculations show that the 5 high pressure wells likely will precipitate in surface pipelines between 4 and 5 tonnes of scales per year with the value of contained metal about \$70,000 (8,000,000 Icelandic krónur).

CHAPTER 3

Cu-rich Scales in the Reykjanes Geothermal System, Iceland

Vigdís Hardardóttir¹, Mark Hannington¹, Jeffrey Hedenquist¹, Ingrid Kjarsgaard²,
Karin Hoal³

¹Department of Earth Sciences, University of Ottawa, Ottawa, K1N 6N5, Ontario,
Canada

²Consulting Mineralogist, 15 Scotia Place, Ottawa, K1S 0W2, Ontario, Canada

³Advanced Mineralogy Research Center, Colorado School of Mines, Golden CO, 80401,
USA

Published in:

Economic Geology, v. 105, p. 1143 - 1155

Presented at:

Annual meeting of the Geological Society of America

Denver, 28 - 31 October, 2007

Paper No. 149-15

Abstract

Seawater-dominated fluids discharge from the subaerial Reykjanes geothermal system, Iceland. There is a sharp pressure decrease in surface pipes at an orifice (throttle point), and Cu-rich scales deposit at this orifice that consist largely of bornite and digenite, along with sphalerite and other sulfides. The bornite and digenite form complex intergrowths with sphalerite and galena, accompanied by high concentrations of gold and silver (up to 590 ppm and 2.3 wt.%, respectively). The precipitates form in response to rapid boiling (flashing) of the hydrothermal fluids due to the sharp decrease in pressure (from ~37 to 22 bar) at the orifice, downstream of the wellhead. The boiling, and concomitant separation of the vapor phase, results in a temperature decrease from 252°C to 220°C across this throttle over distances of centimeters. There is a nearly quantitative deposition of metals from solution, compared to concentrations in reservoir liquids, resulting in formation of the metastable Cu-Fe-S solid solution, rich in silver and gold, plus sphalerite and galena. A high degree of supersaturation of metals in the quenched liquid is indicated by the very fine grain size of the sulfides and dendritic textures. Post-depositional cooling likely caused exsolution of bornite and digenite from the high-temperature solid solution; in addition, silver was expelled from the Cu-Fe-S solid solution and remobilized into late fractures in the scales, whereas the gold appears to have remained in solid solution or as submicroscopic inclusions in the bornite and digenite.

The observed mineral assemblage at Reykjanes contrasts with that of seafloor black smokers, despite similar fluid compositions. The seafloor hydrothermal vents characteristically have Cu-rich linings composed predominantly of chalcopyrite, which is precipitated by a combination of conductive cooling of high-temperature (~350°C)

hydrothermal fluids and mixing with seawater. The difference in sulfide mineralogy between the Reykjanes orifice scales, with Cu sulfides dominated by bornite and digenite, and many seafloor vents may provide an indication of the sub-seafloor mineralization where fluids boil before discharging at seafloor vents.

Keywords: Bornite, digenite, Ag and Au rich, scales, Reykjanes geothermal system, black smoker.

Introduction

Reykjanes is a seawater-dominated geothermal system in Iceland, located where the Mid-Atlantic Ridge emerges on land. The geothermal liquid, harnessed for electrical power generation, is modified seawater heated to temperatures of at least 315°C at 1000 to 2500 m below the surface (Hardardóttir et al., 2009). The deep liquid has major element concentrations that are generally similar to those measured in black smoker fluids discharged at the seafloor from the mid-ocean ridges. However, the reservoir liquid is notably enriched in Au (~30x), Ag (~10x), Pb (~5x) and Cu (~10x) compared to black smoker fluids from 21°N East Pacific Rise (EPR) and the Trans-Atlantic Geotraverse (TAG) hydrothermal field on the Mid-Atlantic Ridge (Table 3.1; Hardardóttir et al., 2009). As the liquid ascends in Reykjanes wells, the decrease in pressure causes boiling and cooling which leads to the precipitation of sulfide minerals as scales within the well and ultimately in surface pipelines.

This paper describes the mineralogy and the composition of Cu-rich scales that are forming in response to sharp pressure decreases in some of the newest wells drilled at Reykjanes, specifically RN-12, 21 and 24, and documents the physical conditions that led to the precipitation of the sulfide assemblage. Because Reykjanes fluids do not

Table 3.1. Calculated reservoir compositions of liquids from wells RN-9, 12, 21, and 24, and measured deep liquid (RN-12DL) in a downhole sample collected from well RN-12 (Hardardóttir et al., 2009).

Source	RN-9	RN-12	RN-21	RN-24	RN-12DL	21°N	TAG	Sea water
Sampling location (m)	Surface	Surface	Surface	Surface	1500	2600	3650	Surface
temperature (°C)	290	295	285	285	295	350-273	366	-
pH	5.0	4.7	4.9	4.8	na	3.4-3.8	3.4	7.4-8.5
Cl	17948	18802	19971	19586	19283	17335	22546	19500
SiO ₂	603	697	619	582	618	1082	1262	2
CO ₂	1067	1886	722	1060	na	251	150	101
H ₂ S	27	58	25	23	na	248	119	nd
SO ₄	16	14	16	17	na	48	0.0	2712
Cu	0.0014	<0.0005	0.0005	0.0012	17	2.2	8.9	0.0004
Fe	0.39	0.07	0.09	0.06	25	93	312	0.00006
Zn	0.0086	0.0009	0.0267	0.0223	27	6.9	3	0.0004
Pb	0.0003	<0.0003	<0.0003	0.0003	0.29	0.06	0.02	0.000002
Ag	ppb	<0.5	na	na	36	4	5.5	0.002
Au	ppb	<0.01	na	na	na	6<0.04-0.2	na	0.004
Mg	0.8	0.8	0.8	0.6	9.9	0.0	0.0	1290
Ba	7.7	8.9	9.5	9.2	10.1	1.1	2.6	0.02
Sr	7	9	9	9	9	7	9	8
Na	9105	9510	9831	9673	9378	9936	12811	10770
K	1311	1363	1537	1469	1542	907	665	380
Ca	1449	1532	1656	1682	1940	625	1242	412
B	7.6	7.3	8.1	7.8	8.0	5.5	na	4.4

All concentrations are in ppm (mg/kg), except where indicated. Except for the deep liquid in RN-12, which was sampled directly at 1500 m depth (Hardardóttir et al., 2009), the compositions of the reservoir liquids were calculated from surface samples by taking into account steam loss due to boiling (Henley et al., 1984). The compositions of the black smoker fluids are from Von Damm (1990), Von Damm et al. (1985), and tables in Hannington et al. (2005). Seawater composition is from Bearman (1989).

mix with cold seawater in the wells, in contrast to the situation at seafloor hydrothermal vents, the scales may provide an indication of what is occurring in the feeder zones of submarine hydrothermal systems prior to discharge on the seafloor. In turn, this may be relevant to the possible origins of some unusually Cu-rich stockworks in volcanic-hosted massive sulfide (VHMS) deposits.

3.1 The Reykjanes Geothermal System

The Reykjanes geothermal area is located 50 km southwest of Reykjavík on the Reykjanes peninsula, which forms the southwestern tip of Iceland. The geothermal system is surrounded by the Atlantic Ocean on three sides, with the ocean no more than

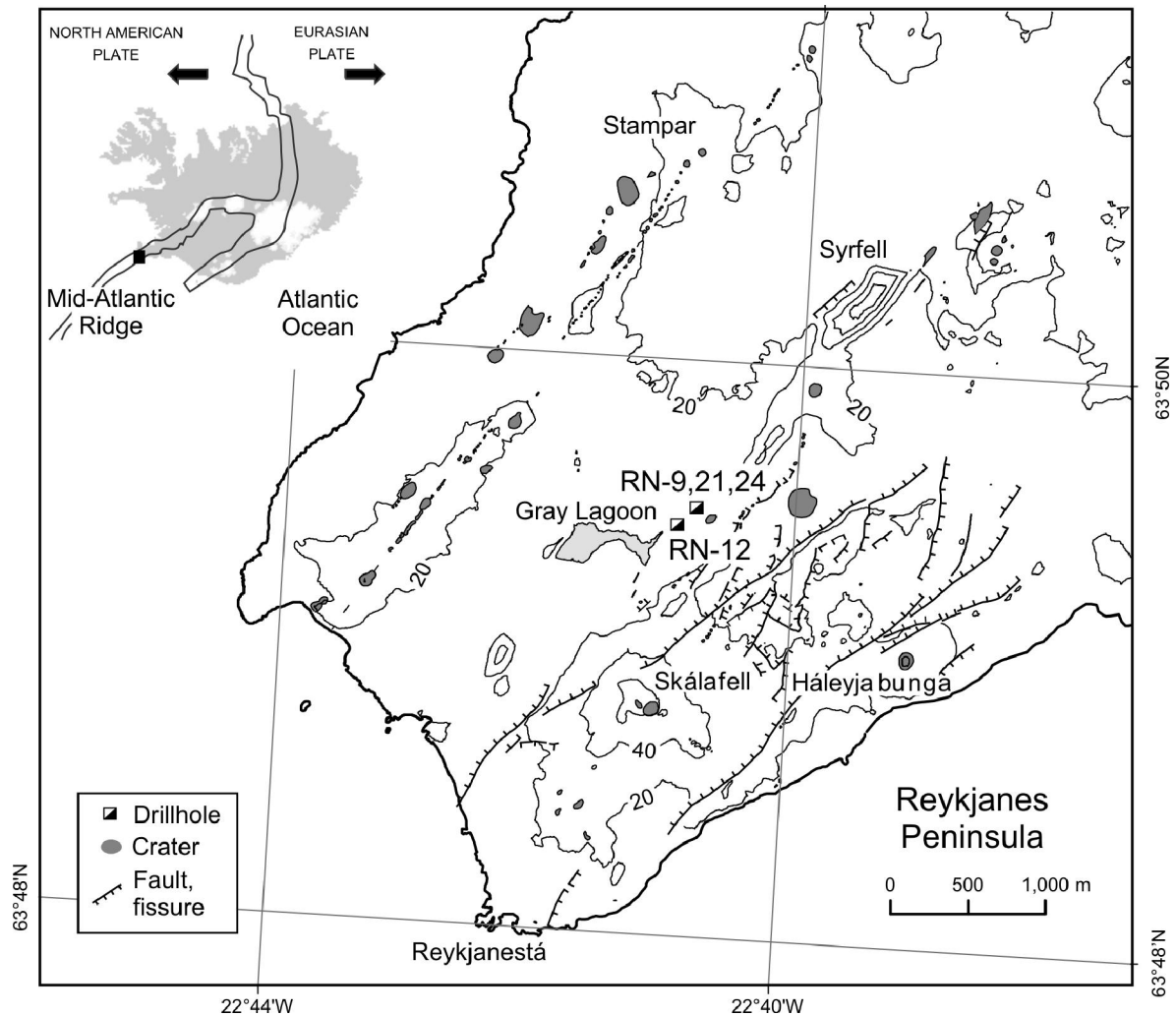


Fig. 3.1. Location of the Reykjanes geothermal system, 50 km southwest of Reykjavík, at the onshore extension of the Mid-Atlantic Ridge (upper left inset). The locations of the wells RN-9, 12, 21 and 24 are shown, along with other wells, in the inset to the upper right.

1.5 km away (Fig. 3.1); the wellheads and surface pipelines are <20 m above sea level. The volcanic section is dominated by tholeiitic basalt flows together with basaltic hyaloclastite and tuffaceous sediments of basaltic origin (Jakobsson, 1978; Kristmannsdóttir, 1984). Geothermal features occur at the surface over an area of ~1 km², and the thermal anomaly at 800 m depth is about 2 km² in size (Björnsson et. al, 1972a); a low resistivity area, thought to represent hydrothermal alteration, may be as large as 10 km² at depth (Karlisdóttir, 2005).

Twenty eight geothermal wells have been drilled in the area, 16 of which have been brought into production (Fig. 3.1). The wells range from 1119 m to 3082 m depth (G. Thórólfsson, pers. comm., 2009). The high-temperature liquid at depth (1 to 2.5 km) is modified seawater, with a salinity of ~3.2 wt percent NaCl. The measured reservoir temperatures range from 270° to 315°C, and the reservoir liquid has a calculated pH of ~5.3 (Björnsson et. al, 1972b; Bjarnason 2002). As in seafloor hydrothermal systems (e.g., Seyfried and Bischoff, 1977), reaction of the heated seawater with the surrounding basalt results in removal of most of the SO_4^{-2} and Mg from the fluid and increases the concentrations of SiO_2 , K and Ca compared to normal seawater (Björnsson et al., 1972b; Arnórsson, 1978b; Kristmannsdóttir, 1984). Based on the compositions of surface-sampled liquids, corrected for vapor loss (Arnórsson et al., 1982; Henley, 1984; Bjarnason, 2002), and the composition of the deep liquid sampled downhole at 1500 m depth (Table 3.1; Hardardóttir et al., 2009), a liquid of essentially constant composition is considered to be feeding all of the wells at Reykjanes. The very low metal contents in the fluids sampled at the surface reflect deposition of metals as scales during liquid ascent and boiling, based on the orders of magnitude higher metal concentrations that are present in the reservoir liquid, as directly measured in samples collected downhole, below the boiling level (Hardardóttir et al., 2009).

3.1.1 Location and conditions of scale formation

The measured pressures at the wellheads range from 52 bar to 15 bar, equivalent to 267°C to 201°C at saturated water vapor pressure, respectively (Keenan et al., 1969); the effect of seawater salinity ($\text{XNaCl} \sim 0.01$) on these properties is minimal and has not been considered here (Driesner, 2007). In the newer wells considered here (RN-12, 21 and 24), a valve is present in the surface pipe immediately downstream from the

wellhead to control the fluid flow from the well. The valve consists of a cone-shaped plug to open and close the orifice, which acts as an adjustable throttle (Fig. 3.2). The position of this cone (% opening) is changed from day to day depending on the daily requirement for high-pressure vapor in the separation station, which is then transmitted to the steam turbine. Variations in the cone position cause a change in the size of the opening at the orifice plate and therefore the amount of the pressure decrease across the orifice plate. In these three wells the pressure at the wellhead ranged from 40 to 22 bar (equivalent to 252°C to 220°C), although the average was 35 to 32 bar (Table 3.2). To prevent the temperatures from dropping below that of amorphous silica saturation (which varies between wells), the pressure at the separation station is maintained between 17 and 18 bar (207-210°C). This is achieved by maintaining a pressure downstream at the orifice plate of about 22 bar (220°C). The maximum temperature

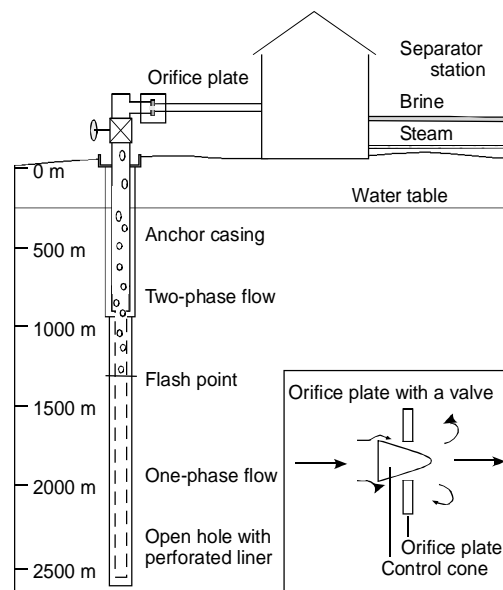


Fig. 3.2. Schematic model of the geothermal wells in the Reykjanes geothermal system, showing the approximate location of initial boiling of rising seawater-dominated liquid, which occurs at depths of 900-1000 (RN-9) to ~1250 m (RN-12, 21, 24). Above the boiling level, flow in the well consists of vapor + liquid. The inset shows the fluid flow-control valve (cone; Fig. 3.3) inserted in the orifice plate immediately downstream of the wellhead in RN-12, 21, and 24, where flashing (extensive boiling) results from a sharp decrease in pressure (from 40 to 22 bar) over a distance of a few cm.

Table 3.2. Summary of the physical parameters for the wells sampled in this study

Well No.	Well depth (m)	Temperature (°C)		Pressure (bars)			Scales in pipe-lines					Production Average day (kg/s)
		T°C _{max} depth (m)	Highest & lowest T°C ¹ at well-head	Average at well-head	Down-stream of orifice plate	ΔP _{MAX} in year of scale formation	At the well-head ²	On the cone	On the orifice plate	6 m down-stream of orifice plate	150 m down-stream of orifice plate	
RN-9	1445	295°C 1402m 314°C	257-201	39	11	23	x	–	xxx	xxxx	xxx	43
RN-12	2506	2495m 285°C	247-239	35	22	15	–	xx	x	–	–	143
RN-21	1664	1593m 286°C	252-165	32	22	18	–	xx	no info	–	–	121
RN-24	2114	1269m	252-236	34	22	15	–	xx	x	–	–	140

Notes: Turbines were operated at ~11 bar when supplied from RN-9, and 18-19 bar when later supplied from RN-12, 21 and 24. From 1983 to July 2000, the average wellhead pressure was 39 bar for well RN-9. From May 2006 to May 2007, the wellhead pressure in RN-12 increased from 32 bar to 37 bar but was 35 bar for 7 months. In RN-21 the wellhead pressure was ~32 bar but ranged from 20 bar (few days) to 40 bar (few days). In RN-24 the pressure was ~39 bar until October 2006, then steady at 30-32 bar. T°C_{max} = maximum measured temperature; T°C¹ = temperature at saturated water vapor pressure (Keenan et al., 1969); ΔP_{max} = pressure at wellhead minus pressure downstream of the orifice plate; xxxx = scales up to 15 cm thick; xxx = scales up to 4 cm thick; xx = scales = 2 cm thick; x = scales < 0.5 cm thick; “-” no scales; no info = no information. At the wellhead² = No scales are deposited between the cone and the wellhead, but color change from brown to blue was seen in the pipes in RN-12, 21, and 24, but no information is available about the wellhead itself.

drop across the orifice plate in these wells is therefore from 252°C to 220°C, which prevents silica supersaturation.

In the sampled wells (RN-12, 21 and 24), metals in the fluids deposited as sulfide scales on the cone and on the downstream side of the orifice plate; scales on the cones are relatively thin (<1.5 cm; Fig. 3.3A) and are dominated by metallic sulfides. This is in contrast to the scales formed in RN-9, one of the old series of wells, which was operated without a cone valve in the orifice plate; the wellhead pressure was ~39 bar (measured in 1983-2000; Table 3.2), and the pressure downstream of the orifice plate was ~11 bar. Scales deposited in RN-9 were up to tens of centimeters thick and consisted mainly of amorphous silica (Hardardóttir et al., 2001; Hardardóttir, 2004a), due to the low pressure and hence temperature (188°C) that led to

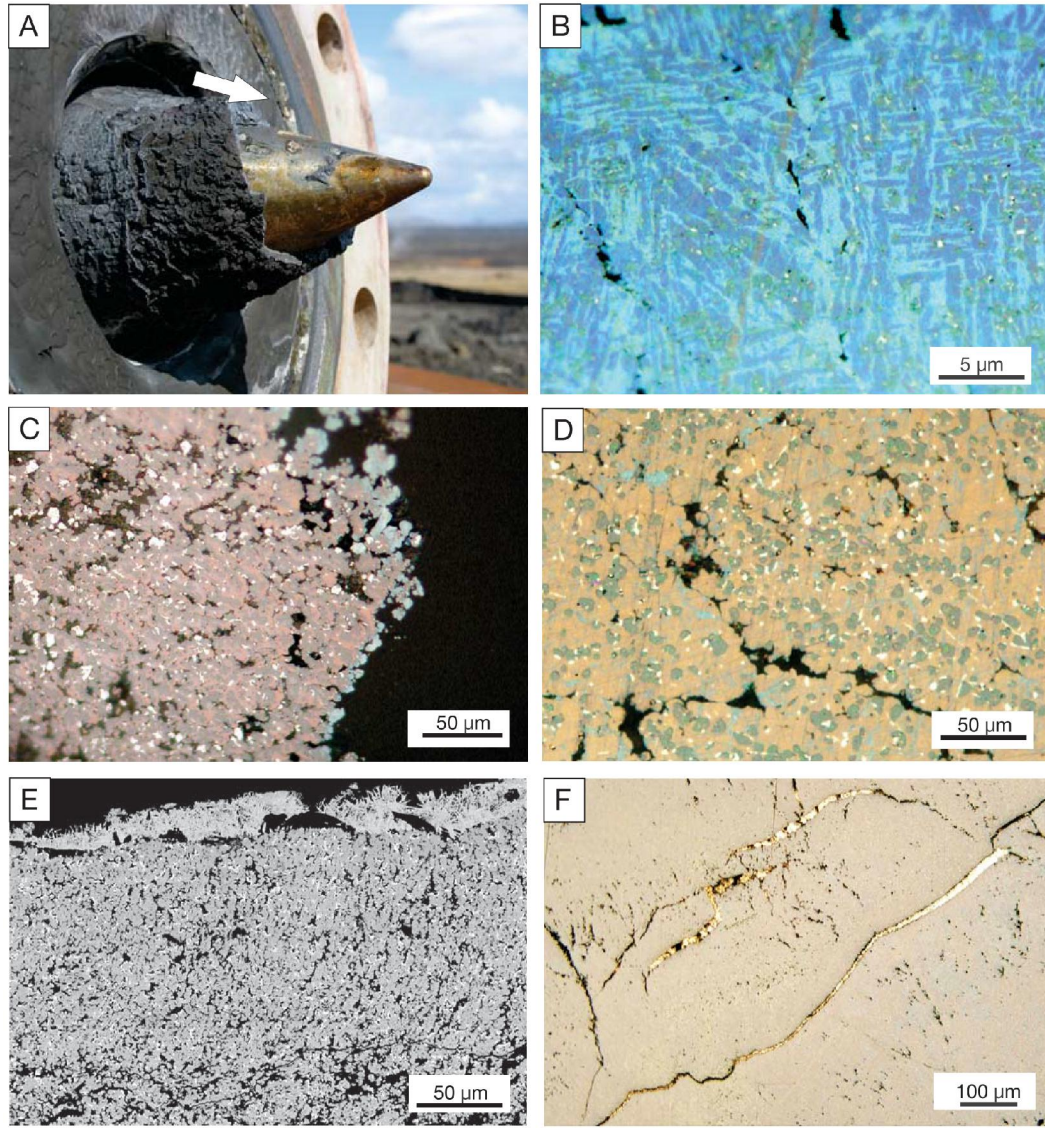


Fig. 3.3. Scales from wells RN-12, 21 and 24. a) Photograph of the Cu-rich scale on the cone-shaped fluid-flow control valve in well RN-24. The cone protrudes through the orifice plate in the direction of fluid flow (see Fig. 2). The cone is 14 cm long and the orifice diameter is 15 cm. A 1-2 cm-thick scale of massive bornite+digenite+sphalerite+galena has precipitated on the cone. Note that the top portion of the scale was broken off during sampling, exposing the steel. b) Photomicrograph of bornite (dark blue to violet) and digenite (light blue) as discrete exsolution lamellae. White grains are native silver. Reflected light, RN-24. c) Photomicrograph showing mass of bornite (pinkish)-sphalerite (light gray) with galena (white), rimmed by digenite (blue gray). Reflected light, RN-21. d) Intimate intergrowth of sphalerite (gray) with bornite (orange), and digenite (light blue). White grains are galena. Reflected light, RN-12 e) Backscattered electron image of the outer 250 μm of the scale from RN-12. Packed dendrites of intimately intergrown bornite, digenite, and sphalerite (all gray) with disseminated galena (white) are coated by a layer of bladed covellite (light gray at the top of the image) and bladed calcite (black). f) Photomicrograph of native silver filling late cooling fractures in massive bornite. The silver is interpreted to have migrated to the late cooling fractures after being expelled from originally deposited Ag-rich Cu-Fe-S solid solution. Reflected light, RN-21.

amorphous silica supersaturation. Although metallic sulfides are present in the RN-9 scales, dominated by fine-grained sphalerite and chalcopyrite with traces of galena, bornite, and pyrrhotite, with amorphous silicates (Hardardóttir et al., 2001; Hardardóttir, 2004a), the concentrations are diluted by the large amounts of amorphous silica downstream of the orifice plate.

In contrast to RN-9, the scales found coating the cone valves at the orifice plate in the new wells, RN-12, 21, and 24, consist almost entirely of sphalerite, bornite, digenite, and with galena and high concentrations of gold and silver. Only a trace (<1 mm) of scales were present between the orifice plate and the wellhead in the new wells, and < 2mm thick downstream of the orifice plates. The scales on the cones formed over a period of not more than one year, from May 2006 to May 2007, and were sampled immediately after shutdown of the wells. The scales in these new wells, at the point of sharp pressure decrease, are the object of study here.

3.2 Mineralogy and Chemical Composition of the Cu-rich Scales

The most Cu-rich scales on the cones in wells RN-12, 21 and 24 consist of very fine-grained (<4 μm) granular sphalerite (~45 vol.%), very fine-grained oriented intergrowths of bornite (~30 vol.%) and digenite (~15 vol.%), fine-grained galena and Ag-sulfides (~10 vol.%), and traces of chalcopyrite, amorphous silica and native silver (<1 vol.% each; Table 3.3). The very fine grain sizes made analyses of some of the minor phases and complex intergrowths difficult, but detailed petrography and electron microprobe data indicate several stoichiometric compositions.

The main Cu minerals in the scales are bornite and digenite in very fine-grained intergrowths (Fig. 3.3B), possibly an exsolution texture. In some samples, they form

Table 3.3. Mineralogy of scale samples from the Reykjanes wells compared to black smoker chimneys from the TAG hydrothermal field.

Source	Well						TAG Black Smoker
	RN-24	RN-21	RN-12	RN-9A	RN-9B	RN-9C	
Bornite	xxx	xxx	xxx	tr	tr		x
Digenite	xxx	xxx	xxx				
Sphalerite/wurtzite	xxx	xxx	xxx	xxx	xxx	x	xxx
Galena	xx	xx	xx	x	tr		tr
Chalcopyrite			x	xxx	xx	tr	xxx
Gold ¹				x	tr		tr
Native silver	x	x					
Covellite			x	tr	x		tr
Pyrrhotite			tr	tr			x
Pyrite			tr			tr	xx
Amorphous SiC ₂	tr	tr	tr	tr	xxx	xxx	x
Anhydrite							xxx
Clay				tr	tr	tr	
Temperature (°C)	252-220	252-220	247-220	257-201	~188	~188	270-360

Notes: xxx = abundant; xx = major; x = minor; tr = trace. ¹Probable mixture of Au+Ag of unknown composition, RN-9A was sampled at the wellhead. RN-9B was sampled ~6 m downstream of the orifice plate (~15 m downstream of wellhead). RN-9C was sampled ~150 m downstream of the orifice plate (Hardardóttir et al., 2001). Data for the TAG hydrothermal field are from Hannington et al. (1995b) and Tivey et al. (1995).

closely packed dendrites (Fig. 3.3E), but in other samples they form granular masses with few pore spaces (Fig. 3.3D). Digenite occurs as graphic intergrowths with bornite, as discrete exsolution lamellae (Fig. 3.3B), and locally concentrated near the outer rims of the packed dendrites (Fig. 3.3C). The bornite and digenite are also intimately intergrown with abundant fine-grained sphalerite as well as galena and minor disseminated Ag minerals (native silver and Ag-sulfides). The sphalerite, in particular, is complexly intergrown with the Cu-Fe-S sulfides (Fig. 3.3D), whereas the galena occurs as small isometric grains varies strongly in abundance from area to area, rimming dendrites of bornite-digenite and in minute open spaces (Figs. 3.3C, D). Minor chalcopyrite occurs in patches and as finely (<1 μm) disseminated grains in bands within the bornite-rich scales. The chalcopyrite is locally intergrown with covellite and rare Fe-sulfides (pyrite and/or pyrrhotite). The outermost layer of the scales in one of the wells (RN-12) is coated by bladed covellite (Fig. 3.3E), which gives the outer

surface a distinctive peacock blue color; this covellite is locally associated with minor bladed calcite. Cracks in the scales, thought to have formed during cooling, are commonly filled by native silver (Fig. 3.3F). Amorphous silica occurs locally as matrix, in open spaces, and intergrown with late covellite in the outermost layers of the scales.

The bulk compositions of the Cu-rich scales from the new wells are given in Table 3.4. Representative analyses of scales from the old well (RN-9) are shown for comparison (Hardardóttir, 2004a). The scales from the new wells are very similar in their base metal contents, with high Cu (20 to 26 wt.%), Zn (20 to 27 wt.%), Pb (13 to 17 wt.%), and relatively low Fe (5 to 9 wt.%). The concentrations of Au and Ag range from 130 to 590 ppm and 0.8 to 2.3 wt. percent, respectively, with a bulk Au:Ag ratio of 0.01 to 0.08. The scales also contain high Mn (430 to 2300 ppm), Se (720 to 1350 ppm), Cd (190 to 430 ppm), and Hg (14 to 46 ppm), and three samples have high Co (19 and 170 ppm). The most sulfide-rich scales from the old well (RN-9A; Table 3.4) have similar Cu and Zn contents (~20 wt.%) but lower Pb (<3.3 wt.%) and higher Fe (up to 20 wt.%) than the Cu-rich scales in the new wells. The Au concentrations in the scales from the RN-9 range from 6 to 147 ppm; Ag concentrations are from <0.01 to 0.04 wt. percent. Concentrations of other elements, except Co and Cd, are also much lower in RN-9.

A false-color backscattered electron image of the surface of scale from RN-12 shows a notable rhythmic banding on a millimeter scale (Fig. 3.4). The individual bands are about 2-4 mm wide, with as many as 18 bands in a 4 cm thickness, and formed as a result of unidirectional growth in the flow direction (from right to left). Each band consists of a Cu-rich zone, a Cu-Zn-rich zone, and a Pb-rich zone. Bulk analyses obtained by rastering the electron beam indicate that the Cu-rich bands contain

Table 3.4. Major and trace element concentrations in scales from the Reykjanes wells and chimneys from the Tag hydrothermal field

Source	Cu	Zn	Pb	Fe	S	SiO ₂	Ag	Au	Mn	Se	Cd	As	Hg	Sb	Ni	Mo	Mineral vol.%,										
Reykjanes	wt.%																Sph	Bn	Di	Gn	Cpy	Ag	Ag in ss				
	ppm																										
RN-12E1	19.9	19.6	13.1	9.1	20	7	7720	589	2300	1199	223	68	170	18	7	<20	<2	47.5	36.0	3.0	13.1	<0.5	0.4				
RN-12E2	25.7	21.2	15.7	7.8	23	2	10700	554	1069	1199	221	88	19	21	7	<20	<2	43.4	38.0	4.5	13.4	0.1	0.6				
RN-21E1	25.9	25.8	12.4	5.7	24	1	23600	154	434	721	435	53	<2	15	9	<20	<2	51.5	18.0	18.6	10.0	0.8	1.1				
RN-21E2	24.1	26.7	13.3	5.4	24	1	21600	127	542	764	391	175	<2	14	17	<20	<2	53.1	17.0	17.1	11.0	0.7	1.1				
RN-24E1	26.3	20.8	16.7	6.3	23	1	20000	359	596	1350	233	100	<2	46	13	<20	<2	43.0	31.0	10.0	14.3	0.6	1.1				
RN-24E2	23.6	22.8	15.3	6.7	22	2	15600	326	1990	1328	192	153	22	24	26	<20	<2	48.0	20.0	17.0	14.0	0.3	0.7				
RN-9A	19.7	20.7	0.6	20.0	28	5	164	147	774	282	236	<1.6	5	na	<0.2	<1	<2	40.0	8.0			0.5	51.5				
RN-9B	6.2	12.3	3.3	4.4	10	47	444	92	5111	199	100	41	51	na	10	10	<2	61.0	19.0			7.0	13.0				
RN-9C	0.2	0.8	0.3	3.1	1	83	79	6	7705	<3	5	25	226	na	2	47	<2										
TAG-Hydrothermal Field																											
ALV2179-1-1B ¹	23.0	0.4	0.003	30.5	34.5	<0.50	6	1	<77	52	<10	51	189	na	6	10	150										
ALV2179-4 ¹	23.5	0.0	<0.002	24.3	28.3	<0.50	6	0.05	<77	630	<10	1	106	na	0	<10	140										
TG1-44 ²	25.0	0.5	0.005	29.3	35.8	2.61	13	1	na	13	17	28	32	0	5	na	190										

Notes: na = not analyzed. Samples RN-12E1, -21E1, and -24E1 are from the base of the cone inserted in the orifice plate. Samples designated E2 are also from the cone, ~ 6 cm downstream of samples E1. Sample RN-9A is from the wellhead, RN-9B is from ~6 m downstream of the orifice plate and ~15 m downstream of wellhead, RN-9C is from ~150 m downstream of the orifice plate (Hardardóttir et al. 2004). Data for Cu-rich sulfides from the TAG hydrothermal field are from Hannington et al. (1991, 1995b), and Tivey et al. (1995). Analyses were performed by Activation Labs, Ancaster, Ontario, by a combination of ICP-ES and ICP-MS following multi-acid digestion, and by instrumental neutron activation. Proportions of minerals in each sample were calculated using a combination of microprobe analyses (Table 3.5) and ideal mineral compositions, assuming galena contains all Pb and 2.5 wt% Ag, sphalerite contains all Zn and 3.2 wt% Fe, bornite and digenite contain 1 wt% Ag, and digenite contains 3.5 wt% Fe. Results were converted to volume % using average mineral densities and normalized to 100% sulfides (plus native Ag). Sph = sphalerite; Bn = bornite; Di = digenite; Cpy = chalcopyrite; Ag = native silver; "Ag in ss" = proportion of Ag in solid solution in bornite, digenite, and galena.

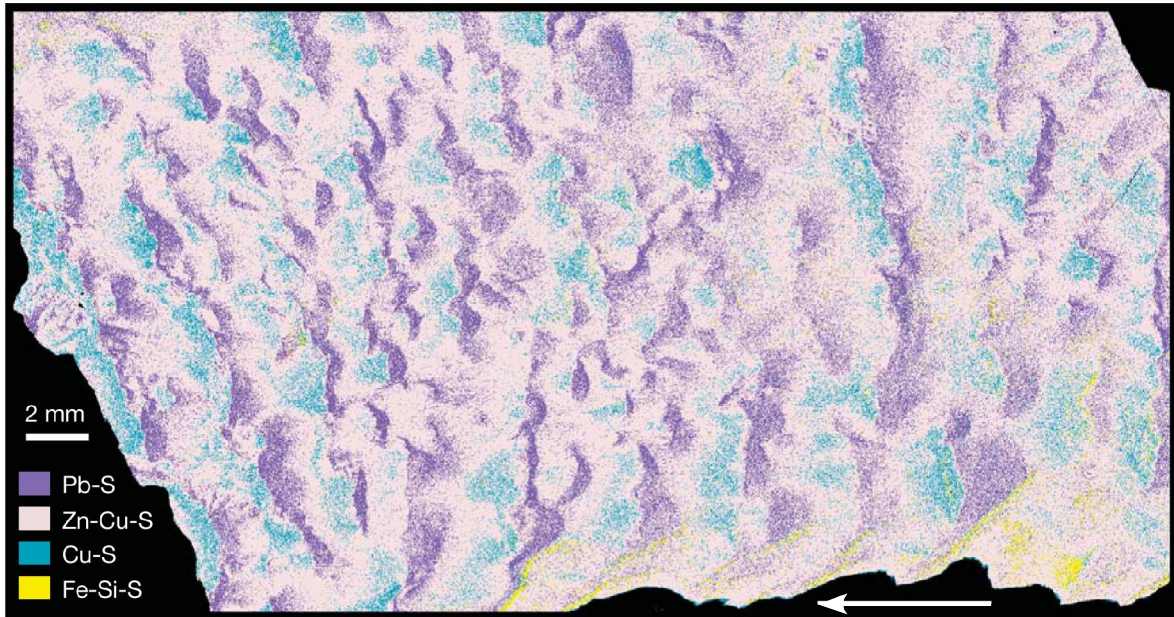


Fig. 3.4. False-color image of the surface of bornite-rich scale in RN-12, showing a crude rhythmic banding of sulfides on a millimeter scale. The image was obtained on a polished specimen of the scale using a QEMSCAN quantitative analytical SEM (scanning electron microscope). The false color map is based on elemental concentrations measured with an automated 4-spectrometer energy dispersive (EDS) analytical system with 25-micron stepping of the electron beam, which determines the pixel size in the final image. Operating conditions were 25 kV accelerating voltage and 5 nA specimen current. The sample was cut to show possible mineralogical zonation in the flow direction (from right to left, indicated by the arrow). The image shows compositional bands (2-4 mm wide) comprising an early Cu-rich zone, an intermediate Cu-Zn-rich zone, and a later Pb-Zn-Cu-rich zone. As many as 18 bands are visible in the sample, which are interpreted to reflect deposition from Cu-rich minerals during pulses of higher-temperature (i.e., higher pressure) fluid, followed by deposition of more sphalerite and galena as the pressure of each pulse subsided and the fluids cooled.

about 45 wt. percent Cu, 19 wt. percent Zn, 9 wt. percent Fe, and 8 wt. percent Pb.

The Pb-rich bands contain about 45 wt. percent Pb, 25 wt. percent Zn, and 6 wt. percent Cu. Silver concentrations are highest in the Pb-rich bands (up to ~8 wt.%).

3.2.1 Mineral analyses

Despite the very fine grain size of the minerals from the samples collected from the cones in RN-12, 21 and 24, discrete mineral phases could be analyzed. These included bornite, digenite, covellite, chalcopyrite, sphalerite, galena, native silver, a Ag-sulfide in the Cu-Ag-S system (Ag-bornite), and an unidentified Cu-rich pyrrhotite-like mineral (Table 3.5).

Table 3.5. Representative electron microprobe analyses (wt.%) of metallic minerals in Cu-rich scales from RN-12, 21, and 24.

Mineral	Well	Cu wt.%	Fe	Zn	Pb	S	Ag	Au	As	Se	Mn
Sphalerite	24RN	5.80	3.74	64.88	<0.01	31.49	0.27	<0.01	<0.01	0.09	0.09
Bornite	24RN	63.76	8.66	0.06	0.00	23.60	1.07	<0.01	<0.01	0.03	0.03
"Ag-bornite"	24RN	30.32	8.19	<0.01	0.08	20.13	35.18	<0.01	0.01	0.07	0.02
Digenite	21RN	71.11	1.15	0.73	<0.01	22.67	1.94	<0.01	<0.01	0.02	0.01
Covellite	12RN	66.91	0.33	0.13	<0.01	28.33	2.19	0.03	0.05	<0.01	<0.01
Galena	24RN	3.22	0.72	3.08	78.39	13.57	2.26	0.03	<0.01	0.58	0.02
Native silver veins	24RN	0.99	0.34	<0.01	<0.01	0.30	98.28	<0.01	0.05	<0.01	0.02
Chalcopyrite	12RN	31.54	30.35	0.19	<0.01	31.49	0.86	<0.01	<0.01	<0.01	0.16
"High-Fe ISS"	12RN	8.57	49.54	0.12	<0.01	36.71	<0.01	<0.01	<0.03	<0.02	0.17

Notes: Cd, Ni, Te, Sb, Hg, Ge, Bi, and V were analyzed but were at or below detection in all cases. Due to the very fine grain size of many phases, some analyses may represent partial intergrowths. Charging of the sample surface also may lead to uneven current distribution and low totals for some analyses. Analyses were performed on a four-spectrometer wavelength dispersive CAMECA Camebax Electron Microprobe at Carleton University, Ottawa. Operating conditions were 20 kV and 30 nA with counting times of 10 seconds and a beam diameter of 2 to 5 μm . Overlap corrections were performed using the PAP procedure. Pure elements (e.g., Au, Ag, Mn, Co) and simple compounds (e.g., FeS, CuS, CdS, PbS, ZnS) were used as standards, and calibrations were checked by analyzing known mineral standards.

Where bornite and digenite are free of fine-grained intergrowths with sphalerite and other phases, the compositions are close to stoichiometric Cu_5FeS_4 and Cu_9S_5 , respectively. A small amount of Fe is present in the analyses of the digenite. The Ag content of both bornite and digenite is about 1 and 1.5 wt. percent, respectively (based on five analyses of bornite and two analyses of digenite); chalcopyrite also contains up to 1 wt. percent Ag, and galena more than 2 wt. percent Ag (Table 3.5). Virtually all the Fe in the scales (5 to 9 wt.%) is accounted for by Fe in bornite, sphalerite and minor chalcopyrite. Minor amounts of Fe-sulfides occur only locally intergrown with chalcopyrite in the outermost parts of the scales. The Fe-sulfides are pyrrhotite-like phases with compositions that are notably Cu-rich. They are interpreted here to be a Cu-Fe-S intermediate solid solution (High-Fe ISS in Table 3.5), although the analytical totals are low owing to contamination by minor calcite gangue. A trace of Mn (~0.5 wt.%) is also present in the scales, most likely in the calcite gangue. The single analysis of sphalerite shows a moderately high Fe content (~7 mole percent FeS). The galena

contains up to 0.7 wt. percent Se in solid solution, which accounts for most of the Se in the bulk samples. However, its composition is far from stoichiometric PbS and also likely reflects a fine-grained intergrowth with other phases.

A brick red Ag-rich bornite with the approximate formula $\text{Cu}_3\text{Ag}_2\text{FeS}_4$ (Ag-bornite in Table 3.5) also occurs with digenite and sphalerite in RN-12. The native silver in veins and cracks in the scales is nearly pure, with Au:Ag <0.001. Silver also occurs as very fine white grains, containing 15 to 80 wt.% Ag, disseminated in the sulfide matrix (Fig. 3.3B); however, the identity of these grains could not be confirmed. The bladed covellite, which coats the scales of well RN-12, is close to stoichiometric CuS but also contains high Ag (more than 2 wt.%; Table 3.5).

3.3 Discussion

3.3.1 Sulfide textures and paragenesis

The textures in the sulfide-rich scales reflect the high discharge velocities of the two-phase fluid (Fig. 3.3A), as well as the sharp pressure decrease and rapid adiabatic cooling downstream of the orifice plates. The fluids in wells RN-12, 21 and 24 are discharged at rates of ~120-140 kg/s (Table 3.2). Since the feed zones are deep (below 1000 m, with solid casing above 611 to 854 m depth), there is no mixing with cooler near-surface waters, as indicated by the absence of Mg in the discharging fluids (Björnsson et al., 1972b; Arnórsson, 1978b; Kristmannsdóttir, 1984; Table 3.1). The high flow rates appear to have strongly influenced the growth of the scales; in many cases, arborescent intergrowths of bornite, digenite, sphalerite, and galena curve in the direction of fluid flow. However, at high magnification, most subgrain textures are too small to establish a clear pattern of crystallization. In these samples, bornite, digenite,

and sphalerite are so intimately intergrown at a fine scale as to be almost indistinguishable as paragenetically distinct phases. In contrast, galena and some native silver appear to have been deposited as discrete phases in micron-sized open spaces and festooning dendrites of bornite, digenite and sphalerite (Figs. 3.3C, D).

The very fine-grained intergrowths of bornite, digenite and sphalerite are typical of the products of rapid quenching, as observed in hydrothermal experiments, and are characteristic of a high degree of supersaturation (Craig and Scott, 1976; Fleet, 2006). The occurrence of dendritic textures (e.g., Fig. 3.3E) is considered by others to be evidence for growth from colloidal suspensions (Saunders and Schoen, 1995), termed orthokinetic colloid aggregation (Stumm and Morgan, 1981). The deposition of such incompletely crystalline material is common at high degrees of supersaturation, reflecting conditions far from equilibrium. Thus, the Cu-rich sulfides may have formed originally as a metastable, high-temperature Cu-Fe-S solid solution, possibly associated with colloids, rather than by direct precipitation as bornite and digenite.

Much of the Ag in the Ag-rich mineral samples may have originated from a higher-temperature Ag-rich Cu-Fe-S solid solution. Reaction rates in the Cu-Ag-S system are fast (Skinner, 1966), explaining the rapid migration of exsolved Ag to contraction fractures in the quenched scales.

Covellite, which rims the bornite-rich layers, likely precipitated directly from hydrothermal fluids rather than by exsolution from Cu-Fe-S-solid solution. This is consistent with its nearly stoichiometric composition, its distinctive bladed habit, and its paragenetically late occurrence and association with late bladed calcite.

intermediate compositions are rare in nature because of the rapid kinetics of exsolution (Grguric and Putnis, 1999). A minor pyrrhotite-like phase in the scales is also notably Cu-rich and may reflect Cu solubility in pyrrhotite or the presence of an intermediate solid solution (e.g., Barton, 1973; Cabri, 1973). The maximum solubility of Cu in pyrrhotite at 350°C is about 0.6 wt. percent (e.g., Fleet, 2006), whereas the pyrrhotite-like phase in the scales has a composition close to $\text{Fe}_{0.85}\text{Cu}_{0.15}\text{S}$ (Table 3.5). This may be analogous to some nonstoichiometric metastable phases formed in the Cu-Fe-S system under conditions of extreme disequilibrium (e.g., cuprian mackinawite; Craig and Scott, 1976). However, the minerals are too fine grained to allow a positive identification.

The composition of sphalerite in RN-12, 21 and 24 (Table 3.5) is similar to that found in RN-9 (Hardardóttir, 2004a; Hardardóttir et al., 2006), about 7 ± 3 mole percent. However, it is unlikely that the Fe content of the sphalerite represents equilibrium with a particular Fe-bearing sulfide, as pyrite and pyrrhotite are rare in the scales. The intimate intergrowth of sphalerite with bornite and digenite may indicate coprecipitation of ZnS with a Cu-Fe-S solid solution, which is known to dissolve considerable amounts of Zn at high temperatures (up to 1.7 at% at $\sim 400^\circ\text{C}$), and this might be enhanced in the absence of pyrite or pyrrhotite (Kojima and Sugaki, 1985; Sugaki et al., 1987). However, the bulk composition of the scales (20 to 26 wt.% Cu, 20 to 27 wt.% Zn, 5 to 9 wt.% Fe and 20 to 24 wt.% S) does not correspond to any known composition on the $\text{CuFe}_2\text{S}_3\text{-CuZn}_2\text{S}_3$ join and is much more Zn-rich than any known zincian intermediate solid solution (e.g., Hutchison and Scott 1981; Kojima and Sugaki 1984, 1985). Zincian isocubanite has been reported from various seafloor hydrothermal sulfide deposits, intergrown with sphalerite (Koski et al., 1988; Peter and Scott, 1988; Paradis

et al., 1988), but the Zn content is typically less than 5 wt. percent. Therefore, it is unlikely that the observed textures and abundant sphalerite can be due to exsolution from a Cu-Fe-Zn-S solid solution and must reflect co-precipitation of ZnS in a complex intergrowth with a Cu-Fe-S solid solution, again favored by the strongly supersaturated conditions.

The bladed covellite observed rimming bornite may be the low-temperature phase commonly referred to as “blue-remaining covellite” (formed at temperatures below 157°C; Craig and Scott, 1976). The covellite may represent precipitation caused by changing conditions shortly before opening of the pipe to sample the scales (i.e., cooling due to the closing of the well).

The abundance of late-stage Ag in fractures and the occurrence of Ag-rich bornite in RN-12 are consistent with substantial Ag solubility in the bornite-digenite solid solutions at higher temperatures of deposition. Studies of the Cu-Ag-S system have shown that very extensive solid solution of Ag can occur in digenite and probably also in bornite (Skinner, 1966; Skinner et al., 1967). Below about 100°C, the solubility of Ag in Cu-Fe-S solid solutions is greatly reduced (Skinner, 1966), accounting for the expulsion of silver from the more massive bornite-digenite intergrowths.

Native Ag and Ag-sulfides are not present in sufficient visual quantity to account for all of the Ag in the bulk analyses, consistent with the Ag contents of about 1 to 2 wt percent in sulfides (Table 3.5; ~40 percent of the silver in the scales). No free gold was observed, despite the high gold content of the bornite-rich scales; in addition, there is insufficient gold in the native silver to account for the bulk gold content of the samples (up to 590 ppm). This indicates that the gold is also present largely as submicroscopic inclusions or in solid solution in other phases.

3.3.3 Causes of sulfide mineral deposition

The difference in the dominant sulfide mineralogy of wells RN-12, 21 and 24 compared to RN-9 may be related to the somewhat smaller pressure decrease (Table 3.2), and thus higher temperatures after cone valves were inserted in the orifice plate. The high metal concentrations in the scales result from the high metal concentrations in the deep liquid (Hardardóttir et al., 2009), coupled with efficient deposition of metals caused by the large and sharp pressure drop and concomitant cooling due to boiling (Brown, 1986; Akaku, 1990; Reed and Palandri, 2006). The proportions of Cu and Zn in the scales correspond generally to that of the deep liquids (Tables 3.1 and 3.4), whereas the Pb/Cu and Pb/Zn ratios in the scales are higher than expected, perhaps due to deposition of Cu and Zn at depth below the wellhead.

The fine, millimeter-scale bands of Cu-, Zn-, and Pb-rich sulfides (Fig. 3.4) may reflect fluctuations in the well, in part due to natural fluctuations but also caused by periodic adjustment of the cone valve position, which will affect the pressure and hence temperature. Each band comprises an early (upstream) Cu-rich zone that may correspond to a pulse of higher temperature (higher pressure) fluid, followed by an intermediate Cu-Zn-rich zone, and a later (downstream) Pb-rich zone. This is repeated in successive bands in the direction of fluid flow.

3.3.4 Comparison with Cu-rich black smoker chimneys

The deep reservoir liquid at Reykjanes (RN-12DL, Table 3.1) is similar in major element composition to the highest temperature fluids discharging from black smokers; trace metals are similar to higher in concentration in the deep Reykjanes liquid (Hardardóttir et al., 2009). Hydrothermal fluids at black smoker vents on the seafloor

discharge at temperatures up to 407°C (Von Damm, 1988, 1990; Koschinsky et al., 2008).

Copper-rich chimneys form where the black smoker vent fluids are cooled rapidly by mixing with seawater; they typically consist of a chalcopyrite core with an outer zone of sphalerite, pyrite, and marcasite (Haymon, 1983). The mineralogy of the scales in RN-9 is generally similar to that of black smoker chimneys (with the important exception of high Au and Ag contents; Hardardóttir et al., 2001; Hardardóttir, 2004). Similar to the Reykjanes scales, abrupt changes in mineralogy are commonly observed in the walls of black smoker chimneys as a result of relatively minor fluctuations in temperature (e.g., Koski et al., 1994, Tivey 1995). However, the apparent cyclic deposition of Cu-, Zn- and Pb-rich bands in the Cu-rich scales of wells RN12- 21 and 24 at Reykjanes (Fig. 3.4) contrasts with the walls of black smoker chimneys, where the mineralogy of the innermost layers (chalcopyrite core) differs dramatically from the outermost layers (zone of sphalerite, pyrite and marcasite; Tivey, 1995; Tivey et al., 1995). Minor amounts of isocubanite are almost always found in black smoker chimneys where rapid cooling of fluids (e.g., from 400° to 350°C) has been documented (e.g., Mozgova et al. 2008), and this may be analogous to the Cu-Fe-S intermediate solid solution observed in the Reykjanes bornite-rich scales (Table 3.5).

Typical black smoker fluids, such as those at 21°N on the East Pacific Rise, are close to calculated equilibrium with bornite (Tivey et al., 1995). Minor amounts of bornite occur locally in many Cu-rich chimneys, but no chimneys have been described that are composed dominantly of bornite and digenite; rather, chalcopyrite dominates. Table 3.1 shows that the Cu/Fe ratio of the deep liquid in RN-12 is more than an order of magnitude higher than that of EPR black smoker fluids, which likely accounts for

the predominance of bornite and digenite in the scales. Similar Cu-rich sulfides may be precipitating in some sub-seafloor stockworks; however, these are rarely exposed, and no systems with demonstrated boiling have been drilled to reveal the nature of the sub-seafloor mineral deposition. During drilling by the Ocean Drilling Program of the Bent Hill massive sulfide deposits at Middle Valley, an anomalous deep Cu zone composed predominantly of isocubanite and chalcopyrite was encountered 200 m below the seafloor (Zierenberg et al., 1998), confirming the presence of unusually Cu-rich fluids at depth that have not reached the seafloor.

The high Cu, Zn, and Pb contents, in addition to mineralogy, of the scales from Reykjanes wells RN-12, 21 and 24 contrast sharply with that of even the most Cu-rich precipitates on the seafloor (Hannington et al., 1991, 1995a; Tivey et al., 1995; Table 3.4), partly reflecting the high metal contents of the geothermal fluids as well as the efficiency of metal deposition on the cones. Hardardóttir et al. (2009) have shown that the deep liquid from Reykjanes is enriched in Au (30x), Ag (10x), Pb (5x) and Cu (10x) compared to many black smoker fluids. Despite the loss of metal due to precipitation at depth in the well, caused by depressurization and boiling during ascent, the scales on the cones still reflect relatively high metal concentrations in the fluid at the orifice plate. These high metal:sulfur ratios are similar to some black smoker fluids (e.g., Cleft, Rainbow), which have been suggested to be a result of phase separation at depth, producing deep metal-rich brines (Butterfield and Massoth, 1994; Douville et al., 2002).

The concentrations of Au and Ag in the scales are also two to three orders of magnitude higher than in the most Au- and Ag-rich mid-ocean ridge black smoker chimneys. The concentrations of Au measured in fluids discharged at surface from RN-

9 and other wells are <0.01 ppb, similar to the concentrations reported for black smoker vent fluids (Table 3.1). However, the orders of magnitude higher Au concentrations measured in the deep liquids at Reykjanes led to the suggestion that hydrothermal fluids deep below the seafloor may also have a much higher Au concentration than in fluids discharging from black smoker vents, with much of the gold (and other metals) deposited below the seafloor chimneys (Hardardóttir et al., 2009).

3.3.5 Comparison with sulfide scales from the Salton Sea

The scales in the Reykjanes geothermal wells are remarkably similar to the black siliceous deposits and metal-rich sulfide scales observed in the highly saline geothermal system of the Salton Sea (Skinner et al., 1967; McKibben and Elders, 1985), even though the salinity of the Salton Sea is an order of magnitude greater than that at Reykjanes. As in the new wells at Reykjanes, Cu-rich scales in the Salton Sea wells consist mainly of bornite, digenite, chalcocite, chalcopyrite, stromeyerite, and native silver. A number of textural features in the Salton Sea scales, including the arborescent growths of fine-grained sulfide phases (Skinner et al., 1967), are also very similar to those observed on the cones in the Reykjanes wells. As in the Reykjanes scales, the abundance of native silver in the Salton Sea scales suggests that an appreciable quantity of Ag was originally present in the Cu-Fe-S solid solutions (Skinner, 1966); the migration of exsolved native silver into fractures in the scales is similar to that observed in the Cu-rich scales at Reykjanes. The high contents of Cu and Ag in the Salton Sea scales is understandable, given the very high salinity of the brines (>25 wt.% NaCl) compared to the seawater salinities (3.2 wt.%) in the Reykjanes system. The lower concentrations of Pb and Zn (not detected) in the Salton Sea scales

compared to those of the Reykjanes wells may also reflect the high salinities, with the solubilities of Pb and Zn greatly enhanced; the high solubilities mean that the Salton Sea fluids do not saturate with Zn and only rarely with Pb minerals.

Skinner et al. (1967) estimated a mass accumulation rate for the Salton Sea scales of about 2000-3000 kg per month with a bulk composition of 20 wt.% Cu, 6 wt.% Ag and 0.1 oz/ton Au. We estimate that a similar quantity of sulfides is presently being deposited in the discharging wells at Reykjanes below the well head, based on the observed flow rates and metal concentrations in the deep liquid, most of which are precipitated prior to sampling at the surface (Hardardóttir et al., 2009). The gold concentration in discharged fluid from the Salton Sea wells is about 0.05 ppb, but McKibben et al. (1990) discussed the possibility that the calculated gold concentrations in the deep fluid, based on samples collected at the surface, may be an underestimate if the fluids lost Au due to scaling in the wells below surface. The highest Au contents in the Salton Sea scales (up to 0.1 wt% Au) occur in the thickest scales forming on downhole steel liners at depths of 500 to 600 m, near the point of first boiling in the well (McKibben and Hardie, 1997). Similar enrichment of Au has been observed in the sulfide scales from other saline geothermal systems (e.g., Clark and Williams-Jones, 1990; Gallup, 1998).

3.3.6 Cu-rich stockworks in volcanic-hosted massive sulfide ore deposits

Bornite is a common trace mineral in the Cu-rich stockwork zones of many VHMS deposits, locally with gold and silver (Hannington et al., 1999). Much of this bornite occurs either as an exsolution product of high-temperature Cu-Fe-S solid solutions, in bornite+pyrite assemblages produced by late-stage, oxidized fluids, or as a secondary mineral resulting from near-surface weathering of Cu-rich ores. However,

small amounts of bornite occur locally in siliceous ores and at the top of the Cu-rich zones in the Kuroko deposits of Japan (Eldridge et al., 1983), and bornite-rich ores have been found to be associated with Au enrichment in high-sulfidation VHMS deposits (Sillitoe et al., 1996). Throttling of hydrothermal upflow may occur across a constriction in sulfide-rich vein stockworks, causing periods of sharp pressure decrease and boiling, similar to the throttling produced by the insertion of cones in the orifice plates of wells at Reykjanes which led to the bornite-rich scales; this observation may help to explain the occurrences described above of high-grade bornite-rich stockwork zones beneath some VHMS deposits.

3.4 Summary and Conclusions

Reykjanes wells RN-12, 21 and 24 have a cone valve inserted into the orifice plate, and this throttle is associated with scales that contain abundant bornite-digenite solid solutions (up to 45 vol. percent of the scales), together with sphalerite and galena. The wellhead pressures for these wells ranged from 40 to 22 bar (252 to 220°C) and decreased to 22 bar (220°C) downstream of the orifice plate. These scales contrast with those in other wells with no such cone valve, e.g., RN-9, where sulfide scales consist of alternating layers of sphalerite and chalcopyrite upstream of the orifice plate and layers of sphalerite, chalcopyrite and Fe-rich amorphous silica downstream of the orifice plate (with a pressure of 11 bar, 188°C).

The textures of the Cu-rich sulfide scale in RN-12, 21 and 24 indicate disequilibrium precipitation from supersaturated solutions, as observed in sulfide-rich scales in other geothermal systems (e.g., Skinner et al., 1967). The observed microtextures are a result of co-deposition of sphalerite and galena with Cu-Fe-S solid solutions and subsequent exsolution of bornite and digenite from the high-temperature

assemblage. There is nonstoichiometric behavior among the major sulfides, and unusual compositions of several phases may reflect incomplete unmixing of the original solid solutions. Native silver formed mainly by exsolution from Ag-rich Cu-Fe-S solid solution, and much of this Ag migrated into late contraction fractures. The high Au content of the bulk scales and the lack of Au in the exsolved Ag-rich minerals indicate that Au occurs in solid solution or as submicroscopic inclusions in the Cu-Fe-sulfides.

The high concentrations of metals in the scales from Reykjanes wells appear to reflect a even greater efficiency of metal deposition than in black smoker chimneys, due to quantitative deposition at the cone in response to the sharp drop in pressure and temperature, similar to that noted for the scales at the Broadlands-Ohaaki geothermal system, New Zealand, and elsewhere (Brown, 1986; Simmons and Brown, 2006, 2007). The bornite-rich mineralogy of the Cu-, Au- and Ag-rich scales at Reykjanes may provide an indication of the nature of sub-seafloor mineralization in some submarine hydrothermal systems, where fluids boil before discharging from seafloor vents.

Acknowledgements

This research has been supported by the Sudurnes Regional Heating Corporation (now HS Orka HF) and the Iceland GeoSurvey (to VH), NSERC grants for field work and other expenses (to JWH) and for analytical work on sulfides from Reykjanes wells 12, 21 and 24 (to MH), and a Hugh E. McKinstry Foundation student research award (to VH) from the Society of Economic Geologists. The manuscript has benefited from reviews by R.A. Binns, D. Teagle, B.J. Skinner, and especially S.F. Simmons. The paper is published with the permission of the Sudurnes Regional Heating Corporation and Iceland Geosurvey.

CHAPTER 4

Metals in Deep Liquid of the Reykjanes Geothermal System, Southwest Iceland: Implications for the Composition of Seafloor Black Smoker Fluids

V. Hardardóttir¹, K.L. Brown², Th. Fridriksson³, J.W. Hedenquist¹, M.D. Hannington¹,
and S. Thorhallsson³

¹Earth Sciences, University of Ottawa, Ottawa, K1N 6N5, Ontario, Canada

²GEOKEM, P.O. Box 95-210, Swanson, Waitakere 0653, New Zealand

³Iceland GeoSurvey, Grensásvegur 9, 108 Reykjavík, Iceland

Published in:

Geology, December 2009; v. 37; no. 12; p. 1103–1106

Presented at:

International Association of Volcanology and Chemistry of the Earth's Interior (IAVCEI)

August 18-22, 2008 in Reykjavík

Abstract

Seafloor hydrothermal systems precipitate Cu, Zn and Fe sulfides at and below black smoker vents on the seafloor; as a result, the metal concentrations in the vent fluids are minimum values. We sampled deep, unboiled liquids from the Reykjanes geothermal reservoir, Iceland, and measured the metal concentrations. This active, seawater-dominated system, situated on the Mid-Atlantic Ridge, is the subaerial equivalent to mid-ocean ridge hydrothermal systems. The liquids, collected at 1350-1500 m depth and 284-295 °C, contain 154-2431 μM Fe (9-140 ppm), 207-261 μM Cu (14-17 ppm), 79-393 μM Zn (5-27 ppm), 0.6-1.4 μM Pb (120-290 ppb), with 6-31 nM Au (1-6 ppb) and 250-960 nM Ag (28-107 ppb). Fluids discharged at surface from the same wells have orders of magnitude lower metal concentrations, due to precipitation caused by boiling and vapor loss during depressurization. The concentrations of Cu, Zn and Pb in the high-temperature reservoir liquids at Reykjanes are similar to those in the highest temperature black smoker discharges, whereas Au and Ag concentrations are 1-2 orders of magnitude higher at Reykjanes; lower temperature seafloor fluids have lower metal contents, suggesting sub-seafloor deposition before discharge. The Reykjanes heat flux of 130 MW requires a liquid flux of ~ 100 kg/s; over 104 years, the minimum life of the system, 0.5 Mt each of Cu and Zn may have precipitated at depth.

Introduction

Iceland is the only location along the length of the Mid-Atlantic Ridge where the largely submarine rift is exposed on land. The seawater-dominated Reykjanes geothermal system, at the southwest tip of Iceland, is the expression of hydrothermal activity associated with the ridge where it comes onshore. Its volcanic and tectonic setting is analogous to that of black smoker hydrothermal systems on the seafloor (Fig. 4.1; Hannington et al., 2005), although oceanic crust here is about three times thicker (Bjarnason, 2008).

We sampled the deep reservoir liquid from Reykjanes, prior to its ascent and depressurization, the first samples of this kind from a seawater-dominated hydrothermal system. The samples were collected with a specially designed titanium sampler at

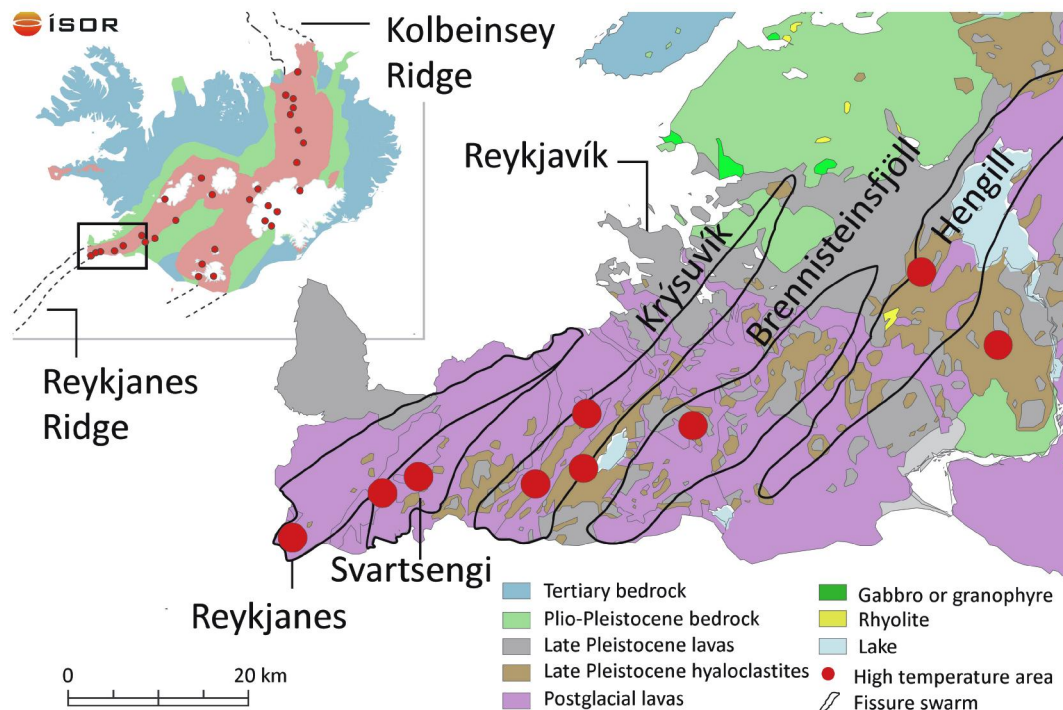


Figure 4.1. Location of the Reykjanes geothermal area on the Reykjanes peninsula, Iceland (modified after Jakobsson et al., 1978, and Saemundsson and Jóhannesson, 2004). Inset shows the location of the Reykjanes Ridge where it comes on-shore Iceland, and the many geothermal systems associated with spreading-center volcanism; Reykjanes is the only seawater-dominated example.

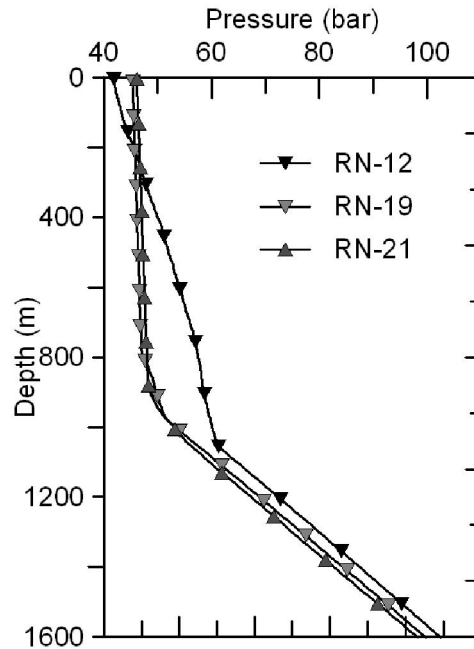


Figure 4.2. Depth versus pressure profiles for wells RN-12, 19 and 21 during the deep liquid sampling of May, 2007.

temperatures between 284° and 295 °C from three wells between 1350–1500 m depth, below the depth of boiling, as indicated by pressure measurements (Fig. 4.2). The metal concentrations are much higher than those in hot fluids sampled at the surface, which have boiled and precipitated metals during ascent.

4.1 Geologic Background and Hydrothermal System

The volcanic zone of the Reykjanes peninsula is the surface manifestation of the obliquely spreading Mid-Atlantic Ridge system (Jakobsson et al., 1978). The Reykjanes geothermal system is located on the onshore extension of the Reykjanes Ridge, surrounded on three sides by the Atlantic Ocean (Fig. 4.1). Surface manifestations of geothermal activity occur over an area of $\sim 1 \text{ km}^2$, but 27 drill holes and resistivity surveys indicate that the subsurface area of the active system is at least 2 km^2 (Björnsson et al., 1972a). Based on drill hole cuttings, the upper 1000 m are dominated by hyaloclastite, volcanic breccias and

tuffaceous units. At greater depths, half the section consists of variably altered basalt flows and intrusions, with the remainder consisting of tuffaceous and sedimentary rocks; basaltic dike intrusions become more common with increasing depth (Tómasson and Kristmannsdóttir, 1972).

Reservoir fluid temperatures are between 275 °C and 315 °C at depths between 1000 and 2500 m. The liquids have reservoir chloride concentrations of 530 mM (18790 ppm), after correcting for concentration due to vapor loss from the liquid phase during standard sampling at surface; this corresponds closely to seawater salinity (Björnsson et al., 1972b; Arnórsson, 1978b). Hydrothermal vent fluids discharged from seafloor black smokers along spreading centers have similar major element concentrations to Reykjanes (Table 4.1; Kristmannsdóttir, 1984; see also Table A4.1).

4.2 Results and Discussion

The deep liquids sampled downhole (methods in Appendix 4) contain orders of magnitude higher concentrations of base metals than fluids sampled at the surface from the same well (Table 4.1, Fig. 4.3A). Iron, Cu and Zn concentrations in the downhole samples range mainly between 200 and 400 μMolal (μM , 15–25 ppm), whereas the Pb concentrations are close to 1 μM (570–1400 ppb). Trace elements that have similar concentrations in both downhole and surface samples include Ba, Sr, B, and Br, all <1 mM; Mg and Al are somewhat higher in the deep liquid, whereas other trace elements are considerably higher. Concentrations of the major elements Na, K, Ca, and SiO_2 in the downhole samples are very similar to concentrations in the surface-collected samples, as are the calculated Cl values (Table 4.1); dissolved H_2S in the reservoir liquid, determined from surface sampling, is ~0.9 mM (RN-19).

Table 4.1. Composition of downhole liquids and surface fluid from Reykjanes, black smoker fluid of 21°N, and seawater

	RN-12 DH	RN-19 DH	RN-21 DH	RN-19 SF	21°N*	Seawater†
Sample depth (m)	1500	1500	1350	Surface	2600	0
T (°C)	296	285	284	275	350-273	2
pH	N.D.	N.D.	N.D.	5.9	3.4-3.8	7.4-8.5
Cl (mM)	524 [§]	511 [§]	528 [§]	532	489	550
Na (mM)	393	389	397	412	432	468
K (mM)	38	38	41	36	23	10
Ca (mM)	47	42	44	40	16	10
SiO ₂ (mM)	10	11	11	10	18	0.07
Mg (mM)	0.39	0.08	0.17	0.02	0 [#]	53.06
Al (µM)	101	15	50	3	5.2	0.04
Ba (µM)	71	76	75	65	>8	0.14
Sr (µM)	100	105	104	98	81	92
B (µM)	709	715	684	712	505	416
Li (µM)	891	901	930	N.D.	891	26
Br (µM)	780	867	740	851	802	838
I (µM)	8	3	3	N.D.	N.D.	0.5
Fe (µM)	430	154	2431	0.8	1664	0.001
Cu (µM)	261	208	207	0.01	35	0.01
Zn (µM)	393	79	189	0.3	106	0.01
Mn (µM)	52	36	49	24	960	0.001
Ni (µM)	4	2	9	<0.01	N.D.	8.0 x 10 ⁻⁶
As (µM)	1.5	1.5	2.0	1.1	0.2	0.005
Pb (µM)	1.3	0.6	1.4	<0.002	0.3	1.0 x 10 ⁻⁵
Cd (µM)	1.2	0.5	1.6	<0.001	0.2	8.9 x 10 ⁻⁴
Cr (nM)	452	212	2611	3	N.D.	6
Ag (nM)	321	250	960	N.D.	3	1.85 x 10 ⁻⁵
V (nM)	243	96	396	N.D.	N.D.	49
Sb (nM)	203	151	375	N.D.	N.D.	1.97 x 10 ⁻³
Mo (nM)	155	128	336	89	N.D.	104
Te (nM)	145	231	474	N.D.	N.D.	0.001
Se (nM)	127	22	53	N.D.	72	3
Tl (nM)	54	54	59	N.D.	N.D.	4.89 x 10 ⁻⁵
W (nM)	34	33	110	N.D.	N.D.	0.54
Au (nM)	31	6	7	N.D.	0.2-1	2.03 x 10 ⁻⁵
Sn (nM)	10	10	57	N.D.	N.D.	0.005
Hg (nM)	3	2	2	<0.01	N.D.	4.98 x 10 ⁻⁶

Note: The surface sample (SF) was corrected for vapor loss to reservoir temperature (Henley et al., 1984). This sample represents the average reservoir fluid composition collected at surface. Be (<1 µM), Bi (<0.05 µM) and Co (<0.2 µM) are below detection in downhole samples (DH); mM–mmol/kg; µM–µmol/kg; nM–nmol/kg. < = below concentration listed, N.D. = not determined. * Von Damm et al., 1985; Von Damm, 1990. †Lide, 1998. §Calculated from Na, K, Ca. #Assumed by authors to be 0 for calculation.

Fluids collected at the surface have boiled over at least the final ~1000 m of their ascent, as indicated by the change in slope of the measured pressure (Fig. 4.2), from a liquid-only profile to liquid plus vapor. As a result of the boiling, metals have precipitated due to saturation of various sulfides, such that these metal concentrations at surface are close to the detection limits of the analytical methods used (Table 4.1).

The one-to-several orders of magnitude higher concentrations of many metals in the downhole liquids indicate that they are almost quantitatively precipitated from the liquid during ascent and boiling prior to reaching the surface. A similar situation was found in geothermal systems of the Taupo Volcanic Zone, New Zealand, where the salinities are an order-of-magnitude more dilute (Simmons and Brown, 2007); boiling and saturation cause deposition of sulfide scales in these wells, which are highly enriched in Au and Ag. The principal metals that form sulfide scales in the wells at Reykjanes are Zn, Cu, Pb and Fe. These scales, collected from surface pipes, typically comprise sphalerite, chalcopyrite, galena, and amorphous Fe-silicate and silica, with traces of bornite, pyrrhotite and pyrite (Hardardóttir, 2004a; Hardardóttir et al., 2007). Gold, Ag, As, and Cd are present at high concentrations in the scales, with Au and Ag concentrations up to 590 ppb and 2.3 wt. %, respectively, in scales from wells RN-12 and RN-21 (Hardardóttir et al., 2007).

4.2.1 Comparison with seafloor black smoker fluids

The concentrations of metals in mid-ocean ridge black smoker fluids have a large range, depending on temperature, pH, chlorinity, tectonic setting, and other factors (reviewed by Hannington et al., 2005). The highest metal concentrations reported are from vent fields at Brandon on the East Pacific Rise (Von Damm et al., 2003), in the Kairei and Edmond vent fields on the Central Indian Ridge (Gallant and Von Damm, 2006), and at 5°S on the Mid-Atlantic Ridge (Koschinsky et al., 2008), the latter from critical fluids discharged at 407°C.

Copper concentrations range from 100 to 400 μM ; Zn ranges from 40 to 160 μM , whereas Pb is typically <1 μM (Fig. 4.3A; Table A4.1). These concentrations and those in the high-temperature reservoir liquid at Reykjanes are similar, although the latter are near the high end of these ranges, except for Fe and Mn⁽¹⁾, which tends to be higher in seafloor fluids. The rather low Fe (up to 2 mM) in Reykjanes reservoir liquid, as well as low H₂S concentrations (0.9 mM), may indicate pyrite deposition prior to ascent to sample depths. The lower Fe and H₂S in the Reykjanes reservoir liquid, compared to the 4 to 10+ mM Fe and up to 11 mM H₂S in high-temperature seafloor discharges (Table A4.1), is consistent with a somewhat greater degree of water-rock interaction at Reykjanes, at slightly higher pH and oxidation state (Seyfried and Ding, 1995), than many high-temperature seafloor systems.

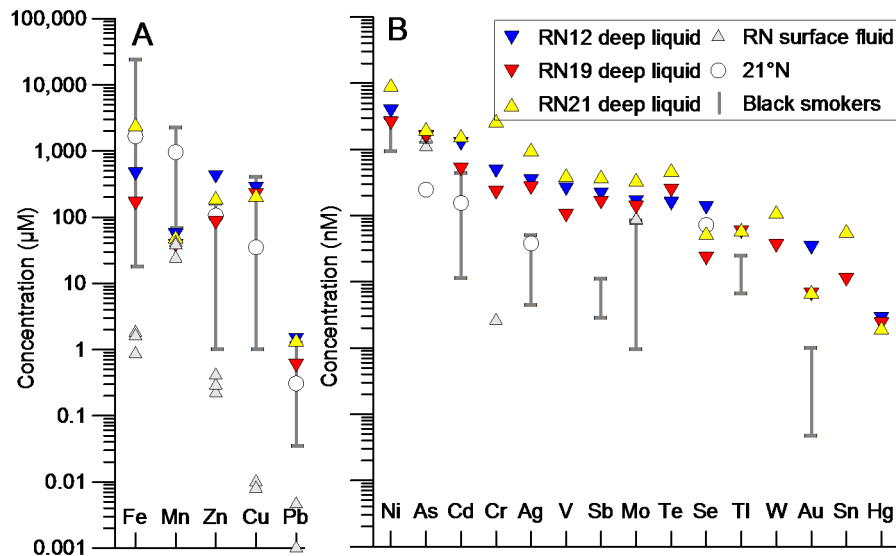


Figure 4.3. Trace-element concentrations in three downhole liquid samples from Reykjanes, and one sample collected from surface, the latter corrected for vapor loss. Also shown are the results for the average black smoker fluid from 21°N (Table 4.1), plus ranges for other seafloor black smoker discharges worldwide, including the high-temperature vents discussed in the text (Table A4.1). A: Concentrations of Cu, Mn, Fe, Zn, and Pb (μM units). B: Concentrations of Ni, As, Cd, Cr, Ag, V, Sb, Mo, Te, Se, Tl, W, Au, Sn, Hg and Co from Reykjanes samples and, where available, from seafloor black smoker discharges (nM units).

High concentrations of metals in vent fluids have been attributed to enriched source rocks (e.g., ultramafic rocks at Rainbow; Douville et al., 2002) or phase separation and discharge of metal-enriched brines (e.g., North Cleft segment of the Juan de Fuca Ridge; Trefry et al. 1994; Butterfield and Massoth, 1994). Alternatively, such high metal concentrations may be due to sources other than host-rock leaching, i.e., intermittent exsolution of metal-rich magmatic fluids from intrusions at depth (de Ronde, 1995; Simmons and Brown, 2006, 2007).

The concentrations of other trace elements, most notably Au and Ag, are 1-2 orders of magnitude higher in the Reykjanes deep liquid than reported in black smoker fluids (Fig. 4.3B, Table A4.1); Cd and Sb are also an order of magnitude higher at Reykjanes. There are few trace-element data for seafloor fluids for species not already mentioned, particularly As, Cr, Hg, Sn, Te, and W (Fig. 4.3B, Table A4.1). Therefore, the Reykjanes data (Table 4.1) help to provide a base line for a wide range of trace-element contents in basalt-hosted seawater-dominated hydrothermal fluids at mid-ocean ridges.

Some vent fluids may be depleted in metals compared to the deep liquids at Reykjanes because of deposition due to boiling, mixing and/or conductive cooling prior to sampling at the seafloor. Boiling, in particular, may be more common in mid-ocean ridge hydrothermal systems than has been previously recognized (Foustoukos and Seyfried, 2007); this is supported by the wide range of Cl content in vent fluids compared to seawater (Table A4.1), which indicates that phase separation is common. Mixing is a less likely explanation because many samples with low Mg concentrations – indicating that there is no direct, unaltered input of Mg-rich seawater – still have low metal concentrations compared to Reykjanes deep liquids. Conductive cooling also is an unlikely factor in the vigorous discharges of high-temperature fluids that are at or close to boiling conditions. The low

metal contents in some mid-ocean ridge hydrothermal systems (Fig. 4.3) imply a significant loss of metal below the seafloor, if the deep liquids have metal concentrations similar to those at Reykjanes.

4.2.2 Metal flux from Reykjanes and seafloor systems

The natural heat flow from the Reykjanes system is at least 130 MW (Fridriksson et al., 2006), which corresponds to an upflow rate of ~100 kg/s of 300°C liquid (less flux for a higher enthalpy liquid). Based on the average metal concentrations in the deep liquid determined here, the annual metal flux is ~47 tons Cu and Zn each, ~740 kg Pb, ~180 kg Ag, and ~9 kg Au. Evidence from the chronology of recent eruptions in the area, which cover altered volcanic units, indicates that the geothermal system has been active at least since the last glacial maximum, 18,000–20,000 yr ago (K. Saemundsson, Iceland GeoSurvey, pers. commun., 2008). If the mass flux and metal concentrations in the deep liquid have been constant over this time, in 104 years the flux of metals would be ~0.5 Mt of Cu and Zn each, 7000 t Pb, 1800 t Ag, and 100 t Au. The majority of this metal would have precipitated in the upper ~1000 m of the system, due to boiling and gas loss prior to natural discharge (similar to what now occurs as scale in wells and pipelines).

For comparison with seafloor systems, the heat flux of the hydrothermal system at 21°N is 220 MW (Converse et al. 1984), TAG is 225 MW (Rona et al., 1993), and the main vent field at Endeavor is 360 ± 70 MW (Ginster et al., 1994); diffuse flow on the margins increase these values. Thus, the heat flow due to high-temperature black smoker venting is ~2-3 times larger than at Reykjanes. Based on inflow temperatures of >350 °C, the liquid flux is also slightly greater in these seafloor systems. Many seafloor systems have been active, albeit episodically, for 20,000–100,000 yr (Hannington et al., 2005). Accepting our argument for similar metal concentrations in deep liquids of many mid-ocean ridge seafloor

systems as we measured in the Reykjanes reservoir, which is supported by the high values in critical fluids at 5°S, as well as at high-temperature Brandon, Kairei and Edmond vent fields, at least 1 Mt of Cu and Zn each may precipitate below the seafloor over the life of typical mid-ocean hydrothermal systems with lower temperature, boiled discharges, with abundant precious metals as well. The effect of transients over the life of all these systems remains to be assessed.

Acknowledgements

We dedicate this paper to the memory of Karen Von Damm, a leader in the geochemical study of seafloor hydrothermal systems. We thank Hitaveita Sudurnesja hf. for funding this sampling, and the Iceland GeoSurvey for their logistic support. This research was also funded by a Natural Sciences and Engineering Research of Canada (NSERC) grant to JWH. The authors thank S.F. Simmons, C.E.J. de Ronde and two Geology reviewers for useful comments. VH also thanks G. Gíslason for discussion, and he and B. Jónsdóttir for assistance with the figures.

⁽¹⁾ “and Mn”, note added in proof

CHAPTER 5

Composition of the Deep Liquid of the Reykjanes Geothermal System, Southwest Iceland: Geochemical Modeling of Fluid-Mineral Interaction

5.1. Introduction

The Reykjanes geothermal system is unique among twenty known high-temperature areas in Iceland, as the geothermal liquid is seawater in origin. The discharged liquid collected at the surface can be corrected for vapor loss to determine the composition of the reservoir liquid; liquids were also collected downhole before boiling and vapor loss, at 1350 and 1500 m depth (Hardardóttir et al., 2009). The first process that affects the composition of the heated seawater is reaction with the basalt reservoir rock; as a result the reservoir liquid is depleted in SO_4^{-2} and Mg^{+2} , whereas the SiO_2 , K^+ and Ca^{+2} concentrations are higher than seawater (Björnsson et al., 1970, 1972a, b; Arnórsson 1978b). As summarized in Figure 5.1 and discussed in Chapter 4, the geothermal liquid is highly enriched in trace

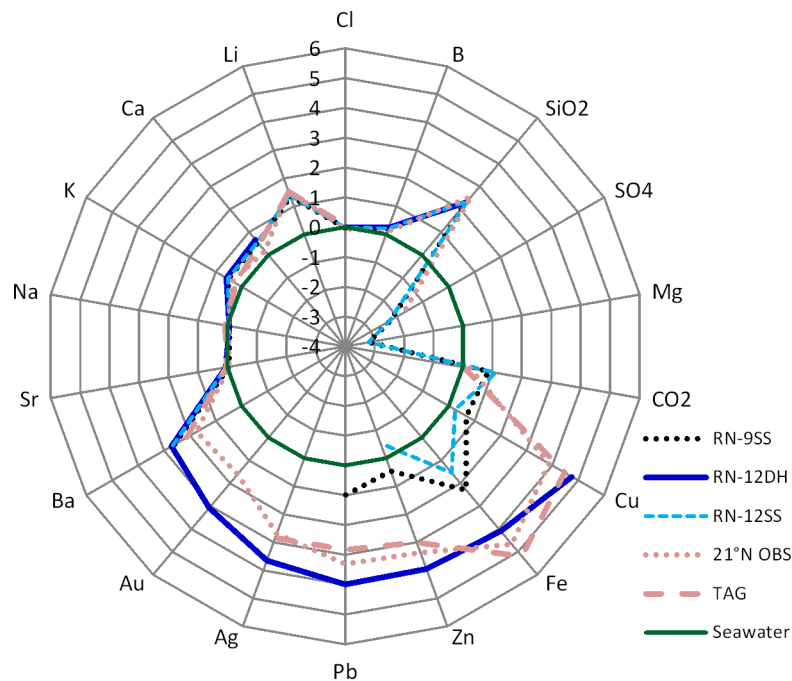


Figure 5.1. A spider diagram with all data normalized to seawater (logarithmic y-axis) for few available species from the Reykjanes discharged fluid and the downhole samples (DH). Zero indicates data with same composition as seawater (green circle); +1 or -1 are data an order of magnitude higher or lower, respectively, than the concentration of seawater. The discharged liquid (RN-9SS and 12SS), sampled at the wellhead, lost the majority of the metals and other trace elements, whereas the major elements are conservative and do not precipitate as the fluid ascends. For comparison, the composition of fluids discharged from TAG (Mid-Atlantic Ridge) and the 21°N OBS (East Pacific Rise) seafloor vents are shown.

metals compared to the surface samples of liquid after vapor separation. Many black smokers on the seafloor, e.g., at 21°N EPR and TAG on the Mid-Atlantic ridge, have metal concentrations lower than those of Reykjanes reservoir liquid (Hardardóttir et al., 2009).

The second major process that alters the composition of the reservoir liquid at Reykjanes is boiling during ascent toward the surface; this causes depletion of the metals, whereas conservative elements like chloride are concentrated due to vapor loss. Boiling is a common process in geothermal systems, whether below the seafloor (Massoth et al., 1989; Butterfield et al., 1990; Foustoukos and Seyfried, 2007) or on land. Subaerial examples, where boiling in the natural system and its effects have been documented, include Broadlands-Ohaaki, New Zealand (Giggenbach and Stewart, 1982; Hedenquist, 1990; Simmons and Christenson, 1994; Simmons and Browne, 2000), Fushime, Japan (Akaku, 1990; Akaku et al., 1991), and Ladolam, Papua New Guinea (Simmons and Brown, 2006); boiling in geothermal wells and pipelines and its effects have been documented at Ngatamariki (Browne et al., 1989), Rotokawa (Reyes et al., 2002), and Broadlands-Ohaaki, New Zealand (Brown and Simmons, 2003; Simmons and Brown, 2007), Cerro Prieto, Mexico (Mercado et al., 1989; Clark and Williams-Jones, 1990; Thomas et al., 1992), and in the Reykjanes wells (Hardardóttir et al., 2009, 2010).

The geothermal liquid of the Reykjanes reservoir is the main topic of this chapter, including the relationship between the discharge fluids corrected for vapor loss and the downhole liquid samples collected at 1350 and 1500 m depth (Chapter 4), and the effect of boiling and mineral reaction on the fluid composition. The data for metal concentration in the deep liquid is based on downhole sampling in wells RN-12, 19, and 21 (Chapter 4). The deep liquid major element composition and pH are recalculated from fluid discharged from wells and sampled at the surface; these are the fluids that precipitated scales on the fluid

flow control valve in wells RN-12, 21, and 24 (Chapter 3), and in well RN-9 and surface pipes (Chapter 2). Well RN-9 was utilized for twenty years, until scaling caused it to be abandoned, whereas the other wells have been in use for only several years.

5.2. Geothermal Fluids at Reykjanes

5.2.1 Calculation of reservoir liquid from the discharged fluid

The reservoir composition of the geothermal liquid has been monitored during the years of operation of the power plant. As liquid rises to the surface, the pressure decreases, resulting in boiling that produces a two-phase fluid of liquid and vapor (Henley et al., 1984; Figure 5.2). A typical high-temperature fluid sample is collected by a Webre-separator, in which the liquid and corresponding vapor are collected separately (Appendix 2.2). The

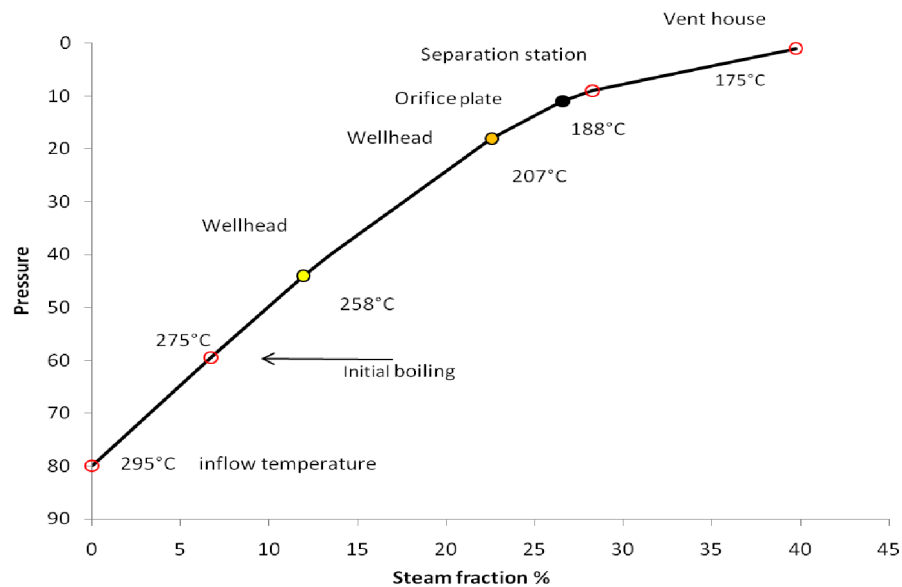


Figure 5.2. Calculated steam fraction versus pressure for RN-9 liquid with the initial inflow temperature 295°C. Boiling starts at 800-900 m depth at 275°C (Fig. A2.2) and the steam fraction increases from 0% to 6.7%. At wellhead the pressure range is between 44 bar (258°C) and 18 bar (207°C) with steam fraction between ~11.9% (44 bar) and 22.6% (18 bar). At the orifice plate the pressure decreases sharply to 11 bar (188°C), increasing the steam fraction to 26.6%, up to 28.3% at the separation station. The filled circles represent 44, 18 and 11 bar (the same as in Figure 2.24). Amorphous silica saturation is reached at ~11 bar (180°C).

vapor fraction depends on the total enthalpy of the discharge and the pressure at the separator. Where a single phase (liquid only, no vapor) enters the well from the reservoir, the total enthalpy is equal to the enthalpy of the liquid at the inflow temperature.

Wells usually have several feed zones at different depths and temperatures. Therefore, a reference temperature (T_r) for each well has to be decided which is used for the calculations of the composition of the reservoir liquid. The reference temperature is a composite temperature of the various feed zone temperatures and is commonly lower than the highest measured temperature in the well (Fridriksson and Giround, 2008). An example that demonstrates how the reservoir liquid composition is calculated from the surface sample information, including the correction for vapor loss, is shown in Appendix 5.1.

After the reservoir liquid is calculated from the discharge fluid by recombining the analyzed liquid and vapor phases, the pH at the reservoir temperature (i.e., reference temperature, T_r) can be calculated with the program WATCH (Arnórsson et al., 1982; version wdens23, Bjarnason, Iceland GeoSurvey, pers. commun., 2007); a similar calculation procedure is shown by Henley et al. (1984).

The major and trace elements in the calculated reservoir liquid (RN-9, 12, 19, 21, 24) and measured in the downhole samples (RN-12, 19, 21) are listed in Table 5.1. These data illustrate the difference in trace element concentrations between the calculated reservoir composition based on sampled surface fluid and the downhole samples. The composition of seawater in a sample collected from the shoreline near Reykjanes (Bjarnason, 1995; ISOR data base) and standard seawater composition (Bearman, 1989) are also listed for comparison.

Table 5.1. Major and trace element concentrations of the reservoir liquid from wells RN-9, 12, 19, 21, and 24, plus downhole liquid samples from wells RN-12, 19, and 21; seawater near Reykjanes, and standard seawater compositions also listed, plus the reconstructed liquid (calculated from CHILLER) for well RN-19

	RN-9	RN-24	RN-12	RN-19	RN-21	RN12	RN19	RN21	Seawater	Seawater	RN19	RN-19
Sample I.D.	20030169	20070113	20070161	20070114	20070112	20070092	20070089	20070086	standard	20060386	CHILLER ⁴	
	Discharge	Discharge	Discharge	Discharge	Discharge	Downhole	Downhole	Downhole	Stóra-	fluid raw	Discharge	Discharge
	fluid	fluid	fluid	fluid	fluid	1500 m	1500 m	1350 m	Sandvík at	data**	sample	sample
Sampling p (bar)	13.2	33.5	30.5	28	32.5	95.93	93.50	80.30	the beach	25		
T°C during sampling	194	234	231	226	232	296	285	284		225		
Enthalpy (calculated)	1290	1263	1317	1211	1263							
Steam fraction	0.24	0.13	0.17	0.12	0.13	None	None	None	None			
Reference	290	285	295	275	285							
pH/°C	5.01	4.79	4.84	4.80	4.89	--	--	--	8.15/23	275	5.9/22	5.74 /20
Cl ppm	17948	19586	18968	19608	19971	19283	18806	19410	18800	19500	22460	22080
Br ppm	64	71	67	71	70	65	72	61	62	67	74	
Na ppm	9105	9673	9590	9812	9831	9378	9299	9493	10560	10770	11285	10200
K ppm	1311	1469	1378	1459	1537	1542	1529	1675	380	380	1630	1530
Ca ppm	1449	1682	1615	1649	1656	1940	17459	1843	337	412	1884	1670
SiO ₂ ppm	603	582	685	635	619	618	7049	671	0.7	2.0	665	599
Al ppm	0.61	0.14	0.10	0.10	0.17	2.8	0.4	1.4	0.001	0.0004	0.05	0.06
Mg ppm	0.82	0.58	0.78	0.61	0.76	9.9	2.0	4.3	1230	1290	1	0.63
Sr ppm	7.1	8.8	8.9	8.9	8.9	9.1	9.6	9.5	na	8.0	10.3	8.9
Ba ppm	7.6	9.2	8.4	9.3	9.5	10.1	10.8	10.8	na	0.02	9.31	9.8
B ppm	7.6	7.8	7.9	8	8.1	8.0	8.0	7.7	4.2	4.4	9.3	
Li ppm	4.0 ⁽³⁾	4.0 ⁽³⁾	4.4 ⁽³⁾	na	na	6.4	6.5	6.8	na	0.2	na	
Mn ppm	1.7	1.7	2.3	1.3	2.2	3.0	2.0	2.8	0.001	0.0001	1.38	1.45
Cu ppm	0.00	0.00	<0.001	0.00	0.00	17.2	13.7	14	na	0.0001	0.0009	0.002
Fe ppm	0.39	0.06	0.10	0.05	0.09	24.9	8.9	141	0.002	0.00001	0.49	0.044
Zn ppm	0.01	0.02	0.01	0.02	0.03	26.7	5.4	13	0.002	0.0	0.009	0.005

Table 5.1 (continued)

Sample I.D.	RN-9	RN-24	RN-12	RN-19	RN-21	RN12	RN19	RN21	Seawater standard	RN19	RN-19
	20030169	20070113	20070161	20070114	20070112	20070092	20070089	20070086	20060386	20060386	CHILLER ⁴
	Discharge fluid	Discharge fluid	Discharge fluid	Discharge fluid	Discharge fluid	Downhole 1500 m	Downhole 1500 m	Downhole 1350 m	Seawater standard	Discharge fluid raw data**	Discharge sample
						Stóra-Sandvík at the beach					
I ppb	188 ⁽³⁾	na	na	na	na	1118	369	460	60	na	na
Pb ppb	0.29	0.32	0.87	up to 1	up to 6	290	118	293	0.002	0.001	0.0003
Ni ppb	0.0005 ⁽³⁾	1	0.6	3	2.9	221	146	554	0.5	0.001	0.008
As ppb	106	95	32	84	114	113	117	154	3.7	0.08	0.07
Cd ppb	0.09	<0.05	<0.05	<0.05	up to 0.1	136	56	181	0.1	na	na
Cr ppb	0.2	0.1	1.3	0.1	<0.0001	24	11	141	0.3	na	na
Sb ppb	0.003 ⁽³⁾	na	na	na	na	26	19	47	0.2	na	na
Ag ppb	0.03	na	na	na	na	36	28	107	0.002	na	na
Te ppb	na	na	na	na	na	19	31	63	1x10-5	na	na
Mo ppb	0.02	10	9	9	10	15	13	34	10.0	0.0	0.02 ⁽⁶⁾
V ppb	na	na	na	na	na	13	5	21	2.5	na	na
Tl ppb	na	na	na	na	na	12	11	13	0.01	na	na
Se ppb	na	na	na	na	na	10	2	4	0.2	na	na
W ppb	na	na	na	na	na	6	6	21	0.0001	na	na
Au ppb	na	na	na	na	na	6	1	1	0.004	na	na
Sn ppb	na	na	na	na	na	1	1	7	6x10-4	na	na
Hg ppb	<2E-06	<2E-06	<2E-06	<2E-06	<2E-06	0.6	0.5	0.4	0.0	0.0	0.0
² S ppm	-	-	-	-	-	40	27	38	na	na	na
SO ₄ ppm	16	17	16	20	16	--	--	--	na	26.9	21.1
CO ₂ ppm	1067	1060	1649	1092	722	--	--	--	na	29.5	35
H ₂ S ppm	27	23	48	33	25	--	--	--	na	2.94	3.7
H ₂ ppm	0	0.2	0.2	0.4	0.2	--	--	--	na	na	na
CH ₄ ppm	0	0.06	0.16	0.06	0.04	--	--	--	na	na	na
N ₂ ppm	0	10	16	11	11	na	na	na	na	na	na

Note: Discharged fluid corrected for vapor loss (Henley, 1984; Appendix 5.1); DH, downhole sample. ¹Fridriksson and Giround 2008; ²total sulfur; ⁽³⁾not analysed in this sample; ⁽⁴⁾Mixed sampled from discharged fluid (raw analytical data) and downhole sample (mg/L) F: 0.21, solution density = 1.023 Kg/L; ⁽⁵⁾calculated from Na, K, Ca and Mg; ⁽⁶⁾As MO4; - analysed as H₂S and SO₄; -- not analysed due to aqua regia, see text; < below detection limits; Bi, Be, Co all below 10 µg/L in deep liquid; ** raw data F=0.2 ppm; gases (ppm): CO₂, 6570; H₂S, 214; H₃BO₃, 20; NH₃; na not analysed.

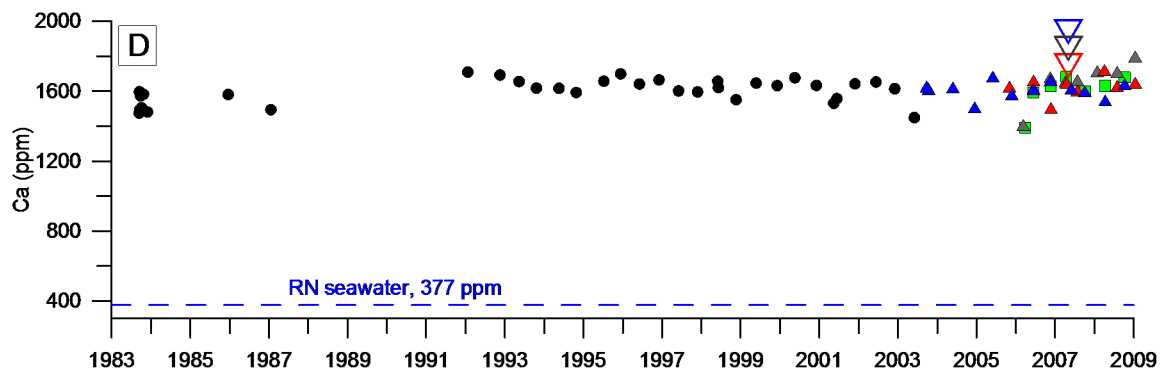
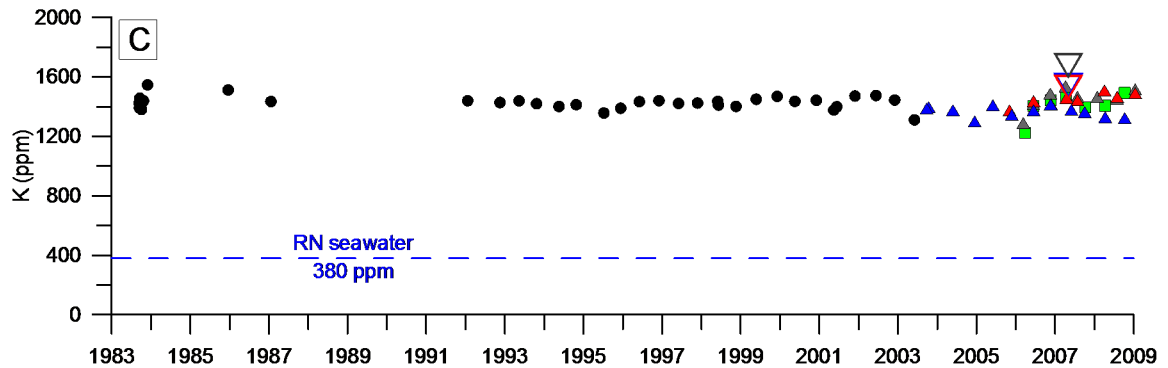
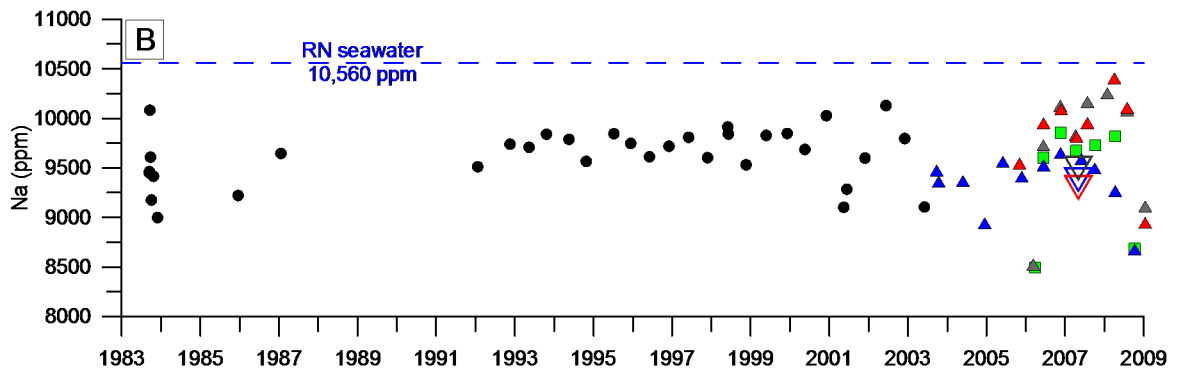
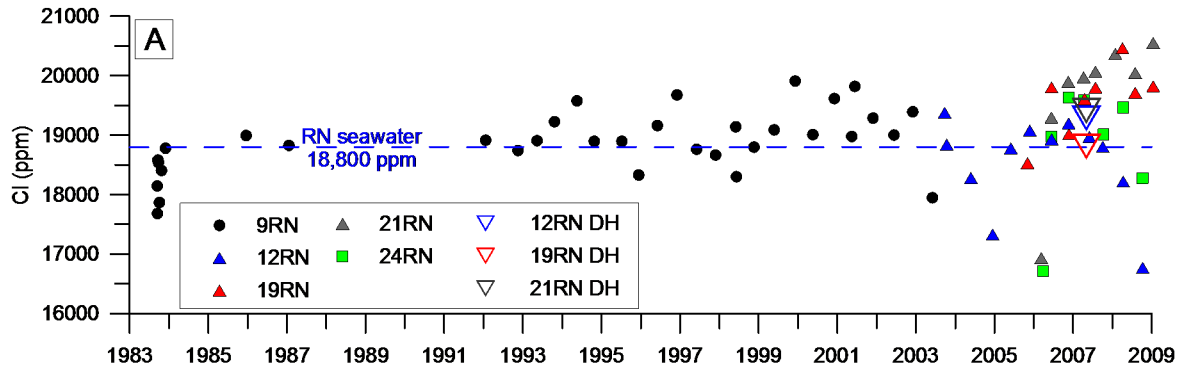
5.2.2 Chemical characteristics of the Reykjanes reservoir liquid determined from surface fluid

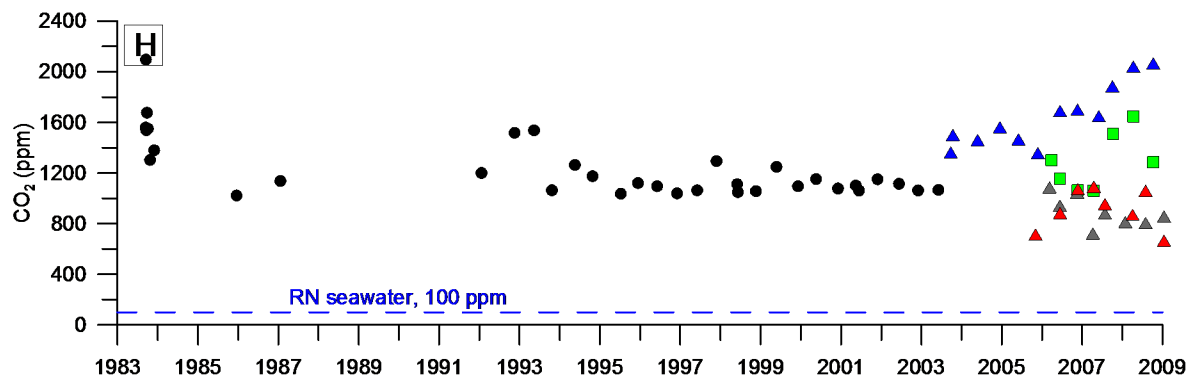
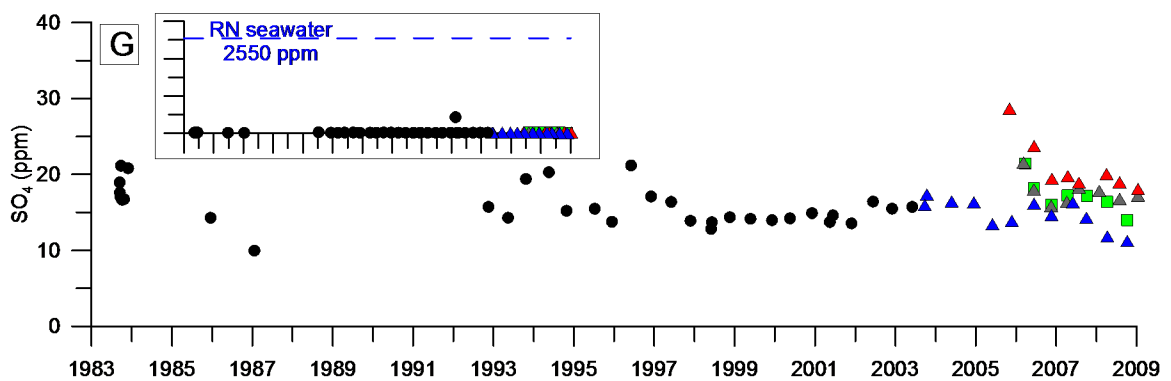
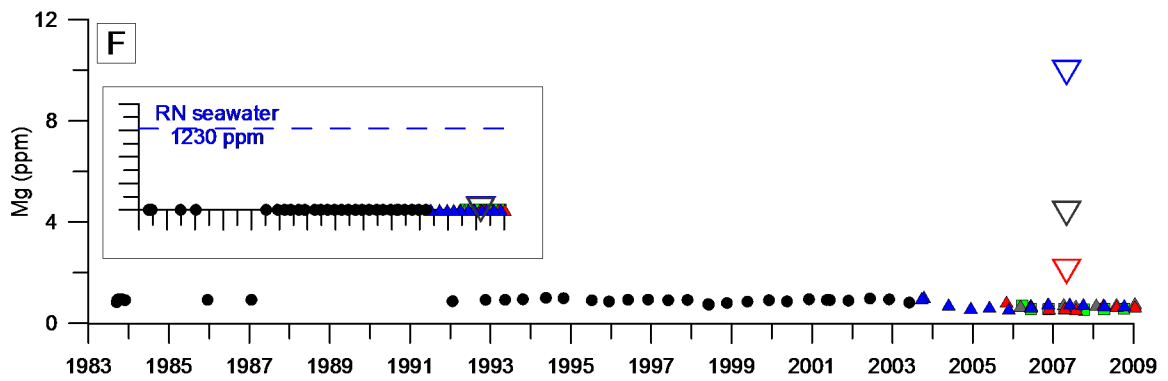
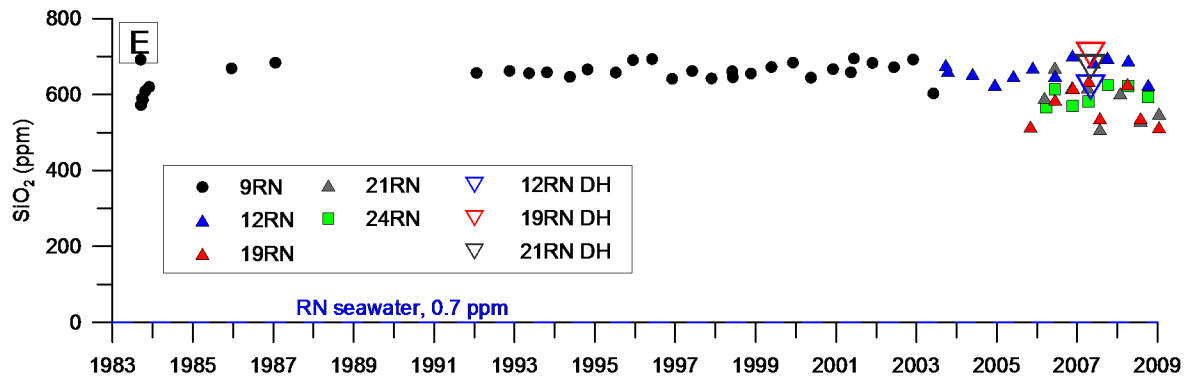
Major and minor elements and dissolved gases

In the Reykjanes area there are three types of fluids: cold seawater that penetrates porous lava, cold meteoric water that occurs as a shallow low-density lens, and the deep high-temperature geothermal liquid (Kristmannsdóttir, 1986). The fresh water lens thickens from nearly zero in the Reykjanes thermal area to ~30 m near the Svartsengi geothermal system, 15 km to the east (Sigurdsson, 1986). Figures 5.3A-L summarize the concentration of major elements, including gases, in the geothermal wells (discharge liquid) versus time, from 1983 to the present, corrected for vapor loss during surface sampling. Figures 5.4 – 5.6 show the concentrations of Na, Ca, and K versus Cl of the calculated reservoir liquid.

The chloride concentration in the calculated reservoir liquid at Reykjanes is close to that of local seawater (18,800 mg/kg), but seawater-rock reaction at temperatures up to at least 348°C has modified the concentration of many other chemical components. The chloride concentrations in the reservoir feeding wells RN-9, 12, 19, 21, and 24, together with that of seawater, are shown on Figure 5.3A. The chloride concentration ranges between 16,700 and 20,550 ppm, with the majority of the samples ranging between 18,000 and 19,000 ppm (Table 5.1). Over time the Cl concentrations in well RN-9 varies slightly from the seawater value, whereas the Cl concentrations in the newer wells have a larger range, commonly above the seawater value, due to boiling in the reservoir and vapor loss.

The concentration of sodium is generally 10% lower in the calculated reservoir liquid than in seawater (Figs. 5.3 and 5.4), whereas calcium and potassium concentrations are up to 13% and 17% higher, respectively (Figs. 5.5 and 5.6; Table 5.1). The sodium concentration is consistent between these wells, ranging between 8,500 and 10,400 ppm,





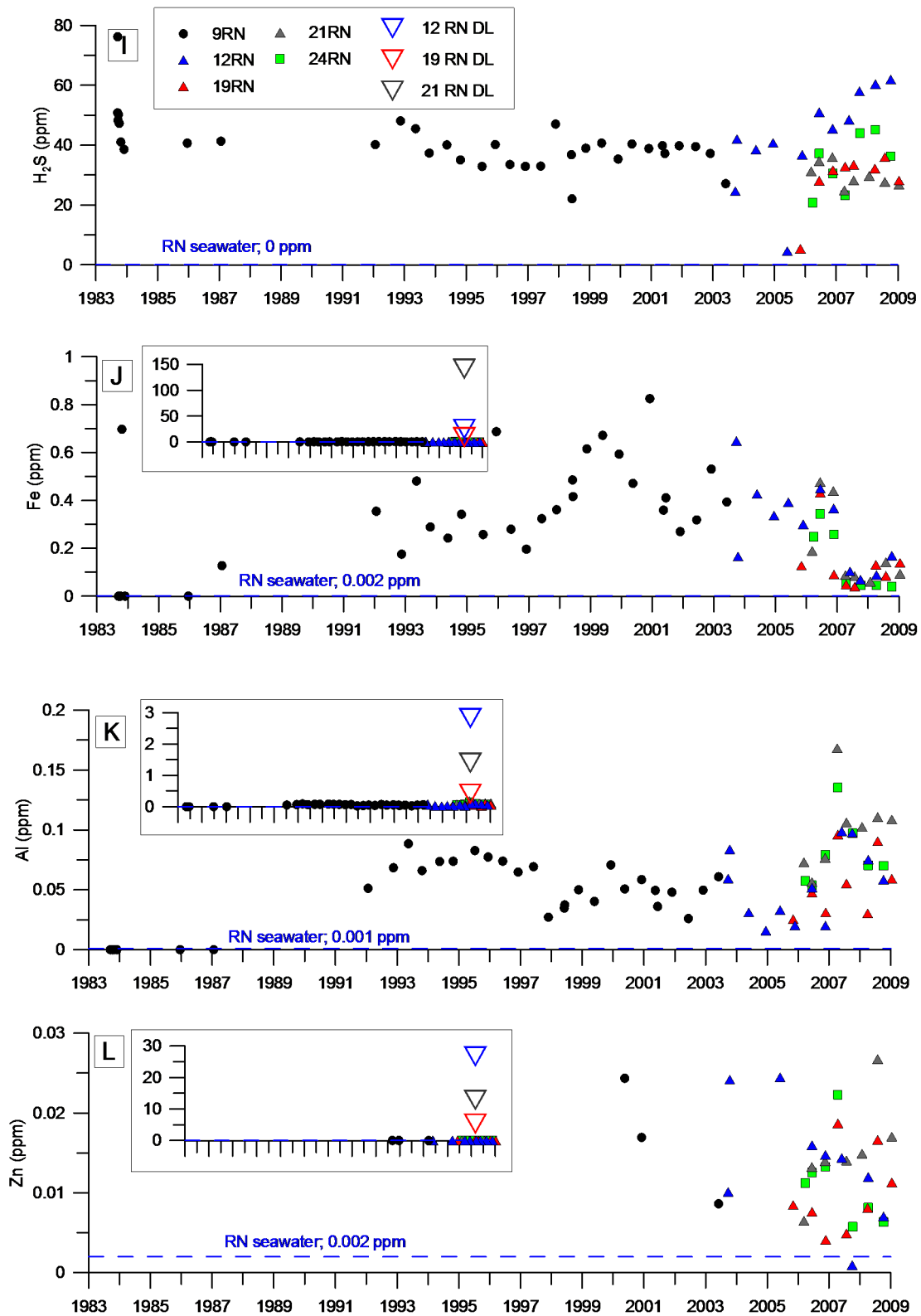


Figure 5.3. Concentrations of elements in the Reykjanes reservoir from 1983 to 2009, calculated from discharges from wells RN-9, 12, 19, 21 and 24. A to L; chloride, sodium, potassium, calcium, silica, magnesium, sulfate, CO_2 , H_2S , Fe, Al and Zn versus time. For comparison, seawater composition is shown by the dashed line.

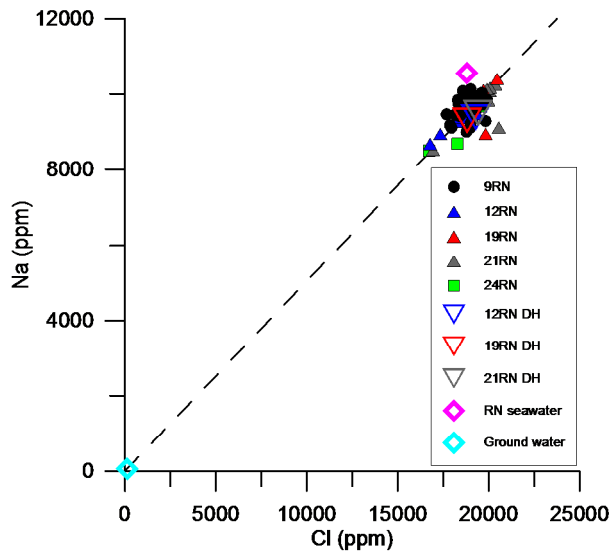


Figure 5.4. Concentrations of Na versus Cl in the geothermal liquids (corrected for vapor loss on boiling) from Reykjanes compared with the surrounding seawater and the ground-water

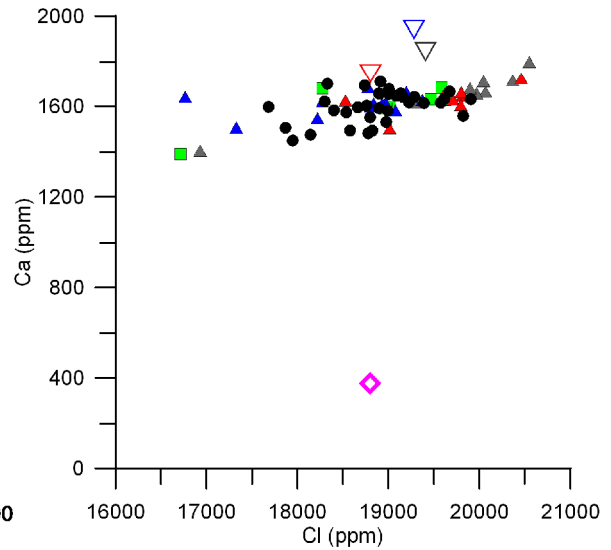


Figure 5.5. Concentrations of Ca versus Cl in the geothermal liquids (corrected for vapor loss on boiling) from Reykjanes compared to local seawater. Legend same as in Fig. 5.4.

with an average composition of 9600 ppm, which is the same as that measured in the downhole samples.

Concentrations of sodium vary slightly with time, with a larger range in the recent years between wells (Fig. 5.3B). Calcium and potassium concentrations in the reservoir liquid

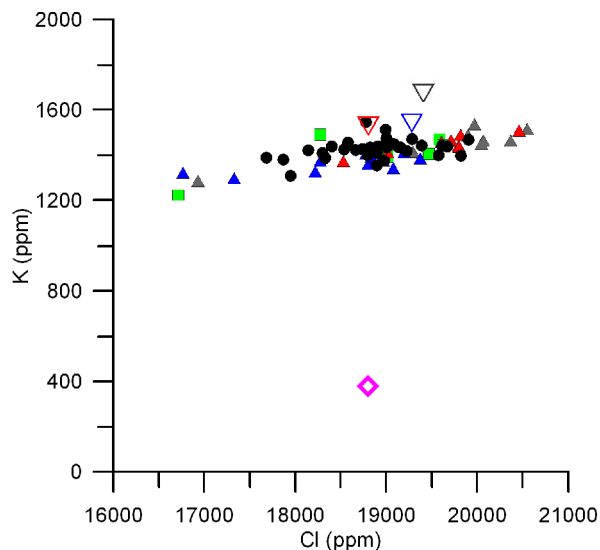


Figure 5.6. Concentrations of K versus Cl in the geothermal liquids (corrected for vapor loss on boiling) from Reykjanes compared with the surrounding seawater. Legend same as in Fig. 5.4

range between 1225 and 1550 ppm and 1390 and 1800 ppm, respectively (Figs. 5.3C, D). In the downhole samples calcium and potassium concentrations are up to 1675 and 1940 ppm, respectively. The concentrations of these two elements have changed little over nearly thirty years of utilization.

The concentration of silica in the reservoir liquid is much higher than in the surrounding seawater, commonly in the range of 600 to 700 ppm, and varies with reservoir temperature (Fridriksson and Giround, 2008), correlating with the solubility of quartz. Well RN-12 has the highest reference temperature for the wells under consideration (295°C) and also has the highest silica concentration (Fig. 5.3E). The silica concentration was largely constant through the ~30 years of utilization of well RN-9, but the silica concentration is notably lower in several newer wells (lower reservoir temperature, in part due to boiling and vapor loss; e.g., RN-19, 21, 24), except for well 12.

The magnesium and sulfate concentrations (~0.7 and 17 ppm) in the reservoir liquid are only a small fraction of their concentrations in seawater (1290 and 2550 ppm, respectively; Fig. 5.3F, G). Magnesium concentration ranges between 0.9 and 0.5 ppm in the calculated reservoir liquid, based on surface samples (the concentration has decreased over time), whereas the magnesium concentrations in the downhole samples are up to an order of magnitude higher (between 2 to 10 ppm).

Aluminium concentrations are from two to four orders higher in the reservoir liquid than in seawater (Fig. 5.3). The concentration in the calculated reservoir liquid is between 0.1 and <1 ppm, whereas the downhole samples have concentrations between 0.4 and 2.8 ppm.

The slightly higher concentration of Ca, K, Mg and Al of the downhole liquids compared to discharge liquid, by up to an order of magnitude for Mg and Al, could indicate contamination during sampling by fine clay particles that were not filtered.

In the reservoir liquid, bromine and strontium concentrations are 60 to 72 ppm and 7 to 9.5 ppm, respectively, similar that of the surrounding seawater (62 and 8 ppm). The concentration of these elements has been constant throughout the utilisation of the wells. The ratio of Br/Cl is generally accepted as one of the most conservative chemical parameters during water/rock interaction (Ellis and Mahon, 1977; Foustoukos and Seyfried, 2007). The ratio ranges between 0.0014 and 0.0017 (molal basis) in the downhole samples and is consistently 0.0015 in the discharged fluid and 0.0015 in seawater.

Lithium was measured only in a few surface samples; the concentration is 4 ppm in RN-9 samples and ~6 ppm in wells RN-2 and RN-8 (Ólafsson and Riley, 1978; ISOR database), similar to concentrations in the downhole samples (6.4 to 6.7 ppm). These values are an order of magnitude higher than in seawater.

Manganese concentrations (1 to 3 ppm) are three orders of magnitude higher than in seawater; the concentrations are slightly higher in the downhole versus surface samples.

The concentration of dissolved gases in the calculated reservoir liquid (Table 5.1; wells RN-8 and 9) are ~0.1 wt.% (Bjarnason 2002), consisting of 96.5% carbon dioxide, 2.5% hydrogen sulfide (Fig. 5.3) and the remaining 1% nitrogen, argon, methane, and hydrogen. The concentration of dissolved gas in the discharge from well RN-9 was low through the years; gas concentrations in fluid discharged from other wells has not changed with time despite considerable increase in utilization (Fridriksson and Giround, 2008; Fridriksson et al., 2010; Fig. 5.3). The dissolved gas was not measured in the downhole samples due to the design of the sample holder (Chapter 4).

Metals and other trace elements

The concentrations of Fe, Cu, Zn, Pb, Ni and Cd in the calculated reservoir liquids, based on samples collected at the surface, are one to four orders of magnitude lower than in the downhole samples (Table 5.1 and Chapter 4) (Hardardóttir et al., 2009). The iron concentrations in the downhole samples are 9 to 140 Fe ppm, compared to 0.2 to 0.6 ppm in the calculated reservoir liquid based on surface samples (Fig. 5.3). Zinc concentrations are between 5 and 27 ppm in the downhole samples (Fig. 5.3), and copper concentrations are ~15 ppm (Table 5.1), versus <0.03 ppm Zn and ~0.003 ppm Cu in the calculated reservoir liquid.

The Pb, Ni, and Cd concentrations are several hundred ppb in the downhole samples, but are only a few ppb or less in the calculated reservoir liquid. Chromium concentrations in the downhole samples are a few 10s of ppb but only ~1 ppb in the calculated reservoir liquid based on discharge samples. Antimony, Ag, Te, Mo, V, Tl, W, Au, and Sn have concentrations of 10s of ppb to 1 ppb in the downhole samples; these trace elements are commonly not measured in the discharge liquid sampled at the surface. Mercury concentrations in the downhole samples are ~0.5 ppb.

5.3. Introduction to the Computational Approach by CHILLER

5.3.1 Reconstruction of the downhole samples

To understand how and why sulfide minerals precipitate on boiling and to understand what chemical species are involved, the program CHILLER was used. Reed (1982) and Spycher and Reed (1989) created the program CHILLER to evaluate the role of various physical and chemical processes such as pH increase, chemical reduction, dilution or cooling in fluid evolution and mineral precipitation. For modeling reservoir liquids, the

calculations start with the program GEOCAL, which recombines the vapor and liquid samples collected downstream from the wellhead and produces an input file for the program SOLVEQ (which speciates the liquid); the results from this program are then incorporated into CHILLER. A short description of the programs follows.

The fluid data can be input as component species in various units (mg/kg, mg/l, etc.): Cl^- , SO_4^{-2} , CO_2 , HS^- , SiO_2 , Al^{+3} , Ca^{+2} , Mg^{+2} , Fe^{+2} , K^+ , Na^+ , Mn^{+2} , Zn^{+2} , Cu^+ , Pb^{+2} , Ag^+ , Au^+ , Hg^{+2} , Sr^{+2} , Ba^{+2} , F^- , Sb^{+3} , As^{+3} , Ni^{+2} , HPO_4^{-2} , Co^{+2} , MoO_4^{-2} , and NH_4^+ . The pH and temperature in ($^\circ\text{C}$) are also specified in the program. The output file converts all aqueous concentrations to molality.

SOLVEQ calculates the aqueous speciation and the mineral assemblage in equilibrium with the liquid at the measured temperature. The programs SOLVEQ and GEOCAL combined are analogous to WATCH (Arnórsson et al., 1982; Bjarnason, 1994), the most commonly used programme in ISOR. WATCH computes a distribution of species (homogeneous equilibrium) in the restored reservoir liquid from surface liquid and vapor analyses.

CHILLER uses the initial aqueous speciation derived from SOLVEQ to begin calculations of equilibrium or partial equilibrium in gas-mineral-aqueous systems, as well as the effects of boiling during fluid ascent, including cooling, wall rock alteration, and scale formation (Reed and Spycher, 1984; Reed, 1998; Palandri and Reed, 2001).

The downhole samples (RN-12, 19, and 21; Chapter 4) were acidified with HCl on collection, precluding analysis of the gases and other components, including Cl^- , F^- , SO_4^{-2} , CO_2 , HS^- , HPO_4^{-2} , and NH_4^+ . The chloride concentration of the downhole sample was

calculated from charge balance at a pH of the reservoir liquid, based on restoration of the vapor and liquid phases sampled at the surface, using the program GEOCAL.

RN-19 was chosen as the representative liquid of the downhole samples, as its composition was intermediate between the other two, and the concentrations of the Al and Mg were the lowest, 0.4 and 2 ppm versus highs of 3 and 10 ppm, respectively; the high values may be due to contamination by clays (Table 5.1). Accurate values for Al and Mg are important; if the Al concentration is too high by an order of magnitude, the Al-bearing minerals are undersaturated which conflicts with SOLVEQ (Pang and Reed, 1998). Magnesium concentrations are likely close to zero, similar to compositions in modern seafloor hydrothermal systems (Seyfried and Mottl, 1982; Berndt et al., 1988). The speciation of the liquid is shown in Appendix 5.2.

5.3.2 Mineral equilibria

To evaluate which minerals were in equilibrium with the geothermal liquid in the reservoir, SOLVEQ was used to calculate the value of $\log(Q/K)$ for selected minerals, where K is the equilibrium constant and Q is the ion activity product. A plot of $\log(Q/K)$ vs temperature identifies the probable minerals with which the fluid equilibrated, and the temperature of equilibrium. The potential for equilibrium is indicated where the calculated $\log(Q/K)$ is 0. Figure 5.7 shows $\log(Q/K)$ values as a function of temperature for the restored reservoir liquid, based on surface samples of discharge liquid and vapor from well RN-19 (Table 5.1). The saturation states of the major alteration minerals identified in thin section were calculated: i.e., actinolite, quartz, wollastonite, epidote, and pyrite, which are present at depths of 1200 to 2200 m in RN-19, as well as in the other wells (Chapter 1). Chalcopyrite, prehnite, albite, anhydrite and sphalerite also occur locally (Fig. 1.5).

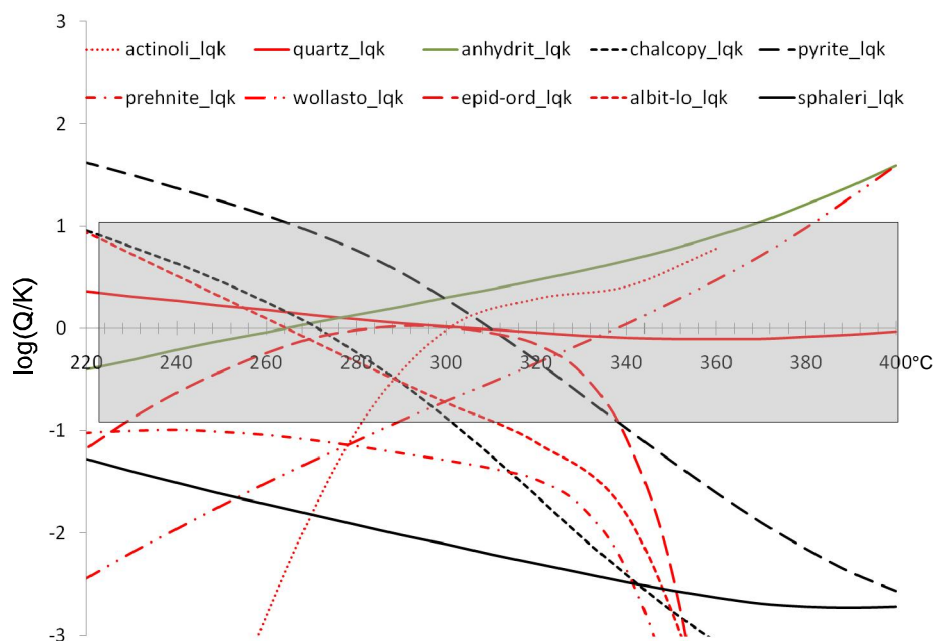


Figure 5.7. Log (Q/K) for mineals vs. temperature for liquid from well RN-19 (20060363, Table 1) calculated at reference temperature 275°C. Convergence of equilibrated minerals to log (Q/K)= 0 occurs in the range from 265° to 330°C with most of the minerals being saturated at temperature around 300° to 315°C. Shaded area indicates close to saturation.

Many of the minerals observed in deep Reykjanes drillholes (Tómasson and Kristmannsdóttir, 1972; Arnórsson et al., 1982; Franzson et al., 2002; Mortensen et al., 2006, Marks et al., 2010a), including actinolite, epidote, pyrite, chalcopyrite, and quartz, are predicted to be saturated in the geothermal liquid in the range of 265° to 330°C (Figure 5.7). The highest measured temperature in well RN-19 is 301°C, with reservoir temperature estimated to be 275°C (Fridriksson and Giround, 2008); the highest measured temperature at Reykjanes was measured in well RN-17 (3000 m depth; ISOR data base) at 348°C. These high temperatures are consistent with the results of calculations of mineral equilibria, based on the SOLVEQ results. Other minerals found in the system, such as albite and K-feldspar, are predicted to precipitate at a lower temperature, either because they are undersaturated at ~300°C or because of problems with analytical results or thermodynamic data for the aqueous species. Issues with thermodynamic data could also be true for wollastonite, which is predicted at temperatures close to 340°C but is observed at ~270°C

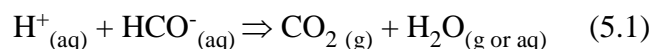
(Chapter 1). Prehnite is present down to 1800 m depth (<300°C). Sphalerite is present sporadically below 2000 m depth in RN-19 (295°C, ISOR data base; Mortensen et al., 2006) and at various depths in well RN-17, where it first appears at 350 m depth (~50°C, ISOR database), together with galena (Mark et al., 2010a), but sphalerite is clearly undersaturated in the calculations shown in Figure 5.7.

The temperature of equilibration for several of the minerals from RN-19 (270 to 310°C) differs slightly from that of RN-8 (280° to 295°C: see Reed and Spycher, 1984).

5.3.3 Result of boiling the reconstructed liquid

The RN-19 liquid that is reconstructed to reservoir conditions for use in CHILLER is a combination of discharge liquid and vapor samples collected at the surface, restored to the reservoir liquid composition, and the concentrations of Mn, Cu, Fe, Zn, Pb, Ag, Au, and Hg from the downhole sample. The measured pH of 5.74 at 20°C from the surface liquid analysis was used. The downhole samples are supersaturated with respect to several sulfides (mainly Cu-sulfides not shown in Figure 5.7) at these metal concentrations, according to SOLVEQ and CHILLER; a pH of 4.5 is required at 275°C to prevent metal sulfide saturation (in contrast to the restored reservoir pH of 5.5 at 275°C).

The change in pH upon calculated boiling of the reconstructed liquid is illustrated in Figure 5.8. The initial pH of the reconstructed liquid changes from 5.5 at 275°C to 6.8 at 100°C, due to continued boiling to 100°C and gas loss. The pH increase upon boiling results mainly from the loss of CO₂ from the liquid:



The computed minerals that saturate as the restored liquid from well RN-19 boils on ascent are shown in Figure 5.9. The y-axis “moles per degree per kg of initial fluid” is the

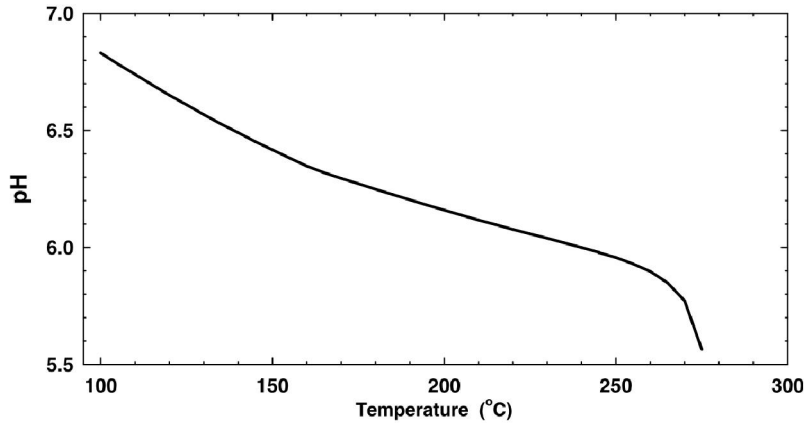


Figure 5.8. pH change during boiling of the reconstructed liquid RN-19 (Table 5.1) with discharge pH 5.7/20°C. Reservoir liquid is calculated to have a pH of 5.5 and continued boiling down to 100°C results in increase of pH to 6.8. See Figure 5.9 and text for further explanations.

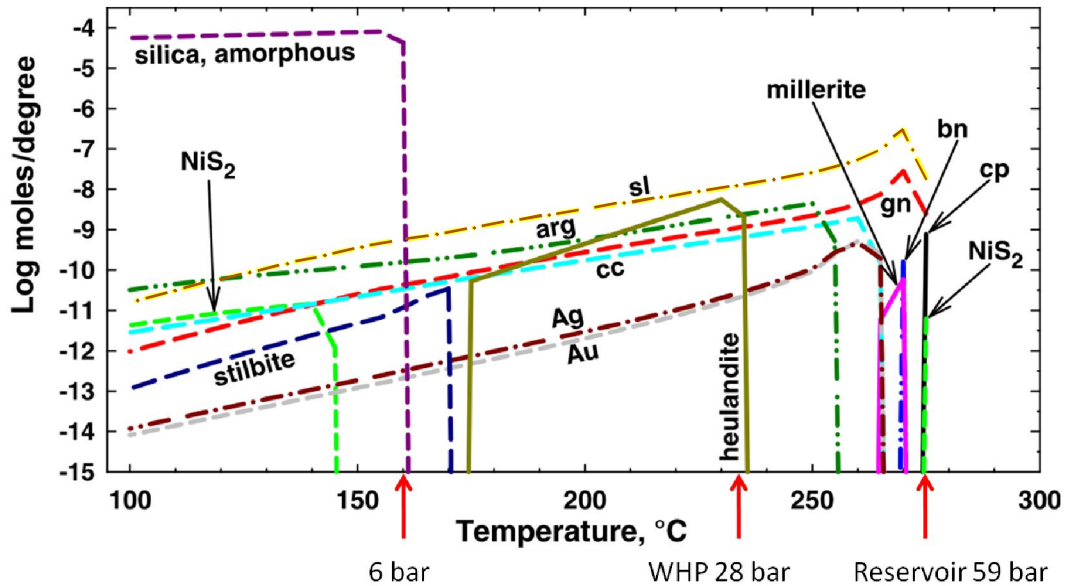


Figure 5.9. Boiling of the reconstructed liquid in the reservoir of RN-19, using the metal concentrations from the downhole sample of RN-19 and discharge liquid (Table 5.1); results from a CHILLER run. The x-axis shows the temperature interval from 300 to 100°C, and the reservoir pressure when precipitation starts, and pressure at wellhead (WHP). Y-axis; Moles per degree is the amount of mineral precipitating with each degree (°C) of temperature decrease per kilogram of initial fluid. The copper sulfides (bornite (Cu_5FeS_4), bn; chalcopyrite (CuFeS_2), cp; nickel sulfides (NiS_2 , and millerite NiS); lead sulfide (galena, PbS), gn; zinc sulfide (sphalerite, ($\text{ZnFe})\text{S}$), sl; all start to precipitate at the same temperature of about 275°C. There is a continuous precipitation of the zinc and lead sulfide up the well followed at slightly lower temperature by gold and silver minerals: Au, Ag, arg (argentite, Ag_2S) and copper sulfide (chalcocite, Cu_2S), cc. Heulandite, a hydrated Ca-Na-Al silicate (zeolite) precipitates from 240-175°C, replaced then by stilbite. Amorphous silica starts to precipitate at 160°C.

amount of mineral that is predicted to precipitate for each degree of temperature decrease (due to boiling) per kilogram of initial liquid. Precipitation proceeds from right to the left with decreasing temperature. Sphalerite (ZnS) and galena (PbS) are predicted to begin to precipitate at 275°C (at pH 4.5) and continue to 100°C (where the program was stopped). Chalcocite (Cu₂S), silver and gold start to precipitate at 265°C and continue to 100°C. Argentite (Ag₂S) starts to precipitate at about 255°C and continues to 100°C. Heulandite [(CaNa)₂-3Al₃(Al,Si)₂Si₁₃O₃₆•12(H₂O)], a zeolite, precipitates over the range of 235°C to 175°C, at which temperature it is replaced by stilbite [(NaCa₄Al₈Si₂₈O₇₂•30(H₂O)], another zeolite. Amorphous silica starts to precipitate at about 160°C and continues downstream to less than 100°C. At high temperature (~275°C), some minerals start to precipitate but are predicted to become undersaturated before the next temperature interval, such as chalcopyrite (CuFeS₂), nickel-disulfide (NiS₂), bornite (Cu₅FeS₄), and millerite (NiS). NiS₂ is predicted to again saturate at much lower temperature (145°C).

CHILLER predicts that the major minerals to precipitate due to boiling are sphalerite followed by galena, whereas chalcopyrite and bornite are minor minerals that precipitate over a very narrow temperature interval. These calculations are consistent with the observed mineralogy in the downhole scales from well RN-22 (there are no downhole samples from RN-19). Sphalerite is the major mineral observed, with minor chalcopyrite followed by bornite at 350 m depth (~265°C); galena occurs at the wellhead and at the fluid-flow control valve. Galena is predicted to saturate at 275°C but it is most abundant at the wellhead in RN-9 (~252°C) and at the fluid flow control valve in medium-pressure wells (RN-12, 21, and 24 at 236-247°C, Table 2.4). Galena is also common where the measured temperature is ~220°C. Bornite, galena and chalcocite are observed in trace to moderate quantities in the surface pipeline from well RN-9, downstream of the orifice plate. A

number of the minor minerals that CHILLER predicts to saturate due to boiling (e.g., NiS₂, millerite, and argentite) have not been observed in the Reykjanes geothermal system. The bulk analyses show that Ag and Au are present in all scale. Analyses of the scales (Table 2.6-2.8) also show a trace amount of Ni, although a Ni mineral was not observed. The computed saturation of argentite and Ni sulfides may indicate that these minerals are present as submicroscopic inclusions in other minerals.

Sources of error in the CHILLER calculations may include the following: 1) the restoration of the deep liquid and pH may not be accurate, although this is a standard calculation from standard analyses; 2) the downhole metal concentrations are not correct, although the three downhole samples agree closely (Chapter 4), and they also agree with the highest seafloor metal concentrations (Hardardóttir et al., 2009); 3) some thermodynamic data are not correct and/or the computational approach needs further work.

5.4. Discussion

Modelling of the reservoir liquid as it rises and boils, together with results of analyses of the downhole samples illustrate the origin of the discharge fluid sampled at the surface and confirm the much higher metal concentrations at depth. Many typical black smoker fluids (21°N), as sampled on the ocean floor, may also have lower metals concentrations than in the corresponding reservoir liquid (Fig. 5.1), possibly due to sub-seafloor boiling (Chapter 4).

The understanding of high-temperature hydrothermal fluids hosted by seafloor basalts comes from the study of submarine hydrothermal systems (Edmond et al., 1979; Thompson et al., 1988; Hannington et al., 1995a; Tivey, 1995; Von Damm, 1990, 1995; Zierenberg et al., 1998). The fluid composition of black smoker discharges has been discussed in the

framework of seawater-basalt experiments (i.e., Bischoff and Seyfried, 1978; Bischoff and Rosenbauer, 1987) followed by modeling of fluid-mineral equilibria (Tómasson and Kristmannsdóttir, 1972; Kristmannsdóttir, 1984; Janecky and Seyfried, 1984; Bowers et al., 1985; Seyfried and Janecky, 1985; Seyfried et al., 1986; Seyfried, 1987; Campbell et al., 1988; Von Damm, 1988; Bowers et al., 1988). These results are summarized below.

As cold seawater penetrates the seafloor along fractures it begins reaction with the basaltic rocks. The alkalis, including K^+ , Rb^+ , Cs^+ and B^{3+} , are fixed at $<100^\circ\text{C}$ by formation of low-temperature clay minerals (smectites, mixed clay), celadonite, zeolites, and Fe-oxides; at higher temperature chlorite starts to form ($\sim 220^\circ\text{C}$). Incorporation of alkalis by hydrothermal minerals is balanced by leaching of Fe^{2+} and SiO_2 from the basaltic glass. At a temperature of about 150°C , anhydrite starts to precipitate due to its retrograde solubility, fixing much of the Ca^{2+} and most of the SO_4^{2-} from the heated seawater. Magnesium and OH^- from the seawater is taken up as a component of magnesium-hydroxy-sulfate hydrate at about 250°C , which leads to a decrease in pH. In black smokers the pH values at 25°C range over nearly 4 orders of magnitude (pH $\sim 2 - 6$, Hannington et al., 2005). The main source of acidity is the reaction:



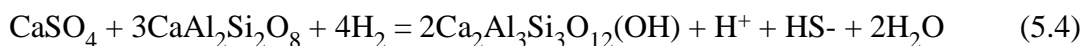
At a temperature of 200°C to 300°C , the alkalis – which were originally added to the basaltic rocks – are leached by the hydrothermal fluid, and balanced by extensive Na metasomatism (albitization), as well as by Ca being added to the rocks (epidotization). The hydrothermal seawater reacts continuously with the basalt, releasing iron, other metals and sulfur to the hydrothermal fluid, for example by the reaction:



Pyrrhotite

Pyrite

At $>350^\circ\text{C}$, deposition of Ca^{2+} to form secondary plagioclase and epidote releases additional H^+ ; the fluid achieves its lowest pH, as shown by the reaction below:



Anhydrite Plagioclase

Epidote

The fluid composition indicate that the liquids are in equilibrium with minerals of the greenschist facies (chlorite, actinolite, albite, epidote, quartz), and the reactions cited above explain most of the data shown in Figures 5.3 to 5.6. Near the critical point of seawater, 407°C and 298 bar, the density of the liquid is very low, resulting in the buoyant fluid rapidly ascending to the seafloor. Some of these fluids may arrive at the seafloor without boiling because of the pressure of the overlying water column.

Species distribution calculations for the Reykjanes reservoir liquid predict that at 300°C a variety of minerals are close to saturation (Figure 5.7). However, some sulfides are predicted to be undersaturated, including sphalerite until a temperature of $<200^\circ\text{C}$. On a stability diagram of $\log f\text{O}_2$ versus $\log [(a^2\text{Cu}^+)/(\text{Fe}^{2+})]$, the downhole liquids (RN-12, 19, and 21) plot in the bornite field at 300°C . By contrast, reservoir liquid RN-9 (the discharged liquid collected at the surface corrected for vapor loss, but without downhole metal concentrations) plots in the pyrite field (Figure 5.10). The same figure also shows the stability fields of these sulfide minerals at 350°C and 250°C . The observation of bornite precipitating on the fluid-flow control valve from the boiled reservoir liquid (Chapter 3 and 4) is consistent with the composition of the reservoir liquid. By contrast, the liquid of RN-9 is not expected to form abundant Cu-sulfides due to the low metal content used. The high

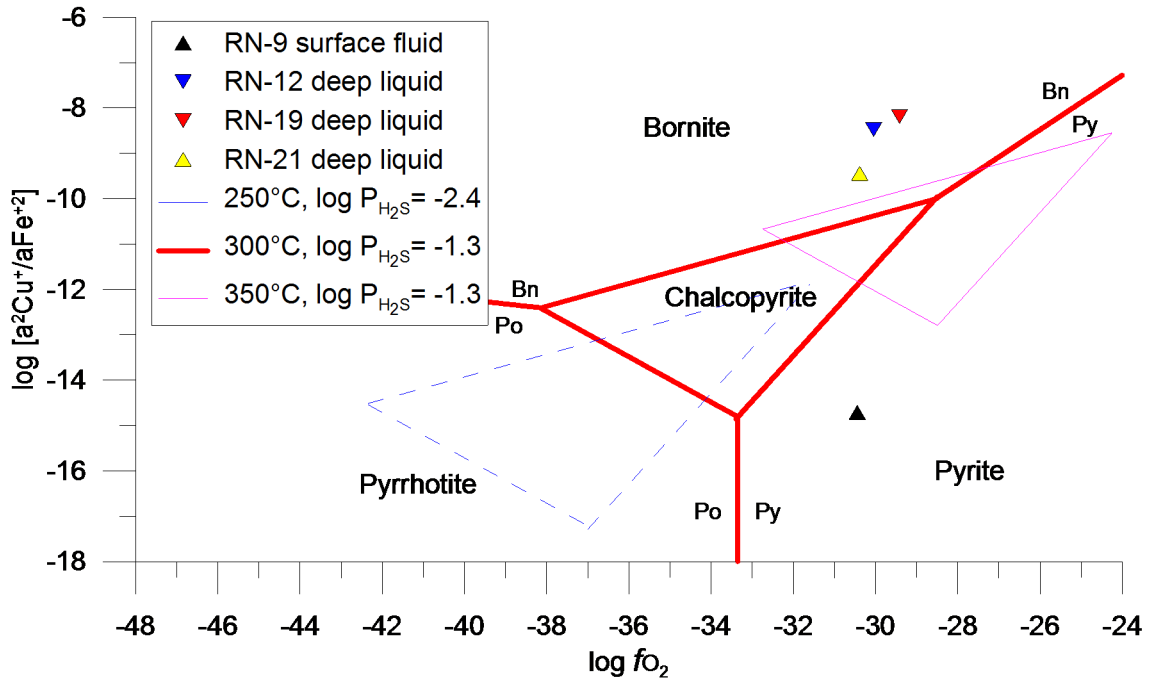


Figure 5.10. Stability diagram of sulfide minerals in terms of $\log f\text{O}_2$ versus $\log (a^2\text{Cu}^+/a\text{Fe}^{+2})$ determined from SUPCRT92. Downhole liquids with metal concentrations from downhole samples are in equilibrium with bornite, consistent with this sulfide in scales (Chapter 3). Boiled liquid (RN-9), as sampled at the surface with low metal contents (and restored to reservoir conditions, except for the metals) plots in the pyrite field. The high Cu/Fe ratio of the deep fluids in RN-12 and RN-19 explains the abundant bornite in the scales of these wells.

Cu/Fe ratio of the reservoir liquid in RN-12 also contrasts with that of typical black smokers (Table 4.1) and may reflect a slightly different redox buffer in the deep reaction zone (e.g. Seyfried et al., 1999). In contrast to Reykjanes observations and predictions, bornite is rarely observed in most seafloor hydrothermal systems. Tivey et al. (1995) predicted seafloor fluid to be chalcopyrite stable.

5.5. Summary

The Reykjanes reservoir liquid shows little variation in concentration of the major elements during production from 1983 to 2009. The reservoir liquid sampled downhole has slightly higher K, Ca, Al and Mg concentrations than the restored discharge liquid,

suggesting the possibility of some contamination of the downhole samples by clay minerals. The alteration minerals that are predicted by the computer program SOLVEQ to be in equilibrium with the reservoir liquid, over a range of 310° to 270°C, include actinolite, epidote, pyrite, chalcopyrite, and quartz, which agree with the observed alteration minerals and mineral buffers in seafloor hydrothermal systems. The downhole liquid appears to be saturated with chalcopyrite and bornite, according to SOLVEQ and CHILLER calculations; these minerals may have precipitated in the well (RN-19), but they are observed only as trace minerals in RN-22 (downhole). The abundance of bornite in some wells at the surface, on the fluid flow control valve (Chapter 3) likely reflects the high Cu/Fe ratios of the fluids which may in turn reflect different redox buffers at depth (e.g., hem-mt-py-cpy versus po-py-mt-cpy)

CHAPTER 6

Summary and Comparison with Other Geothermal systems

6.1 Summary

The Reykjanes high-temperature geothermal system is situated at the toe of the Reykjanes Peninsula where the submarine Mid-Atlantic Ridge comes onshore. The surface thermal manifestations are $\sim 1.5 \text{ km}^2$ in area, whereas the size of the geothermal system at $\sim 1 \text{ km}$ depth is up to 10 km^2 (Karlsdóttir, 2005). From 1956 to 2010, 29 wells have been drilled in the area, with 14 wells presently under production. Electrical production increased from a few MWe in 2005 to 100 MWe in May, 2006, when the Reykjanes Power Plant was commissioned. This sudden increase in mass withdrawal caused a pressure decrease in the production zone by $\sim 35 \text{ bar}$, leading to an increase in boiling which extended to a depth of 1200 – 1300 m (Jónsson 2008; Fridriksson et al., 2010), compared to a boiling depth of 900-1000 m depth in well RN-9 during the 1980s and 1990s. This pressure decline has caused a steam cap in the upper part of the production zone. The average mass withdrawal in 2006 was 455 kg/s, then 736 kg/s in 2007, 614 kg/s in 2008 and 590 kg/s in 2009. The lower mass intake in the last two years was due to the increase in enthalpy of discharge (i.e., caused by the change from liquid to liquid plus vapor feed to the well from the reservoir), from 1330 kJ/kg in 2007 to 1420 kJ/kg in 2008 and 1440 kJ/kg in 2009 (Vatanskil, 2010; Jónsson et al., 2010).

The Reykjanes geothermal field is surrounded by the ocean on three sides at a distance of only 1.5 km. The reservoir liquid is of seawater salinity (Björnsson et al., 1972a, b; Arnórsson, 1978b), with reservoir temperature between 275° and 315°C . Comparison of the reservoir liquid (discharge liquid after vapor separation corrected for the vapor loss) and the sampled downhole liquid to seawater composition shows that the reservoir liquid and the downhole liquids are higher in SiO_2 , K^+ and Ca^{+2} , where as Mg^{+2} and SO_4^{-2} are close to zero. The metals measured in the downhole liquids (Cu, Fe, Zn, Pb, Ag and Au) are

between 5 and 3 orders of magnitude higher than the surrounding seawater as summarized in Fig. 5.1. Utilization of geothermal fluid from two wells (mainly RN-8 and RN-9) until 2005 and 14 additional wells from 2006 has not resulted in a noticeable increase or decrease in the major element concentrations of the reservoir liquid (Bjarnason, 2002; Fridriksson and Giround, 2008; Fridriksson et al., 2010).

Pressure and temperature measurements define where the liquid starts to boil as it ascends up the well. Such boiling causes the precipitation of sulfides at high pressure (>22 bar) and amorphous SiO_2 at lower pressure (<17 bar). In early 2007, downhole liquid samples were collected from 1350 to 1500 m depth in wells RN-12, RN-19, and RN-21, below the level of boiling in each well. Comparison of the downhole liquid analyses and those of the discharge liquid sampled at the surface indicates that the downhole liquids contain orders of magnitude higher concentrations of most metals than the discharge liquid, due to precipitation during boiling. The concentrations of Cu, Zn, and Pb in the downhole liquid are similar to those from the highest-temperature black smoker discharges from the seafloor, whereas Au and Ag are one to two orders of magnitude greater at Reykjanes.

RN-9 was a high-pressure well, indicating relatively little boiling at depth, with wellhead pressure generally about 40 bar; it was the principal producing well for the heating company from 1983 to 2003. The well was clogged twice with scale, in late 1993 and late 2003. In 1993 the well was cleaned of scales to 552 meters depth but the scaling in 2003 led to it being abandoned and filled with concrete in 2005. Chemical analyses on the downhole scales showed that they mainly consisted of Fe-sulfides together with Zn and Cu with traces of SiO_2 and Mg. Confirmation of the composition of scales formed downhole was obtained when scales were drilled out of well RN-22, a high-pressure well, in August, 2009. The scales were collected from 141 m to 664 m depth and formed at pressures of 46

to 52 bar (260° – 267°C); they consisted mainly of sphalerite/wurtzite [(ZnFe)S] with minor chalcopyrite (CuFeS₂) and bornite (Cu₅FeS₄). In the upper part of the well the samples contained maghemite (γ-Fe₂O₃), although some Fe in the samples is apparently contamination from the steel casing. High concentrations of Au (80 ppm) and Ag (40 ppm) were found in scales at the greatest depth, with concentrations increasing up the well to 125 ppm Au and 580 ppm Ag at 150 m depth and ~100 ppm Au and 900 ppm Ag at wellhead.

During a maintenance break in early 2007 it was evident that the newer wells RN-10 to RN-24 had various surface scale characteristics, and that these varied with wellhead pressures (high: ~40 bar; medium: ~33 bar; and low: ~25 bar). In the high-pressure wells a considerable amount of scales were deposited downstream of the orifice plate, whereas the low-pressure wells did not have any scales in the surface pipe. Most of the deposition in the low-pressure wells is argued to occur in the host rock and in the well due to deep boiling. In the medium-pressure wells most scales were deposited at the orifice plate (on the fluid-flow control valve). Scales formed in the medium-pressure wells consist of a complex intergrowth of fine-grained sphalerite, bornite, and digenite (Cu₉S₅), together with variable amounts of fine isometric grains of galena (PbS). The bornite contains a high concentration of Ag (up to 35 wt.%) and native silver occurs in veins cutting scale. A layer of covellite gives the scales on the fluid-flow control valve a distinctive peacock blue colour. This covellite layer is locally associated with bladed calcite. In the high-pressure wells, the scales formed upstream and downstream of the orifice plate, have high Zn concentrations (up to 60 wt.%) with lower Cu and Fe concentrations (up to 20 and 23 wt.%). Gold and Ag concentrations in these scales are the highest measured in Icelandic scales (up to 950 ppm and 2.2 wt.%, respectively). Three main types of textures were observed in the sulfides: i) skeletal sulfides (mainly upstream of the orifice plate), ii) dendritic sulfides (downstream

og the orifice plate), and iii) solid solutions with partial to complete exsolution textures (mainly on the fluid flow control valve). These different textures reflect different degrees of supersaturation and quenching related to different pressure and temperature regimes, flow rates, and laminar versus turbulent flow in the wells and pipelines.

The iron contents of sphalerite range from 1 to 4.7 wt.% Fe (at 300 to 290°C) downhole and increase towards the wellhead where they are ~ 3 wt.% (at 257 to 230°C). The highest observed FeS contents in sphalerite are further downstream in well RN-9, and range from 5 to 8.5 wt.% (at 220°C). The unexpected increase in the FeS content of sphalerite that is observed downstream of the orifice plate is not consistent with boiling and equilibrium degassing, suggesting that some other process must be controlling the change in Fe content with decreasing temperature. Conversely, cadmium contents are highest in downhole sphalerites, at 0.5 to 4.4 wt.%, and decrease significantly towards the surface, where they range from 0.03 to 0.5 wt.%. Selenium concentrations in sphalerite are 0.1 wt.% downhole and decreases down to 0.06 wt.% in the surface pipelines. The antithetic relationship between Fe, Cd and Se, suggests that CdS and CdSe both enter the sphalerite structure by solid solution, substituting for ZnS at high temperature, which may explain the unexpectedly low FeS content of sphalerite down the well.

When well RN-9 was still in operation the pressure downstream of the orifice plate was 11 bar, which lead to considerable accumulation of scale that was cleaned out regularly. In mid 2000 the surface pipeline of RN-9 was cleaned out from the orifice plate to the separation station and from there to the valve house, a total of 500 m. At high pressure (upstream of the orifice plate), scaling was minimal, with a few millimetres thickness of chalcopyrite and sphalerite and a trace of galena and bornite. Downstream of the orifice plate the principal scale was amorphous silica with alternating layers of sphalerite and

chalcopyrite. The scales that deposited in a year nearly clogged the pipeline. The metal-rich scales contained up to 175 ppm Au and 1 wt.% Ag, with the highest concentration upstream and a few centimetres downstream of the orifice plate. Well RN-9 became clogged in 1993 and 2003, and based on metals in the reservoir liquid (estimated from downhole samples from other wells), internal well measurements, sulfide mineralogy and densities, and the assumption that boiling starts at 1000 m depth, ~11 tonnes of sphalerite (~7 tonnes Zn) was precipitated downhole per year from 1983 to 1993. Mass balance calculations indicate that between 4 and 5 tonnes of scales are deposited by the high-pressure wells (RN-10, 11, 14b, 22, and 23) per year at surface, including 1.5 tonnes of Zn, 8 kg of Ag and ~1 kg of Au.

Based on drill cuttings the stratigraphy of well RN-9 in the upper 1000 m is mainly basaltic hyaloclastite and breccias interbedded with basaltic lava flows and pillow lavas. Dykes and pillow lavas increase below 1000 m depth. The alteration assemblage includes wollastonite, garnet, actinolite, epidote, pyrite, chalcopyrite and quartz, which formed in the range of 270° to 310°C. The composition of the altered rocks from 500 m to 1346 m depth in well RN-9, compared to basalt lava from surface, indicates an increase in LOI, major oxides (SiO_2 , Al_2O_3 , FeO , MnO , and CaO), and a slight increase in K_2O . The major metals Zn and Cu have a small range of concentrations in the altered rocks (average 95 ppm Zn and 163 ppm Cu), similar to the unaltered host rocks. Lead, Cd, Ag and Au in the cuttings are all below the detection limits. These data indicate that there was little net loss or gain in major elements in the cuttings, which suggests that these immediate host rocks were not the source of the metals in the scales that precipitate in the pipelines.

Precipitation of the sulfides downhole in the Reykjanes wells cannot be prevented because of the pressure release and boiling. However, maintaining high pressures at the wellhead will mitigate precipitation downhole. The high pressure (22 bar) downstream of

the orifice plate will prevent amorphous silica from precipitating, but abrupt change in pressure at the orifice plate will cause substantial precipitation of sulfides. In the surface pipeline, the pressure must be at least ~22 bar downstream of the fluid flow control valve, and the surface pipelines should be as straight as possible, avoiding bends and other disruptions of flow that cause turbulence and scale deposition. Sulfide-rich scales that might be recovered from the five high-pressure wells examined in this study could contain metals valued at close to \$73,000 per year at today's metal prices.

6.2 Comparison of Reykjanes Scales to Other Geothermal Systems

Precipitation of scales in geothermal pipelines can be an issue for production in some systems, and scales are well known from many locations around the world. These systems have a range of salinities spanning two orders of magnitude, from low salinity (0.2 wt.% NaCl at Broadland-Ohaaki, New Zealand: Hedenquist, 1990; Simmons and Browne, 2000) to high salinity (32 wt.% NaCl at Salton Sea, USA: Skinner et al., 1967; McKibben et al., 1990; Gallup, 1998). The characteristics of systems with seawater salinity, directly comparable to Reykjanes, plus other high-temperature geothermal systems, with lower and higher salinity, are summarized in Table 6.1.

The most notable contrast between Reykjanes and the other geothermal systems (Table 6.1) is the tectonic setting. Reykjanes is the only system formed on a mid-ocean ridge; all the other geothermal areas are located either in volcanic arcs or back arcs, or continental rifts. These systems are comparable to Reykjanes in that all have high-temperature reservoir liquids (~300°C), and scales generally consist of sulfides at higher temperature and amorphous silica at lower temperatures. The Cu, Zn, Fe and Pb concentrations vary depending on the locations in the pipelines but tend to decrease sharply once the pressure

Table 6.1. High-temperature geothermal systems with various range of salinity compared to Reykjanes of seawater salinity

Location	Scale mineralogy									
	wt.% NaCl, T °C (1)	Wellhead p (bar-a), °C	Separation pressure (bar-a), °C	Well	Wellhead	Orifice plate (OP)	Downstream pipeline	Composition average or range (or highest concentration), wt.-%	Tectonic setting (Fluid sources)	Reference
Ohaaki-Broadland New Zealand	0.2% >310°C	~40 bar ~250°C	~11 bar, ~185°C	am-SiO ₂ -py-cc-Ag-Au	cpy>gn>sph>mt-py+Au-Ag	cpy>gn>sph>mt-py+Au-Ag	cpy>gn>sph>mt-py+Au-Ag	Fe 30-50%, Cu 9-21%, Au 2.8-4.5%, Ag 2.2-6.9%, Zn 1-3%, Pb 1-4%	Volcanic arc- back arc; rhyolite, minor andesite & basalt (meteoric water, minor magmatic component)	Brown, 1986; Hedenquist, 1990; Simmons & Browne, 2000
Rotokawa	0.2% >310°C	25 bar 224°C	19.25 bar, 210°-224°C	No info	black SiO ₂ >> Te (Ag, Pb, Cu, Au); sulf (Cu, Pb, Zn)	No info	same mineral as upstream decrease fast	(WH:75% Am-Si)>> 25% ore forming minerals (Cu 5.6%, Ag 4%, Te 3%, Zn 1.5%, Pb 0.6%, Au 0.2%)	Volcanic arc- back arc: rhyolite, minor andesite & basalt (meteoric water, minor magmatic component)	Reyes et al., 2002
Cerro Prieto Mexico downhole/pipeline	3.1% 250-367°C	9-103 bar	13-5.5 bar, 162°-195°C	Top:am-SiO ₂ >>10% sulf (Po>>sph, Ag, Au); m depth 60% sulf (icb-gn-sph), am-SiO ₂ , Ag, Au. Other wells:Top:sph>gn>py>cb>py>iss>sil-Au; >1400 m depth: sph>cpy>bn>gn>sil-Au-Ag±mht±cb±iss; WH & OP No info	Top:am-SiO ₂ >>10% sulf (Po>>sph, Ag, Au); >1200 m depth 60% sulf (icb-gn-sph), am-SiO ₂ , Ag, Au. Other wells:Top:sph>gn>py>cb>py>iss>sil-Au; >1400 m depth: sph>cpy>bn>gn>sil-Au-Ag±mht±cb±iss; WH & OP No info	>1200	silica, sulfides	well: Cu 12.87%, Zn 8.88%, Pb 8.28, Ag ~280 ppm (2.3 wt%), Au 0.1 ppm (270 ppm); pipe Fe 0.1-0.3%, Zn 0.1-0.3%, Cu 0.07-0.3, Pb<0.1%, silica<0.05%	Continental rift (setiments; originated from a mixture of oceanic brine and river water)	Truesdell et al., 1981, Mercado et al.,1989; Clark & Williams-Jones 1990; Thomas et al., 1992
Reykjanes 9RN; RN12, 21, 24 (MP: medium pressure)	3.3% 295°C	40 bar & 27 bar, 253° & 230°C/ 36-30 bar, 247-236°C	12 bar, 188°C/23 bar, 220°C	RN-22: mainly sph, tr cpy & bn	sph>bn- (dl)>>>cpy>gn, Au, Ag/bn=df=sph>gn>>>cpy, Au, Ag	Am-SiO ₂ >>>sph>>>cp y>>>bn, py, Au, Ag		Cu 21-5%; Fe 17-4.5%; Zn 18-10%; Pb 0.5-3%; SiO ₂ 4-50%; Au150-100 ppm; Ag 500-5000 ppm; MP Cu 20-26%; Fe 5-9%; Zn 20-26%; Pb 12-17%; SiO ₂ 1-7%; Au 130-590 ppm; Ag 0.7-2.3%	Mid-ocean ridge rift, basalt (on the coast, seawater)	Hardardóttir et al., 2001, 2005, 2009
Fushime Japan, 755-2600 md	3.5% 240-320°C	No info	25 bar	well: anh=Am-SiO ₂ >> gn=sph=mt±po; am-SiO ₂ , gn, sph	well: anh=Am-SiO ₂ >> gn=sph=mt±po; am-SiO ₂ , gn, sph		gn>sph + am-SiO ₂ ±po, ±mt	Two-phase line: Pb 40%, Zn 17%, Cu 7.8%, FeO 3.6%, SiO ₂ 3.5%	volcanic arc- back arc; silicic (on the coast, seawater)	Akaku, 1990; Akaku et al., 1991
Milos Greece, production, scaling test	8.1-11 ~310°C	No info	24-25 bar ~225°C	No info	gn, sph, Cu-sulfide	gn>cpy>sph-opal	SiO ₂ , sph	Pb 34-0.2%, Fe 33-10%, Zn 30-0.4%, Si 12-48%, Ag 0.1%	Island-volcano arc (Felsic rocks, dacite & andesites, phreatic breccias) on the coast	Karabelas et al., 1989; Christianis & St. Seymour, 1995
Asal Djibouti	11.6% 260°C	20 bar	17.7 bar ~206°C	No info	gn	gn	gn, sph, Fe-silicate, ±cpy, ±siderite, Ag2S	WH; Fe2O3 22%, Pb 22, SiO ₂ 20%, Zn 8.8, Cu 0.4, (test<18-10 bar); SiO ₂ 38%, Zn 4%, Fe 14%, Pb 3% Cu 0.7%, Ag 320 ppm, Au 780 ppm	Continental rift (mainly basalt, containing thick layers of clays, and intermediate products up to trachytes and rhyolites)	Ármansson & Hardardóttir, 2010
Salton Sea, production test	26 - 32% 300-365°C	220°C	2.7-7.9 bar 170°-130°C	Mt, gn, sph, cc	bornite, digenite, HP polyform of Cu ₂ S/gn+cc+oxides+sulf	No info	general: gn, sph, opaline (tr of str, As-py, th, cpy, py)	Fe-rich (7 wt.-%) opaline & Cu 0.1-30%, Pb 0.1-76 %, Zn 0.1-16%, <6% Ag, <820 ppm Au	Continental rift, sedimentary rocks (evaporate brines)	Skinner et al., 1967; Harrar, et al., 1979; McKibben & Elders, 1985; Gallup, 1998, McKibben et al., 1990

(1) T°C = reservoir. No info-no information, WH-wellhead, OP-orifice plate, Hp-high pressure, MP-medium pressure, mb-most abundant, md- meter depth, gn- galena, sph-sphalerite, te-tellerite, el-elctrum, am-SiO₂ amorphous silica, mt-magnetite, cc-calcite, po-pyrrhotite, icb-isocubanite, cb-cubanite, iss-intermediate solid solution, sil-amorphous silicate, mh-mooihoekite, %-wt.%, bbb-back pressure plate = orifice plate

decreases, similar to the Reykjanes pipelines. The Ag and Au concentrations in the scales have a large range, as in the Reykjanes scales, depending on the location of precipitation; in all cases, the highest concentration of precious metals occurs in surface pipelines close to the orifice plate where pressure sharply decreases.

The scales that precipitate from the low salinity fluid at Ohaaki-Broadlands, at pressures similar to those in RN-9, are less voluminous and are composed mainly of chalcopyrite with lesser amounts of galena, sphalerite, magnetite and pyrite. Amorphous silica, pyrite and calcite precipitate in the slotted liner below the surface (Simmons and Browne, 2000). Concentrations of Au and Ag in scales at Broadlands are significantly higher than in the Reykjanes scales, up to 6.4 wt.% and 30 wt.%, respectively, although the Au concentration in the deep liquid ($\sim 1.5 \mu\text{g}/\text{kg}$; Brown, 1986) is similar to that measured in the downhole liquid in well RN-12 at Reykjanes. The deposition of most of the amorphous silica at Ohaaki-Broadlands is restricted by engineering design to the surface pipeline downstream of the steam separator vessels (at $<180^\circ\text{C}$), whereas at Reykjanes the fluid is already supersaturated with amorphous silica at 11 bar ($\sim 188^\circ\text{C}$) in RN-9 upstream of the separator.

The Rotokawa geothermal system has similar salinity, reservoir temperature and tectonic setting as Ohaaki but the wellhead pressure is lower, and the separation pressure is higher. In the surface pipelines at Rotokawa, scales are dominantly amorphous silica together with metal tellurides, sulfides, salts and native sulfur (Reyes et al., 2002). The silica precipitation is minimized by the high separation pressure; the separated liquid is also diluted with condensate to produce the same effect. At the wellhead, 25% of the scales are sulfides and other metal minerals, including chalcopyrite, hessite/stützite, altaite, galena, pyrite, sphalerite, native Au, and hessite-petzite solid solution, in addition to opal. This variation in mineral composition, including the tellurides, differs significantly from

Reykjanes scales, most likely because of the source rocks and contributions from a magmatic-hydrothermal fluid.

Geothermal areas with a significantly higher salinity than Reykjanes include Salton Sea, California, Milos, Greece and Assal, Djibouti, with 32 wt.% to 8 wt.% NaCl. Two of these areas, Salton Sea and Assal, are located in a continental rift setting, whereas Milos is part of an island arc a short distance to the ocean (Karabelas et al, 1989; Christanis and St.Seymour, 1995; Ármannsson and Hardardóttir, 2010; McKibben et al., 1990). Galena is the major sulfide formed at high pressure and at the orifice plate, decreasing sharply downstream of the orifice plate. Amorphous silica together with sphalerite becomes the most abundant scale in the downstream pipelines of these systems. The high content of galena compared to Reykjanes may reflect the source rocks. Somewhat lower abundances of galena in scales from the Salton Sea likely reflect the bulk composition of host greywackes. In scales from the Salton Sea (Skinner et al., 1967), the main minerals are bornite, digenite, a high-pressure polymorph of chalcocite (Cu_2S), and silver together with traces of chalcopyrite and pyrite. This assemblage is remarkably similar to bornite-digenite-sphalerite that forms together with galena and silver on the fluid-flow control valves in the newer Reykjanes wells (RN-12, RN-21, RN-24).

The geothermal areas with salinities similar to Reykjanes are Cerro Prieto, Mexico, and Fushime, Japan. Cerro Prieto is located ~30 km southeast of Mexicali, Baja California, Mexico, in the southern portion of the Salton Sea basin. In 1989 over 150 wells had been drilled and scaling in the wells and surface installations has been a large problem (Mercado et al., 1989). The reservoir temperature is variable but reaches close to 370°C. Due to the high temperature, the wellhead pressure is highly variable, from 9 to 120 bar (Mercado et al., 1989). In general, downhole scales in wells contain amorphous silica > calcite > sulfides

(commonly sphalerite or pyrrhotite) together with Ag (280 ppm) and Au (0.1 ppm: Table 6.1). The mineralogy is also variable from well to well; sphalerite may be the major mineral in one well, whereas pyrrhotite is dominant in another well (Clark and Williams-Jones, 1990; Thomas et al., 1992). In the surface pipeline amorphous silica is the major precipitate together with sulfides. The major difference from Reykjanes is the abundance of amorphous silica forming downhole.

The Fushime geothermal area is located at the southeastern extremity of the Satsuma Peninsula, Kyushu, on the coast line. The hydrothermal system is dominated by seawater and the salinity is up to 3.5%. The host rocks are mostly dacitic to andesitic pyroclastic rocks and lavas interbedded with marine sediments (Akaku et al., 1991). Galena and sphalerite are commonly the dominant scale minerals in the high-temperature sections of the surface pipes, whereas amorphous silica is dominant in the low-temperature portions (Akaku, 1990). Here again, galena is one of the major minerals precipitating both downhole in the wells and in the surface pipeline.

Compared to Reykjanes, the scale mineralogy is somewhat more variable in geothermal systems in continental and arc-back arc environments. Metal precipitation is considerably greater from fluids that are more saline and hotter. The abundance of galena closely reflects the source rocks. The Au and Ag concentration does not appear to be related to the salinity, however, most likely because Au, in particular, is transported as a bisulfide rather than chloride complex (Brown, 1986).

References

References

- Akaku, K., 1990, geochemical study on mineral precipitation from geothermal waters at the Fushime field, Kyushu: Japan, *Geothermics*, v. 19, No. 5, 455-467.
- Akaku, K., Reed, M.H., Yagi, M., Kai, K., and Yasuda, Y., 1991, Chemical and physical processes occurring in the Fushime geothermal system, Kyushu, Japan: *Geochemical Journal*, v. 25, p. 315-333.
- Albertsson, A., Thórólfsson, G., and Jónsson, J., 2010, Three decades of power generation- Svartsengi power plant: Proceedings World Geothermal Congress 2010 Bali, Indonesia, 25-29 April 2010, extended abstract.
- Angenheister, G.H., Gebrande, H., Miller, H., Goldflam, P., Weigel, W., Jacoby, W.R., Pálmason, G., Björnsson, S., Einarsson, P., Pavlenkova, N.I., Zverev, S.M., Litvinenko, I.V., Loncarevic, B., and Solomon, S.C., 1980, Reykjanes Ridge Iceland seismic experiment: *Journal of Geophysics*, v. 47, p. 228-238.
- Arnórsson, S., 1978a, Progress report, about the scale composition from wells in Krafla (in Icelandic): National Energy Authority Report OS JHD 7832, p. 33.
- Arnórsson, S., 1978b, Major element chemistry of the geothermal sea-water at Reykjanes and Svartsengi, Iceland: *Mineralogical Magazine*, v. 42, p. 209-220.
- Arnórsson, S. 1995a, Geothermal systems in Iceland: Structure and conceptual models. I. High-temperature areas. *Geothermics*, v. 24, 561-602.
- Arnórsson, S., 1995b, Geothermal systems in Iceland: Structure and conceptual models. II. Low-temperature areas. *Geothermics*, v. 24, 603-629.

- Arnórsson, S., Grönvold, K., and Sigurdsson, S., 1978, Aquifer chemistry of four high-temperature geothermal systems in Iceland: *Geochimica et Cosmochimica Acta*, v. 42, p. 533-536.
- Arnórsson, S., Sigurdsson, S., and Svavarsson, H., 1982, The chemistry of geothermal waters in Iceland. I. Calculation of aqueous speciation from 0°C to 370°C: *Geochimica et Cosmochimica Acta*, Vol. 46, p. 1513-1532.
- Arnórsson, S., Axelsson, G., and Saemundsson, K., 2008, Geothermal systems in Iceland: *Jökull*, v. 58, p. 269-302.
- Ármannsson, H., 1989, Predicting calcite deposition in Krafla boreholes: *Geothermics*, v. 18, no. ½, p. 25-32.
- Ármannsson, H., 1993, The geothermal system at Námafjall (in Icelandic): National Energy Authority Report OS93053/JHD-29B, 30 p.
- Ármannsson, H., 2005, Monitoring the effect of geothermal effluent from the Krafla and Bjarnarflag power plants on groundwater in the Lake Mývatn area, Iceland, with particular reference to natural tracers: *Proceedings World Geothermal Congress 2005 Antalya, Turkey, 24-29 April 2005*, 8 p.
- Ármannsson, H., Benjamínsson, J., and Jefferey, A.W.A., 1989, Gas changes in the Krafla geothermal systems, Iceland: *Chemical Geology*, v. 76, p. 175-196.
- Ármannsson, H., Gíslason, G., and Hauksson, T., 1982, Magmatic gasses in well fluids aid the mapping of the flow pattern in a geothermal system: *Geochimica et Cosmochimica Acta*, v. 46, p. 167-177.
- Ármannsson, H. and Ólafsson, M., 2006, Collection of geothermal fluids for chemical analysis, internal report at Iceland Geosurvey, ÍSOR-2006/016, 17 p.

- Ármansson, H. and Hardardóttir, V., 2010, Geochemical patterns of scale deposition in saline high temperature geothermal systems: Proceedings of the thirteenth international symposium on water-rock interaction, Guanajuato, México. In Birkle and I.S. Torres-Alvarado (eds), Water-Rock Interaction, Taylor and Francis Group, London, p. 133-136.
- Árnadóttir, Th, Geirsson, H., and Einarsson, P., 2004, Coseismic stress changes and crustal deformation on the Reykjanes Peninsula due to triggered earthquakes on June 17, 2000: *Journal of Geophysics Research*, v. 109, B09307, doi: 10.1029/2004JB003130.
- Axelsson, G., Björnsson, G., Flóvenz, Ó.G., Gautason, B., Hauksdóttir, S., Ólafsson, M., Smáráson, Ó.B., and Saemundsson, K., 2005, Nature and properties of recently discovered hidden low-temperature geothermal reservoirs in Iceland: World Geothermal Congress, Antalya, Turkey, 10 p.
- Barton, P.B., Jr., 1973, Solid solutions in the system Cu-Fe-S. Part I: The Cu-S and CuFe-S joins: *Economic Geology*, v. 68, p. 455-456.
- Båth, M., 1960, Crustal structure of Iceland: *Journal of Geophysical Research*, v. 65, p. 1793-1807.
- Bearman, G., ed., 1989, *Ocean Chemistry and Deep-Sea Sediments*: Pergamon, London, 134 p.
- Berndt, M.E., Seyfried, W.E. Jr., Beck, J.W., 1988, Hydrothermal alteration processes at midocean ridges: experimental theoretical constraints from Ca and Sr exchange reactions and Sr Isotopic ratios: *Journal of geophysical Research*, v. 93. No.B5, p. 4573-4583.

- Bethke, P.M. and Barton, P.B., 1971, Distribution of some minor elements between coexisting sulfide minerals: *Economic Geology*, v. 66, p. 140-163.
- Bischoff, J. L., and Seyfried, W. E., 1978, Hydrothermal chemistry of seawater from 25° to 350°C: *American Journal of Science*, v. 278, p. 838-860.
- Bischoff, J.L., and Rosenbauer, R.J., 1987, Phase separation in seafloor geothermal systems: An experimental study on the effects of metal transport: *American Journal of Science*, v. 287, p. 953-978.
- Bjarnason, I. Th., Menke, W., Flóvenz, Ó.G., and Caress, D., 1993, Tomographic image of the Mid-Atlantic plate boundary in southwester Iceland: *Journal of Geophysical Research*, v. 98, p. 6607-6622.
- Bjarnason, I.Th., 2008, An Iceland hotspot saga: *Jökull* No. 58, p. 3-16.
- Bjarnason, J.Ö., 1994, The speciation programme WATCH: version 2.1: Reykjavík, National Energy Authority, 7 p.
- Bjarnason, J.Ö., 1995, Chemical composition of freshwater, saltwater, and seawater in the Reykjanes area, south western Iceland: Internal report of the National Energy Authority (in Icelandic), JÖB-95/04, 3 p.
- Bjarnason, J.Ö., 2002, Reykjanes: elements in geothermal seawater and steam 1971 – 2001: Internal report of the National Energy Authority (in Icelandic with English abstract), No .OS-2002/038, 69 p.
- Björnsson, S., Arnórsson, S., and Tómasson, J., 1970, Exploration of the Reykjanes thermal brine area: *Geothermics*, v. 2, special issue 2, p. 1640-1650.

- Björnsson, S., Ólafsdóttir, B., Tómasson, J., Jónsson, J., Arnórsson, S., and Sigmundsson, S.G., 1971, Reykjanes. Final report, research of the geothermal area (in Icelandic): National Energy Authority Report, 171 p.
- Björnsson, S., Arnórsson, S., and Tómasson, J., 1972a, Economic evaluation of Reykjanes thermal brine area, Iceland: American Association of Petroleum Geologists Bulletin, v. 56, p. 2380-2391.
- Björnsson, S., Arnórsson, S., and Tómasson, J., 1972b, Exploration of the Reykjanes thermal brine area: Geothermics, special issue 2, v. 2, part 2, p. 1640-1650.
- Björnsson, A., Saemundsson, K., Einarsson, P., Tryggvason, E., and Grönvold, K., 1977, Current rifting episode in north Iceland: Nature, v. 266, p. 318-323.
- Björnsson, A., Johnsen, G., Sigurdsson, S, Thorbergsson, G. Tryggvason, E., 1979, Rifting of the plate boundary in North Iceland 1975-1978: Journal of Geophysical Research, v. 84, p. 3029-3038.
- Björnsson, A., Axelsson, G., and Flóvenz, Ó.G., 1990, The nature of hot spring systems in Iceland (in Icelandic with English summary): Náttúrufræðingurinn, v. 60, p. 15-38.
- Björnsson, G., Arason, Th., and Bödvarsson, G.S., 1993, The wellbore simulator HOLA, vesion 3.1: user guide, 36 p. (ISOR data base).
- Bowers, T. S., Von Damm, K. L., and Edmond, J. M., 1985, Chemical evolution of mid-ocean ridge hot springs: Geochimica et Cosmochimica Acta, v. 49, p. 2239-2252.
- Bowers, T.S., Campell, A.C., Measures, C.I., Spivack, A.J., Khadem, M., and Edmond, J.M., 1988, Chemical controls on the composition of vent fluids at 13°-11°N and 21°N, East Pacific Rise, Journal of Geophysical Research, v. 93, p. 4522-4536.

- Bödvarsson, G., 1961, Physical characteristics of natural heat resources in Iceland: *Jökull*, v. 11, p. 29-38.
- Brandsdóttir, B., and Menke, W.H., 2008, The seismic structure of Iceland: *Jökull*, v. 58, p. 17-34.
- Brown, K.L., 1986, Gold deposition from geothermal discharges in New Zealand: *Economic Geology*, v. 81, p. 979-983.
- Brown, K. L. and Simmons, S. F., 2003, Precious metals in high-temperature geothermal systems in New Zealand: *Geothermics*, v. 32, p. 619-625.
- Browne, P.R.L., Courtney, S.F., and Wood, C.P., 1989, Formation rates of calc-silicate minerals deposited inside drill hole casing, Ngatamariki geothermal field, New Zealand: *American Mineralogist*, v. 74, p. 759-763.
- Butterfield, D.A., Massoth, G.J., McDuff, R.E., Lupton, J.E., and Lilley, M.D., 1990, Geochemistry of hydrothermal fluids from Axial Seamount hydrothermal emissions study vent field, Juan de Fuca Ridge: Subseafloor and subsequent fluid-rock interaction: *Journal of Geophysical Research*, v. 95, No. B8, p. 12,895–12,921.
- Butterfield, D. and Massoth, G.J., 1994, Geochemistry of north Cleft segment vent fluids: Temporal changes in chlorinity and their possible relation to recent volcanism: *Journal of Geophysical Research*, v. 99, No. B3, p. 4951-4968.
- Cabri, L.J., 1973, New data on phase relations in the Cu-Fe-S system: *Economic Geology*, v. 68, p. 443-454.
- Campbell, A.C., Bowers, T.S., and Edmond, J.M., 1988, A time-series of vent fluid compositions from 21°N EPR (1979, 1981, 1985), and the Guaymas Basin Gulf of California (1982, 1985): *Journal of Geophysical Research*, v. 93, p. 4537-4549.

- Christanis, K. and St.Seymour, K., 1995, A study of scale deposition: An analogue of meso- to epithermal ore formation in the volcano of Milos, Aegean arc, Greece: *Geothermics*, v. 24, No. 4, p. 541-552.
- Christenson, B.W., Ármannsson, H., Kennedy, B.M., von Soest T.J., 2010, Geochemical reconnaissance of fluids from the Krafla and Nesjavellir thermal areas, Iceland: Baseline studies in support of the IDDP: Proceedings World Geothermal Congress 2010, Bali, Indonesia, p. 1-7.
- Clark, J.R. and Williams-Jones, A.E., 1990, Analogues of epithermal gold-silver deposition in geothermal well scales: *Nature*, v. 346, p. 644-645.
- Clifton, A.E. and Schlische, R.W., 2003, Fracture populations on the Reykjanes Peninsula, Iceland: comparison with experimental clay models of oblique rifting: *Journal of Geophysical Research*, v. 108, No. B2, 2074, doi: 10.1029/2001jb000635, p. 4-1 to 4-17.
- Clifton, A.E. and Kattenhorn, S.A., 2007, Structural architecture of a highly oblique divergent plate boundary segmen: *Tectonophysics*, v. 419, p. 27-40.
- Converse, D.R., Holland, H.D., and Edmond, J.M., 1984, Flow rates in the axial hot springs of the East Pacific Rise (21°N): Implications for the heat budget and the formation of massive sulfide deposits: *Earth and Planetary Science Letters*, v. 69. 159-175.
- Craig, J.R., and Scott, S.D., 1976, Sulfide phase equilibria: Mineralogical Society America, *Reviews in Mineralogy*, v. 1, p. CS1-110.

- Darbyshire, F., Bjarnason, I.Th., White, R.S., and Flóvenz, O.G., 1998, Crustal structure above the Iceland mantle plume imaged by the ICEMELT refraction profile: *Journal of Geophysical Research*, v. 135, p. 1121-1149.
- Darbyshire, F. A., White, R.S., and Priestley, K.F., 2000, Structure of the crust and uppermost mantle of Iceland from a combined seismic and gravity study: *Earth and Planetary Science Letter*, v. 181 (3), p. 409-428.
- Darling, W.G. and Ármannsson, H., 1989, Stable isotopic aspects of fluid flow in the Krafla, Námafjall and Theistareykir geothermal systems of northeast Iceland: *Chemical Geology*, v. 76, p. 197-213.
- De Ronde C.E.J., 1995, Fluid chemistry and isotopic characteristics of seafloor hydrothermal systems and associated VMS deposits: potential for magmatic contributions in J.F.H. Thompson, eds., *Magmas, Fluids, and Ore Deposits*, short course series: Mineralogical Association of Canada, Short course v. 23, p. 479-509.
- Douville, E., Charlou, J.L., Oelkers, E.H., Bienvenu, P., Jove Colon, C.F., Donval, J.P., Fouquet, Y., Prieur, D. and Appriou, P., 2002, The rainbow vent fluids (36°14'N, MAR): the influence of ultramafic rocks and phase separation on trace metal content in Mid-Atlantic Ridge hydrothermal fluids: *Chemical Geology*, v. 184, p. 37-48.
- Driesner, T., 2007, The system H₂O-NaCl: Part II: Correlations for molar volume, enthalpy, and isobaric heat capacity from °C to 1,000°C, 1 to 5000 bar, and 0 to 1 XNaCl: *Geochimica et Cosmochimica Acta*, v. 71, p. 4902-4919.
- Edmond, J.M., Measures, C., McDuff, R.E., Chan, L.H., Collier, R., Grant, B., Gordon, L.I., and Corliss, J.B., 1979, Ridge crest hydrothermal activity and the balances of the

- major and minor elements in the ocean: The Galapagos data: *Earth and Planetary Science Letters*, v. 46, p. 1-18.
- Einarsson, P., 1978, S-wave shadows in the Krafla caldera in NE-Iceland, evidence from magma chamber in the crust: *Bulletin of Volcanology*, v. 43, p. 1-9.
- Einarsson, P., 1991, Earthquakes and present-day tectonism in Iceland: *Tectonophysics*, v. 189, p. 261-279.
- Einarsson, P., 2001, Structure and evolution of the Iceland hotspot: *Deutsche Geophysikalische Gesellschaft, Mitteilungen*, 1/2991, p. 11-14. http://www.dgg-online.de/mitteilungen/2001_1/island-hotspot.html
- Einarsson, P., 2008, Plate boundaries, rifts and transforms in Iceland: *Jökull*, v. 58, p. 35-58.
- Einaudi, M.T., Hedenquist, J.W., and Inan, E.E., 2003, Sulfidation state of fluids in active and extinct hydrothermal systems: transitions from porphyry to epithermal environments. In Simmons, S.F. and Graham, I.J., eds., *Volcanic, geothermal, and ore-forming fluids: Rulers and witnesses of processes within the Earth (Giggenbach Volume): Society of Economic Geologists Special Publication 10 2003*, p. 285-313.
- Eldridge, C.S., Barton, P.B., Jr., and Ohmoto, H., 1983, Mineral textures and their bearing on formation of the Kuroko orebodies: *Economic Geology Monograph 5*, p. 241—281.
- Ellis, A.J. and Mahon, W.A.J., 1977, *Chemistry and geothermal systems*, Academic press, New York, A Subsidiary of Harcourt Brace Jovanovich, Publishers, 392 p.
- Eysteinnsson, H., and Hermance, J., 1985, Magnetotelluric measurements across the eastern neovolcanic zone in south Iceland: *Journal of Geophysical Research*, v. 90, p. 10,093-10,103.

- Flanagan, F.J., 1984, Three USGS mafic rock reference samples, W-2, DNC-1, and BIR-1: U.S. Geological Survey Bulletin 1623, p. 54.
- Fleet, M.E., 2006, Phase equilibria at high temperatures, in Vaughan, D.J., eds., Sulfide Mineralogy and Geochemistry: Reviews in Mineralogy and Geochemistry, v. 61, p. 365-419.
- Foustoukos, D.I., and Seyfried Jr., W. E., 2007, Fluid phase separation processes in submarine hydrothermal systems: Reviews in Mineralogy & Geochemistry, v. 65, p. 213-239.
- Fournier, R.O., and Rowe, J.J., 1977, The solubility of amorphous silica in water at high temperatures and high pressure: American Mineralogy, v. 62, p. 1052-1056.
- Franzson, H., 1978, Structure and petrochemistry of the Hafnarfjall-Skardsheidi central volcano and the surrounding basalt succession, W-Iceland: Unpublished PhD Dissertation, University of Edinburgh, 264 p.
- Franzson, H., Gudmundsson, G., Tómasson, J., and Thorsteinsson, Th., 1983, Drilling of well RnG-9, Reykjanes (in Icelandic): National Energy Authority Report No. OS-83040/JHD-12, 31 p.
- Franzson, H., 1995; Geological aspects of Svartsengi high-T field, Reykjanes peninsula Iceland: Proc. of the 8th International Symposium on Water Rock Interaction, Vladivosto, Russia, 1-19 August, p. 671-674.
- Franzson, H., 1998, Reservoir geology of the Nesjavellir high-temperature field in SW-Iceland: Proceedings 19th Annual PNOC-EDC Geothermal Conference Manila, Philippines, March 5-6th 1998, p. 13-20.

- Franzson, H., 2000, Reykjanes high-temperature system. A study of fluid inclusions in wells RN-9 and RN-10 (in Icelandic): National Energy Authority Report No. OS-2000/021, 20 p.
- Franzson, H., 2004, The high-temperature system at Reykjanes (in Icelandic): Internal report of Iceland Geosurvey ISOR-2004/012, 68 p.
- Franzson, H., Gudmundsson, G., Tómasson, J., Thorsteinsson, Th., 1983, Drilling of Well RnG-9, Reykjanes, National Energy Authority Report No, OS-83040/JHD-12 B, 31p.
- Franzson, H., Thordarson, S., Bjornsson, G., Gudlaugsson, S.Th., Richter, B., Fridleifsson, G.Ó., and Thorhallsson, S., 2002, Reykjanes high-temperature field, SW-Iceland. Geology and hydrothermal alteration of well RN-10: Proceedings, 27th Workshop on Geothermal Reservoir Engineering. Stanford University, p. 233-240.
- Fridleifsson, I.B., 1979, Geothermal activity in Iceland: Jökull v. 29, p. 47-56.
- Fridleifsson, G.Ó., Blischke, A., Kristjánsson, B.R., Richter, B., Einarsson, G.M., Jónasson, H., Franzson, F., Sigurðsson. Ó., Danielsen, P.E., Jónsson, S.S., Thordarson, S., Þórhallsson, S., Harðardóttir, V., and Egilson, T., 2005, Reykjanes – Well Report RN-17 and RN-17ST, Iceland GeoSurvey report No. ÍSOR-2005/007, ISBN-9979-780-26-6, 198 p.
- Fridriksson, Th., Kristjánsson, B.R., Ármannsson, H., Margrétardóttir, E., Ólafsdóttir, S., Chiodini, G., 2006, CO2 emissions and heat flow through soil, fumaroles, and steam heated mud pools at the Reykjanes geothermal area, SW Iceland: Applied Geochemistry, v. 21, p. 1551-1569.
- Fridriksson, Th. and Giround, N., 2008, Geochemical production monitoring 2006 and 2007 at Reykjanes (In Icelandic). Iceland GeoSurvey Report No ÍSOR-2008/021, 52 p.

- Fridriksson, Th., Óladóttir, A.A., Jónsson, P., and Eyjólfsdóttir, E.I., 2010, The response of the Reykjanes geothermal system to 100 MWe power production: Fluid Chemistry and surface activity: Proceedings World Geothermal Congress 2010 Bali, Indonesia, 25-29 April 2010.
- Gallant, R.M. and Von Damm, K.L., 2006, Geochemical controls on hydrothermal fluids from the Kairei and Edmond vent fields, 23°-25°S, Central Indian ridge: *Geochemistry Geophysics Geosystems*, v. 6, p. 1-24, doi: 10.1029/2005GC001067.
- Gallup, D.L., 1998, Geochemistry of geothermal fluids and well scales, and potential for mineral recovery: *Ore Geology Reviews* v. 12, p. 225-236.
- Giggenbach, W. F., 1980, Geothermal gas equilibria: *Geochimica et Cosmochimica Acta*, v. 44, p. 2021-2032.
- Giggenbach, W. F. and Stewart, M. K. 1982, Processes controlling the isotopic composition of steam and water discharges from steam vents and steam-heated pools in geothermal areas: *Geothermics II*, p. 71-80.
- Ginster, U, Mottl, M.J., and Von Herzen, R.P., 1994, Heat flux from black smokers on the Endeavour and Cleft segments, Juan de Fuca Ridge: *Journal of Geophysical Research*, v. 99, p 4937-4950.
- Gíslason, G. and Arnórsson, S., 1976, Progress report on changes in flow rate and chemical composition in wells 3 and 4 in Krafla (in Icelandic): Internal report of the National Energy Authority, no. OS-JHD-7640, 14 p.
- Grguric, B.A., and Putnis, A., 1999, Rapid exsolution behavior in the bornite-digenite series and implications for natural ore assemblages: *Mineralogical Magazine*, v. 63, p. 1-12.

- Grguric, B.A., Harrison, R.J., and Putnis, A., 2000, A revised phase diagram for the bornite-digenite join from in situ neutron diffraction and DSC experiments: *Mineralogical Magazine*, v. 64, p. 213-231.
- Gudmundsson, Á., 1986, Mechanical aspects of postglacial volcanism and tectonics of the Reykjanes peninsula, Southwest Iceland: *Journal of Geophysical Research*, v. 91, p. 12711-12721.
- Gudmundsson, Á., Mortensen, A.K., Hjartarson, A., Karlsdóttir, R., and Ármannsson, H., 2010, Exploration and utilization of the Námafjall high temperature area in N-Iceland: *Proceedings World Geothermal Congress 2010 Bali, Indonesia, 25-29 April 2010*.
- Gudmundsson, B.T. and Arnórsson, S., 2002, Geochemical monitoring of the Krafla and Námafjall geothermal areas, N-Iceland: *Geothermics*, v. 31, p. 195-243.
- Gunnarsson, Á., Steingrímsson, B., Gunnlaugsson, E., Magnússon, J., and Maack, R., 1992, Nesjavellir geothermal co-generation power plant: *Geothermics*, v. 21, p. 559-583.
- Gunnarsson, I. Ívarsson, G., Sigfússon, B., Thrastarson, E.Ö., and Gíslason, G., 2010, Reducing silica deposition potential in waste waters from Nesjavellir and Hellisheidi power plants, Iceland: *Proceedings World Geothermal Congress 2010 Bali, Indonesia, 25-29 April 2010*.
- Haas, J.L. Jr., 1971, The effect of salinity on the maximum thermal gradient of a hydrothermal system at hydrostatic pressure: *Economic Geology*, v. 66, p. 940-946.
- Haneda, K. and Morrish, A.H., 1977, Magnetite to maghemite transformation in ultrafine particles: *Journal de physique*, v. 38, p.C1-321.

- Hannington, M. D.; Herzig, P. M., Scott, S. D., Thompson, G., and Rona, P. A., 1991, Comparative mineralogy and geochemistry of gold-bearing sulfide deposits on the mid-ocean ridges: *Marine Geology*, v. 101, p. 217-248.
- Hannington, M.D., Jonasson, I.R., Herzig, P.M. and Peterson, S., 1995a, in Humphris, S.E., Zierenberg, R.A., Mullineaux, L.S., and Thomson, R.E., eds., *Seafloor Hydrothermal Systems: Geophysical Monograph 91*, American Geophysical Union, Washington, DC, p. 115-157.
- Hannington, M.D., Tivey, M.K., Larocque, A.C.L., Petersen, S. and Rona, P.A., 1995b, The occurrence of gold in sulfide deposits of the TAG hydrothermal field, Mid-Atlantic Ridge: *The Canadian Mineralogist*, v. 33, p. 1285-1310.
- Hannington, M. D., Poulsen, K. H., Thompson, J. F. H., and Sillitoe 1999, Volcanic gold in the massive sulfide environment: *Reviews in Economic Geology*, v. 8, p. 325-356.
- Hannington, M.D., de Ronde, C.E.J., and Petersen, S., 2005, Sea-floor tectonics and submarine hydrothermal systems, in Hedenquist et al., eds., *100th Anniversary Volume of Economic Geology: Society of Economic Geologists*, Littleton, Colorado, p. 111-141.
- Hardardóttir, V., 1983, The petrology of the Hengill volcanic system, southern Iceland: Unpubl. M.Sc. thesis, Department of Geological Sciences McGill University, Montreal Canada, 260 p.
- Hardardóttir, V., 2002, Scales from well RN-9 Reykjanes (in Icelandic): Internal report by National Energy Authority, No OS-2002/011, 48 p. <http://www.os.Is/gogn/Skyrslur/OS-2002/OS-2002-011.pdf>

- Hardardóttir V., 2004a, Major and trace elements in scales in pipes from well 9, Reykjanes, Iceland: in Water-Rock Interaction, in Wanty, R.B., and Seal, R.R., (eds) II: Proceedings of the 11th Symposium on Water-Rock Interaction: Leiden, Netherlands, A.A. Balkema, p. 1521-1525.
- Hardardóttir, V., 2004b, Scaling studies on brine from wells 9 and 11, in the Reykjanes high temperature area, Iceland, extended abstract: 13. Scandinavian Corrosion Congress (Nordisk Korrosionsmöte). NKM 13 in Reykjavík Iceland 18-20, April 2004.
- Hardardóttir, V., Kristmannsdóttir, H., and Ármannsson, H., 2001, Scale formation in wells RN-9 and RN-8 in the Reykjanes geothermal field Iceland, in Cidu R. eds., Water-Rock Interaction: Swets and Zeitlinger, Lisse, ISBN90 2651 824 2, v. 2. p. 851-854.
- Hardardóttir, V., Ármannsson, H., and Thórhallsson, S., 2005, Characterization of sulfide-rich scales in brine at Reykjanes: Proceedings World Geothermal Congress Antalya, Turkey, 24-29 April 2005, extended abstract. http://www.geothermal-energy.org/310,proceedings_from_past_world_geothermal_congresses.html
- Hardardóttir, V., Hannington, M., and Hedenquist, J., 2006, Mineralogy and textures of metal-rich scales from the Reykjanes seawater-dominated system, Iceland: Comparison with seafloor hydrothermal systems: Extended abstract, International Geothermal Association conference held in Tucson Arizona 5-10 September 2006, 4 p., http://pangea.stanford.edu/ERE/db/IGAstandard/search_results.php
- Hardardóttir, V., Hannington, M.D., Hedenquist, J.W., and Kjarsgaard, I., 2007, Quenched black-smoker fluids: evidence from bornite scales precipitated from seawater-dominated geothermal fluids on the Reykjanes peninsula, Iceland: Geological Society of America Abstracts with Programs, v. 39, no. 6, paper no. 149-15.

- Hardardóttir, V., Brown, K., Fridriksson, T., Hedenquist, J., and Hannington, M., 2009, Thorhallsson, S., Metal in deep liquid of the Reykjanes geothermal system, southwest Iceland: implications for the composition of seafloor black smoker fluids: *Geology*, v. 37; no 12, p. 1103-1106.
- Hardardóttir, V., Hannington, M., Hedenquist, J., Kjarsgaard, I., and Koal, K., 2010, Cu-rich scales in the Reykjanes geothermal system, Iceland, *Economic Geology*, v, 105, p. 1143-1155.
- Harrar, J.E., Otto, C.H., Jr., Deutscher, S.B., Ryon, R.W., and Tardiff, G.E., 1979, Studies of brine chemistry, precipitation of solids, and scale formation at the Salton Sea geothermal field: Lawrence Livermore Laboratory Report UCRL-52640, 17 p.
- Hauksson, T., 1981, Concentrations of major elements in geothermal water: National Energy Authority Report No. OS-81015/JHD-10, 53 pages.
- Haymon, R.M., 1983, Growth history of hydrothermal black smoker chimneys: *Nature*, v. 301, p. 695-698.
- Hedenquist, J.W., 1990, The thermal and geochemical structure of the Broadlands-Ohaaki geothermal system, New Zealand: *Geothermics*, vol. 19, No. 2, p. 151-185.
- Henley, R.W., Truesdell, A.H., and Barton, P.B., Jr., 1984, Fluid-Mineral Equilibria in Hydrothermal Systems: Chelsea, UK, Society of Economic Geologists, *Reviews in Economic Geology*, v. 1, 267 p.
- Hjartarson, A., 2004, Go devil runs, temperature and pressure logging í well RN-9 in Reykjanes in October 2004 (in Icelandic). Iceland GeoSurvey Report No ÍSOR-04133, 12 p.

- Hjartarson, A., and Júlíusson, E., 2007, Numerical model of the Reykjanes Geothermal System and predictions of its response to 100 MW electricity generation (in Icelandic): Iceland GeoSurvey report No. ISOR-2007/025, 147 p.
- Hoffman, E.L., 1992. Instrumental Neutron Activation in Geoanalysis: *Journal of Geochemical Exploration*, v. 44, p. 297-319.
- Hreinsdóttir, S., Einarsson, P., and Sigmundsson, F., 2001, Crustal deformation at the oblique spreading Reykjanes Peninsula, SW Iceland: GPS measurements from 1993 to 1998: *Journal of Geophysical Research*, v. 106, p. 13303-13816.
- Hutchison, M.N., and Scott, S.D., 1981, Sphalerite geobarometry in the Cu-Fe-Zn-S system: *Economic Geology*, v. 76, p. 143-153.
- Jakobsson, S.P., 1972, Chemistry and distribution pattern of recent basaltic rocks in Iceland: *Lithos*, v. 5, p. 365-386.
- Jakobsson, S.P., 1979, Petrology of Recent basalts of the eastern volcanic zone, Iceland: *Acta Naturalia Islandica*, v. 26, 103 p.
- Jakobsson, S.P., 1980, Outline of the petrology of Iceland: *Jökull*, v. 29, p. 57-73 and 96-99.
- Jakobsson, S.P., Jónsson, J., and Shido, F., 1978, Petrology of the Western Reykjanes Peninsula, Iceland: *Journal of Petrology*, v. 19, p. 669-705.
- Jakobsson, S.P. and Gudmundsson, M.T., 2008, Subglacial and intraglacial volcanic formations in Iceland: *Jökull*, v. 58, p. 179-196.
- Jakobsson, S.P., Jónsson, J., and Sigurdsson, I.A., 2008, The three igneous rock series of Iceland: *Jökull* v. 58, p. 117-138.

- Janecky, D.R., and Seyfried, W.E., Jr., 1984, Formation of massive sulfide deposits on oceanic ridge crests: Incremental reaction models for mixing between hydrothermal solutions and seawater: *Geochimica et Cosmochimica Acta*, v. 48, p. 2723-2738.
- Johnsson, G.L. and Jakobsson, S.P., 1985, Structure and petrology of the Reykjanes Ridge between 62°55'N and 63°48'N: *Journal of Geophysical Research* v. 90, p. 10073-10083.
- Jolley, D.W., and Bell, B.R., 2002, The evolution of the Tertiary North Atlantic igneous province, and the opening of the NE Atlantic rift: *Geology Society London, Special Publication* v. 197, p. 1-13.
- Jóhannesson, H., 1975, Structure and petrochemistry of the Reykjadalur central volcano and the surrounding areas, Midwest Iceland: Unpublished PhD from Durham University, 273 p.
- Jóhannesson, H., and Einarsson, S., 1988, Age of Illahrauns at Svartsengi (in Icelandic with English abstract): *Fjölrit Náttúrufræðistofnunar* No. 7, 12 p.
- Jóhannesson, H. and Saemundsson, K., 2009, Geological Map of Iceland. 1:600 000. Bedrock Geology: Icelandic Institute of Natural History, Reykjavík (1st edition).
- Jónsson, J., 1968, Changes in the geothermal area at Reykjanes in 1967 (in Icelandic): National Energy Authority Report 10421 OST 5, 5 p.
- Jónsson, J., 1978, Geological map of Reykjanes Peninsula: National Energy Authority Report No. OS JHD 7831, p. 303.
- Jónsson, J., 1983; Historic eruptions on the Reykjanes Peninsula (in Icelandic): *Náttúrufræðingurinn* v. 52, p. 127–139.

- Jónsson P., 2008, Svartsengi – Reykjanes heat and pressure measurements 2006 and 2007 (in Icelandic): Iceland GeoSurvey Report No ÍSOR/020, 95 p.
- Jónsson, P., Björnsson, H., and Halldórsdóttir, S., 2010, Svartsengi – Reykjanes, Temperature and pressure measurements 2009 (in Icelandic): Iceland Geosurvey report No. ÍSOR-2010/020 61 p.
- Jónsson, S.S., Kristjánsson, B.R., Guðmundsson, Á., Björnsson, G., Gunnarsson, G., Danielsen, P.E., and Thórhallsson, S., 2003, Reykjanes – well RN-12, 3. stage: Drilling from 854 m to 2506 m depth (in Icelandic): National Energy Authority Report No. OS-2003/010, 62 p.
- Karabelas, A.J., Andritsos, N., Mouza, A., Mitrakas., M., Vrouzi, F., and Christanis, K., 1989, Characteristic of scales from the Milos geothermal plant: *Geothermics*, v. 18, p. 169-174.
- Karlsdóttir, R., 1997, TEM-resistivity measurement on the outer Reykjanes Peninsula (in Icelandic): National Energy Authority Report No. OS-97002, 64 p.
- Karlsdóttir, R., 2005, TEM-measurements at Reykjanes 2004 (in Icelandic): Iceland Geosurvey report No. ÍSOR-2005/002, 23 p.
- Keenan, J.H., Keyes, F.G., Hill, P.G., and Moore, J.G., 1969, *Steam Tables – thermodynamic properties of water including vapor, liquid, and solid phases, (International Edition – metric units)*: Wiley, New York, 162 p.
- Kojima, S., and Sugaki, A., 1984, Phase relations in the central portion of the Cu-Fe-Zn-S system between 800°C and 500°C: *Mineralogical Journal*, Mineralogical Society of Japan, v. 12, p. 15-28.

- Kojima, S., and Sugaki, A., 1985, Phase relations in the Cu-Fe-Zn-S system between 500° and 300°C under hydrothermal conditions: *Economic Geology*, v. 80, p. 158-171.
- Koschinsky, A., Garbe-Schönberg, D., Sander, S., Schmidt, K., Gennerich, H.H., Strauss, H., 2008, Hydrothermal venting at pressure-temperature conditions above the critical point of seawater, 5°S on the Mid-Atlantic Ridge: *The Geological Society of America* 36, 615-618.
- Koski, R.A., Shanks, W.C. III, Bohrson, W.A., and Oscarson, R.L., 1988, The composition of massive sulfide deposits from the sediment-covered floor of Escanaba Trough, Gorda Ridge: Implications for depositional process: *Canadian Mineralogist*, v. 26, p. 655-673.
- Koski, R. A., I. R. Jonasson, D. C. Kadko, V. K. Smith, and F. L. Wong, 1994, Compositions, growth mechanisms, and temporal relations of hydrothermal sulfide-sulfate-silica chimneys at the northern Cleft segment, Juan de Fuca Ridge: *Journal of Geophysical Research*, v. 99, no. B3, p. 4813-4832.
- Kristmannsdóttir, H., 1975, Hydrothermal alteration of basaltic rocks in Icelandic geothermal areas: Reprinted from *Second UN Symposium on the Development and use of Geothermal Resources*, San Francisco, Proceedings, Lawrence Berkeley Lab., University of California, p. 441-445.
- Kristmannsdóttir, H., 1984, Chemical evidence from Icelandic geothermal systems as compared to submarine geothermal systems: in Rona, P.A., Bostrom, Laubier, L., and Smith, K. L. Jr, eds., *Hydrothermal processes at seafloor spreading centers*: Plenum Press, London and New York, p. 291-320.

- Kristmannsdóttir, H., 1986, Saline groundwater and geothermal brine on the Reykjanes Peninsula: Fifth International Symposium on Water-Rock Interaction, Reykjavik, Iceland, August 8-17, 1986, Reykjavík: Orkustofnun, 1986, p. 337-340.
- Kristmannsdóttir, H., 1989, Types of scaling occurring by geothermal utilization in Iceland: *Geothermics*, v. 18, p. 183-190.
- Kristmannsdóttir, H., and Svantesson, J., 1978, Analyses of precipitations from wells KJ-7, KG-10 and KJ-9 from Krafla (in Icelandic): National Energy Authority report No. OS-JHD 7820, 31 p.
- Kristmannsdóttir, H., Ildefonse, Ph., Bertaux, J., and Flank, A.M., 1999, Crystal-chemistry of Mg-Si and Al-Si scales in geothermal waters, Iceland, in Ármannsson ed., *Geochemistry of the Earth's Surface*: Balkema, Rotterdam, ISBN 90 5809 073 6, p. 519-522.
- Lide, D.R., ed., 1998, *CRC Handbook of Chemistry and Physics* (78th edition, 1997-1998): New York, CRC Press, p. 14-14.
- Líndal, B., 1975, Development of industry based on geothermal energy, geothermal brine and sea water in the Reykjanes peninsula, Iceland: *Proceedings Second U.N. on Development and use of geothermal resources*, v. 3, p. 2223-2229
- Lonker, S.W., Franzson, H., and Kristmannsdóttir, H., 1993, Mineral-fluid interactions in the Reykjanes and Svartsengi geothermal systems, Iceland: *American Journal of Science*, v. 293, p. 605-670.
- Marks, N., Schiffman, P., Zierenberg, R., Zierenberg, R.A., and Fridleifsson, G.Ó., 2010a, Hydrothermal alteration in the Reykjanes geothermal system: insights from Iceland

- deep drilling program well RN-17: *Journal of Volcanology and Geothermal Research*, v. 189, p. 172-190.
- Marks, N., Schiffman, P., Zierenberg, R., Elders, W.A., Fridleifsson, G.Ó., and Franzson, H., 2010b, Isotopic evidence of hydrothermal exchange and seawater ingress from alteration minerals in the Reykjanes geothermal system: Results from the IDDP: Proceedings World Geothermal Congress, Bali, Indonesia, 25-29 April 2010.
- Massoth, G.J., Butterfield, D.A., Lupton, J.E., McDuff, R.E., Lillry, M.D., and Jonasson, I.R., 1989, Submarine venting of phase separated hydrothermal fluids at Axial Volcano, Juan de Fuca ridge, *Nature*, v. 340, p. 702-705.
- McDonough, W.F. and Sun, S.-s., 1995, The composition of the earth: *Chemical Geology*, v. 120, 223-253.
- McKibben, M.A. and Elders, W., 1985, Fe-Zn-Cu-Pb mineralization in the Salton Sea geothermal system, Imperial Valley, California: *Economic Geology*. v. 80, p. 539-559.
- McKibben, M.A., Williams, A.E., Hall, G.E.M., 1990, Solubility and transport of platinum-group elements and Au in saline hydrothermal fluids: constraints from geothermal brine data: *Economic Geology*, v. 85, p. 1926-1934.
- McKibben, M.A. and Hardie, L.A., 1997, Ore-forming brines in active continental rifts, in Barnes, H.L., ed, *Geochemistry of hydrothermal ore deposits: 3rd ed.*: New York, Wiley and Sons, p. 877-935.
- Menke, W., Brandsdóttir, B., Einarsson, P., and Bjarnason, I., 1996, Reinterpretation of the RRISP-77 Iceland shear wave profiles: *Geophysical Journal International*, v. 126, p. 166-172.

- Mercado, S., Bermejo, F., Hurtado, R., Terrazas, B., and Hernández, L., 1989, Scale incidence on production pipes of Cerro Prieto geothermal wells: *Geothermics*, v. 18, p. 225-232.
- Mortensen, A.K., Gudmundsson, Á., Richter, B., Sigurdsson, Ó., Fridleifsson, G.Ó., Franzson, H., Jónsson, S.S., Danielsen, P.E., Ásmundsson, R.K., Thordarson, S., Egilsson, Th., Skarphéðinsson, K., and Thórirsson, S., 2006, Well report for RN-19. 1st stage: Drilling for 18? in anchor casing from 84 m to 349. 2nd stage: Drilling for 13? in production casing from 349 m to 763 m. Spot-coring from 2245 m to 2248: Iceland Geosurvey report ÍSOR-2006/025, 141 p.
- Mortensen, A.K., Ingimarsdóttir, A., Egilsson, Th., Fridriksson, Th., and Ólafsson, M., 2008, Well KJ-35 at Krafla. Cleaning of the downhole well (in Icelandic): Iceland Geosurvey Report ÍSOR-2008/068, 46 p.
- Mortensen, A.K., Gudmundsson, Á., Steingrímsson, B., Sigmundsson, F., Axelsson, G., Ármannsson, H., Björnsson, H., Ágústsson, K., Saemundsson, K., Ólafsson, M., Karlsdóttir, R., Halldórsdóttir, S., and Hauksson, T., 2009a, The geothermal system at Krafla. Summary of researches and reviewed model (in Icelandic): Iceland Geosurvey Report ÍSOR-2009/057, 206 p.
- Mortensen, A.K., Egilsson, Th., Gudfinnsson, G.H., Jónsson, S.S., Ingimarsdóttir, A., Gunnarsson, H.S., Tryggvason, H.H., and Jónsson, R.B., 2009b, Krafla – Leirbotnar Well KJ-39. Removal of the liner and studies of the scales (in Icelandic): Iceland Geosurvey Report ÍSOR-2009/044, 73 p.
- Mozgova, N.N., Trubkin, N.V., Borodaev, Y.S., Cherkashev, G.A., Stepanova, T.V., Semkova, T.A., and Uspenskaya, T.Y., 2008, Mineralogy of massive sulfides from the

- Ashadze hydrothermal field, 13°N Mid-Atlantic Ridge: *Canadian Mineralogist*, v. 46, p. 545 – 567.
- Mungania, J. 1993; Borehole Geology of well RN-9, Reykjanes, SW-Iceland: United Nations University Geothermal Training Program, Gensásvegur 9, 108 Reykjavík, Iceland, 37 p.
- Mutonga, M.W., Sveinbjörnsdóttir, Á., Gíslason, G., and Ármannsson, 2010, The isotopic and chemical characteristics of geothermal fluids in Hengill area, SW- Iceland (Hellisheidi, Hveragerdi and Nesjavellir Fields), Proceedings World Geothermal Congress 2010, Bali, Indonesia, 25-29 April, p. 1-13.
- Ólafsson, E., 1975, The travel book of Eggerts Ólafssonar and Bjarna Pálssonar, their traveling in Iceland the years 1752-1757, 2. Volume (in Icelandic): Örn og Örlygur hf. 1975, p. 149-266.
- Ólafsson, J., and Riley, J.P., 1978, Geochemical studies on the thermal brine from Reykjanes (Iceland): *Chemical Geology*, v. 21, p. 219-237.
- Óskarsson, N, Steinhórsson, S., and Sigvaldason, G.E., 1985, Icelandic geochemical anomaly: origin, volcano tectonics, chemical fractionation and isotopic evolution of the crust: *Journal of geophysical Research*, v. 90, p. 10011-10025.
- Pang, Z.H. and Reed, M., 1998, Theoretical chemical thermometry on geothermal waters: problems and methods: *Geochimica et Cosmochimica Acta*, v. 62, p. 1083-1091.
- Palandri, J.L. and Reed, M.H. (2001), Reconstruction of in situ composition of sedimentary formation waters: *Geochimica et Cosmochimica Acta*, v. 65, p. 1741-1767.

- Paradis, S., Jonasson, I.R., Le Cheminant, G.M., and Watkinson, D.H., 1988, Two zinc-rich chimneys from the Plume Site, southern Juan de Fuca Ridge: *Canadian Mineralogist*, v. 26, p. 637-654
- Pálmason, G., 1970, Crustal structure of Iceland from explosion seismology: Science Institute, University of Iceland and National Energy Authority, Reykjavík, 239 p.
- Pálmason, G., 1971, Crustal structure of Iceland from explosion seismology: *Societas Scientiarum Islandica*, Reykjavík, 187 p.
- Pálmason, G., 1981, An assessment of the geothermal resources in Iceland (in Icelandic): Proceedings of the Energy Conference, Reykjavík, June 1981, p. 121-137.
- Pálmason, G. and Saemundsson, K., 1974, Iceland in relation to the Mid-Atlantic Ridge: *Annual Reviews of Earth and Planetary Sciences*, v. 2, p. 25-63.
- Pálmason, G., Johnsen, G.V., Torfason, H., Saemundsson, K., Ragnars, K., Haraldsson, G.I., and Halldórsson, G.K., 1985, Assessment of geothermal energy in Iceland (in Icelandic): Report by National Energy Authority No. OS-85076/JHD-10, 134 p.
<http://www.os.is/gogn/Skyrslur/OS-1985/OS-85076.pdf>
- Peach, C.L., Mathes, E.A., and Keays, R.R., 1990, sulfide melt-silicate melt distribution coefficients for noble metals and other chalcophile elements as deduced from MORB: Implications for partial melting: *Geochimica et Cosmochimica Acta*, v. 54, p. 3379-3389.
- Peter, J.M., and Scott, S.D., 1988, Mineralogy, composition, and fluid inclusion microthermometry of seafloor hydrothermal deposits in the southern trough of Guaymas basin, Gulf of California: *Canadian Mineralogist*, v. 26, p. 567-588.

- Pope, E.C., Bird, D.K., Arnórsson, S., Fridriksson, Th., Elders, W., and Fridleifsson, G.Ó., 2009, Isotopic constraints on ice age fluids in active geothermal systems: Reykjanes, Iceland: *Geochimica et Cosmochimica Acta* v. 73, p. 4468-4488.
- Reed, M.H., 1982, Calculation of multicomponent chemical equilibria and reaction processes in systems involving minerals, gases and an aqueous phase: *Geochimica et Cosmochimica Acta* v. 46, p. 513-528.
- Reed, M.H., 1998, Calculation of simultaneous chemical equilibria in aqueous-mineral-gas systems and its application to modeling hydrothermal process. In: Richards, J., and Larson, P. eds., *Techniques in Hydrothermal Ore Deposits Geology: Reviews in Economic Geology*, v. 10, p.109-124.
- Reed, M. H. and Spycher, N., 1984, Calculation of pH and mineral equilibria in hydrothermal waters with application to geothermometry and studies of boiling and dilution: *Geochimica et Cosmochimica Acta*, v. 48, p 1479-1492.
- Reed, M.H., and Palandri, J., 2006, Sulfide mineral precipitation from hydrothermal fluids, in Vaughan, D.J., ed., *Sulfide Mineralogy and Geochemistry: Reviews in Mineralogy and Geochemistry*, v. 61, p. 609-631.
- Reyes, A.G., Trompeter, W.J., Britten, K., and Searle, J., 2002, Mineral deposits in the Rotokawa geothermal pipelines, New Zealand: *Journal of Volcanology and Geothermal Research*, v. 119, Issues 1-4, p. 215-239.
- Richter, B., Franzson, H., Kristjánsson, B.R., Jónsson, S.S., Gudmundsson, Á., Gunnarsson, G., Sigurdsson, Ó., and Skarphéðinsson, K., 2003, Reykjanes – well 12, 1. Stage, drilling from 119 to 300 m depth and 2. Stage, drilling from 300 to 854 m depth: National Energy Authority Report No., OS-2003/008, 50 p.

- Rimstidt, J.D., 1997, Gangue mineral transport and deposition. In Barnes, H.L. (ed): Geochemistry of hydrothermal ore deposits. John Wiley & Sons, New York, p. 487-516.
- Rona, P. A., Hannington, M. D., Raman, Thompson, G. Tivey, M. K. Humphiris, S. E. Lalou, C. Petersen, S. 1993, active and Relict sea-floor hydrothermal mineralization at the TAG hydrothermal field, mid-Atlantic ridge: *Economic Geology*, v. 88, p. 189-217.
- Saemundsson, K., 1967, Vulkanismus und Tektonik des Hengill-Gebietes in Sudwest – Island: *Acta Nat Islandica*, v. 2, p. 1-105.
- Saemundsson, K., 1974, Evolution of the axial rifting zone in northern Iceland and the Tjörnes fracture zone: *Geological Society of America Bulletin*, v. 85, p. 495-504.
- Saemundsson, K., 1978, Fissure swarms and central volcanoes of the neovolcanic zones of Iceland: *Geological Journal Special Issue 10*, p. 415-432.
- Saemundsson, K., 1979, Outline of the geology of Iceland: *Jökull*, v. 29, p. 7-28.
- Saemundsson, K., 1983, Fractures in the Krafla area. On the status of the Krafla geothermal power station (in Icelandic): *Proceedings of meeting held in Akureyri, Iceland 2-3 March 1983*, p. 4-8.
- Saemundsson, K., 1986, Subaerial volcanism in the western North Atlantic, in Vogt, P.R., and Tucholke, B.E., eds, *The Geology of North America*, v. M, the Western North Atlantic Region: *Geological Society of America*, p. 69-86.
- Saemundsson, K., 1991, Geology of the Krafla system, in Gardarsson, A. and Einarsson, P., Eds, *the Natural History of Lake Mývatn (in Icelandic): The Icelandic Natural History Society, Reykjavík*, p. 24-95.

- Saemundsson, K. and Noll, H., 1974, K/Ar ages of rocks from Húsafell, western Iceland and the development of the Húsafell central volcano: *Jökull*, v. 24, p. 40-59.
- Saemundsson, K. and Fridleifsson, 1980, Application of geology in geothermal research in Iceland (in Icelandic with English summary): *Nátturufraedingurinn*, v. 60, p. 157-188.
- Saemundsson, K., and Jóhannesson, H., 2004, Geothermal map of Iceland. Iceland GeoSurvey and National Energy Authority.
- Saemundsson, K., Jóhannesson, H., Kristinsson, S.G., and Sigurgeirsson, M. A., 2010, Geological map of Southwest Iceland, 1:100,000. Iceland GeoSurvey.
- Saunders, J.A., and Scholenley, P.A., 1995, Boiling, colloid nucleation and aggregation, and the genesis of bonanza Au-Ag ores of the Sleeper deposit, Nevada: *Mineralium Deposita*, v. 30, 199-210.
- Schilling, J.G., 1973, Iceland Mantle Plume: Geochemical study of Reykjanes Ridge: *Nature* vol. 242, 565-571.
- Schilling, J.G., Meyer, P.S., and Kingsley, R.H., 1982, Evolution of the Iceland hotspot: *Nature*, v. 296, p. 313-296.
- Seyfried, 1987. Experimental and theoretical constraints on hydrothermal alteration processes at mid-ocean ridges. *Annual Review of Earth and Planetary Sciences* v. 15, p. 317-335.
- Seyfried, W., and Bischoff, J., 1977, Hydrothermal transport of heavy metals by seawater: the role of seawater/basalt ratio: *Earth and Planetary Science Letters*, v. 34, p. 71-77.
- Seyfried, W.E. Jr., and Mottl, M.J., 1982, Hydrothermal alteration of basalt by seawater under seawater-dominated conditions, *Geochimica et Cosmochimica Acta*, 46, p. 985-1002.

- Seyfried, W.E., Jr., and Janecky, D.R., 1985; Heavy metal and sulfur transport during subcritical and supercritical hydrothermal alteration of basalt; Influence of fluid pressure and basalt composition and crystallinity: *Geochimica et Cosmochimica Acta*, v. 49, p.2545-2560.
- Seyfried W.E., Jr., Berndt, M.E., and Janecky, D.R., 1986; Chloride depletions and enrichments in seafloor hydrothermal fluids; Constraints from experimental basalt alteration studies: *Geochimica et Cosmochimica Acta*, v. 50, p. 469-475.
- Seyfried W.E., Ding, K., Berndt, M.E., and Chen, X., 1999, Experimental and theoretical controls on the composition of mid-ocean ridge hydrothermal fluids In: *Volcanic-Associated Massive Sulfide Deposits; Processes and Examples in Modern and Ancient Settings*. Barrie CT, Hannington M.D. (eds). *Reviews in Economic Geology*, v. 8, p. 181-200.
- Seyfried, W.E. Jr., and Ding, K., 1995, Phase equilibria in Subseafloor hydrothermal systems: A review of the role of redox, temperature, pH and dissolved Cl on the chemistry of hot spring fluids at mid-ocean ridges, in Humphris, S.E., Zierenberg, R.A., Mullineaux, L.S., and Thomson, R.E., eds., *Seafloor Hydrothermal Systems: Physical, Chemical, Biological, and Geological Interactions: American Geophysical Union Geophysical Monograph 91*, p. 248-272.
- Seward, T.M., 1973, Thio complexes of gold and the transport of gold in hydrothermal ore solutions. *Geochimica et Cosmochimica Acta*, v. 37, p. 379-399.
- Sigurdsson, F. 1986, Hydrogeology and groundwater on the Reykjanes Peninsula: *Jökull*, v. 36. P. 11-29.

- Sigurdsson, Ó., 2010, The Reykjanes Seawater Geothermal System – Its exploitation under regulatory constraints: Proceedings World Geothermal Congress 2010, Bali, Indonesia, 25-26 April, extended abstract.
- Sigurðeirsson, M.Á., 1995, The younger Stampar eruption at Reykjanes (in Icelandic): Náttúrufræðingurinn v. 64, p. 211–230
- Sigurðeirsson, M.Á., 2004, A chapter on the eruption history of Reykjanes: eruption episode two thousand years ago (in Icelandic): Náttúrufræðingurinn, v. 72, p. 21–28.
- Sigvaldason, G., 1959, Mineralogische untersuchungen über gesteinszersetzung durch postvulkanische aktivität in Island: Beiträge zur Mineralogie und Petrographie, v. 6, p. 405-426.
- Sillitoe, R.H., Hannington, M.D., and Thompson, J.H., 1996, High- sulfidation deposits in the volcanogenic massive sulfide environment: Economic Geology, v. 91, p. 204-212.
- Simmons, S.F. and Christenson, B.W., 1994, Origins of calcite in a boiling geothermal system: American Journal of Science, v. 294, p. 361–400.
- Simmons, S.F, and Browne, P.R.L., 2000, Hydrothermal minerals and precious metals in the Broadlands-Ohaaki Geothermal system: Implications for understanding low-sulfidation epithermal environments: Economic Geology, v. 95, p. 971-999.
- Simmons, S. F. and Brown, K. L., 2006; Gold in Magmatic Hydrothermal Solutions and the Rapid Formation of Giant Ore Deposit: Science, v. 314, p 288-291.
- Simmons, S.F. and Brown, K.L., 2007, The flux of gold and related metals through a volcanic arc, Taupo Volcanic Zone, New Zealand. Geology, v. 35, No. 12, p. 1099-1102.
- Skinner, B.J., 1966, The system Cu-Ag-S: Economic Geology, v. 61, p. 1-26.

- Skinner B.J., White, D.E., Rose, H.J., and Mays, R.E., 1967, Sulfide associated with the Salton Sea geothermal brine: *Economic Geology*, v. 62, p. 316-330.
- Spycher N.F., and Reed M.H., 1989, Evolution of a Broadlands-type epithermal ore fluid along alternative P-T paths: Implications for the transport and deposition of base, precious, and volatile metals: *Economic Geology*, v. 84, p. 328-359.
- Stanton, R.L., 1972, *Ore Petrology*, McGraw-Hill Book company, New York, 713 p.
- Stefánsson, V., 1985, The Nesjavellir high-temperature geothermal field in Iceland: Proceedings 10th Workshop on Geothermal Reservoir Engineering. Stanford University, Stanford, California, January 22-24, SGP-TR-84, p. 23-30.
- Stefánsson A. and Seward, T. M. 2003, The hydrolysis of gold(I) in aqueous solutions to 600°C and 1500 bar. *Geochim. Cosmochim. Acta* 67, 1677–1688.
- Stefánsson, A. and Seward, T.M. 2004, Gold(I) complexing in aqueous sulphide solutions to 500°C at 500 bar: *Geochimica et Cosmochimica Acta*, v. 68, p. 4121-4143.
- Steingrímsson, B., Gudmundsson, A., Franzson, H, and Gunnlaugsson, E., 1990, Evidence of a supercritical fluid at the depth in the Nesjavellir field, Iceland: Proceedings of the 15th Workshop on Geothermal Reservoir Engineering, Stanford University Report, 36p-TR-130, p. 81-88.
- Steingrímsson, B., and Björnsson, G., 1992, Well RnG-9 at Reykjanes. Measurements in March 1992 (in Icelandic): National Energy Authority Report No BS/GrB-92/01, 5 p.
- Steingrímsson, B., and Björnsson, G., 1993, Logging of well 9 on Reykjanes in September 1993 (in Icelandic): National Energy Authority Report No BS/GrB-93/01, 10 p.
- Steingrímsson, B., and Björnsson, G., 1994. Cleaning of well 9 on Reykjanes fall 1993 (in Icelandic): National Energy Authority Report No BS/GrB-94/01, 8 p.

- Stumm, W., and Morgan, J.J., 1981, Aquatic chemistry: 2nd ed.: New York, Wiley, 780 p.
- Sugaki, A., Kitakaze, A., and Kojima, S., 1987, Bulk compositions of intimate intergrowths of chalcopyrite and sphalerite and their genetic implications: *Mineralium Deposita*, v. 22, p. 26-32.
- Sveinbjörnsdóttir, Á.E., Coleman, M.L., and Yardley, B.W.D., 1986, Origin and history of hydrothermal fluids of the Reykjanes and Krafla geothermal fields, Iceland. A stable isotope study: *Contributions to Mineralogy and Petrology*, v. 94, p. 99-109.
- Thomas, D., McKibben, M.A., and Ruiz, M.C., 1992, Sulfide scaling in Cerro Prieto geothermal wells: *Geothermal Resources Council TRANSACTIONS*, v. 16, p. 371-376.
- Thompson, G., Humphris, S.E., Schroeder, B., Sulanowska, M., and Rona, P.A., 1988, Active vents and massive sulfides at 26°N (TAG) and 23°N (Snakepit) on the Mid-Atlantic Ridge, *Canadian Minealogist*, v. 26, 697-712.
- Thorkellsson, Th., 1928, On thermal activity in Reykjanes, Iceland: *Rit Vísindafélag Íslendinga III*, 42 p.
- Thórólfsson, G., 2010, Maintenance history of a geothermal plant: Svartsengi Iceland: *Proceedings World Geothermal Congress 2010 Bali, Indonesia, 25-29 April 2010*, extended abstract.
- Thórhallsson, S., Ragnars, K., Arnórsson, S., and Kristmannsdóttir, H., 1975, Rapid scaling of silica in two district heating systems: *National Energy Authority Report OSJHD 7534*, 17 p.

- Tivey, M. K., 1995, The influence of hydrothermal fluid composition and advection rates on black smoker chimney mineralogy: insights from modeling transport and reaction: *Geochimica et Cosmochimica Acta*, v. 59, No. 10, p. 1933-1949.
- Tivey, M. K., Humphris, S. E., Thompson, G., Hannington, M. D., and Rona, P. A., 1995, Deducing patterns of fluid flow and mixing within the TAG active hydrothermal mound using mineralogical and geochemical data: *Journal of Geophysical Research*, v. 100, No. B7, p. 12527-12555.
- Tómasson, J. and Kristmannsdóttir, 1972: High temperature alteration minerals and geothermal brine, Reykjanes, Iceland: *Contributions to Mineralogy and Petrology*, v. 36, p. 123-134
- Trefry, J.H., Butterfield, D.B., and Metz, S., 1994, Trace metals in hydrothermal solution from Cleft segment on the southern Juan de Fuca Ridge: *Journal of Geophysical Research*, v. 99, p. 4925-4935.
- Truesdell, A.H., Thompson, J.M., Coplen, T.B., Nehring, N.L., and Janik, C.J., 1981, The origin of the Cerro Prieto geothermal brine: *Geothermics*, v. 10, p. 225-238.
- Tryggvason, E., 1962, Crustal structure of the Iceland region from dispersion of surface waves: *Bulletin of the Seismological Society of America* v. 52, p. 359-388.
- Tryggvason, K., E., Husebye, E.S., and Stefánsson, R., 1983, Seismic image of the hypothesized Icelandic hot spot: *Tectonophysics* v. 100, p. 97-118.
- Vaughan, D.J., and Craig, J.R., 1978, *Mineral Chemistry of the Metal Sulphides*: Cambridge, England, Cambridge University Press, Earth Science Series, 493 p.
- Verkfræðistofan Vatnaskil hf 1993, Reykjanes. Monitoring July 1992 – July 1993: National Energy Authority Report No OS-93043/JHD-23 B, 16 p.

- Verkfraedistofan Vatnaskil sf 2000, Svartsengi – Reykjanes. Monitoring July 1999 – July 2000, National Energy Authority Report No OS-2000/062, 36 p.
- Verkfraedistofan Vatnaskil 2010, Svartsengi – Reykjanes. Monitoring 2009, Report no 10.04, xx p.
- Vine, F.J. and Mathews, D.H., 1963, Magnetic anomalies over ocean ridges: *Nature*, v. 199, p. 947-949.
- Vine, F.J., 1966, Spreading of the ocean floor: New evidence: *Science*, v. 154, p. 1405-1415.
- Von Damm, K.L., 1988, Systematics of and postulated controls on submarine hydrothermal solution chemistry: *Journal of geophysical research*, v. 93, No. B5, p 4551-4561.
- Von Damm, K. L., 1990, Seafloor hydrothermal activity: Black smoker chemistry and chimneys: *Annul Rev. Earth Planet. Sci*, v. 18, p. 173-204.
- Von Damm, K.L., 1995, Controls on the chemistry and temporal variability of seafloor hydrothermal fluids, in Humphris, S.E., Zierenberg, R.A., Mullineaux, L.S., and Thomson, R.E., eds., *Seafloor Hydrothermal Systems: Geophysical Monograph 91*, American Geophysical Union, Washington, DC, p. 222-247.
- Von Damm, K.L., Edmond, J.M., Grant, B., Measures, C.I., Walden, B., and Weiss R.F., 1985, Chemistry of submarine hydrothermal solutions at 21°N, East Pacific Rise: *Geochimica et Cosmochimica Acta*, v. 49, p. 2197-2220.
- Von Damm, K.L., Bray, A.M. Bray, Buttermore, L.G., and Oosting, S.E., 1998, The geochemical controls on vent fluids from the Lucky Strike vent field, Mid-Atlantic Ridge: *Earth and Planetary Science Letters*, 160, 521-536.

- Von Damm, K.L., Lilley, M.D., Shanks, W.C., III, Brockington, M., Bray, A.M., O'Grady, K.M., Olson, E., Graham, A., Proskurowski, G., and the SouLEPR Science Party, 2003, Extraordinary phase separation and segregation in vent fluids from the southern East Pacific Rise: *Earth and Planetary Science Letters*, v. 206, p. 365-378.
- Walker, G.P.L., 1959, Geology of the Reydarfjörður area eastern Iceland: *Quarterly Journal of the Geological Society of London*, v. 114, p. 367-393.
- Walker, G.P.L., 1960, Zeolite zones and dike distribution in relation to the structure of the basalts of eastern Iceland: *Journal of Geology*, v. 68, p. 515-528.
- Walker, G.P.L., 1963, The Breiddalur central volcano eastern Iceland: *Quarterly Journal of the Geological Society of London*, v. 119, p. 29-63.
- Walker, G.P.L., 1974, The structure of eastern Iceland, in L. Kristjánsson, ed., *Geodynamics of Iceland and the North Atlantic Area*: D. Reidel, Dordrecht, p. 177-188.
- Weir, N.R.W., White, R.S., Brandsdóttir, B., Einarsson, P., Shimamura, H., Shiobara, H., Darbyshire, F., Smallwood, J., Staples, R., Gunnarsson, G., Hjörleifsdóttir, Jónsdóttir, K., Mochizuki, M., and Nakanishi, A., 2001, Crustal structure of the northern Reykjanes Ridge and Reykjanes Peninsula, Southwest Iceland: *Journal of Geophysical Research*, v. 106, p. 6347-6368.
- Wilson, J.T., 1963, Continental drift: *Scientific American*, v. 208, p. 86-100.
- Zierenberg, R. A., Fouquet, Y., Miller, D.J., and Shipboard Scientific Party, 1998, The deep structure of a sea-floor hydrothermal deposit: *Nature*, v. 392, no. 6675, p. 485-488.

Appendices

Appendix 2.1

2.1.1 Well logging in RN-9 September 1993 and October 2004

In June 1993 the orifice plate in well RN-9 was changed from an opening of 115 mm to 150 mm. As a result, the well head pressure dropped from 28 bars to 20 bars, and this large pressure decrease led to abundant scaling in the well. The wellhead pressure then started to decrease by 1 bar per month from July 1993. During a stop in production in September, 1993, the well diameter was measured by sinkers of variable diameter (also referred to as a Go-devil). In these simple diameter measurements a sinker with known diameter descends into the well to gauge the minimum inside diameter of the well and identify the depth where the sinker bar stops due to an obstruction. This is followed by measurements with a smaller sinker. The results are shown in Table A2.1 and in Figure A2.1.

Table A2.2 shows pressure and corresponding temperature (°C) in the well. All pressures referred to are gauge (g) pressure, which is 0 at atmospheric pressure, unless otherwise noted (e.g., absolute, which is gauge plus 1 bar). The well diameter was reduced up to 50% at 567 m depth (Steingrímsson and Björnsson, 1993). An attempt was made to clean the well with a drill rig, but due to technical problems the well was only cleaned to 552 m depth (Steingrímsson and Björnsson, 1994).

Table A2.1. Measured diameter of well RN-9 in 1983 when new, and 10 and 20 years later

Date	Well Pipe			
	Well length (m)		Pipe thickness (")	Inside dia-meter (mm)
1983	525	13.375	0.55	312
Slotted liner 1983	from 503	9.625	0.45	222
1993	498	13.375	0.55	190
1993	567	9.625	0.45	150
2003	505	9.625	0.45	205
2003	506	9.625	0.45	<40

Note Temperature and pressure instruments are ~32 mm (1 1/4") in diameter. Data from Steingrímsson and Björnsson, 1993, 1994; Hjartarson, 2004

Table A2.2. Pressure and corresponding temperature for water at saturated vapor pressure

Pressure bar-g	Pressure bar-a	Temperature °C
48	49	263.0
47	48	262.0
46	47	260.0
45	46	258.7
44	45	257.4
43	44	256.0
42	43	254.7
41	42	253.2
40	41	251.8
39	40	250.3
38	39	248.8
37	38	247.3
36	37	245.8
35	36	244.2
32	33	239.2
31	32	237.5
30	31	235.7
28	29	232.0
27	28	230.0
26	27	228.0
25	26	226.0
24	25	224.0
23	24	222.0
22	23	219.6
20	21	214.9
19	20	212.4
15	16	201.5
13	14	195.0
12	13	191.6
11	12	188.0
10	11	184.1
9	10	179.9
6	7	165.0
5	6	159.0

Keenan et al., 1969

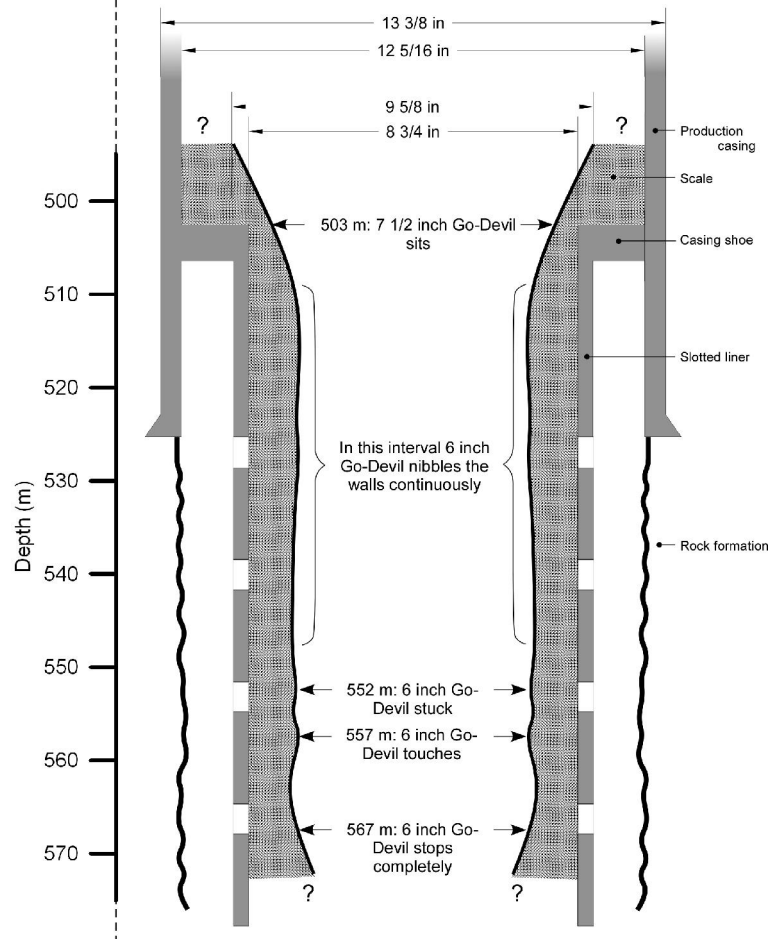


Figure A2.1 Well RN-9, 28 September 1993 profile of scales, from surface to 600 m depth (Modified from Steingrímsson and Björnsson 1993). For more detail see A2. 1.

As the fluid ascends in the well its starts to boil due to pressure release (equation 2.1, Figure A2.2). The boiling in the system depends on height of the overlying column of water (h), the density of water ($\rho(w)$) at the boiling point and the acceleration due to gravity (g). Dissolved gas leads to an increase in the boiling point depth for a given temperature, whereas salinity decreases the boiling point depth (Henley et al., 1984).

$$dP/dh = \rho(w)g \quad (2.1)$$

Temperature and pressure measurements from well RN-9 were few, since the wellhead pressure (WHP) was high and the instrument did not work well at high pressure and temperature, and was also affected by the high salinity. To determine where boiling (also

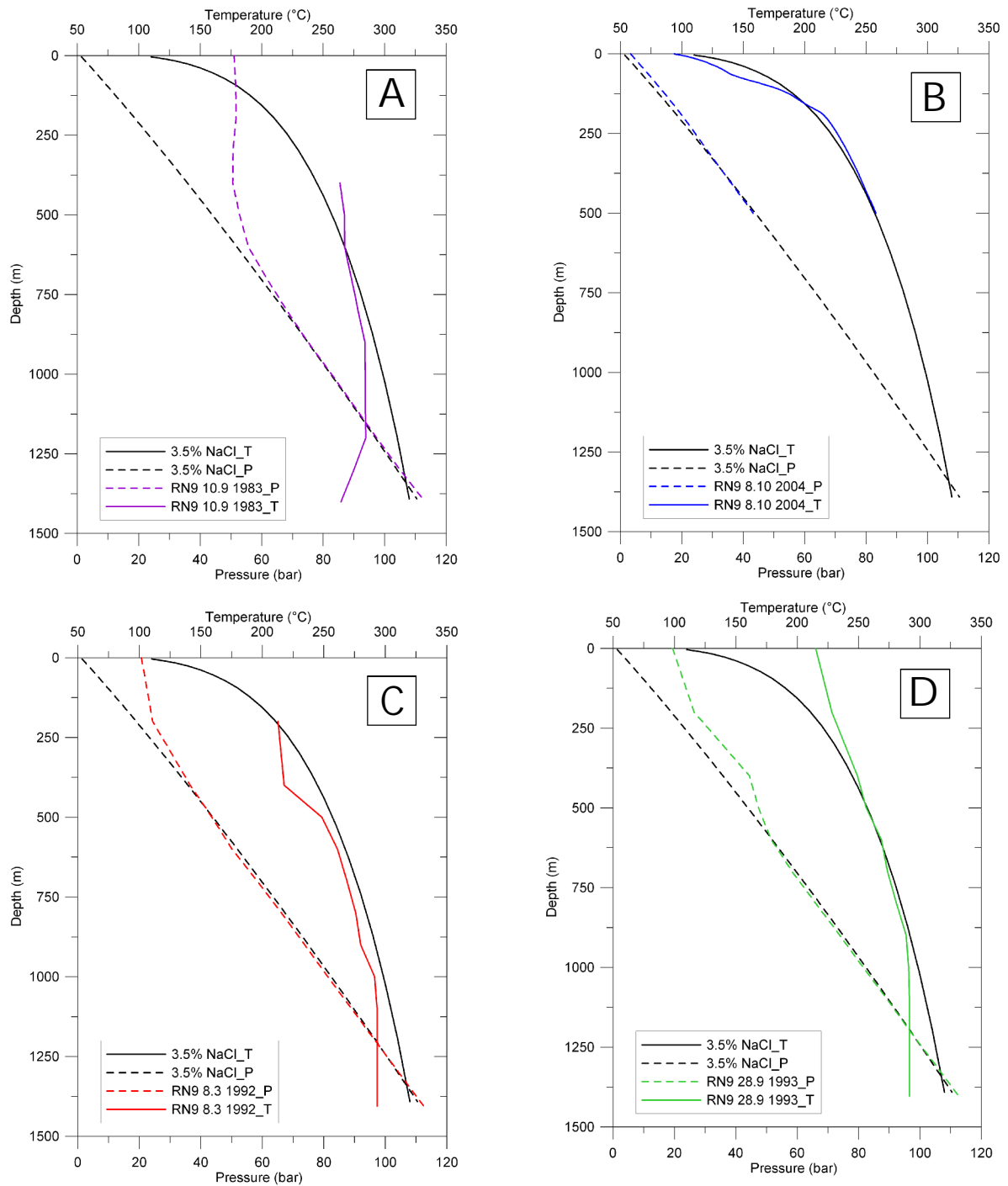


Figure A2. 2. Well logging of RN-9; temperature (solid line in color, upper x-axis) and pressure measurements (broken line in color, lower x-axis) compared to boiling-point curves (black lines) for seawater (3.5 wt.% NaCl, Haas, 1971). The boiling-point curves for seawater are calculated at atmospheric pressure, meaning ~0 wellhead pressure. (A) 31 May 1983, (B) 10 September 1983, (C) 8 March 1992, (D) 28 September 1993. See text for further explanation.

called flashing) begins in a well, the well must be logged in a dynamic state (i.e., it has to be discharging). The best results are when both pressure and temperature logs are measured at the same time. Björnsson et al. (1993) have simulated the physical conditions in the well and determined that boiling would start at about 1000 m depth when the flow rate is 80 kg/s and wellhead pressure is 30 bars absolute, whereas when the flow rate is lower (30 kg/s) and the wellhead pressure is higher (43 bar absolute), boiling will not begin until 670 m depth. Figure A2.2 shows the measurements in which both pressure and temperature was logged at the same time. For comparison, the boiling curve for 3.5 wt% NaCl seawater is shown, assuming a 1 bar absolute WHP (i.e., 0 bar gauge); this has not been corrected for actual WHP at the time of measurement.

The first measurement was done in 31 May 1983 (Figure A2.2A) while the well was heating up after drilling, with 1 bar absolute WHP; the water level was at 32 m depth. The pressure log indicates a hydrostatic pressure profile from the water surface to the bottom of the well. The pressure profile at all depths was below the boiling pressure depth curve (BPD curve) for water level at surface (0 m, i.e., there was no boiling). The temperature log started at 200 m and also plots below the BPD curve. The highest temperature was 260°C.

The second logging was done from 10 September 1983 (Figure A2.2A, b). The well was closed during logging, with WHP =50 bars. The pressure log shows that boiling started above 800 m depth. The temperature log, which started at 400 m depth, shows that the highest temperature was about 280°C at a feed-zone at 1200 m. Another temperature measurement was made shortly after the discharge test and shows a temperature of 295°C from 1400 to 1000 m depth and wellhead temperature of 255°C (Figure A2.2).

The third logging took place nine years later, on 8 March 1992 (Figure A2.2C). RN-9 had been under production for several years but was closed a day before the pressure and temperature logs. The shut-in pressure was 45-50 bars but the well was put on bleed and the WHP decreased to 26 bars when the logging started the next day, and decreased to 20 bars at the end of the logging operation. The well continued on bleed after the logging and the WHP continued to drop. It was 12.4 bars on March 9 (Steingrímsson & Björnsson, 1992). The pressure log indicates boiling above about 400 m depth. The temperature log shows a maximum temperature of 290°C.

The fourth complete logging (pressure and temperature) was done on 28 September 1993 (Figure A2.2). The well was closed on 24 September and one hour later the WHP was 32 bars. Six hours after closing the well the WHP was 29 bars (on bleed?). The well diameter was measured with logging baskets, which showed that the diameter had been reduced by 50 % at 567 m depth (Figure A2.1). The pressure log shows that conditions were unstable (some boiling) between 400 and 600 m depth (Steingrímsson and Björnsson, 1992). The temperature log (Figure A2.2) shows temperature close to boiling above 900 m depth.

Comparisons between the 1983 and the 1992 and 1993 logs show no pressure decline due to production, whereas the well appears to have cooled by about 4-5°C, from the highest measured temperature (295 to 290°C) at ~1400 m depth. The accuracy with the Kuster tool at that time was $\pm 3^\circ\text{C}$ but since 2004 the accuracy has been $\pm 0.1^\circ\text{C}$ (Hjartarson, 2004). The well was drilled out in late 1993, as discussed in main text.

2.1.2 The Orifice plate and the fluid flow control valve (the cone)

An orifice plate is a steel plate with a circular opening which controls the fluid flow from the well (Figure A2.3). In well RN-9 the thickness of the plate was 2 cm (G. Thórólfsson, pers. commun., 2009). To change the fluid flow, orifice plates with

different diameter openings are inserted in the flow line. Upstream of the orifice plate is the wellhead, and the opening in the orifice plate controls the wellhead pressure (WHP). The wellhead for well RN-9 was located ~14 m upstream of the orifice plate, but for the new wells it is ~3 m. When the fluid flows through the orifice plate, the fluid flows faster through the opening than in the upstream pipe, and therefore the pressure decreases after the orifice plate (according to Bernoulli's principle), with a concomitant temperature decrease according to the saturated water vapor pressure. The sudden decrease in pressure and temperature results in flashing of the fluid, referring to the very vigorous boiling that occurs (Henley et al., 1984). This phase separation and temperature decrease leads to precipitation of minerals and/or amorphous phases in the opening and on the downstream side of the

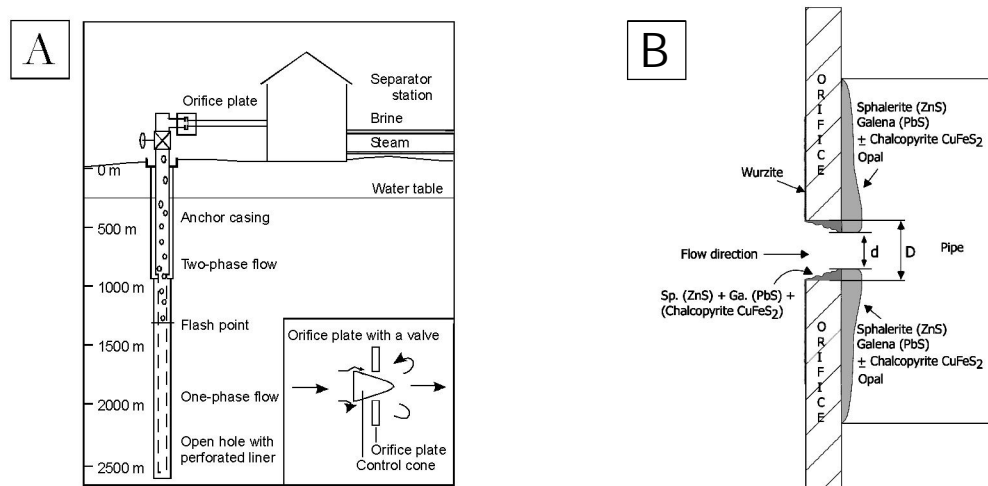


Figure A2.3. (A) Schematic model of geothermal wells in the Reykjanes geothermal system, showing the approximate location of initial boiling (flash point) of ascending seawater-dominated liquid, which occurs at depths of 900-1000 m (RN-9) to ~1250 m. Above the level that boiling starts, flow in the well consists of vapor + liquid. The inset shows the fluid flow-control valve (cone; Fig. 3A) inserted in the orifice plate immediately downstream of the wellhead in the newer wells (RN-10 to RN-24), where flashing (extensive boiling) is caused by a sharp decrease in pressure (from 40 to 22 bars as the fluid passes the narrow orifice plate) over a distance of a few cm. (B) Cross section of an orifice plate showing the scales and their locations.

orifice plate (Figure A2.3). Note that the precipitation in the opening of the orifice plate reduces the diameter and therefore causes more pressure drop downstream of the orifice plate. With time and depending on the pressure, scales also precipitate in the pipeline upstream of the orifice plate as well as on the upstream side of the orifice plate.

Appendix 2.2

Scale samples from boreholes used in this PhD work were collected by various colleagues at various times when the wells were tested before utilization and/or during maintenance break. The majority of the samples are from RN-9 from the cleaning of the surface pipeline in 2000 and were collected by the author but samples from other times were collected by various colleagues. Samples from downhole RN-22 were collected by workers of the Sudurnes heating company late summer 2009. Samples from 10, 11, 12, 13, 14, 15, 18, 21, 22, 23 and 24 were collected by author. Many of the samples were cleaned out from the pipeline by a high-pressure water pump and other with hammer and chisel. The samples weighed from <5 g up to few kg.

Mineral identification and textural features were documented using an XRD (X-ray diffraction) instrument at ISOR and Scanning electron microscope at Innovation Center Iceland, and petrographic microscope at the University of Ottawa, and electron microprobe at Carleton University.

2.2.1 Microprobe analyses

Mineral analyses were performed on a four-spectrometer wavelength dispersive CAMECA Camebax Electron Microprobe at Carleton University, Ottawa. Overlap corrections were performed using the PAP procedure. Calibrations were checked by analyzing known standards.

Sulfides were analyzed at 20 kV and 30 nA with counting times of 10 seconds. Elements analyzed were V, Mn, Fe, Co, Ni, Cu, Zn, Ge, As, Se, Ag, Cd, Sb, Te, Au, Hg, Pb, Bi and S. Pure elements (V, Mn, Co, Ge, Te, Sb, Ag, Au) and simple compounds (FeS, CuS, CdS, NiAs, BiSe, HgTe, PbS, ZnS) were used as standards.

Note that most of the grains analyzed were extremely small (< 2 μm), i.e., smaller than

the diameter of the electron beam (2 to 3 μm diameter) or closely intergrown with another phase (e.g., bornite-digenite) which causes contamination of the analyses with the surrounding material. Some analyses like in sample 12RN have low totals, either due to high levels of Ca or due to charging of the sample surface which leads to uneven current distribution and low totals. Detection limits were 0.01 wt% for most measured elements.

Oxides were analyzed at 20kV accelerating voltage, 25 nA beam current, focused beam \sim 2-3 microns in diameter. Counting times 10 to 20 seconds per element or 40,000 accumulated counts. Element analyzed (standard); Si (CaSiO_3); Ti (synthetic MnTiO_3); Al (synthetic MgAl_2O_4); Cr (Cr_2O_3); V (V); Fe (synthetic FeTiO_3); Mn (synthetic MnTiO_3); Ni (synthetic NiO), Co (Co), Zn (ZnAl_2O_4); Mg (MgAl_2O_4), and, Ca (CaSiO_3).

Sulfides and were analyzed at 20kV accelerating voltage, 30 nA beam current, focused (2 micron diameter). Counting times were 10-20 seconds or 40,000 accumulated counts. Element analyzed (standard): S (synthetic Fe_{1-x}S); Fe (synthetic Fe_{1-x}S); Mn (synthetic MnS); Co (Co); Ni (synthetic NiAs); Cu (synthetic CuFeS_2); Zn (synthetic ZnS); V (V); Ga (GaAs); Ge (Ge); As (synthetic NiAs); Se (Bi_2Se_3); Ag (Ag); Cd (CdS); In (InP); Sn (Sn); Sb (Sb_2S_3); Te (Te); Au (Au); Hg (HgS); Pb (PbS); and Bi (Bi_2Se_3).

Digital BSE (back-scattered electron) images were collected with an Electron Optic Services digital imaging system at 512 x 512 pixel resolution with a Lamont 4 element solid state BSE detector and BSE Quad Summing Amplifier interfaced to a 4Pi Analysis Inc. digital imaging and EDX X-ray system and Power Macintosh computer.

2.2.2 Bulk chemical analyses

Bulk samples were analyzed by Activation Laboratories Ltd. (ActLabs, <http://www.actlabs.com/>) for major and trace elements by a variety of methods including INAA, XRF,

ICP-ES, and ICP-MS. Instrumental Neutron Activation Analysis (INAA) is a non-destructive trace element technique, capable of measuring up to 35 elements at the ppb to percent level in most materials. The sample is bombarded by neutrons from a nuclear reactor, producing new, radioactive isotopes as they interact with atoms in the sample. The new isotopes decay fast and emit gamma rays in the process. Measuring the radiation enables identification of elements and determination of their concentration. Neutron activation is generally most useful for trace elements such as the rare earths, the platinum group elements, and other heavy elements. Sample preparation for INAA is simple, the method is free from matrix effects and has an unmatched long-term instrument stability (Hoffman, 1992).

The Inductively Coupled Plasma (ICP) technique relies on placing the sample material into solution using mixed acids and fusion techniques with a variety fluxes. Fusion involves melting the sample at high temperature. Flux was typically added (e.g., Na_2O_2) to promote fusion, and the resulting fused material was then dissolved using a multiacid digestion. The sample solution is then introduced into radio frequency excited plasma ($\sim 8000^\circ\text{K}$). Atoms within the samples are excited to the point that they emit wavelength-specific photons which are characteristic of particular elements. The number of photons produced is directly related to the concentration of that element in the sample. A sample solution is nebulized into flowing carrier gas, usually argon, and passed through a coil where electric current produces oscillating magnetic field, which in turn sets up electric current in the support gas.

Inductively Coupled Plasma Optical Emission Spectrometry (ICP-OES) is used for analysis of a variety of major and minor elements to ppm and ppb levels. The major rock forming elements and some important trace elements can be determined simultaneously (SiO_2 , Al_2O_3 , CaO , Na_2O , MnO , MgO , Ti , V , Zn , Cu , Pb , Be , P , Sr , Ba , Zr).

Inductively coupled plasma mass spectrometry (ICP-MS) is used for analysis of selected trace elements at very low concentrations (Rb, Cs, Mo, Ga, Bi, Sn, U, Th, Y, La, Ce, Pr, Nd, Sm, Eu, Gd, Tb, Dy, Ho, Er, Tm, Yb, Lu). The detection limit for most elements in solution is in the sub-ppb range. The ICP-MS instrument employs ICP and a quadrupole mass spectrometer to detect the ions produced. The positive ions in the plasma are focused down a mass spectrometer where they are separated according to mass and counted.

Loss of Ignition (LOI) was determined by measuring the loss of volatiles in a sample when heated. The sample is kept at elevated temperature until the mass remains stable. The volatiles in a mineral sample consists of “combined water” (hydrates and hydroxy-compounds) and carbon dioxide from carbonates.

Analytical precision and accuracy by Actlabs is provided by analysis of reference standards (for accuracy), certificated standards, duplicates (for precision) and blanks. The company analyzes up to 25 reference standards, with every 5th sample being a duplicate; blanks are every 25th sample or so.

2.2.3 X-Ray diffraction (XRD analysis at ISOR)

XRD was used to provide information about the mineralogical makeup of solid samples as well potentially the crystallographic structure of its phases. Generally XRD will only provide an estimate of phases present and usually 2-5% of that phase must be present to be detectable. The samples were ground in a mortar, placed and packed in a PMMA sample holder and measured from $2\theta=2^\circ$ to $2\theta=70^\circ$ (parameter file malmur.dq1). Measurement times were 1 second and step size was 0.04° . A Bruker AXS, D8 Focus diffractometer was used, with Ni-filtered Cu $k\alpha$ radiation at 1.54 \AA wavelengths at 40 mA and 40 kV with fixed 1° slits and NaI scintillation counter, with 0.2 mm detector slit. Reference patterns were obtained from ICDD, PDF-2, Release 2007.

Table A2.3 Brief description of sample treatment and analytical methods

	Sample treatment ¹⁾	Method ²⁾	Brief description	Standard	Detection limit
pH	Ru	Electrometric	A glass electrode in combination with a reference potential is inserted into the sample and pH and temperature values recorded	Merck Titrisol. pH 4, 7, 10	(±0.1 pH unit)
CO ₂ (t)	Ru	Electrometric	Determined by titration with 0.1N HCl from pH=8.2 to pH=3.8	Merck Titrisol. pH 4, 7, 10	1 ppm
H ₂ S	Ru	Titration	Determined by titration with 0.001M Hg(CH ₃ COO) ₂ solution and dithizone indicator		30 ppb
Conductivity	Ru	Bridge	Specific conductance is measured using a Wheatstone type bridge using temperature compensation to 25°C	KCl	
TDS	Fu	Weighing	Weighing the residue after evaporating a known weight of sample		
O ₂ dissolved	Ru	Chemet kit	Measured with Chemét test kit, based on reaction with rhodazine or indigocarmin		1 ppb
SiO ₂	Ru/Rd	SPH	Measured spectrophotometrically as yellow silicomolybdate complex or reduced molybdenum blue complex	Icelandic water standard	0,5 ppm
B	Fu	SPH	Sample is complexed with azomethine-H and measured spectrophotometrically	Merck Titrisol H ₃ BO ₃ /H ₂ O	30 ppb
Na	Fa	AAS-DA	A small amount of Cs solution is added and the sample directly aspirated into an oxidizing air-acetylene flame. Absorbtion read at 589.6 nm	Merck Titrisol NaCl / H ₂ O	10 ppb
K	Fa	AAS-DA	A small amount of Cs solution is added and the sample directly aspirated into an oxidizing air-acetylene flame. Absorbtion read at 766.5 nm	Merck Titrisol KCl / H ₂ O	10 ppb
Mg	Fa	AAS-DA	A small amount of La solution is added and the sample directly aspirated into an oxidizing air-acetylene flame. Absorbtion read at 285.2 nm	Merck Titrisol MgCl ₂ / HCl	1 ppb
Ca	Fa	ASS-DA	A small amount of La solution is added and the sample directly aspirated into an oxidizing air-acetylene flame. Absorbtion read at 422.7 nm	Merck Titrisol CaCl ₂ / HCl	10 ppb
F	Fu	IC	Anions from a small volume of sample are separated by means of a guard column, a separator column and a suppressor column. F determined using a conductivity detector	Merck Titrisol NaF/H ₂ O	20 ppb
Cl	Fu	IC	Anions from a small volume of sample are separated by means of a guard column, a separator column and a suppressor column. Cl determined using a conductivity detector	Merck Titrisol HCl/H ₂ O	25 ppb

Table A2.3 Continued

Sample treatment ¹⁾	Method ²⁾	Brief description	Standard	Detection limit
NO ₃	IC	Anions from a small volume of sample are separated by means of a guard column, a separator column and a suppressor column. NO ₃ determined using a conductivity detector	Merck Titrisol NaNO ₃ /H ₂ O	100 ppb
SO ₄	IC	Anions from a small volume of sample are separated by means of a guard column, a separator column and a suppressor column. SO ₄ determined using a conductivity detector	Merck Titrisol H ₂ SO ₄ /H ₂ O	50 ppb
Al	AAS-GF	Dried 30 s 125°C, ashed 30 s 1500°C, atomized 3 s 2400°C. Purge gas Ar. 309.3nm	Merck Ni(NO ₃) ₃ 0.5M HNO ₃	1 ppb
Cr	AAS-GF	Dried 30 s 125°C, ashed 30 s 1200°C, atomized 3 s 2300°C. Purge gas Ar. 357.9 nm	Merck Cr(NO ₃) ₃ 0.5M HNO ₃	0.1 ppb
Mn	AAS-GF	Dried 30 s 125°C, ashed 30 s 1000°C, atomized 2 s 1900°C. Purge gas Ar. 279.5nm. Aspiration directly into flame.	Merck Mn(NO ₃) ₂ 0.5M HNO ₃	0.1 ppb
Fe	IC	Dried 30 s 125°C, ashed 30 s 1200°C, atomized 2 s 2000°C. Purge gas Ar. 248.3nm. Aspiration directly into flame.	Merck Fe(NO ₃) ₂ 0.5M HNO ₃	0.1 ppb
Cu	AAS-GF	Dried 30 s 125°C, ashed 30 s 900°C, atomized 2 s 2000°C. Purge gas Ar. 324.7nm	Merck Cu(NO ₃) ₂ 0.5M HNO ₃	0.1 ppb
Zn	AAS-GF-DA	Dried 30 s 125°C, ashed 30 s 400°C, atomized 2 s 1000°C. Purge gas Ar. 213.9nm. Aspiration directly into flame.	Merck Zn(NO ₃) ₂ 0.5M HNO ₃	0.1 ppb
As	AAS-HG	As is reduced and converted to AsH ₃ using NaBH ₄ . The hybrid is swept into a cell placed in the beam of an As EDL lamp and As determined at 193.7 nm	Merck HgAsO ₄ 0.5M HNO ₃	0.1 ppb
Cd	AAS-GF	Dried 30 s 125°C, ashed 30 s 700°C, atomized 10 s 2000°C. Purge gas Ar. 228.8nm	Merck Cd(NO ₃) ₂ 0.5M HNO ₃	0.05 ppb
Hg	AAS-FI	Hg is reduced and converted to HgH ₂ with NaBH ₄ . The hydride is swept into a cell placed in the beam of an Hg EDL lamp and the atomic absorption determined at 253.7 nm	Merck Hg(NO ₃) ₂ 0.5M HNO ₃	0.005 ppb
Pb	AAS-GF	Dried 30 s 125°C, ashed 30 s 750°C, atomized 2 s 2000°C. Purge gas Ar. 283.3nm	Merck Pb(NO ₃) ₂ 0.5M HNO ₃	0.1 ppb
Ni	AAS-GF	Dried 30 s 125°C, ashed 30 s 1000°C, atomized 3 s 2300°C. Purge gas Ar. 232.0 nm	Merck Ni(NO ₃) ₂ 0.5M HNO ₃	1 ppb

¹⁾ Ru, raw untreated sample; Rd, raw diluted sample; Fu, filtered with 0.45µ or 0.22µ Membrane filter, untreated sample; Fa, filtered, acidified sample, ²⁾ AAS, Atomic absorption spectroscopy; DA, direct aspiration; GF, Graphite furnace; HG, Hydride generation; FL, Flameless; IC, Ion chromatography, SPH, Spectrophotometer; Cs solution, cesium solution added to prevent ionic disturbances.

Table A2.4. Fractionation of samples from high-enthalpy well; field treatment and elements to be determined

Phase	Treatment	Specification	To determine
vapour	None; amber glass bottle	Ru	$\delta^2\text{H}$, $\delta^{18}\text{O}$
	0.5 ml 0.2 M ZnAc_2 added to sample in 100 ml volumetric glass flask to precipitate sulphide	Rp	SO_4
	None	Ru	Anions
	0.8 ml conc. HNO_3 (Suprapur) added to 200 ml sample	Ra	Cations
	Added to 50 ml 40% NaOH in evacuated doubleport bottle	Gas sample, Ai	CO_2 , H_2S in NaOH, residual gases in gas phase, $\delta^{34}\text{S}$ in H_2S in
Liquid	None	Ru	Mg, SiO_2 if < 100 ppm
	Dilution; 10 ml of sample added to 90 ml of distilled, deionized water	Rd (1:10)	SiO_2 if > 100 ppm
	None; amber glass bottle with ground glass stopper	Ru	pH, CO_2 , H_2S (if not in field)
	Filtration	Fu	Anions
	Filtration; 2 ml 0.2 M ZnAc_2 added to sample in 100 ml volumetric glass flask and ≥ 10 ml to ≥ 500 ml bottle containing ≥ 25 mg SO_4 to precipitate sulphide	Fp, Fpi	SO_4 , $\delta^{34}\text{S}$ and $\delta^{18}\text{O}$ in SO_4
	Filtration; 160 ml and 2 1000 ml amber glass bottle, with ground glass stoppers	Fui, Fuc, Fut	$\delta^2\text{H}$, $\delta^{18}\text{O}$, ^{13}C , ^3H
	Filtration; 0.8 ml conc. HNO_3 (Suprapur) added to 200 ml sample	Fa	Cations

2.2.4 Chemical analyses of water samples (at ISOR)

Sampling of a two-phase flowing geothermal well requires advanced sampling skills and the appropriate sampling equipment. A detailed description of the methods used is given by Ármannsson and Ólafsson (2006). Samples were collected at well head (Figs, A2.4). The various samples collected are described in Tables A2.3 and A2.4 with the procedure summarized in Figure A2.5

The samples were collected using a Webre separator (Figure A2.4) to separate vapor and liquid (Ármannsson and Ólafsson, 2006). Both phases were cooled to ambient temperature in a cooling coil and the samples treated according to the instruction from the laboratory (Tables A2.3 and A2.4). The major elements analyzed at ISOR, treatment when sampled, standard analytical methods, and a brief description of the analytical methods and detection limits are given in Tables A2.3 and A2.4.

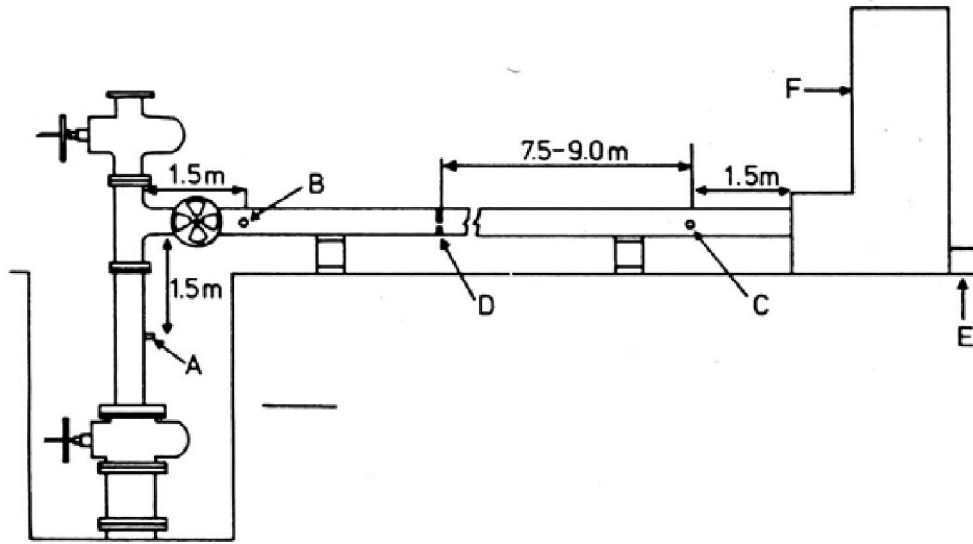


Figure A2.4. Drawing of geothermal well. A, B, and C are sample points; D, a back pressure plate or valve; F, silencer; E, weir box (Ellis and Mahon, 1977).

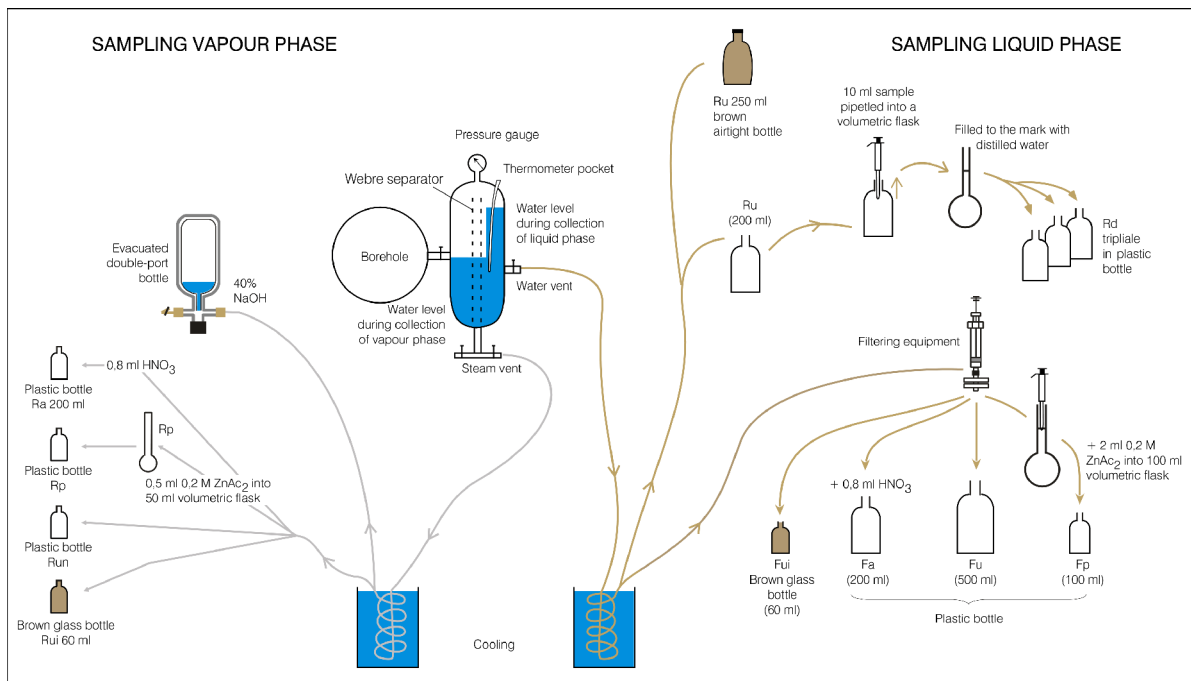


Figure A2.5. Treatment of sub-samples from two-phase geothermal wells (Ármansson and Ólafsson, 2006).

Appendix 2.3

Table A2.5. Composition of sphalerites upstream (group 1, 40 bar) and downstream (group 2, 11 bar) of the orifice plate in well RN-09

Sample #	Group	Zn	Fe	S	Se	Cu*	Cd	Mn	Co	Pb	As	Ni	Sb	Te	total	FeS* mole%	ZnS mole%	S/ (Fe+Zn)	
Wellhead, pressure range 47-15 bar																			
9RN5_2005G	1	61.47	5.00	32.99	0.05	1.26	0.40	0.07	<0.01	0.26	<0.01	<0.01	<0.01	0.01	101.5	6.97	93.00	1.00	
9RN5_2005	1	64.49	3.17	32.17	0.04	0.89	0.02	0.05	0.03	<0.01	<0.01	<0.01	0.01	0.03	100.9	4.20	95.84	0.96	
9RN5_2005	1	64.62	3.36	32.11	0.09	0.56	0.03	0.05	<0.01	<0.01	0.02	0.03	<0.01	<0.01	100.9	5.00	95.00	0.96	
9RN5_2005	1	62.46	3.61	32.84	0.07	1.53	0.06	0.10	0.01	0.30	<0.01	<0.01	0.03	0.01	101.0	4.06	95.93	1.00	
9RN5_2005G	1	63.21	3.51	33.61	0.09	0.60	0.14	0.05	<0.01	0.09	<0.01	<0.01	0.01	<0.01	101.3	5.20	94.76	1.00	
9RN09_2001	1	62.36	3.02	32.29	0.09	0.24	0.16	0.05	<0.01	0.03	0.01	<0.01	<0.01	0.03	98.3	5.01	94.99	1.00	
9RN09_2001	1	63.45	2.76	32.09	0.07	0.19	0.07	0.06	0.01	0.01	<0.01	<0.01	0.01	0.02	98.7	4.57	95.43	0.98	
9RN1_2005G	1	58.12	7.54	33.71	0.03	0.37	0.22	0.13	0.01	0.21	<0.01	0.01	<0.01	0.03	100.4	12.69	87.31	1.03	
9RN1_2005G	1	62.29	4.03	32.44	0.06	0.65	0.16	0.07	<0.01	0.61	<0.01	<0.01	<0.01	<0.01	100.3	6.11	93.89	0.99	
9RN1_2005G	1	62.57	3.06	32.64	0.07	0.22	0.05	0.08	0.03	0.25	<0.01	0.02	<0.01	<0.01	99.0	5.09	94.91	1.01	
Upstream of the orifice plate, pressure range 47-15 bar																			
9RN20_2000	1	61.03	4.68	31.79	0.10	2.68	0.08	0.07	0.02	0.05	<0.01	0.01	<0.01	<0.01	100.5	4.27	95.73	0.97	
9RN20_2000	1	65.25	3.40	32.46	0.05	1.01	<0.01	0.05	0.02	<0.01	0.02	0.01	<0.01	<0.01	102.3	4.32	95.68	0.96	
9RN20_2000	1	65.25	3.56	32.87	0.05	1.11	0.03	0.03	0.01	<0.01	<0.01	<0.01	<0.01	<0.01	102.9	4.43	95.57	0.97	
9RN20_2000	1	62.40	3.17	31.17	0.11	0.58	0.06	0.04	0.01	<0.01	<0.01	<0.01	<0.01	0.03	97.6	4.76	95.24	0.96	
9RN20_2000	1	64.53	3.17	32.91	0.02	0.58	0.04	0.03	<0.01	<0.01	<0.01	<0.01	<0.01	<0.01	101.3	4.61	95.39	0.98	
9RN20_2000	1	63.67	3.07	32.58	0.08	0.90	0.10	0.04	<0.01	0.02	0.01	0.01	<0.01	0.03	100.5	4.02	95.98	0.99	
9RN20_2000	1	61.94	4.78	32.87	0.09	3.27	0.05	0.04	<0.01	0.03	<0.01	0.01	<0.01	0.01	103.1	3.48	96.52	0.99	
9RN21_2000	1	61.92	3.12	33.52	0.02	0.03	<0.01	0.05	<0.01	<0.01	<0.01	<0.01	<0.01	<0.01	98.7	5.53	94.47	1.04	
9RN21_2000	1	63.03	3.43	33.38	0.06	1.35	0.10	0.02	<0.01	0.45	0.03	0.01	<0.01	0.01	101.9	4.00	96.00	1.02	
9RN21_2000	1	64.46	2.88	33.55	0.12	0.20	0.03	0.07	<0.01	<0.01	<0.01	0.02	<0.01	0.01	101.3	4.68	95.32	1.01	
9RN21_2000#	1	62.90	3.93	33.52	0.08	0.51	0.15	0.06	<0.01	0.01	<0.01	0.01	0.02	<0.01	101.2	6.09	93.91	1.01	
9RN21_2000#	1	63.25	3.46	33.36	0.13	0.35	0.07	0.07	0.02	0.16	<0.01	0.03	<0.01	<0.01	100.9	5.52	94.48	1.01	
9RN21_2000	1	64.32	2.85	33.32	0.08	0.31	0.08	0.06	<0.01	<0.01	<0.01	0.01	0.03	<0.01	101.1	4.48	95.52	1.00	
9RN21_2000	1	63.83	3.47	33.58	0.10	0.36	0.03	0.03	0.01	<0.01	<0.01	<0.01	0.02	0.03	101.5	5.47	94.53	1.01	
9RN21_2000	1	64.43	3.03	33.56	0.04	0.44	0.04	0.05	<0.01	0.30	0.01	<0.01	0.01	<0.01	101.9	4.58	95.42	1.01	
9RN21_2000	1	64.64	2.63	33.34	0.06	0.21	0.09	0.08	0.01	<0.01	<0.01	<0.01	<0.01	<0.01	101.1	4.24	95.76	1.00	
9RN21_2000	1	63.75	3.33	33.33	0.09	0.64	0.07	0.09	<0.01	<0.01	0.05	<0.01	<0.01	<0.01	101.4	4.84	95.16	1.01	
9RN21_2000	1	64.77	2.94	33.21	0.12	0.07	0.15	0.04	0.01	<0.01	<0.01	<0.01	<0.01	<0.01	101.3	4.95	95.05	0.99	
9RN21_2000	1	64.99	2.66	33.32	0.02	0.05	0.11	0.09	<0.01	<0.01	<0.01	<0.01	<0.01	0.01	101.3	4.50	95.50	1.00	
9RN21_2000	1	64.22	2.93	33.17	0.03	0.10	0.03	<0.01	<0.01	0.08	<0.01	0.01	0.03	0.02	100.6	4.93	95.07	1.00	

Table A2.5 Continued

Sample #	Group	Zn	Fe	S	Se	Cu*	Cd	Mn	Co	Pb	As	Ni	Sb	Te	total	FeS*	ZnS	S/ (Fe+Zn)	
		wt%	wt%	wt%	wt%	wt%	wt%	wt%	wt%	wt%	wt%	wt%	wt%	wt%		mole%	mole%		
9RN21C_2000#	1	64.32	2.53	33.39	0.01	0.08	0.11	0.07	0.01	<0.01	<0.01	<0.01	0.03	0.02	100.6	4.29	95.71	1.01	
9RN21C_2000#	1	63.62	2.58	33.56	0.07	0.21	0.06	0.07	<0.01	<0.01	<0.01	0.01	0.03	<0.01	100.2	4.22	95.78	1.03	
9RN21C-2000	1	65.29	2.56	33.45	0.05	0.16	0.07	0.05	0.02	<0.01	0.08	<0.01	<0.01	<0.01	101.7	4.16	95.84	1.00	
9RN21C-2000	1	64.97	2.63	32.75	0.11	0.06	0.06	0.09	<0.01	0.18	0.01	<0.01	<0.01	<0.01	100.9	4.44	95.56	0.98	
Bend three and downstream of it, pressure ~11 bar																			
9RN1_2004_2	2	62.62	3.44	32.90	0.09	0.02	0.21	0.07	<0.01	0.03	<0.01	<0.01	<0.01	<0.01	99.4	6.02	93.98	1.01	
9RN1_2004_2	2	63.91	2.89	33.15	0.12	0.08	0.16	0.06	0.01	0.01	0.03	<0.01	0.01	<0.01	100.4	4.91	95.09	1.00	
9RN1_2004_2	2	61.04	5.36	33.17	0.08	0.05	0.51	0.15	<0.01	0.22	0.03	<0.01	<0.01	0.01	100.6	9.26	90.74	1.01	
9RN1_2004_2	2	60.61	5.76	33.20	0.05	0.02	0.41	0.10	0.03	0.38	<0.01	<0.01	0.01	0.03	100.6	9.99	90.01	1.01	
9RN4B_2000	2	63.09	4.39	31.97	0.09	0.04	0.47	0.12	0.01	<0.01	<0.01	<0.01	<0.01	<0.01	100.2	7.48	92.52	0.96	
9RN4B_2000	2	62.35	3.66	32.41	0.05	0.06	0.59	0.13	0.01	0.17	<0.01	<0.01	<0.01	<0.01	99.4	6.35	93.65	0.99	
9RN4B_2000	2	63.08	3.27	32.24	0.12	0.05	0.17	0.10	0.01	0.20	<0.01	<0.01	<0.01	<0.01	99.2	5.65	94.35	0.98	
9RN4B_2000	2	60.93	4.79	32.92	0.09	0.08	0.40	0.10	0.01	0.00	<0.01	<0.01	<0.01	0.01	99.3	8.32	91.68	1.01	
At the bridge, pressure ~11 bar																			
9RN-3-2006#	2	61.85	5.30	32.92	0.03	<0.01	0.46	0.10	0.01	0.00	<0.01	<0.01	0.02	<0.01	100.7	9.12	90.88	0.99	
9RN-3-2006#	2	62.06	5.07	32.59	0.06	0.02	0.42	0.08	0.03	0.13	0.03	0.01	<0.01	0.03	100.5	8.71	91.29	0.98	
9RN-3-2006#	2	61.72	5.25	32.65	0.03	0.00	0.40	0.07	0.03	0.10	<0.01	0.02	<0.01	<0.01	100.3	9.06	90.94	0.98	
9RN-3-2006#	2	61.54	6.18	31.88	0.07	0.03	0.30	0.08	0.03	0.24	<0.01	0.01	<0.01	<0.01	100.4	10.48	89.52	0.95	
9RN-3-2006#	2	62.97	4.86	32.30	0.04	0.01	0.31	0.08	0.02	0.03	<0.01	<0.01	<0.01	<0.01	100.6	8.28	91.72	0.96	
9RN-3-2006#	2	61.44	5.84	32.30	0.08	<0.01	0.45	0.07	0.01	0.00	0.02	<0.01	<0.01	<0.01	100.2	10.02	89.98	0.96	
9RN-3-2006#	2	61.98	5.18	32.80	0.06	<0.01	0.36	0.10	0.05	0.10	0.03	<0.01	<0.01	<0.01	100.7	8.92	91.08	0.98	
9RN-3-2006	2	58.67	6.97	32.21	0.05	0.01	0.24	0.09	0.05	0.06	<0.01	<0.01	<0.01	<0.01	98.4	12.20	87.80	0.98	
9RN-3-2006	2	58.50	6.79	32.54	0.05	0.05	0.19	0.12	0.02	0.22	<0.01	<0.01	<0.01	<0.01	98.5	11.90	88.10	1.00	
9RN-3-2006#	2	62.41	4.31	32.23	0.04	0.05	0.48	0.08	0.01	0.10	<0.01	<0.01	<0.01	0.01	99.7	7.41	92.59	0.97	
9RN-3-2006#	2	61.45	4.62	32.12	0.05	0.03	0.43	0.09	0.03	0.20	<0.01	<0.01	<0.01	0.01	99.0	8.05	91.95	0.98	
9RN-3-2006#	2	61.88	5.04	32.40	0.05	0.05	0.41	0.10	0.04	0.07	<0.01	<0.01	<0.01	<0.01	100.0	8.64	91.36	0.98	
9RN-3-2006#	2	60.97	6.08	32.10	0.06	0.04	0.40	0.09	0.02	0.24	<0.01	<0.01	<0.01	<0.01	100.0	10.40	89.60	0.96	
9RN-3-2006#	2	60.33	6.13	32.20	0.05	0.02	0.41	0.10	0.01	0.01	<0.01	<0.01	<0.01	<0.01	99.3	10.61	89.39	0.97	
9RN-3-2006	2	62.41	4.17	32.25	0.04	0.03	0.70	0.10	0.02	0.07	<0.01	<0.01	<0.01	<0.01	99.8	7.22	92.78	0.98	
9RN-3-2006	2	63.04	4.00	32.37	0.04	0.04	0.73	0.10	0.01	0.10	<0.01	<0.01	<0.01	0.01	100.4	6.86	93.14	0.97	
9RN-3-2006	2	60.86	6.35	32.21	0.03	0.03	0.36	0.12	0.02	0.25	<0.01	<0.01	<0.01	<0.01	100.2	10.85	89.15	0.96	
9RN-3-2006	2	60.57	6.23	31.91	0.05	0.05	0.35	0.12	0.02	0.10	<0.01	<0.01	<0.01	<0.01	99.4	10.68	89.32	0.96	
9RN-3-2006	2	58.48	7.22	33.15	0.08	0.01	0.23	0.12	0.04	0.00	0.01	<0.01	<0.01	<0.01	99.3	12.62	87.38	1.01	

Table A2.5 Continued

Sample #	Group	Zn wt%	Fe wt%	S wt%	Se wt%	Cu* wt%	Cd wt%	Mn wt%	Co wt%	Pb wt%	As wt%	Ni wt%	Sb wt%	Te wt%	total	FeS* mole%	ZnS mole%	S/ (Fe+Zn)
9RN-3-2006	2	63.02	4.43	32.57	0.05	0.03	0.59	0.07	0.03	0.01	<0.01	<0.01	<0.01	0.01	100.8	7.56	92.44	0.97
9RN3_2006†	2	63.56	3.53	32.56	0.08	0.03	0.45	0.08	0.02	0.09	<0.01	<0.01	<0.01	0.01	100.4	6.06	93.94	0.98
9RN3_2006†	2	63.35	3.14	32.47	0.05	0.01	0.43	0.07	0.02	0.00	<0.01	<0.01	<0.01	<0.01	99.5	5.47	94.53	0.99
9RN3_2006	2	60.59	5.56	32.23	0.05	0.03	0.27	0.07	0.03	0.00	<0.01	<0.01	<0.01	<0.01	98.8	9.66	90.34	0.98
9RN3_2006	2	57.36	7.91	32.14	0.09	0.85	0.25	0.12	0.01	0.25	<0.01	<0.01	<0.01	0.01	99.0	12.76	87.24	0.98
9RN3_2006	2	52.77	8.52	30.26	0.09	1.25	0.21	0.17	<0.01	<0.01	<0.01	<0.01	<0.01	<0.01	93.3	14.14	85.86	0.98
9RN3_2006	2	55.07	7.33	30.38	0.08	0.11	0.28	0.10	0.01	<0.01	<0.01	<0.01	<0.01	<0.01	93.4	13.33	86.67	0.97
9RN3_2006	2	58.78	6.66	32.36	0.07	0.01	0.43	0.10	0.01	0.24	0.01	<0.01	<0.01	<0.01	98.7	11.70	88.30	0.99

* Cu in analyses of individual sphalerite grains was assumed to have been present as inclusions of chalcopyrite smaller than the resolution of the

microprobe beam. Results of these analyses were corrected for excess Fe by subtracting an amount of Fe equal to Cu on an atomic basis. Gold was not detected. † microprobe analysis from the same crystal. <0.01 below the detection limits of the microprobe.

Table A2.6. Bulk chemical compositions of scales from coupons from the scaling experiments in wells RN-9, RN-11 and RN-10

	Zn	Fe	Cu	Pb	S	SO4	CTotal	SiO2	Al2O3	CaO	Na2O	K2O	MnO	MgO	LOI	Ag	Au	As	
pressure	ICP-OES	FUS-ICP	ICP-OES	ICP-OES	IR	IR	%	FUS-ICP	%	ppm	ppm	ppm							
bar	0.001	0.01	0.001	0.003	0.01	0.01	IR	0.01	0.01	0.01	0.01	0.01	0.001	0.01	5	2	0.5		
Well RN-9																			
Scale pressure experiments																			
1.1	18	17.2	3.8	14.7	11.9	15.5	na	24.7	3.3	0.8	1.0	0.7	0.1	0.1	8.1	1052	67	2500	
2.1+3.1*	17	18.7	5.7	15.3	17.7	na	na	13.5	1.5	0.6	0.6	0.3	0.5	0.2	8.7	1819	102	6370	
4.1	10	16.3	3.0	13.9	10.4	15.1	na	26.1	3.5	0.8	1.0	0.8	0.1	0.0	8.4	1542	53	1610	
1.4+1.5+1.6*	7	7.9	1.8	3.4	4.5	6.5	na	56.2	6.5	1.3	2.1	1.4	0.035	0.1	9.5	1669	22	813	
Critical pipe	1	2.4	2.4	1.4	1.5	2.3	na	74.4	4.4	1.5	1.2	0.9	0.1	0.6	8.4	680	7	93	
Well RN-10																			
1.1	34	31.4	23.3	1.4	0.7	30.1	na	5.5	0.4	0.3	0.6	0.1	0.3	0.3	14.0	1129	161	8	
3.1	18	21.4	21.9	1.2	2.2	22.3	na	21.9	0.4	0.3	0.8	0.1	0.6	0.2	12.3	3258	151	92	
2.1	12	16.1	18.5	1.3	2.3	16.9	na	37.5	0.5	0.3	0.8	0.1	0.8	0.2	10.7	2390	105	47	
4.1	20	21.9	22.5	1.2	1.8	22.3	na	22.5	0.4	0.3	0.8	0.2	0.5	0.2	12.6	3027	150	35	
1.6	8	18.5	15.4	1.4	6.3	16.7	na	33.3	0.5	0.3	0.7	0.1	0.6	0.2	10.0	6270	161	233	
Well RN-11																			
1.1	41	21.9	16.4	3.9	0.6	15.3	na	20.5	3.2	1.0	1.3	0.7	0.3	2.8	16.0	234	273	33	
1.2	41	26.7	15.8	7.5	1.7	20.6	na	14.1	1.5	0.9	0.6	0.2	0.4	1.6	14.7	1856	296	360	
1.3	13	17.3	8.4	6.0	3.1	13.9	na	43.2	1.1	0.6	0.5	0.2	0.5	0.3	10.6	1379	157	410	
1.4	9	13.4	7.9	5.0	2.7	10.2	na	52.3	1.4	0.6	0.7	0.3	0.3	0.2	9.5	1191	118	280	
1.6	5	6.6	4.3	2.0	1.8	4.5	na	71.3	1.5	0.5	0.9	0.4	0.1	0.1	7.3	575	67.8	486	

Scales at locations 2.1 + 3.1 and 1.4+ 1.5 +1.6 were combined for whole-scale analysis because the amount at each station was not enough for individual analysis. *This is justified by the very similar pressure at these stations. ICP-OES, Inductively coupled plasma optical emission spectrometry; FUS-ICP, Fusion inductively coupled plasma; IR, infrared; INAA, instrumental neutron activation analysis; FUS-MS, Fusion mass spectrometry

Table A2.6. (continue)

	pressure bar	Sb	Cd	Hg	Tl	Ga	Ge	Mo	Co	Ni	Se	Bi	In	Sn	W	V	Cr	Nb	Zr
		ppm INAA	ppm TD-ICP	ppm INAA	ppm FUS-MS	ppm FUS-MS	ppm FUS-MS	ppm FUS-MS	ppm FUS-MS	ppm INAA	ppm INAA	ppm INAA	ppm FUS-MS	ppm FUS-MS	ppm FUS-MS	ppm INAA	ppm FUS-ICP	ppm INAA	ppm FUS-MS
Well RN-9																			
1.1	18	815	32	na	0.1	2	<0.1	7	<1	19	320	<0.4	<0.2	<1	<1	<5	<5	<1	<5
2.1+3.1	17	803	44	na	<0.1	1	<0.1	33	<1	49	440	<0.4	<0.2	<1	<1	<5	<5	<1	<5
4.1	10	1120	28	na	0.3	3	<0.1	4	<1	21	292	<0.4	<0.2	<1	<1	<5	<5	<1	<5
1.4+1.5+1.6	7	1530	11	na	0.4	8	<0.1	3	5	20	210	<0.4	<0.2	<1	<1	<5	<5	<1	<5
Critical pipe	1	60	3	na	0.6	82	<0.1	24	5	32	54	<0.4	<0.2	<1	<1	22	32	<1	<5
Well RN-10																			
1.1	34	5	180	na	<0.1	5	<0.1	9	9	62	245	0.6	<0.2	<1	<1	48	<5	<1	na
3.1	18	34	76	na	<0.1	13	<0.1	11	6	19	172	10.7	<0.2	<1	2	96	27	<1	na
2.1	12	47	57	na	0.2	17	1	9	4	32	148	0.5	<0.2	<1	<1	87	<5	<1	na
4.1	20	23	79	na	<0.1	13	<0.1	11	4	48	180	0.8	<0.2	<1	<1	99	55	<1	na
1.6	8	142	20	na	0.5	21	<0.1	9	<1	10	180	0.6	<0.2	<1	<1	88	25	<1	na
Well RN-11																			
1.1	41	7	145	na	0.1	10	15	33	13	432	387	<5	<0.2	5	4	81	662	13	<5
1.2	41	23	121	na	<0.1	7	8	77	20	68	472	<5	<0.2	3	<1	73	187	8	<5
1.3	13	29	72	na	0.1	7	4	22	8	45	340	<5	<0.2	1	2	29	72	6	<5
1.4	9	25	51	na	<0.1	10	3	14	7	22	339	<5	<0.2	1	<1	27	40	<1	24
1.6	5	115	53	na	<0.1	24	2	13	4	32	232	<5	<0.2	<1	<1	15	35	4	6

Table A2.6. (continue)

	Hf	Ta	Sc	Ti	Ir	Ba	Sr	Rb	Cs	Be	Br	P	U	Th	Y	La	Ce	Pr	
pressure	ppm	ppm	ppm	ppm	ppb	ppm	ppm	ppm	ppm	ppm	ppm	ppm	ppm	ppm	ppm	ppm	ppm	ppm	
bar	INAA	FUS-MS	INAA	FUS-ICP	INAA	FUS-ICP	FUS-ICP	FUS-MS	FUS-MS	FUS-ICP	INAA	FUS-ICP	FUS-MS	FUS-MS	FUS-ICP	INAA	FUS-MS	FUS-MS	
	<2	0.1	0.1	10	5	3	2	2	0.5	1,3	5	200	0.1	0.1	2	0.5	0.1	0.05	
Well RN-9																			
1.1	<0.2	<0.1	1	36	<5	191	44	26	1	<1	<0.5	<200	<0.1	<0.1	<1	<0.1	<0.1	<0.1	
2.1+3.1	<0.2	<0.1	<0.1	12	<5	86	24	11	<0.5	<1	<0.5	<200	<0.1	<0.1	<1	<0.1	<0.1	<0.1	
4.1	<0.2	<0.1	<0.1	72	<5	205	45	33	1	<1	<0.5	<200	<0.1	<0.1	<1	<0.1	<0.1	<0.1	
1.4+1.5+1.6	<0.2	<0.1	<0.1	12	<5	331	74	67	3	<1	24	<200	<0.1	<0.1	4	<0.1	<0.1	<0.1	
Critical pipe	<0.2	<0.1	2	611	<5	147	48	44	2	2	3	458	<0.1	<0.1	4	<0.1	<0.1	<0.1	
Well RN-10																			
1.1	0.2	-0.1	0.8	54	<5	18	6	3	<0.5	<3	17	<200	3.1	<0.1	<1	1	0.7	0.17	
3.1	<0.2	-0.1	0.6	144	<5	21	6	7	<0.5	<3	11.6	<200	1.2	<0.1	<1	1.1	0.7	0.19	
2.1	<0.2	-0.1	0.3	<10	<5	18	6	4	<0.5	<3	10.6	<200	2.3	<0.1	<1	0.7	0.7	0.12	
4.1	<0.2	-0.1	-0.1	288	<5	21	15	7	<0.5	<3	21.7	<200	3.3	<0.1	<1	1.3	0.9	0.23	
1.6	<0.2	-0.1	-0.1	<10	<5	18	6	7	<0.5	<3	<0.5	<200	1.1	<0.1	<1	0.9	0.6	0.15	
Well RN-11																			
1.1	0.7	0.3	0.8	533	<5	87	34	36	1.5	<1	47.5	458	0.4	1.2	1	2.7	4.5	0.53	
1.2	0.3	0.2	1.1	258	<5	30	26	12	0.6	<1	42.5	<200	0.2	0.7	1	2.8	3.9	0.58	
1.3	<0.2	-0.1	0.7	84	<5	34	16	9	<0.5	2	18.2	<200	<0.1	<0.1	<1	1	0.8	0.17	
1.4	<0.2	-0.1	0.7	240	<5	36	15	12	0.6	2	14.1	<200	<0.1	0.1	<1	1.1	1	0.2	
1.6	<0.2	-0.1	0.6	144	<5	31	14	16	0.8	4	10.8	458	<0.1	0.1	<1	0.8	0.9	0.15	

Table A2.6. (continue)

	pressure bar	Nd		Sm		Eu		Gd		Tb		Dy		Ho		Er		Tm		Yb		Lu	
		ppm FUS-MS	ppm INAA	ppm FUS-MS	ppm INAA	ppm FUS-MS	ppm INAA	ppm INAA															
Well RN-9																							
1.1	18	<0.1	<0.1	<0.1	<0.1	<0.1	<0.1	<0.1	<0.1	<0.1	<0.1	<0.1	<0.1	<0.1	<0.1	<0.1	<0.1	<0.1	<0.1	<0.1	<0.1	<0.1	<0.1
2.1+3.1	17	<0.1	<0.1	<0.1	<0.1	<0.1	<0.1	<0.1	<0.1	<0.1	<0.1	<0.1	<0.1	<0.1	<0.1	<0.1	<0.1	<0.1	<0.1	<0.1	<0.1	<0.1	<0.1
4.1	10	<0.1	<0.1	<0.1	<0.1	<0.1	<0.1	<0.1	<0.1	<0.1	<0.1	<0.1	<0.1	<0.1	<0.1	<0.1	<0.1	<0.1	<0.1	<0.1	<0.1	<0.1	<0.1
1.4+1.5+1.6	7	<0.1	<0.1	<0.1	<0.1	<0.1	<0.1	<0.1	<0.1	<0.1	<0.1	<0.1	<0.1	<0.1	<0.1	<0.1	<0.1	<0.1	<0.1	<0.1	<0.1	<0.1	<0.1
Critical pipe	1	<0.1	<0.1	<0.1	<0.1	<0.1	<0.1	<0.1	<0.1	<0.1	<0.1	<0.1	<0.1	<0.1	<0.1	<0.1	<0.1	<0.1	<0.1	<0.1	<0.1	<0.1	<0.1
Well RN-10																							
1.1	34	0.4	0.1	<0.05	<0.1	<0.1	<0.1	<0.1	<0.1	<0.1	<0.1	<0.1	<0.1	<0.1	<0.1	<0.1	<0.1	<0.1	<0.05	<0.1	<0.1	<0.1	<0.04
3.1	18	0.5	0.1	<0.05	<0.1	<0.1	<0.1	<0.1	<0.1	<0.1	<0.1	<0.1	<0.1	<0.1	<0.1	<0.1	<0.1	<0.1	<0.05	<0.1	<0.1	<0.1	<0.04
2.1	12	0.4	0.1	<0.05	<0.1	<0.1	<0.1	<0.1	<0.1	<0.1	<0.1	<0.1	<0.1	<0.1	<0.1	<0.1	<0.1	<0.1	<0.05	<0.1	<0.1	<0.1	<0.04
4.1	20	0.6	0.2	<0.05	<0.1	<0.1	<0.1	<0.1	<0.1	<0.1	<0.1	<0.1	<0.1	<0.1	<0.1	<0.1	<0.1	<0.1	<0.05	<0.1	<0.1	<0.1	<0.04
1.6	8	0.4	0.1	<0.05	<0.1	<0.1	<0.1	<0.1	<0.1	<0.1	<0.1	<0.1	<0.1	<0.1	<0.1	<0.1	<0.1	<0.1	<0.05	<0.1	<0.1	<0.1	<0.04
Well RN-11																							
1.1	41	1.7	0.3	0.12	0.3	0.12	0.3	<0.1	<0.1	<0.1	<0.1	0.2	<0.1	<0.1	<0.1	<0.1	0.1	<0.05	<0.1	<0.05	0.1	<0.05	<0.04
1.2	41	1.9	0.4	0.09	0.3	0.09	0.3	<0.1	<0.1	<0.1	<0.1	0.2	<0.1	<0.1	<0.1	<0.1	0.1	<0.05	<0.1	<0.05	0.1	<0.05	<0.04
1.3	13	0.6	0.1	<0.05	<0.1	<0.05	<0.1	<0.1	<0.1	<0.1	<0.1	<0.1	<0.1	<0.1	<0.1	<0.1	<0.1	<0.1	<0.05	<0.1	<0.1	<0.1	<0.04
1.4	9	0.6	0.2	<0.05	<0.1	<0.05	<0.1	<0.1	<0.1	<0.1	<0.1	<0.1	<0.1	<0.1	<0.1	<0.1	<0.1	<0.1	<0.05	<0.1	<0.1	<0.1	<0.04
1.6	5	0.4	0.1	<0.05	<0.1	<0.05	<0.1	<0.1	<0.1	<0.1	<0.1	<0.1	<0.1	<0.1	<0.1	<0.1	<0.1	<0.1	<0.05	<0.1	<0.1	<0.1	<0.04

Appendix 2.4

2.4.1 Scaling experiments 2002 and 2003

Scaling tests were conducted in July 2002, using the fluid discharged into the surface pipeline from well RN-9, and in October 2002 using the fluid from RN-11 from October 2003 with well RN-10 (Hardardóttir et al., 2005). The purpose was to determine the relationship between pressure and the characteristics of the scale, as well as scaling rate. The following section summarizes the test equipment, the procedures, and the results for each well.

2.4.2 Test equipment

The test equipment consisted of a manifold with four parallel branches (pipe 60 mm in diameter; Figure A2.6). Each branch contained 2 to 6 stations, with steel coupons and pressure gauges (Figure A2.6B, C, D). The manifold was connected directly to the wellhead, with the flow to each branch throttled by an orifice. Different pressures were maintained in each branch by adjusting a flow valve at the exit, which had a back-up orifice plate designed to control fluid flow. Small adjustments were made 3-5 times a week to maintain constant pressure conditions for the coupons throughout the test period. The wellhead pressure at the beginning of each experiment was 22, ~42 and ~50 bar-g for wells RN-9, RN-11, and RN-10, respectively (Figures A2.7 – A2.11).

A set of coupons (Figure A2.6D) were located close to the inlet just downstream of the flow-controlling orifice (stations 1.2 – 1.6, 2.1, 3.1, 4.2; Figure A2.6C). Five (RN-9) or four (RN-11, RN-10) sets of coupons were used in stations 1.1. Another set of coupons was located in each branch near the exit (stations 2.2, 3.2, 4.2). The mild steel coupons (50 mm x 15 mm x 2 mm) were aligned perpendicular to the flow direction. The distance between

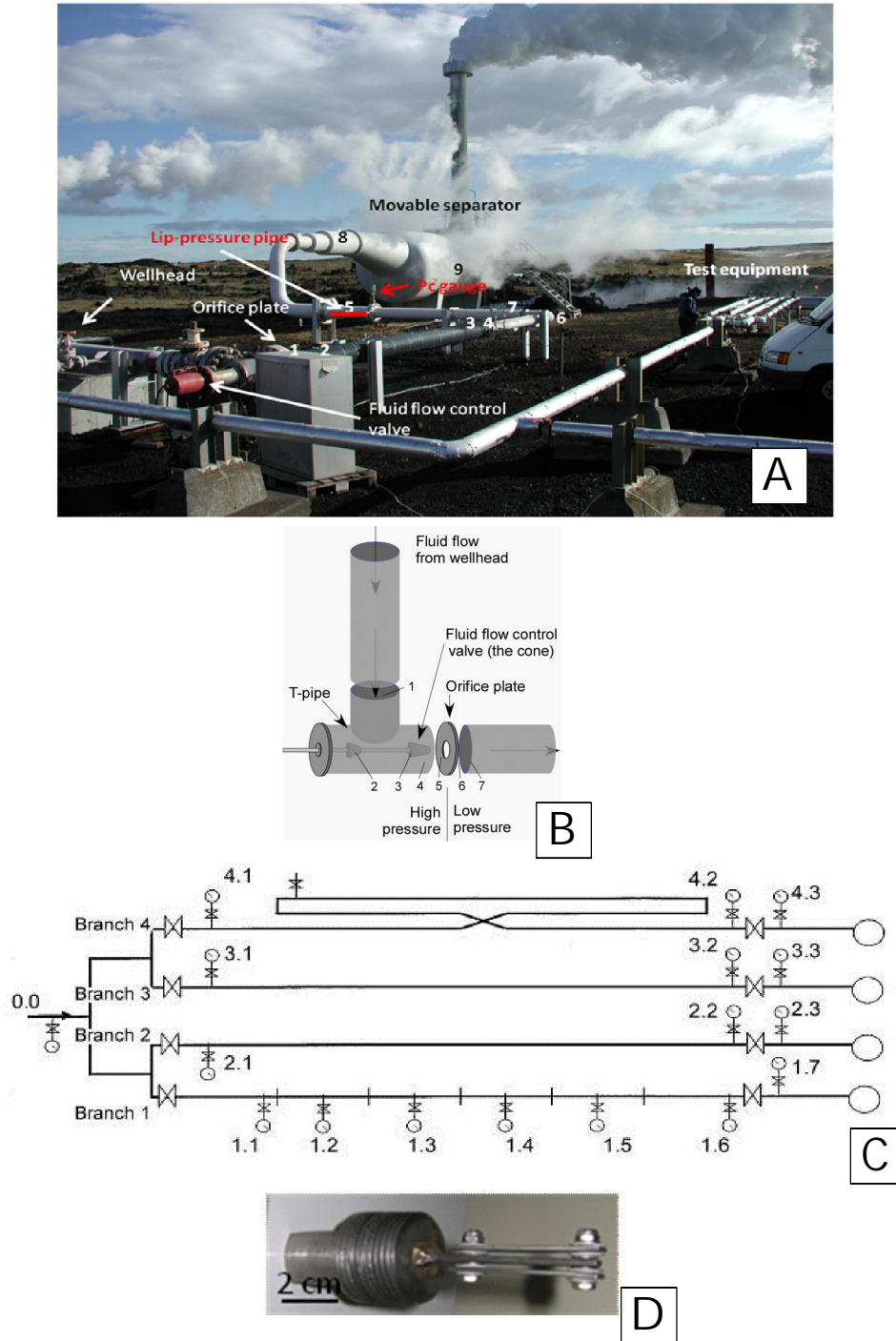


Figure A2.6. A) Photo of the equipment used in the scaling test experiments in 2002 and 2003, including the movable horizontal vapor/liquid separator used for well output measurements. Numbers 1-9 refer to sample locations in the scaling test for well R-10. B) Schematic drawing of the pipeline from wellhead to ~1 downstream of the orifice plate showing the fluid-flow control valve (choke valve; stainless steel stem) and the valve stem (T-pipe). C) Schematic drawing of the test equipment (experimental manifold). Individual branches are labelled 1 to 4 and the locations of individual stations are indicated by numbers (0.0, 1.1, 1.2 etc). D) Photo of a set of new coupons used in the scaling test experiments.

stations 4.1 and 4.2 was three times the distance between 2.1 and 2.2, and between 3.1 and 3.2. Branch one had six orifice plates equally spaced along its length to decrease the pressure in six stages (stations 1.1 – 1.6, Figure A2.4C) whereas branch two, three and four had two orifice plates (in front and at the end of the branch). After 4 to 6 weeks the coupons were removed from the manifold, the thickness of the scales measured, and the crystalline scale phases identified by XRD; chemical analysis on selected bulk-scale samples was carried out as well as scanning electron microscopy (Leo Supra 25 SEM).

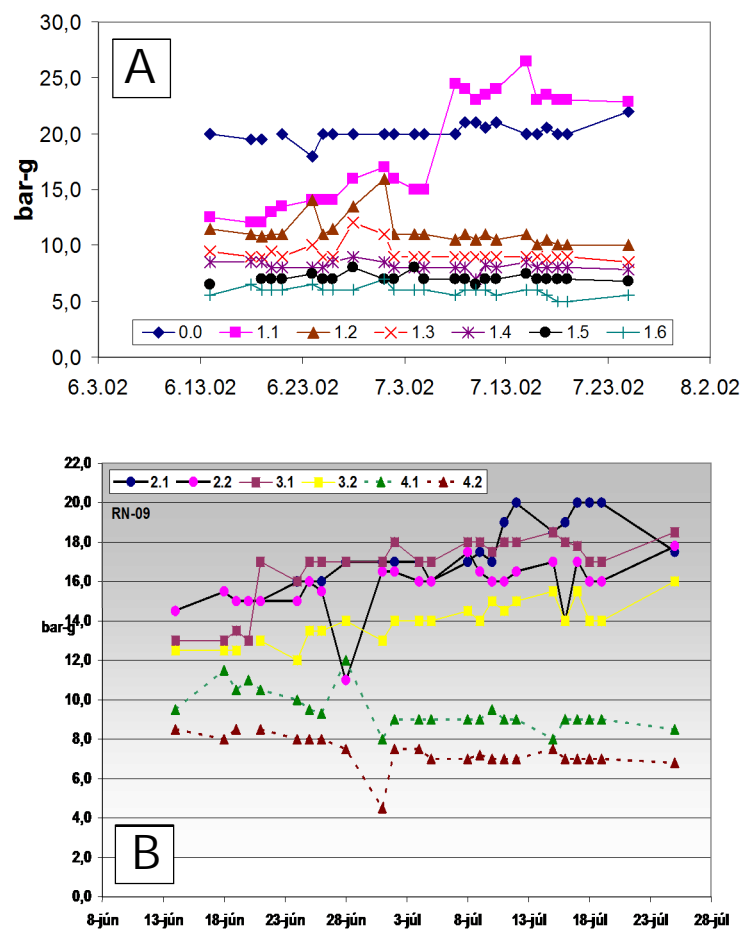


Figure A2.7. A) Results of pressure measurements in RN-9 at station 0.0 and in branch one at stations 1.1 to 1.6 as a function of time. B) Pressure at branches two, three and four as a function of time (Hardardóttir et al., 2005).

Table A2.7. Pressure range and average pressure measured in scaling tests in 2002 and 2003 in well RN-9, -10, and -11

RN-9	Station	0	1.1	1.2	1.3	1.4	1.5	1.6	2.1	2.2	3.1	3.2	4.1	4.2
Average pressure	bar	20.1	18.5	11.2	9.2	8.1	7	5.9	17.2	15.7	16.7	13.9	9.4	7.3
Lowest pressure	bar	18	12	10	8.5	7	6.5	5	14.5	11	13	12	8	4.5
Highest pressure	bar	22	26.5	16	12	9	8	7	20	17.8	18.5	16	12	8.5
RN-11														
Average pressure	bar	42.3	41.1	40.5	12.6	9.1	6.4	5.3	37.2	35	25.9	25.6	11.7	10.4
Lowest pressure	bar	32	32	32	7	5.5	4	3	30	0	13	12	4.7	4.2
Highest pressure	bar	46	46	46	19	14	10	9	45	45	38	37	20	17
RN-10														
Average pressure	bar	50.4	34.3	30.3	26	21.8	17.7	8.1	11.5	11	17.6	17.5	20	19.4
Lowest pressure	bar	46.5	13	10.8	12.7	7	5.2	4	4.3	4.3	5.5	5.4	7.2	6.8
Highest pressure	bar	52.5	43.5	41.5	40	38.5	37.5	13.2	18.5	18.5	24	24	29.5	28.5

Table A2.8. XRD results for precipitates on coupons from wells RN-9, RN-11, RN-10

Station- branche No	Pressure	chalco-							clay	unidentified
		bar-g	sphalerite	galena	pyrite	bornite	opal			
RN-9										
0.0	20		x	x	x					
2.1	16		x	x	x	x				
3.1	14		x	x	x	x				
1.1	14		x	x	x	x				
1.2	11		x	x	x	x	x			
1.3	9		x	x	x	x				
4.1	9		x	x	x	x		x	x	
1.4	8		x	x	x	x				
1.5	7		x	x	x	x				
1.6	6		x	x	x	x				x
RN-11										
1.1	41		x	x	x					
2.2	35		x	x	x					
1.4	9		x	x	x		x			
1.5	6		x	x	x		x			
RN10										
0	50	w*								
1.1	34	w								
4.1	20	x+w								
3.2	17	x								
2.1	11	w								

*w wurtzite

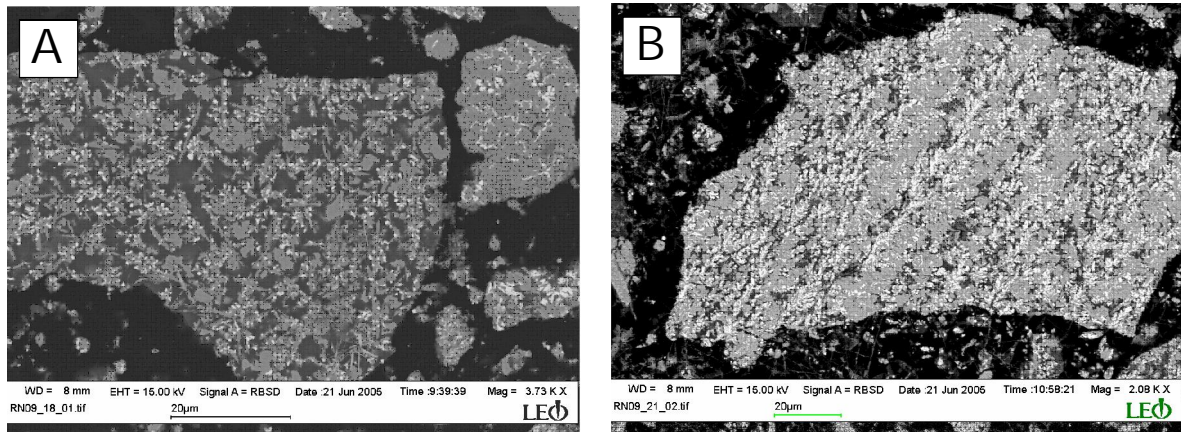


Figure A2.8. Electron backscatter image of scales precipitated in a scaling test in July 2002, in well RN-9. (A) At ~17 bar, the scale mainly consists of needles and anhedral grains of sphalerite (gray) and chalcopryrite (white) and galena (white). (B) Same minerals as above at ~8-10 bar, with mainly dendritic texture.

2.4.3 RN-9 Results

The coupon scales in well RN-9 formed at a range of pressures, from ~22 bar down to 6 bar-g. The average pressures at each location are shown in Table A2.7 and also plotted versus time over the 41-day test (Fig. A2.7). The pressure on each branch typically varied by ± 2 bar, with except for station 1.1, and at stations in branches 2 and 3 where the pressure increased during the scaling test (Hardardóttir et al., 2005). At station 1.1 the measurements (Figs. A2.7A and Table A2.7) indicated that the pressure increased, but this is unlikely, as the pressure downstream of station 0.0 could not be higher than the measured wellhead pressure. Either the wellhead pressure increased during this time, which was not detected (ISOR data base), or the gauge became blocked. If scaling occurred inside the orifice or if a fragment blocked the orifice, the pressure downstream of the orifice plate could increase up to the wellhead pressure.

The results from XRD analysis are shown in Table A2.8. Sphalerite and galena formed in all pressure intervals (average 20, 16, 14, 11, 9, 8, 6 bar) whereas chalcopryrite was found

between 20 and 14 bar and bornite from 16 to 6 bar. A broad hump, characteristic of amorphous silica, was observed in the XRD patterns for samples from 11 bar pressure.

Scanning electron microscopy was conducted on a few of the scale samples, mainly on the amorphous phase, formed at an average pressure between ~17 and 10 bar (location 2.1, 3.1 and 4.1). The EDS images showed fine-grained minerals, with anhedral forms and needles common at higher pressure and dendrites forming at lower pressure. Semi quantitative EDS analyses indicated an intimate intergrowth of an anhedral chalcopyrite and sphalerite at ~17 – 14 bar together with galena that crystallized at the ends of the needles (Figure A2.8A). At ~10 bar elongated dendrites together with long needles were the principal textures (Figure A2.8B).

Major element concentrations in scales from selected coupons are listed in Table A2.6 together with average pressure at each location. From ~20 to 10 bar, Cu, Zn and Pb were present at similar concentrations (~15 wt.%, 17 wt.%, and 15 to 10 wt.%, respectively), with Fe between ~ 3 and 6 wt.% (Hardardóttir et al., 2005). At lower pressure the metals were present in similar proportions, totaling ~8 wt.%. At pressure of 20 to 10 bar, SiO₂ constituted ~13 to 26 wt.% of the scales, whereas at lower pressure SiO₂ concentration reached 75 wt.%, thus diluting the metals. The Al₂O₃ concentration was ~1.5 to 6.5 wt.%, and other oxides were < 2% (Hardardóttir et al., 2005).

Trace element concentrations that correlate with pressure are As, Se and Au, which decrease from higher to lower pressure (Table A2.6). Arsenic concentrations reached ~6400 ppm at 17 bar and decreased to ~90 ppm at 1 bar. The Se and Au concentrations also decreased with pressure from 17 bar to 1 bar, from 440 to 54 ppm and 102 to 7 ppm, respectively. Silver and Sb concentrations did not correlate with pressure, from 1819 to 680 ppm and from 1530 ppm to 60 ppm, respectively.

The amount of scale deposited increased as the pressure decreased. At ~20 bar and ~7 bar the scale rate was ~1.2 mm and 6 mm per year, respectively (Hardardóttir et al., 2005).

2.4.4 RN-11 Results

The manifold tests at well RN-11 were discontinued after four weeks, and the coupons were left in the pipes for four more weeks (Hardardóttir et al., 2005). The inlet pressure was ~45 bar; the pressure range was ~45 to 5 bar in branch one, 45 to 30 bar in branch two, 37 to 12 bar in branch three and ~20 to 5 bar in branch four (Figure A2.9). The pressure in branch one both decreased and increased during the test, whereas the pressure decreased in the other branches.

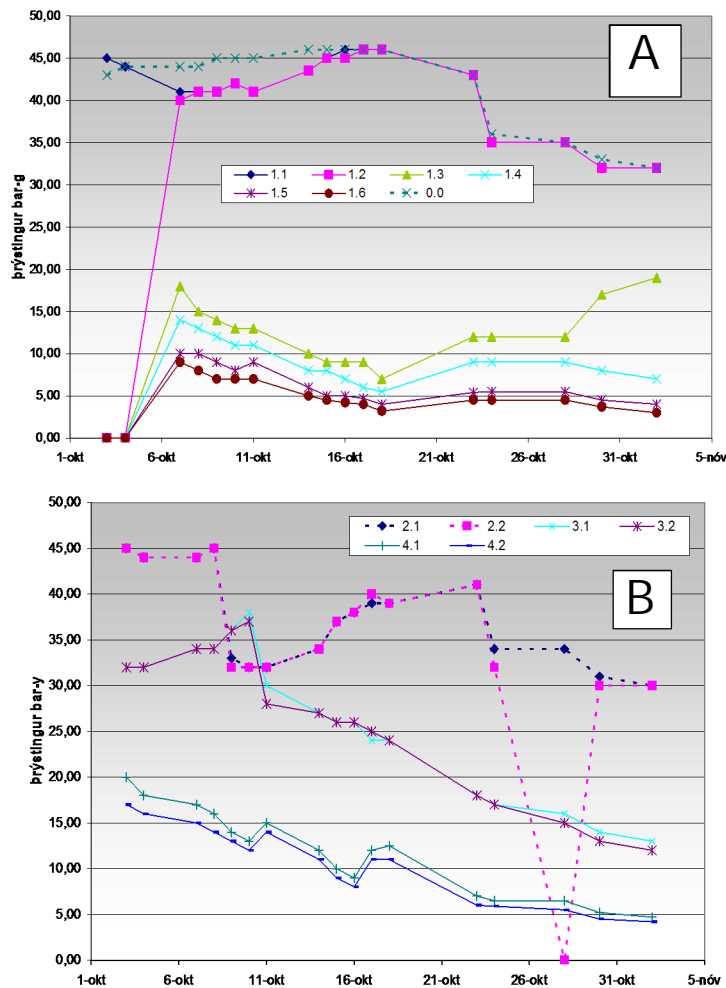


Figure A2.9. A) Results of pressure measurements in RN-11 at station 0.0 and branch one at stations 1.1 to 1.6 as a function of time B) Pressure at branches two, three and four as a function of time.

XRD results indicate that sphalerite and chalcopyrite formed at all pressures together with a trace of galena, and opal below 10 bar (Table A2.8).

Chemical analyses on scale samples from branch one (Table A2.6), where the pressure was ~45 to 5 bar, indicate Zn concentrations from ~27 wt.% to 7 wt.%, from higher to lower pressure. Similarly, the Fe concentration ranged from ~16 wt.% to 4 wt.%, and Cu from <8 wt.% to 2 wt.%. The Pb concentration ranged from 3 to 0.5 wt.%, and was greatest at ~10 bar. Silica concentration is lowest at 41 bar (14 wt.%), and highest (~75 wt.%) at ~5 bar. Other oxides were commonly <1 wt.% (Hardardóttir et al., 2005).

The Ag ranged from 1856 ppm to 234 ppm at a pressure of ~40 bar. Arsenic and Se ranged from ~500 to 30 ppm and did not correlate with pressure, whereas Au decreased from 300 (~40 bar) to 70 ppm (at 5 bar) (Table A2.6).

Scaling rate was 6 mm per year at ~41 bar and 12 mm at =15 bar (Hardardóttir et al., 2005).

2.4.5 RN-10 Results

The coupon scaling tests in RN-10 were carried out in October 2003 for six weeks. This well had the highest measured temperature at that time, 319°C (ÍSOR database). Wellhead pressure was ~50 bar. The pressure range in this scaling test was ~42 to 5 bar in branch one, ~18 to 4 bar branch two, ~22 to 5 bar in branch three, and ~29 to 6 bar in branch four (Table A2.7, Figure A2.10) The pressure was very unstable during this period (Hardardóttir et al., 2005).

XRD analyses indicate wurtzite at all pressures except in branch 3 (station 3.2) where the average pressure was ~17 bar and sphalerite was present instead. Chalcopyrite formed as a trace at the highest pressure (50 bar, just downstream of station 0.0), and galena was present at =20 bar (Table A2.7).

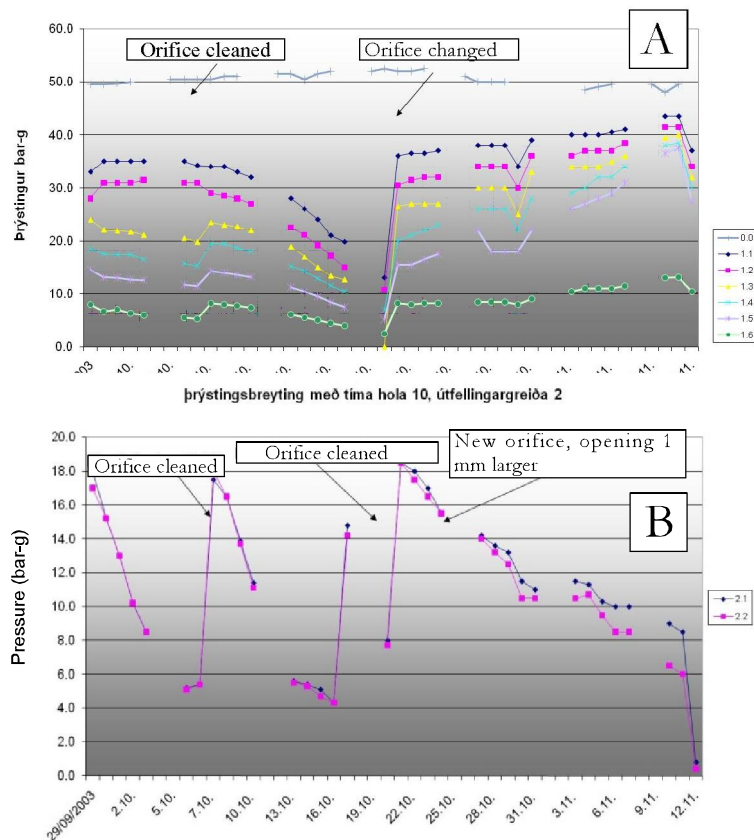


Figure A2.10. A) Results of pressure measurements in RN-10 at station 0.0 and branch one at stations 1.1 to 1.6. as a function of time. B) Pressure at branch two as a function of time.

SEM analyses on scale samples formed at 34 bar (station 1.1, Figure A2.11A), 20 bar (station 4.1), 11 bar (station 2.1; Figure A2.11B), and 8 bar (station 1.6) indicated deposition of mainly iron-rich sphalerite and wurtzite, galena, amorphous iron silicate and amorphous silica, in that order. The sphalerite contained on average 56 wt.% ZnS, 42 wt.% FeS and 2 wt.% CuS ($\text{Cu}_{0.02}\text{Fe}_{0.42}\text{Zn}_{0.56}$); the FeS concentration ranged from 27 to 60 mole%. The iron-rich amorphous phase was interpreted to be of minnesotaite composition $[\text{Fe}_6\text{Si}_8\text{O}_{19}(\text{OH})_6]$, also observed in in well RN-8 (Kristmannsdóttir, 1984). The principal texture at all pressures was dendritic; skeletal crystals were common at 34 bar (Figure A2.11).

Copper concentration was ~1.3 wt.% for all pressure intervals, from ~34 bar to 8 bar, whereas Fe decreased from ~23 wt.% to 12 wt.%, and Zn from ~30 wt.% to 18 wt.%. Pb increased as the pressure decreased, from ~0.7 to 10 wt.%. The SiO₂ concentration generally increased with pressure decrease, from 5 to 38 wt.%. Most other oxides were typically <0.5 wt.% (Table A2.6).

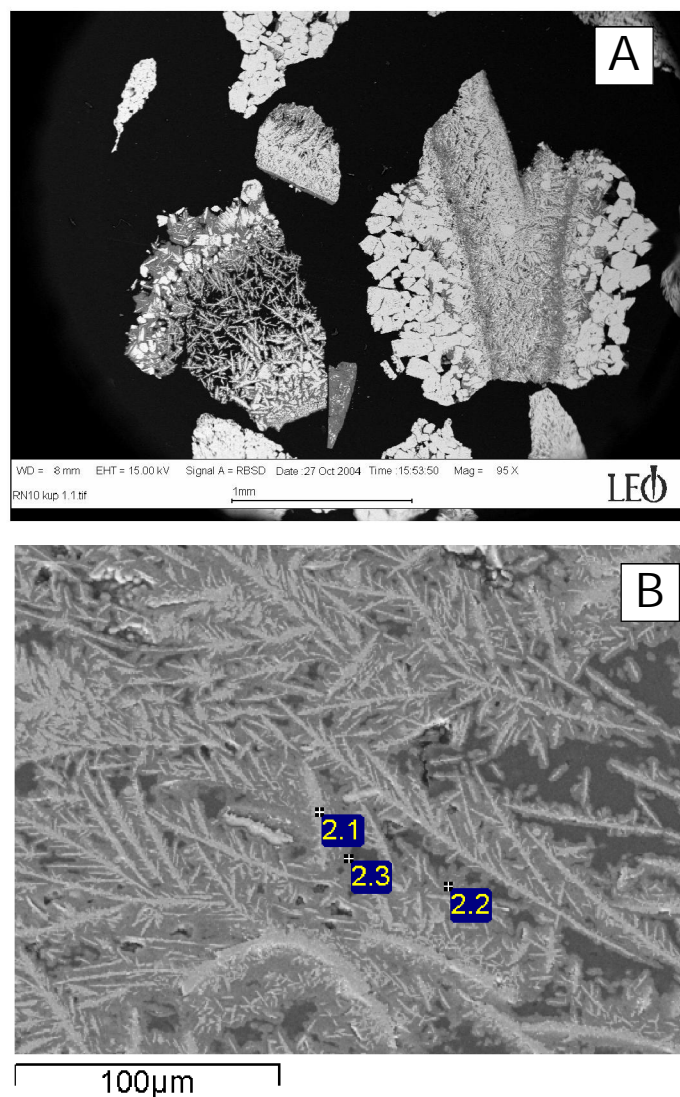


Figure A2.11. Electron Backscatter image of scales formed during a test of scaling rate, October 2003, well RN-10. A) Needles and skeletal sphalerite/wurtzite in amorphous iron-rich phase (34 bar). The skeletal crystals are formed at higher pressure (~34 bar) whereas the needles are precipitated at lower pressure (30 to 12 bar). B) Dendritic feathery structures of sphalerite with bright galena crystals at the rims, surrounded by amorphous Fe-rich silicate followed by amorphous silica (11 bar). Numbers refer to analyses.

Appendix 2.5

2.5.1 Normative calculations

Table A2.9. Normative calculations for well RN-9

Sample No.	mol sph		mol gn		mol cpy		S/sph wt%		S/gn wt%		S/cpy wt%		S/bn wt%		Σ S wt%		Δ S		Fe/sph wt%		Fe/cpy wt%		Fe/bn wt%		Σ Fe		Δ Fe left over		Sph wt%		bn		Sum Sulfides			
	wt%	wt%	wt%	wt%	wt%	wt%	wt%	wt%	wt%	wt%	wt%	wt%	wt%	wt%	wt%	wt%	wt%	wt%	wt%	wt%	wt%	wt%	wt%	wt%	wt%	wt%	wt%	wt%	wt%	wt%	wt%	wt%	wt%			
9RN20-2000	0.28	0.00	0.00	0.52	9.1	0.0	18.2	0.4	27.2	0.4	0.9	15.8	16.8	0.74	27.7	0.2	52.0	79.8																		
9RN31A-2000	0.38	0.07	0.02	0.25	12.5	0.9	0.8	6.4	20.6	-1.5	1.3	0.7	4.8	1.20	37.4	6.8	2.3	24.4	70.8																	
9RN2-2005G	0.24	0.15	0.02	0.22	7.8	2.0	0.7	5.6	16.1	-0.1	0.8	0.6	3.9	0.55	23.3	14.9	2.1	21.9	62.2																	
9RN3-2005G	0.27	0.17	0.02	0.24	8.7	2.2	0.8	6.2	17.9	-0.7	0.9	0.7	4.3	0.19	26.0	16.5	2.3	24.2	69.0																	
29	0.20	0.02	0.09	0.05	6.5	0.3	3.1	1.3	11.1	-0.1	0.7	2.7	4.0	0.47	19.4	2.0	9.0	35.4																		
9RN29-2000	0.15	0.03	0.08	0.02	4.9	0.4	2.9	0.6	8.8	-0.4	0.5	2.6	3.3	0.78	14.5	3.0	8.4	28.3																		
9RN28-2000	0.17	0.03	0.10	0.03	5.5	0.5	3.5	0.7	10.2	-0.3	0.6	3.0	3.9	0.55	16.5	3.5	10.0	31.3																		
9RN27B-2000	0.15	0.03	0.09	0.02	5.0	0.4	3.2	0.6	9.3	-0.3	0.5	2.8	3.6	0.92	15.1	3.1	9.1	29.8																		
4	0.04	0.04	0.05		1.2	0.5	1.6		3.3	-1.7	0.1	1.4	1.6	0.85	3.6	3.8	3.6	11.0																		

Factor used for above calculations

Sample No.	S wt%		Cu wt%		Fe wt%		Zn wt%		Pb wt%		SiO ₂ wt%		Al ₂ O ₃ wt%		CaO wt%		Na ₂ O wt%		K ₂ O wt%		MgO wt%		MnO wt%		Sum oxides												
	wt%	wt%	wt%	wt%	wt%	wt%	wt%	wt%	wt%	wt%	wt%	wt%	wt%	wt%	wt%	wt%	wt%	wt%	wt%	wt%	wt%	wt%	wt%	wt%	wt%	wt%	wt%										
9RN20-2000	27.6	18.0	17.5	17.7	0.1	6.1	0.7	0.2	0.1	0.1	1.5	0.1	15.0	8.8																							
9RN31A-2000	19.1	16.0	6.0	23.6	5.9	14.4	0.5	0.6	0.4	0.1	0.6	0.7	14.9	17.4																							
9RN2-2005G	16.0	14.6	4.4	14.7	12.9	26.9	2.9	0.6	0.8	0.7	0.1	0.1	10.2	32.2																							
9RN3-2005G	17.2	16.1	4.5	16.4	14.3	21.3	2.4	0.7	0.7	0.5	0.1	0.1	10.6	25.8																							
29	11.0	6.2	4.4	12.3	1.8	47.0	2.9	0.9	0.8	0.6	0.3	0.7	14.3	53.1																							
9RN29-2000	8.4	4.4	4.1	9.2	2.6	54.6	3.3	1.4	0.9	0.6	0.3	0.8	12.0	61.7																							
9RN28-2000	9.9	5.2	4.5	10.4	3.0	49.8	2.8	1.4	0.8	0.5	0.2	0.6	15.2	56.0																							
9RN27B-2000	9.0	4.7	4.5	9.5	2.7	53.4	3.3	1.2	1.0	0.6	0.3	0.7	12.2	60.4																							
4	1.6	0.6	2.4	2.3	3.3	82.6	1.7	0.5	0.9	0.5	0.3	0.8	6.4	87.3																							

proportion of Bn/Cpy ratio

	BN	CPY
0.05	0.10	0.15
0.25	0.20	0.25
0.33	0.33	0.33
0.5	0.55	0.6
0.6	0.70	0.75
0.75	0.85	0.9
0.8	0.95	1.0
0.9	1.0	1.0

probe	Sphalerite group		gn		cpy		bn	
	1	3	stoci					
Zn	63.9	61.85	64.1	Pb	86.6	Cu	34.6	63.3
Fe	3.4	5.3	2.9	Fe	30.4	11.1		
S	32.7	32.9	33.1	S	13.4	S	34.9	25.6
ZnFeS				Pbs		CuFeS		Cu5FeS4

2.5.2 Volume calculations

Scale and volume calculations downhole in well RN-9

Table A2.10. Volume of scales ($V \text{ (m}^3\text{)} = \pi * r^2 * h$) formed in the first 8 m in the surface pipeline of RN-9

	Radius (m)	Volume (m ³)	volume (m ³)
Diameter empty pipe (m)	40 cm	0.2	1.01
Diameter of fluid flow	10 cm	0.05	0.06
Pipe length	8 m		0.94

To calculate the volume of scale in the well a few assumptions are made regarding the volume of the empty well; the well is divided into two cylinders (i.e., the production casing and the slotted liner) with the volume:

$V = r^2 * \pi * h$ where r = radius of the well, h = well length. For the production casing, h = from surface to 500 m depth, casing diameter = 312 mm (Table A2.1 and A2.12). For the slotted liner, h = 500 m depth 1000 depth, and the casing diameter = 222 mm. Thus the empty volume of well RN-9 in 1983, 1000 m long, is 57.6 m³ (Figure A2.12).

2.5.3 Amount of scales precipitated in well RN-9 from 1983 to 1993

Data from the well logging in the fall 1993 were used for the calculations (Tables A2.1 and A2.13). The scales are assumed to form layers of even thickness on the well wall between measuring points. The remaining empty volume in the well can be calculated using the formula for a cut-off cone cylinder as shown in Figure A2.13.

$$V = h * \pi / 12 * [D^2 + d^2 + (D * d)] \quad (2.3)$$

h is the well length; D the upper/bigger diameter; d the lower diameter. The volume of scale in the calculated section is the difference between the volume of the casing and the volume of empty space.

Sphalerite (identified by XRD) was the main precipitate in the well in 1993 (ISOR database). The average density of sphalerite is 4050 kg/m³. Therefore assuming that only

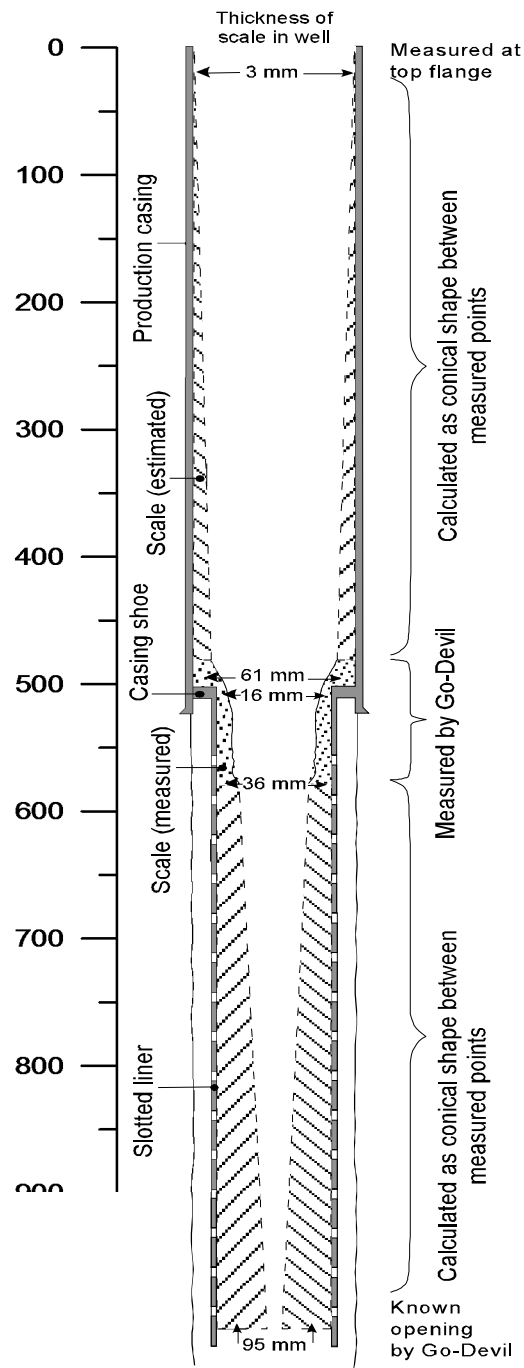


Figure A2.12. Schematic drawing of scaling in well RN-9. The interval from 500 to 570 m depth is from Steingrímsson and Björns-son (1993); the upper and lower part are estimated.

Table A2.11. The amount of each mineral formed in the first 8 m downstream of the orifice plate RN-9

	4 m		8 m	
	downstream of		downstream of	
	OP Average		OP Average	
	(wt%)	mole /100g	(wt%)	mole /100g
SiO ₂	25.14	0.42	51.18	0.85
Al ₂ O ₃	1.33	0.03	3.03	0.06
Fe	5.65	0.10	4.37	0.08
MnO	0.40	0.01	0.69	0.01
MgO	0.22	0.01	0.25	0.01
CaO	0.89	0.02	1.21	0.02
Na ₂ O	0.48	0.02	0.87	0.03
K ₂ O	0.43	0.01	0.55	0.01
Total S	16.90	0.53	9.59	0.30
Ag	0.52	0.00	0.14	0.001
Cu	12.59	0.20	5.13	0.08
Pb	5.03	0.02	2.53	0.01
Zn	19.07	0.29	10.34	0.16
ZnS		0.29		0.16
FeS=S _t -AgS-ZnS-CuS-PbS		0.01		0.05
CuS= Cu mol		0.20		0.08
PbS= Pb mol		0.02		0.01
mol Fe ₃ Si ₄ O ₁₀ (OH) ₂ *		0.03		0.01
mol Si in (Fe ⁺⁺ ,Mg) ₃ Si ₄ O ₁₀ (OH) ₂		0.12		0.04
mol Si í SiO ₂ amorph		0.29		0.81
<u>total mol</u>		<u>0.94</u>		<u>1.15</u>
mol% Fe in sph		2.74		22.77
		g/100g		g/100g
ZnS		28.43		15.42
FeS		0.72		4.10
CuS		18.94		7.72
PbS		5.81		2.92
mol Si í Fe _{2,1} Si _{3,5} O ₁₀		14.67		4.99
mol Si í SiO ₂ amorph		17.67		48.58
<u>total mole</u>		<u>86.24</u>		<u>83.73</u>
	Density g/cm ³	volume%	sum sul	volume%
	average			
Sphalerite/ZnS	4.1	27.27		12.22
Sphalerite/FeS	4.1	0.69		3.25
Chalcopyrite	4.1	18.17		6.11
Galena	7.5	3.05		1.27
"Minnesotaite"	3	19.24		5.41
Am-Si	2.2	31.59		71.74
Total volume of scale ⁽¹⁾				0.94
Sphalerite/ZnS				0.11
Sphalerite/FeS				0.03
Chalcopyrite				0.06
Galena				0.01
"Minnesotaite"				0.05
Am-Si				0.67
Sphalerite/ZnS				471
Sphalerite/FeS				125
Chalcopyrite				236
Galena				89
"Minnesotaite"				153
Am-Si				1484
<u>Total</u>				<u>2557</u>

It was assumed that all Zn, Cu and Pb occurs as sulfides, and the remaining S goes with Fe sulfide. What is left of Fe precipitates as "minnesotaite" (used here as a substitute for amorphous iron silicate) which takes Si in the ratio 3:4. What is left of Si is precipitated as amorphous silica. ⁽¹⁾ from Table A2.9. *mole mass = 473.877

Table A2.12. Measurements of a new well RN-9 (1983), 10 years later (1993), and 20 years later (2003) and volume of scales formed in that time

	Casing		Opening				Volume of casing	Empty volume	Volume of scale		%
	Length	Diameter (internal)	Opening at top		Opening at bottom				If sphalerite	If chalcopyrite	
	m	mm	m	mm	m	mm	m	m ³	m ³	m ³	
Production casing	500	312	0.312	306	0.31	190	0.19	38.23	24.59	13.63	35.67
Top of liner	67	222	0.222	190	0.19	150	0.15	2.59	1.53	1.07	41.09
Bottom part of scaling	433	222	0.222	150	0.15	31.8	0.03	16.76	3.20	13.56	80.88
Total								57.58	29.33	28.26	49.07

ρ -sph, 4050 kg/m³; ρ -cpy; 4190 kg/m³

volume for cylinder is $V = r^2 * \pi * h$

volume for cut-off cone is $V = H * \pi / 12 * (D^2 + d^2 + (D*d))$

sphalerite precipitates downhole ~11 tons/year are formed. The results are shown in Table A2.12.

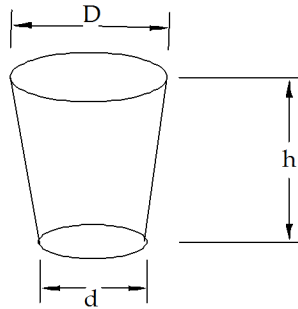


Figure A2.13. Drawing of a cut-off cone used to calculate the amount of precipitation in the RN-9 well; h is the well length; D the upper diameter; d the lower diameter.

2.5.4 Amount of scales in well RN-9 in 2003

Flashing starts at ~1000 m depth based on the temperature and pressure curves in Figure A2.2D. Data from Hjartarson (2004) for well RN-9 in 2003 do not have as much detail (Table A2.1). Therefore, the precipitation in 2003 was assumed to be similar to the 1993 scaling in tonnes per year. The average fluid flow was 34.3 kg/s.

Appendix 4

Table A4.1. Major and Trace Concentrations from Selected Seafloor Black Smoker Vents

	Seamount	Lucky Strike	Lucky Strike	Crystal [†]	Rainbow [‡]	Logatche	Menez Gwen [§]	Broken Spur [§]	Snakepit	TAG [#]	Red Lion ^{**}	Turtle Pits	Turtle Pits	Sisters Peak ^{**}	Brandon brine ^{††}	Brandon vapor ^{††}	Kairei 4 ^{§§}	Kairei 6 ^{§§}	Edmond ²	Edmond ¹⁰
depth, m	1540	1687	1726	2300	2300	2950	850	3090	3480	3650	3000	3000	3000	3000	2834	2834	2452	2452	3300	3303
T°C	328	325	281	365	353	271	271	360	341	366	349	407	407	400	376	405	315	365	273	293
pH	3.5	4.1	4.2	2.8	3.3	4.4	4.4	N.D.	3.7	3.4	N.D.	N.D.	N.D.	N.D.	3.3	<3.7	3.35	3.62	<3.02	<2.97
Cl (mM)	624	438	535	750	515	400	469	550	550	636	552	291	271	224	557	338	571	620	929	926
Na (mM)	499	386	431	553	438	313	420	515	557	557	480	230	237	209	441	303	492	528	698	718
K (mM)	27	21	29	20	24	24	19	23	17	17	20	8	9	7	14	9	13	15	45	45
Ca (mM)	47	30	35	67	28	33	12	11	11	31	19	8-11	9	12-17	33	21	29	31	58	65
SiO ₂ (mM)	15	16	15	7	8	11	N.D.	20	21	21	22	11	12	14	13	9	17	17	20	19
Mg (mM)	0 ^{##}	0 ^{##}	0 ^{##}	0 ^{##}	0 ^{##}	0 ^{##}	0 ^{##}	0 ^{##}	0 ^{##}	0 ^{##}	0 ^{##}	0 ^{##}	0 ^{##}	0 ^{##}	0 ^{##}	0 ^{##}	0 ^{##}	0 ^{##}	0 ^{##}	0 ^{##}
Al (µM)	N.D.	(4-11)	N.D.	2	4	6	N.D.	12	10	10	N.D.	N.D.	N.D.	N.D.	N.D.	N.D.	4.35	5.29	7.28	19.1
Ba (µM)	26	(>6)	N.D.	>67	>4.5	>12	>21	>4	19	19	N.D.	N.D.	N.D.	N.D.	N.D.	N.D.	N.D.	N.D.	N.D.	N.D.
Sr (µM)	192	77	91	200	138	108	45	54	99	99	63	28	25	35-52	94	63	70	80	165	182
B (µM)	590	N.D.	N.D.	N.D.	N.D.	N.D.	N.D.	N.D.	N.D.	N.D.	520	536	547	591	465	431	N.D.	N.D.	N.D.	N.D.
Li (µM)	636	303	356	340	245	280	1030	835	850	850	1217	416	427	343	488	335	553	545	1080	1070
Br (µM)	956	N.D.	N.D.	N.D.	N.D.	N.D.	N.D.	N.D.	N.D.	N.D.	873	494	482	392	890	920	970	1440	1390	1390
I (µM)	1065	623	56	24000	2500	18	1970	2400	5590	5590	803	3120	3940	3380	8680	3540	6010	10500	13100	13100
Fe (µM)	10	(<2-30)	N.D.	140	27	<2	43	35	140	140	5	111	9-76	110-374	105	51	276	118	146	403
Cu (µM)	111	(<2-40)	N.D.	160	29	<2	72	53	46	46	60	55	28-69	50-155	121	81	67	85	122	149
Mn (µM)	1150	267	73	2250	330	68	254	400	680	680	730	454	473	704	1300	790	811	857	1450	1430
Ni (µM)	N.D.	(<2)	N.D.	3	<2	<2	N.D.	<2	<2	<2	N.D.	N.D.	N.D.	N.D.	N.D.	N.D.	N.D.	N.D.	N.D.	N.D.
As (µM)	N.D.	N.D.	N.D.	N.D.	N.D.	N.D.	N.D.	N.D.	N.D.	N.D.	N.D.	N.D.	N.D.	N.D.	N.D.	N.D.	N.D.	N.D.	N.D.	N.D.
Pb (µM)	0.3	(0.035-0.130)	N.D.	0.1	0.1	0.1	N.D.	0.3	0.1	0.1	0.4	0.2	0.1-0.2	0.1-0.4	N.D.	N.D.	0.3	0.3	0.8	1.3
Cd (µM)	N.D.	(0.018-0.079)	N.D.	0.13	0.063	0.01	N.D.	0.44	0.07	0.07	N.D.	N.D.	N.D.	N.D.	N.D.	N.D.	0.07	0.11	0.22	0.28
Cr (mM)	N.D.	N.D.	N.D.	N.D.	N.D.	N.D.	N.D.	N.D.	N.D.	N.D.	N.D.	N.D.	N.D.	N.D.	N.D.	N.D.	N.D.	N.D.	N.D.	N.D.
Ag (mM)	N.D.	(5-25)	N.D.	47	11	17	N.D.	31	51	51	N.D.	N.D.	N.D.	N.D.	N.D.	N.D.	N.D.	N.D.	N.D.	N.D.
V (mM)	N.D.	(<3-6)	N.D.	3	<3	5	N.D.	11	4	4	N.D.	N.D.	N.D.	N.D.	N.D.	N.D.	N.D.	N.D.	N.D.	N.D.
Sb (mM)	N.D.	(3-84)	N.D.	2	1	10	N.D.	3	5	5	16	101	15-57	80-270	N.D.	N.D.	N.D.	N.D.	N.D.	N.D.
Mo (mM)	N.D.	N.D.	N.D.	N.D.	N.D.	N.D.	N.D.	N.D.	N.D.	N.D.	N.D.	N.D.	N.D.	N.D.	N.D.	N.D.	N.D.	N.D.	N.D.	N.D.
Te (mM)	N.D.	N.D.	N.D.	N.D.	N.D.	N.D.	N.D.	N.D.	N.D.	N.D.	N.D.	N.D.	N.D.	N.D.	N.D.	N.D.	N.D.	N.D.	N.D.	N.D.
Se (mM)	N.D.	(7-16)	N.D.	9	7	11	N.D.	25	13	13	N.D.	N.D.	N.D.	N.D.	N.D.	N.D.	N.D.	N.D.	N.D.	N.D.
Tl (mM)	N.D.	N.D.	N.D.	N.D.	N.D.	N.D.	N.D.	N.D.	N.D.	N.D.	N.D.	N.D.	N.D.	N.D.	N.D.	N.D.	N.D.	N.D.	N.D.	N.D.
W (mM)	N.D.	N.D.	N.D.	N.D.	N.D.	N.D.	N.D.	N.D.	N.D.	N.D.	N.D.	N.D.	N.D.	N.D.	N.D.	N.D.	N.D.	N.D.	N.D.	N.D.
Au (mM)	N.D.	N.D.	N.D.	N.D.	N.D.	N.D.	N.D.	N.D.	N.D.	N.D.	N.D.	N.D.	N.D.	N.D.	N.D.	N.D.	N.D.	N.D.	N.D.	N.D.
Sn (mM)	N.D.	N.D.	N.D.	N.D.	N.D.	N.D.	N.D.	N.D.	N.D.	N.D.	N.D.	N.D.	N.D.	N.D.	N.D.	N.D.	N.D.	N.D.	N.D.	N.D.
Hg (mM)	N.D.	N.D.	N.D.	N.D.	N.D.	N.D.	N.D.	N.D.	N.D.	N.D.	N.D.	N.D.	N.D.	N.D.	N.D.	N.D.	N.D.	N.D.	N.D.	N.D.

Note: H₂S concentrations for these fluids range from 0.8 to 11.2 mM, averaging ~4.7 mM. N.D. No data.

* Butterfield et al., 1990.

† Von Damm et al., 1998.

‡ Douville et al., 2002.

Douville et al., 2002; Hannington et al., 2005.

** Koschinsky et al., 2008

†† Von Damm et al., 2003.

§§ Gallant and Von Damm, 2006.

Assumed by authors to be 0 for calculation.

Appendix 4.1: Sampling and Analytical Methods, plus Discharge Compositions of Seafloor Black Smokers

The deep liquid at Reykjanes was sampled in May, 2007, from the only three wells that were available that were also vertical; deviated wells have the potential for the down-hole sampler tool, unique in the world (Simmons and Brown, 2006, 2007), to become stuck. Two wells are fitted with slotted liners, open to the reservoir through the slots, that extend below the solid production casing (from depths of 763 and 611 m in RN19 and 21, respectively), whereas the third well (RN-12) has no slotted liner, just an open hole below the solid production casing (base at 854 m). Bottom depths of the wells are 2506 m (RN12), 2235 m (RN19), and 1664 m (RN21). All three wells were sampled during a short period of power station maintenance, with the wells discharging at a very low rate, 3-5 kg/s, to prevent non-condensable gases from accumulating; normal production flow rates are ~110 kg/sec. The pressure and temperature in the wells were logged using a Kuster K-10 tool, less than 4 hours prior to sampling. In each case the depth of sampling was at least 150 m below the boiling level in the well, as defined by the change in slope of the measured pressure (Fig. 4.2). This change in slope is due to the transition from liquid to a boiling, two-phase mixture at ~1300 m depth, above which the vapor phase controls the pressure profile.

A titanium down-hole sampler, designed specifically to provide reservoir liquid samples for trace element analysis (particularly metals), was used to collect the deep liquid, as previously described by Brown and Simmons (2003) and Simmons and Brown (2006, 2007). After lowering the sampler to the sample depth, it was opened by an inertial trigger; the internal volume of the sampler is 800 ml. Although the deep liquid samples were

collected below the boiling zone, contamination by previously precipitated metal sulfide, either well bore scale or particulate (colloidal) sulfide suspended in the boiling zone, cannot be totally ruled out (although the narrow range of trace element concentrations from the three separate wells argue against ingestion of foreign particles; Fig. 4.3). Simmons and Brown (2007) showed that blanks using this down-hole sampler indicate little or no contamination when samples are being collected; in addition, because the samples were collected below the boiling level (Fig. 4.2), the presence of scales at this depth is not likely. All components of the sample vessel in contact with the liquid are titanium. Copper seals in the sampler are isolated from the liquid sample by viton O-rings. These O-rings are replaced before each sampling.

The sealed container prevents the liquid from boiling on ascent to the surface, by the use of a non-return valve so the sample maintains the same pressure as that collected; there was no evidence of leakage during recovery of the samples. At the surface the sampler was cooled below atmospheric boiling point by pouring cold water on its exterior, after which the sampler was opened and the solution collected (425-625 ml). All liquid samples were greyish in color due to the suspension of fine precipitates, assumed to have formed after sampling, due to mineral saturation (largely sulfides) on cooling. The sampler was then rinsed with 40 ml aqua regia to dissolve any precipitate that may have adhered to the internal titanium wall of the vessel, followed by rinsing with 40 ml of distilled water; this was repeated again with acid and distilled water. The total diluent (160 ml) was added to the original sample, and this dilution was later corrected for in the final reported analyses (Table 4.1).

Samples were analyzed at CSIRO Australia, Lucas Heights. Analytical methods include: CSIRO; Ag, Au, Be, Bi, Br, Cd, Co, Cr, Cu, I, Mo, Ni, Pb, Sb, Sn, Te, Tl, V, W by ICP-MS

(Inductively coupled plasma-Mass spectrometry), B, Ba, Ca, Cu, Fe, K, Na, Li, Mg, Mn, Na, S, Si, Sr, Zn by ICP-OES (Inductively coupled plasma-Optical emission), As and Se by Hydride-AAS (Atomic absorption spectrometric) analysis, Hg by AFS (Atomic fluorescence spectroscopy). The pH, CO₂, H₂S and SO₄ were not measured in the downhole samples due to acid addition upon sample retrieval. Surface-collected fluids have pH measured in the field, and are then analyzed by the Iceland GeoSurvey (B, Br, Cl, K, Mg, Na, SiO₂, CO₂, H₂S and SO₄ by spectrophotometer, ion chromatography, AAS) and at ALS Scandinavia AB Sweden (Al, Ba, Sr, Li, I and trace elements by ICP-SFMS, ICP-AES, ICP-SMS).

Surface samples are collected 2-3 m downstream of the wellhead, at pressures of 28-32.5 bar absolute (i.e., equivalent to 230-238°C, respectively) from the production wells at regular intervals for production monitoring purposes by the Iceland GeoSurvey. These samples consist of liquid and vapor phases of known proportion, determined from sample pressure and discharge enthalpy (Henley et al., 1984), with volatile species largely fractionated into the vapor sample. After analysis of all major components, including gases, from both samples they are recombined to provide the composition of the reservoir liquid, prior to boiling, using standard methods (Henley et al., 1984); a typical H₂S concentration in the reservoir liquid is 0.8 mM (sample collected at the surface from RN19). The surface samples of liquid are also analyzed for their trace element composition (a typical composition from RN19 is given in Table 4.1, corrected for concentration due to vapor loss at the sample point, i.e., equivalent to reservoir concentrations except for elemental changes due to precipitation on ascent prior to sampling).

Appendix 5

5.1. Calculation of reservoir liquid composition from surface samples

The wells selected at Reykjanes are assumed to have a liquid inflow (i.e., at aquifer depth only liquid phase exists) based on the measured enthalpy of discharge being close to the liquid saturated geothermometer temperature (Henley et al., 1984).

During discharge, boiling occurs due to pressure decrease; a mixture of liquid and vapor forms, causing concentration changes in both phases as boiling progresses (species which fractionate to the liquid are concentrated, whereas the volatile gas species are fractionated to the vapor phase). Recovering a representative sample at the well head requires sampling of both phases present (i.e., liquid and vapor phases). The sampled liquid is corrected for the vapor loss; no gain or loss of heat in the well is assumed. The steam fraction at the wellhead sampling point can be calculated as follows:

$$H_0 = y H_v + (1 - y) H_l \quad \text{or} \quad y = (H_0 - H_l) / (H_v - H_l)$$

Where y represents the vapor fraction, H_0 is the total enthalpy (at inflow temperature) and H_v and H_l represent the enthalpy of vapor (largely steam, H_2O) and liquid at the sampling point. These values can be derived from pressure (P_s) and/or temperature measurement at the sampling port.

At the sample point, $P_s = 27$ bar for well RN-19 is equivalent to a sampling temperature of 226°C ; the enthalpy at this temperature is 2803 J/g (vapor) and 971.4 J/g (liquid). The reservoir temperature for well RN-19 is 275°C , with an enthalpy of 1210 J/g, and the Cl in the discharge sample (RN-19) is 22010 mg/ kg. Therefore

$$y = (1210 - 971.4) / (2803 - 971.4) = 0.1302$$

The above calculation with the analyses of vapor and liquid phases at surface can be used to calculate the deep liquid concentrations.

$$MR = yM_v + (1-y)M_l$$

MR is the concentration of element M in reservoir, and M_v and M_l the concentration in the steam and liquid, respectively.

Appendix 5.2

Table A5.1. Example of calculated species (from SOLVEQ) for discharge liquid RN-9 to reservoir liquid composition by recombining the vapor (sample No. 200030169)

	Species	Molality	Tot Moles	ppm	Tot Molality	Log(a)
1	H ⁺	1.50E-03	0.2750E-01 CM	2.77E+01	2.84E-02	-3
2	H ₂ O	1.00E+00	5.38E+01	9.68E+05	5.55E+01	-0.0066
3	Cl ⁻	3.61E-01	0.5044E+00 AD	1.79E+04	5.21E-01	-0.8441
4	SO ₄ ⁻⁻	2.41E-06	1.64E-04	1.57E+01	1.69E-04	-7.1622
5	HCO ₃ ⁻	2.94E-07	2.42E-02	1.48E+03	2.50E-02	-6.9102
6	HS ⁻	8.81E-08	7.96E-04	2.63E+01	8.22E-04	-7.4534
7	SiO _{2(aq)}	1.04E-02	1.00E-02	6.03E+02	1.04E-02	-1.9848
8	Al ⁺⁺⁺	3.26E-09	2.26E-06	6.09E-02	2.33E-06	-12.0807
9	Ca ⁺⁺	9.52E-03	3.62E-02	1.45E+03	3.73E-02	-3.6314
10	Mg ⁺⁺	1.79E-05	3.36E-05	8.17E-01	3.47E-05	-6.4142
11	Fe ⁺⁺	1.45E-06	7.04E-06	3.93E-01	7.27E-06	-7.4926
12	K ⁺	3.15E-02	3.35E-02	1.31E+03	3.46E-02	-1.8736
13	Na ⁺	2.83E-01	3.96E-01	9.10E+03	4.09E-01	-0.9463
14	Mn ⁺⁺	4.63E-08	3.15E-05	1.73E+00	3.25E-05	-8.9772
15	Zn ⁺⁺	1.51E-11	1.32E-07	8.63E-03	1.36E-07	-12.4744
16	Cu ⁺	1.68E-11	2.24E-08	1.42E-03	2.31E-08	-11.1747
17	Pb ⁺⁺	1.70E-12	1.37E-09	2.84E-04	1.42E-09	-13.3451
18	Sr ⁺⁺	2.65E-05	8.10E-05	7.10E+00	8.36E-05	-6.1654
19	Ba ⁺⁺	1.15E-05	5.61E-05	7.70E+00	5.79E-05	-6.4922
20	F ⁻	2.70E-08	9.32E-06	1.77E-01	9.62E-06	-8.016
21	H ₂ AsO ₃ ⁻	1.79E-11	1.42E-06	1.77E-01	1.46E-06	-10.9995
22	MoO ₄ ⁻⁻	1.74E-07	1.69E-07	2.70E-02	1.74E-07	-8.3023